RCA REVIEW

a technical journal

RADIO AND ELECTRONICS
RESEARCH • ENGINEERING

VOLUME XV SEPTEMBER 1954 NO. 3

RCA REVIEW, published quarterly in March, June, September, and December by RCA Laboratories, Radio Corporation of America, Princeton, New Jersey. Entered as second class matter July 3, 1950 at the Post Office at Princeton, New Jersey, under the act of March 3, 1879. Subscription price in the United States and Canada; one year $2.00, two years $3.50, three years $4.50; in other countries: one year $2.40, two years $4.30, three years $5.70. Single copies in the United States, $.75; in other countries, $.85.

RCA REVIEW

a technical journal

RADIO AND ELECTRONICS
RESEARCH • ENGINEERING

Published quarterly by
RCA LABORATORIES
in cooperation with all subsidiaries and divisions of
RADIO CORPORATION OF AMERICA

VOLUME XV | SEPTEMBER, 1954 | NUMBER 3

CONTENTS

RCA REVIEW is regularly abstracted and indexed by *Industrial Arts Index, Science Abstracts* (I.E.E.-Brit.), *Electronic Engineering Master Index, Chemical Abstracts, Proc. I.R.E., and Wireless Engineer.*

RCA REVIEW

BOARD OF EDITORS

FACSIMILE SCANNING BY CATHODE-RAY TUBE*†

By

WARREN H. BLISS AND CHARLES J. YOUNG

Research Laboratory, RCA Laboratories,
Princeton, N. J.

Summary—*The use of cathode-ray tubes to perform the scanning function in facsimile scanners and recorders was first demonstrated on a large scale in the system called "Ultrafax."[1] This was in 1949. Since then a number of electronic facsimile equipments have been developed, largely under government supported contracts. The speeds, for practical reasons, have been much slower than "Ultrafax's" 400 pages per minute, but faster than the conventional facsimile devices which obtain their scanning by mechanical and optical means. In one exception, a cathode-ray system was developed to match the present wire-line standard of one page (8½ × 11 inches) in approximately ten minutes.*

This paper contains a survey of these developments along with an evaluation of the merits and handicaps of cathode-ray-tube scanning as applied to facsimile communication. Preceding the discussion a brief description is given of five systems which have been developed and tested.

INTRODUCTION

THE application of cathode-ray-tube scanning to facsimile may be accomplished in several different ways. As in television, both horizontal and vertical scanning are needed. At the sending end the preferred method is flying-spot scanning, the moving spot on the phosphor screen being projected optically onto the subject copy and the reflected light caught in a phototube, which then provides the facsimile signal. The rapid horizonal scanning is provided by deflection of the beam of the cathode-ray tube, the vertical scanning, either by the tube or by vertical motion of the subject copy. The cathode-ray tubes which are best suited for facsimile use are those known as "flying-spot" tubes.

At the receiving end the transient image on the cathode-ray tube screen must be photographed to get "hard copy." Here again two modes

---

* Decimal Classification: R581.

† The facsimile systems referred to in this paper were developed under research projects for the U. S. Department of the Navy, the U. S. Army Signal Corps, the Atomic Energy Commission and the U. S. Air Force—Project Lincoln.

[1] Donald S. Bond and Vernon J. Duke, "Ultrafax," *RCA Review*, Vol. X, No. 1, pp. 99-115, March, 1949.

of operation are possible. In one case horizontal scanning is by cathode-ray tube while vertical scanning is obtained by moving the film. In the second case, both horizontal and vertical scanning are by cathode-ray tube, so that a television-like raster is employed. It is not essential, of course, to record by cathode-ray tube at the lower speeds. Mechanical facsimile recorders have been used with electronic scanners.

Ultrafax

In the Ultrafax[1] system the horizontal or line scanning was provided by cathode-ray tube at both the sending and receiving terminals. The pages of subject copy were prepared in advance by photographing them on microfilm, which was then moved at constant speed through the optical system in the scanner. At the receiver the image was again photographed from the cathode-ray tube on a moving microfilm. Final copy was made by enlargement from this film. The use of microfilm at each terminal was necessary to handle pages at 400 per minute. At slower communication rates the extra photographic procedures are a handicap. In the devices to be described, with one exception, scanning was always by reflection from the actual subject copy, and the recorder made a print on paper ready for delivery.

Remote Duplicator

The objective here was to develop a medium-speed facsimile system which would deliver at branch libraries copies of reference material on file in a central main library. Scanning of pages in bound volumes and high definition of recorded copy were essential requirements. The speed of the system was 15 linear inches of 8½ inch wide copy per minute.

Flying-spot scanning made it possible to handle subjects in flat form and to vary the magnification at the scanner. The arrangement of the scanner is shown schematically in Figure 1. Figure 2 shows the outside appearance with the enclosure opened for insertion of subject copy on the scanner carriage.

The projection optical system is similar to that of a photographic enlarger. The cable drive from pulley D to the lens, and the connected lever system moving the cathode-ray tube, keep the scanning line in focus on the subject at any magnification ratio from 2:1 to 1:2. For a constant 4$\frac{1}{16}$-inch scanning line on the tube face, the width of copy scanned could be varied from 2$\frac{1}{32}$ to 8$\frac{1}{8}$ inches. The mechanism also varied the rate of vertical feed so that the scanned field was kept in proportion. Thus the copy received at the recorder, where the scan-

ning line was always 9 inches long, was reproduced either at normal size or enlarged to whatever extent necessary to make fine print clearly readable. The over-all length of the optical system from subject to tube socket was 35 inches with the 5.3-inch focal length lens. The very small amount of light reflected from the flying spot projected on the

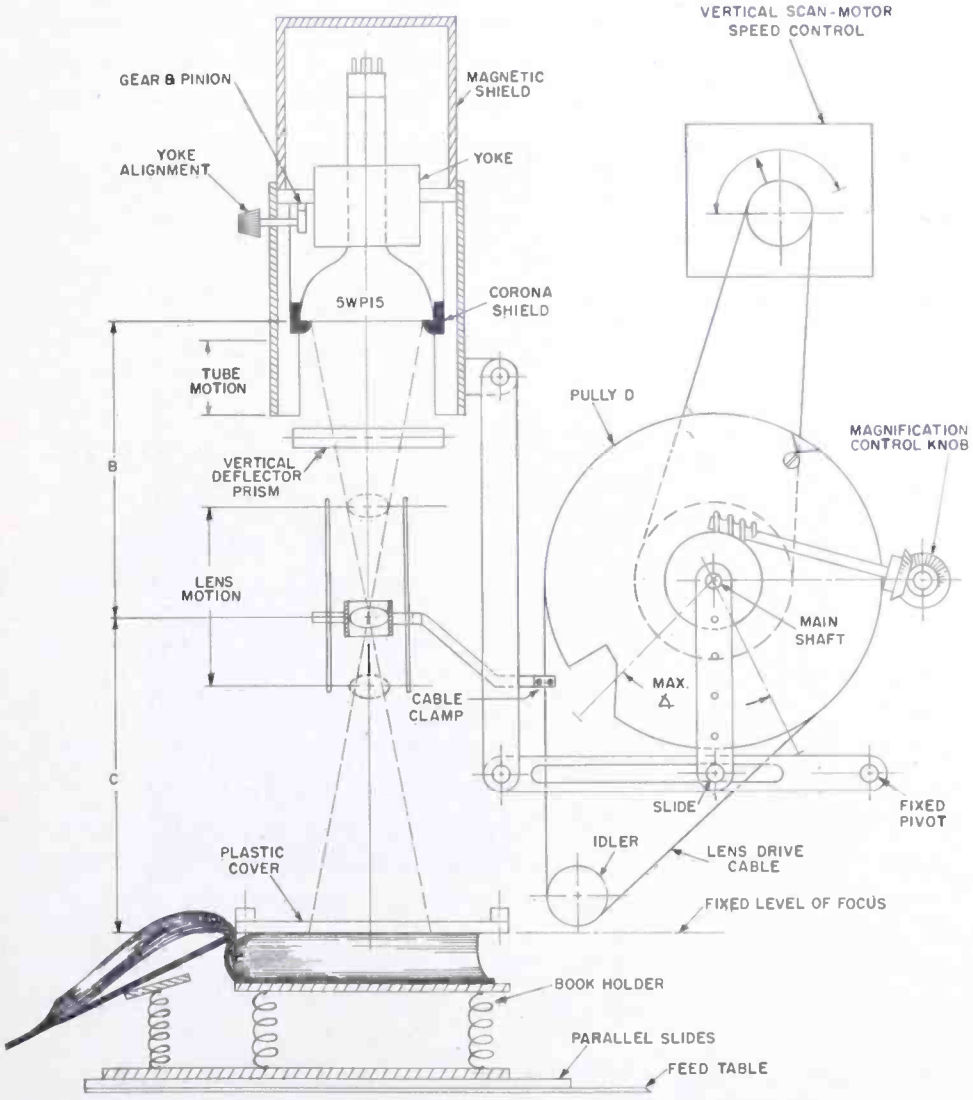

Fig. 1—Optical system for flat-bed scanner.

subject was collected by four photomultipliers distributed along the line, their outputs being balanced to produce a uniform facsimile signal.

The receiving unit of the system was mechanical, scanning being provided by a printer bar and rotating helix. The latter was driven by an 1800 revolutions-per-minute synchronous motor to provide the 30 scanning lines per second. The image was formed electrolytically on paper treated with a sensitizing solution and subsequently fixed and

dried, all these functions being performed automatically and continuously in the recorder mechanism.

Standard-Speed System

The development and test of the two systems described above gave a background of experience on cathode-ray-tube facsimile scanning at very high (400 pages per minute) and at medium (1½ pages per minute) speeds. Fortunately, an opportunity was next provided, under

Fig. 2—Loading the flat-bed scanner.

sponsorship of the U. S. Army Signal Corps, to make a similar study at slow speeds, at the standard rate of 90 lines per minute, 96 lines per inch.

The scanner which resulted from this work is shown in Figure 3, the case on the right being the scanner proper. Here the optical system from the cathode-ray tube socket to the subject copy is 48 inches long but is so folded that the length of the case is only 20 inches. Ambient light was excluded by placing the subject face down on the glass of the moving carriage and covering with a black curtain, a great simplification as compared with the enclosure in Figure 2.

A major problem in this system was the provision for accurate beam deflection in the flying-spot tube at the very low rate of 1.5 sweeps per second. Conventional deflection circuits were impractical,

and any departure from linearity was immediately apparent because the associated recorder used constant speed mechanical scanning. The solution of this problem is discussed in a later section.

Electronic Xerographic System

The most recent and most promising cathode-ray facsimile system was developed under U. S. Navy sponsorship for transmission at a speed of ten $8\frac{1}{2} \times 11$ inch pages per minute. In this case the recorder

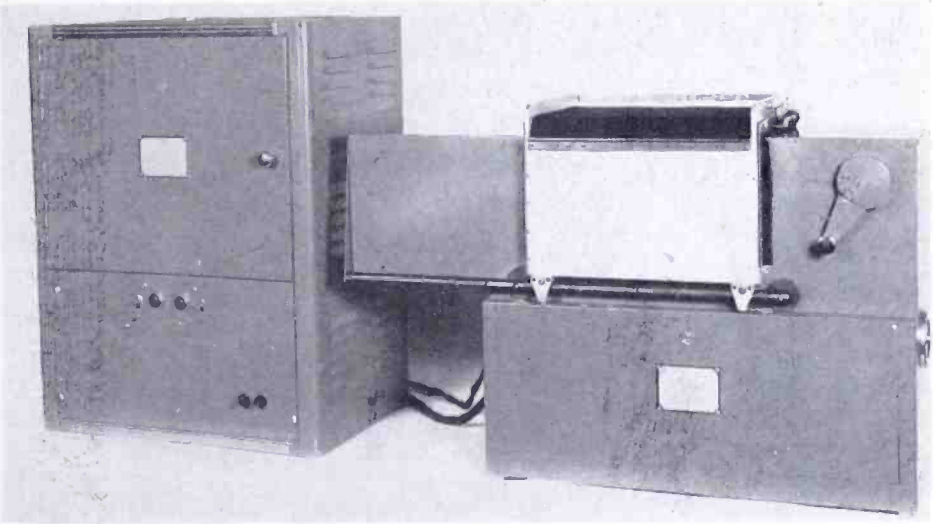

Fig. 3—Cathode-ray tube facsimile scanner with folded optical system.

as well as the scanner was based on optical projection from a flying-spot tube. Direct, continuous, and economical printing of "hard copy" was made possible for the first time at these speeds by use of xerographic printing.*,[2,3]

The optics in the scanner were similar to those already described in that the flying spot on the tube was projected on the subject copy as a scanning line, and the reflected light collected in a photomultiplier tube. Variable magnification provided a choice of 4-, 6-, or 8-inch scanning lines. In this case there was no requirement to handle books. The subject sheets were carried past the scanning point on a rotating drum, being held in place on its porous surface by vacuum. The design made it possible to load sheets conveniently at the rate of one every six seconds. Figure 4 shows the scanner in operation.

---

* A Xerographic Printer and Processor was obtained from the Haloid Company of Rochester, N. Y. for this purpose.

[2] W. L. Carlson, U. S. Patent 2,297,691.

[3] Shaffert and Oughton, "Xerography: A New Principle of Photography and Graphic Reproduction," *Jour. Opt. Soc. Amer.*, Vol. 38, pp. 991-998, December, 1948.

In the recorder, the flying spot on the face of the cathode-ray tube was projected by a lens and mirror to produce a scanning line on the surface of a selenium-coated cylinder which, by its rotation, provided the vertical component of scanning. The intensity of the beam was modulated by the incoming facsimile signal.

In the Xerographic process, the surface of this cylinder is first charged to a potential of several hundred volts as it moves under a

Fig. 4—Scanner for the Electronic-Xerographic System.

corona unit. Exposure to the light image causes a selective discharge due to photoconductivity, leaving a latent electrostatic image on the surface. A developer consisting of a mixture of fine carrier beads and a much finer black powder is then cascaded over the surface. The fine black toner particles, having acquired an appropriate electric charge by friction with the beads, adhere to the proper areas on the selenium and form an image. This powder image is then transferred to a moving web of paper and fixed thereon by thermal fusion. The method gives inexpensive paper prints and has sufficient photographic sensitivity to function well at the speed of 10 feet per minute.

A Raster Scanning System

In all of the equipments so far described, the horizontal or line scanning was supplied by sweep of the spot on the cathode-ray tube and the vertical component by continuous motion of the copy. In one development, carried on under Air Force sponsorship, complete raster scanning was provided for both sending and receiving. Here the subject was an image on a frame of 35-millimeter film and the output at the receiver was a similar frame on film.

In this case, with a 4:1 size reduction from the tube face to the film, the optics are simpler and more compact. At the sending end the photomultiplier can be put immediately behind the film and receives much more light by transmission than was available by reflection from a page-size print on paper. Reduced beam currents are possible with consequent improvement in definition.

The scanning speed in this case was 50 lines per second, 15 seconds per frame. The resolution was 700 lines each way. It was observed that strict proportionality of the reproduced image is more readily obtained with identical deflection circuits at each end of the system, the usual "S" shaped distortion in deflection being automatically compensated.

Selection of Cathode-Ray Tube

Although there are a large number of commercially available cathode-ray tubes at the present time, only a few meet the exacting requirements of facsimile scanning. The major requirements are (1) a flat screen, (2) a very small spot of light and (3) ample spot brightness. These requirements automatically exclude practically all television kinescopes and most of the oscilloscope tubes. This work has been done with the flat face flying-spot cathode-ray tubes. These have a 4.25-inch flat screen and can be operated at 25 to 30 kilovolts to give a small, bright spot of light. Types of this category are the 5WP11, the 5WP15 and 5ZP16.

Spot size determines the definition that may be attained. In television, definition is usually expressed as the maximum number of alternate black plus white lines that can be resolved across a picture raster. In facsimile a more critical view is taken. Alternate lines must not only be discernible but should have a good contrast ratio. Measurements made on a type 5ZP16 tube gave spot diameters of 0.005 to 0.006 inch when measured between points 10 per cent down from the maximum. This figure was obtained by use of a very low value of beam current—of the order of 1 to 2 microamperes. The spot size increases as the beam current goes up. A spot diameter of 0.005 inch will give

825 lines across the diameter of a 4.25-inch screen. High-frequency signal boost can be used to compensate for a certain amount of signal drop as the limiting action of spot size is approached. In the Standard-Speed System this method was used to obtain 1000-line resolution from a pickup signal that dropped to 60 per cent on fine bars.

It is unfortunate that the use of a low beam current to get high resolution also gives a low level of spot brightness. Operation at a high value of beam current not only results in a bigger, brighter spot but other effects occur. A high level of light is usually required from electronic flying-spot recorders, but phosphor screens and glass are subject to burning or browning when bombarded with too great a concentration of energy. To verify this a new type 5WP11 was operated at 30 microamperes and 27 kilovolts for a 30-hour test with continuous single line scan of 90 per cent duty cycle. At the end of the test the light output from this "burned" phosphor line was down to 50 per cent. A compromise can usually be reached depending on what performance is required.

Although electronic devices are generally characterized by tremendous speed, the rate of light decay on a phosphor is often an exception. The P-16 phosphor emission decays to 10 per cent in 4.5 microseconds, but the P-11 phosphor requires 2 milliseconds to reach the same value under some operating conditions. This factor may become prominent in scanning since it tends to produce a "tail" of light behind the flying spot. Decay must be rapid enough that the pickup cell receives light from only one picture element at a time. In cathode-ray-tube recording by line sweep, the decay time may extend over the major part of the line-sweep period with no detrimental effect.

In some applications the spectral emission characteristic of available phosphors must be checked. This becomes important if colored copy is to be handled, but is of lesser consequence for black and white. There is also the matter of matching the sensitivity characteristic of the pickup device to the light source. For black-and-white copy the 5ZP16 cathode-ray tube and the 5819 photomultiplier work well together. Since the emission from a P-16 phosphor is mostly in the ultraviolet (and hence, invisible), focussing is best accomplished by means of oscillographic observation of the scanner output signal.

Optical Projection Considerations

A much more elaborate but no less precise optical system is required for cathode-ray-tube scanning than for conventional, mechanical facsimile scanning. This is due to the fact that a whole scanning line (or raster in one case) must be projected from the phosphor screen onto the subject copy. The choice of lens is governed by several factors.

A flat field of focus over as large a projected area as possible is desirable. If the focal length is too great the system becomes bulky. A magnification other than unity increases the length of the optical path. For available lenses the maximum subtended angle of use has been found to be about 30 degrees (±15 degrees). Some lenses do not give good performance for magnifications of unity or less than unity.

In one case a standard enlarging lens of 5.33-inch focal length and f/4.5 gave fairly good results, but definition fell off at the ends of an 8-inch projected scanning line. A lens of the symmetrical anastigmatic type having a focal length of 8 inches and f/6.3 gave superior performance.

The optical spacings required for lens operation follow these two simple laws:

$$\frac{1}{F}=\frac{1}{B}+\frac{1}{C} \quad \text{and} \quad X=\frac{C}{B}.$$

Here F is the focal length of the lens, B is the distance from the cathode-ray-tube screen to the lens, C is the distance from the lens to the subject copy, and X is the magnification ratio. Application of these rules to an 8-inch lens set for a 2-to-1 magnification gives an over-all path length of four feet if the length of the cathode-ray tube is included. If means for handling the subject copy to give vertical scanning and adjustable magnification are also included, the space problem is even more critical.

A good solution to this problem was worked out and used in the Standard-Speed System. The details are shown schematically in Figure 5. The desired range of magnification ratio was from 2-to-1 to 1-to-2. A folded optical path is used to project a 4.33-inch scanning line onto the copy which may vary in width from 8.66 to 2.16 inches. Three mirrors M_1, M_2, and M_3 are used to break the optical path into four sections. An L-shaped member pivoted at the toe point carries mirror M_2 at its heel and moves mirror M_3 in a vertical slide. A carriage holding the lens rides on the longer side of the member by cable drive from the magnification-ratio control crank. A roller on the lens carriage traverses a fixed cam as shown to impart the required motion to the L-shaped member. Mirror M_1 is fixed in position and the angular position of mirror M_3 is controlled by a small pantograph. Accurate focus is maintained throughout the whole range.

Although this appears to be somewhat complicated, the maximum dimension of the complete scanner was reduced to 20 inches as mentioned before. This machine (Figure 3) scans the flat copy, which is carried on a motor-driven carriage to provide the vertical scan.

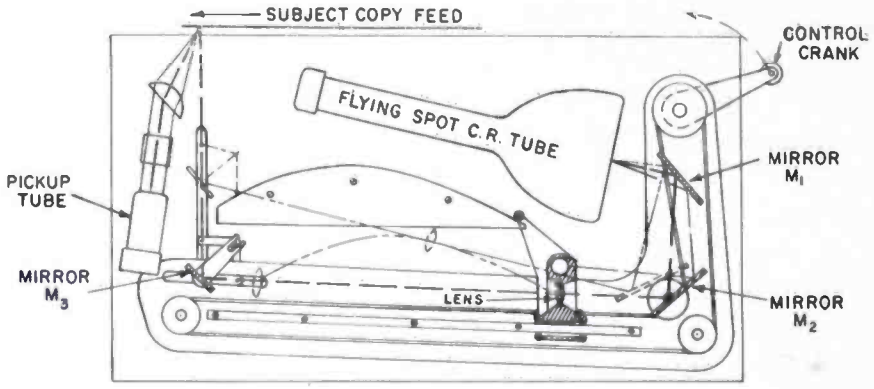

Fig.5—Folded optical system schematic.

Light Pickup

When electronic scanning is used on opaque copy the collection or pickup of reflected light requires a special optical system. A design must be achieved that will not only collect as much light as possible but will produce uniform response all along the scanning line. The efficiency of light collection is important for a high signal-to-noise ratio because the illumination from the flying spot is very low. In one of the developments, four type 5819 phototubes were spaced in a row to give uniform pickup over an 8-inch line. Their outputs were combined in parallel and individual controls were used for matching purposes. This did not prove to be satisfactory since the balance was difficult to maintain, partly because of tube aging, and the parallel arrangement gave a signal-to-noise ratio of only 25 decibels.

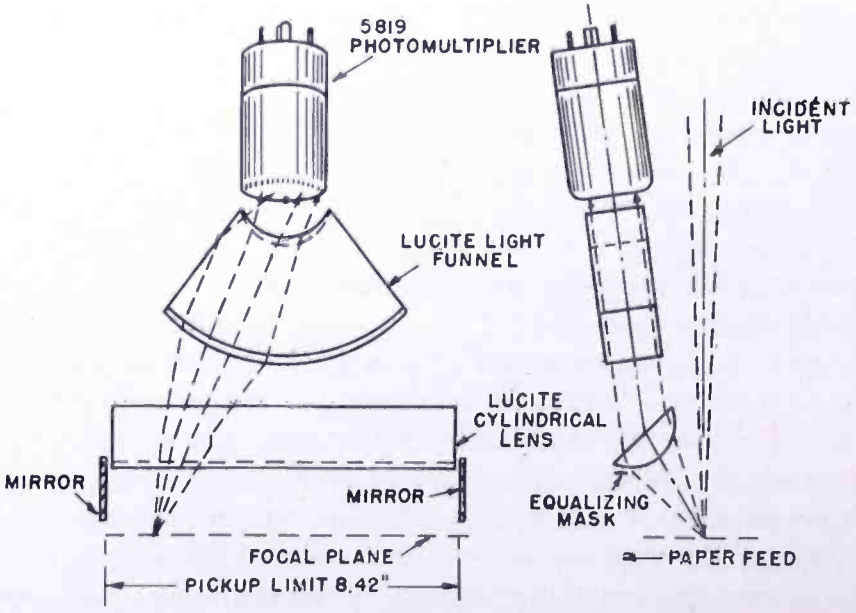

Fig. 6—Optical pickup for standard-speed scanner.

A better solution to this problem is illustrated in Figure 6 and was used on the Standard-Speed System. A single type 5819 photomultiplier was employed with a cylindrical lens and a light funnel to direct the reflected light onto the photoemissive cathode. Two small mirrors were used as shown to increase the pickup from the extreme ends of the line. As a final detail to completely equalize the response, a paper mask was adjusted point-by-point along one edge of the cylindrical lens. A signal-to-noise ratio of 40 decibels was obtained in this case. This was for a beam current of 2 to 5 microamperes in the type 5WP15 scanner tube operating at 25 kilovolts. The photomultiplier output was 2 volts for white areas on the subject copy.

Screen Coverage

Except for raster scanning, the systems described operate from a single scanning line across the phosphor screen of the cathode-ray tube. This limitation obviously results in very inefficient use of the screen. As mentioned previously, continued use of a single line would also shorten the life of the tube, particularly with a high level of beam current. To overcome this difficulty, manually adjustable vertical deflection may be included so that the scanning line may be changed from time to time to different places on the screen. In order to hold the projected scanning line in the same position on the subject copy, a compensating optical shift of opposite sense must be made. This has been accomplished by physically moving the cathode-ray tube or by rocking a prism or mirror in the light path.

A somewhat more elegant as well as practical way to accomplish this function is to link the electrical and mechanical adjustments together and drive the system with a single control. If a motor is used for this drive a considerable area of the total screen may be used and it will age uniformly and slowly.

Uniformity of Spot Brightness

Until experiments were made with cathode-ray tubes as facsimile scanners, it was not apparent that lack of uniformity in spot brightness would present a problem. However, phosphor grains are deposited on the inner glass surface by settling them out of a liquid suspension, and this does not produce an absolutely uniform thickness. In single-line scanning, variations from this cause can produce vertical streaks in the reproduction. Another observable variation in spot brightness as the beam is deflected can be attributed to beam defocussing produced at wide deflection angles. Still another possible source of variation is the projection lens. The combined effect of these factors has been

observed to produce light output variations as great as 2 to 1 in some cases.

When reproduction includes half-tones this much variation cannot be tolerated, nor can it be removed by limiters as it is for line cuts. A scheme called automatic white control has been devised to solve this problem. Figure 7 illustrates the details of one such device. A sample of the light emitted by the cathode-ray tube as the spot sweeps across the screen is "viewed" by a type 931A photomultiplier tube mounted adjacent to the projection lens. The electrical output of this tube is amplified by a triode T_4 and fed back as control bias to the cathode of the cathode-ray tube.

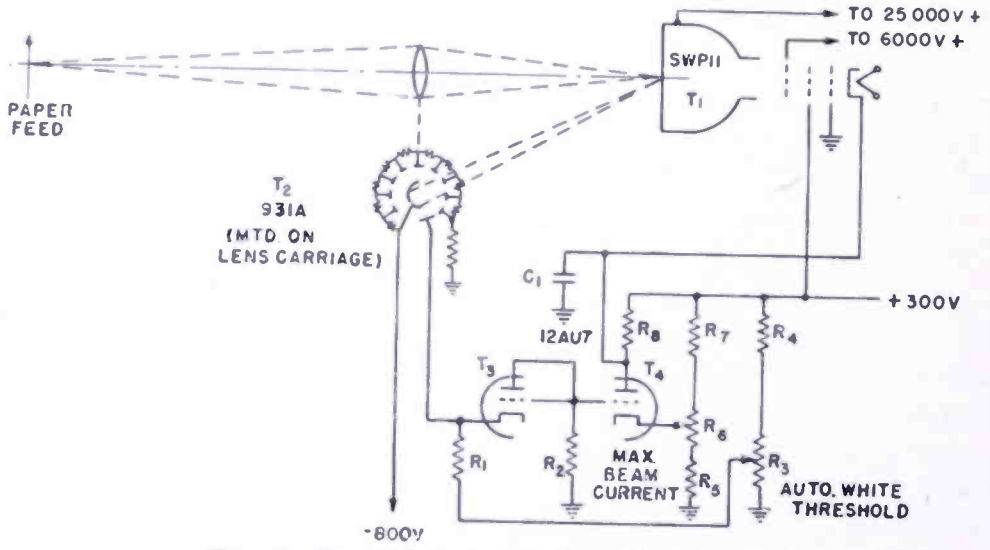

Fig. 7—Simplified automatic white circuit.

Any tendency toward brightness variation is instantly recognized and proper control is effected to counteract it. The speed of operation should be sufficiently high relative to the scanning rate to correct for phosphor variations even smaller than the light spot dimension. In variable magnification systems the 931A tube may be mounted on the lens carriage so that light variations resulting from lens position changes can also be compensated. In the circuit shown, a potentiometer R_6 is provided for setting the maximum attainable beam current at a safe value and the desired operating level of brightness can be set by means of control R_3. A condenser C_1 prevents oscillation at very-high frequencies.

Automatic white control was used in the Remote Duplicator, the Standard-Speed System, and the Electronic-Xerographic System.

Linearity of Sweep

Although linear line sweep occurs naturally in most mechanical

systems, it is considerably more difficult to attain in an electronic system. Not only must a suitable sawtooth waveform be generated, but it must be applied to the cathode-ray tube so as to produce uniform spot motion. Most deflection yokes are not linear so that the drive current characteristic must be slightly S-shaped to produce suitable correction. The difficulties from an electronic point of view increase

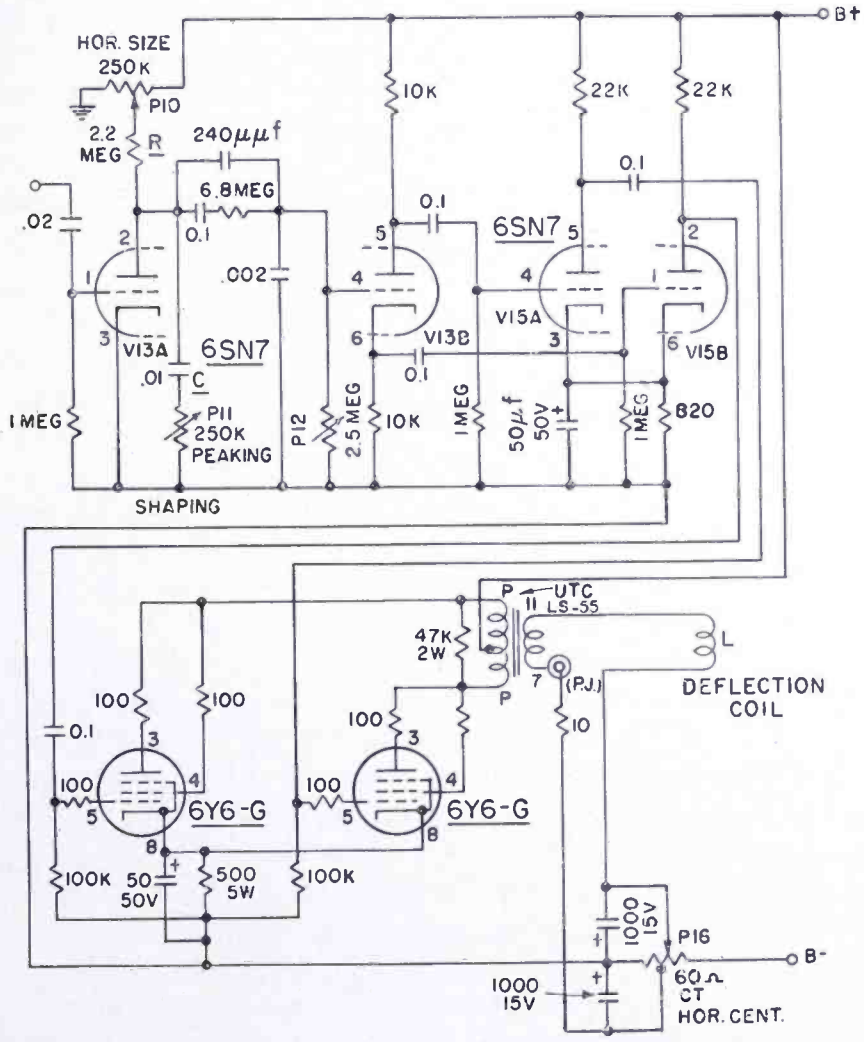

Fig. 8—Electronic scanner deflection circuit.

as the sweep frequency decreases. Two other related factors are stray field pickup and regulation of the high-voltage anode potential supply. For precision work the cathode-ray tube must not only be shielded from stray magnetic fields (primarily from power supplies) but the deflection current must be free from "hum." Variations in the anode potential cannot be tolerated since this changes the beam "stiffness" and, hence, the deflection sensitivity.

A typical sweep circuit as used in the Electronic-Xerographic

System to operate at 240 lines per second is shown in Figure 8. The basic sawtooth waveform is developed as a potential across condenser C which is slowly charged through resistor R and quickly discharged by triode V13A. Variable resistor P12 and the other associated condensers and resistors provide a means of adjusting the waveform so that the result produced in the deflection yoke coil L is reasonably linear. Variable resistor P11 causes a sharp reverse pulse to be produced at flyback time to help overcome the inductive effect of the yoke. The other tubes act as phase splitter, triode amplifiers, and push-pull drivers. Two other controls which are invariably used in deflection circuits are the size control (P10) and the centering control (P16). A system of this type will give an over-all characteristic that does not deviate more than 3 per cent from perfect linearity.

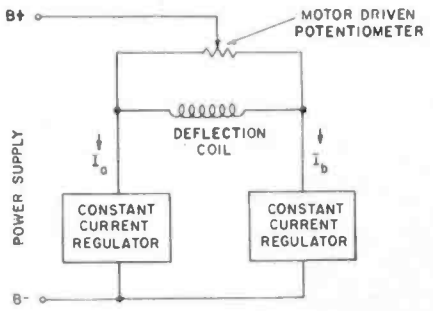

Fig. 9—Low-speed deflection circuit.

For the Standard-Speed System better linearity was required and the slow speed of 1.5 sweeps per second imposed very high precision and stability requirements for an electronic sweep. The deflection system selected for this is partly mechanical and partly electronic as depicted briefly in Figure 9. With this simple arrangement, the linear motion applied to the potentiometer slider by the motor drive produces a linear variation of deflection current from a positive value through zero to a negative value. The two current regulators, which provided about 50 milliamperes each in this case, can be adjusted to set the length and centering of scan. This system gave an over-all deflection linearity that deviated not more than 1 per cent from the ideal condition.

Miscellaneous Items

When flying-spot cathode-ray tubes are operated at more than a few microamperes beam current, there is likely to be screen damage if the beam is allowed to remain stationary. It is good practice to provide protection against this possibility by automatically turning the beam off in case of loss of deflection. One method is to rectify a

portion of the deflection signal and use it to hold the beam on by relay control.

The synchronizing problem with electronic scanning is not fundamentally different from that for conventional mechanical systems. Reference frequencies can be provided by (1) locally maintained frequency standards at both terminals, (2) 60-cycle power line tie-in or (3) a single standard with sync pulse transmission. Since these methods are well known in the facsimile art there is no need for detailed discussion here. In electronic scanning, as in television, it is the usual practice to trigger the sweep circuit at the beginning of each line, the trigger or phasing pulses being supplied from the standard.

The recording means, if electronic, may use the same trigger pulse if it is transmitted with the signal. The bandwidth of the transmission circuit for the required speed of operation is usually sufficient to handle the sync pulses with the necessary precision and stability. A special difficulty arises when electronic equipment at one terminal is to be synchronized with motor driven equipment at the other. The inertia of the mechanical device may prevent it from following any rapid changes in the electronic units. In the Remote Duplicator System the scanner sync pulses were generated from a motor having the same inertia as the motor driving the recorder.

The flying light spot produced on the flat screen of these cathode-ray tubes provides a means of scanning flat copy which cannot readily be accomplished by mechanical means. For the case where reproductions from pages of books and magazines is necessary this flat-bed scanning is essential. However, in attempting to utilize the speed capabilities of electronics the input copy feeding problem may become a limiting factor.

Conclusions

Although these systems have not been developed beyond the experimental prototype stage and very little operational data has been accumulated, certain reasonable conclusions can be drawn. In all cases, a completely workable, practical facsimile system was obtained which could be engineered further for commercial use. However, there are certain limitations as well as a few advantages in the electronic system.

Attainment of good sweep or scanning linearity is more difficult to reach with the deflection of an electron beam than with a rotating drum, especially at low speeds. Even though the yoke current is made to follow a precise saw tooth pattern, this does not result in absolutely linear spot movement. The linearity of electronic scanning can be

improved further, but this increases the complexity of the system. A high degree of linearity is easier to get in a mechanical scanner.

The limit of definition for cathode-ray-tube scanners is in the spot size produced on the phosphor screen. The use of 25- to 30-kilovolt accelerating potentials and low values of beam current such as 2 to 5 microamperes give a very small area of light, but the maximum definition attainable with standard tubes is about 1000 lines across the whole screen. A mechanical scanner can do better than this with a relatively simple optical system. Future developments in cathode-ray tubes may be expected to give 2000-line definition.

The obvious and outstanding advantage for the electronic device is speed. All the systems discussed, except "Ultrafax," operated at relatively low speeds for electronic scanners. Good sweep linearity and circuit stability can be more readily attained at speeds which start at the upper limit of mechanical systems. For continuous scanners this comes at one to two pages per minute. For high-speed transmission the electronic scanner must be used.

Although the optical systems for flying-spot scanners are somewhat cumbersome, they do offer a means for efficiently handling subject copy for a variety of types and sizes. Practical flat-fed scaning opens up new applications. In spite of the nonlinearities of the lens law, the variable magnification problem can be practically solved as was done in three of the projects. This feature of flexibility is not practical to attain with the mechanical scanner.

The experimental and developmental work on applying cathode-ray tubes to facsimile systems has resulted in a good background of information. With this accumulation of data one will be able to judge better as to how much electronics should be used when new facsimile applications arise. When flat-bed scanning is required, when high speed of transmission is necessary, or when photographic reproduction is used, electronic scanning of the subject copy should be considered. As transmission speeds get higher and higher, the ultimate limitation may be the available bandwidth or the sensitivity of the photographic reproducer.

Acknowledgment

The authors wish to acknowledge the work of H. C. Allen, Maurice Artzt, and K. J. Magnusson, who carried out the development work on three of the projects and supplied much of the information included in this paper.

CIRCULAR POLARIZATION IN WAVEGUIDES AND CAVITIES*

By

R. W. Klopfenstein

Research Laboratory, RCA Laboratories,
Princeton, N. J.

Summary—A filter element suitable for high-power ultra-high-frequency television applications is described. This element consists of a radial transmission line cavity coupled in series to a circular waveguide which is operated in a circularly polarized mode. The theory relevant to the design of these filter elements is presented. Curves displaying the required design data are given.

I. Introduction

IN CONNECTION with the development of components with high power handling ability for use at ultra-high frequencies, a structure consisting of a circular waveguide series-loaded by radial line cavities appears to have many desirable features. For the structure envisaged, the circular waveguide would transmit circularly polarized energy in the dominant mode of the guide. While a rather complete treatment of the radial line excited in uniform amplitude and phase is given in the literature, it is not believed that a published treatment of the radial line excited in rotating phase exists. Also, some additional results in regard to circular polarization in cylindrical waveguides are needed.

It is the object of this study to develop specific design formulas that can be used in connection with the structures mentioned in the previous paragraph. In Section II a rather complete theory for radial lines excited in rotating phase is presented. Input impedance expressions have been derived, and design curves showing the resonant lengths for open and short circuit terminated radial lines are presented. A formula for the Q of radial line cavities is derived and a comparison with other types of cavities is given.

In Section III two different definitions of the characteristic impedance for a circular waveguide transmitting circularly polarized energy are presented. The first is useful in determining the reflection coefficient on the guide due to a given series load, while the second relates the power transfer on a matched guide to the axial wall current.

* Decimal Classification: R119.35.

Throughout this paper the time dependence of the field quantities has been taken as that given by the factor $e^{j\omega t}$, and, as usual, this factor has been dropped from all the equations.

II. Radial Transmission Lines—Rotating Phase Mode

A. *General Considerations*

A considerable amount of work has been done in connection with radial transmission lines whose inner radii are excited by a constant-phase voltage.[1-3] The theory for radial transmission lines whose inner conductors are excited by a constant magnitude voltage of rotating phase will be devcloped here. One application of such transmission lines is encountered in the series loading of circular waveguides which are transmitting power in a circularly polarized mode.

A radial transmission line and the coordinate system associated with it is illustrated in Figure 1. Circular cylindrical coordinates are used with the Z axis perpendicular to the plane of the paper.

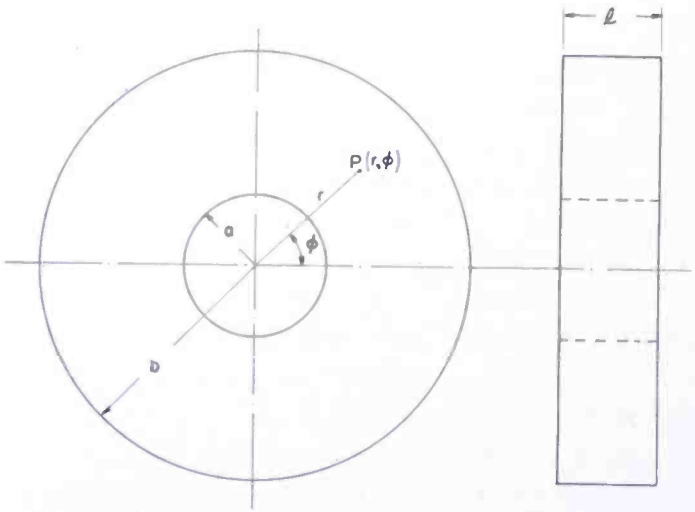

Fig. 1—Radial transmission line and associated terminology.

It is assumed that there is no z variation of the field quantities, and that the aperture at $r = a$ is excited by a phase rotated wave.

$$E_z(a,\phi) = E_0 e^{-j\phi}. \tag{1}$$

Elementary solutions to the wave equation in cylindrical coordinates

[1] H. Salinger, "A Coaxial Filter for Vestigial-Sideband Transmission in Television," *Proc. I.R.E.*, Vol. 29, pp. 115-120, March, 1941.
[2] N. Marcuvitz, *Waveguide Handbook*, McGraw-Hill Book Company, New York, N. Y., 1951, pp. 29-47.
[3] W. Ramo and J. R. Whinnery, *Fields and Waves in Modern Radio*, John Wiley and Sons, New York, N. Y., 1949, pp. 354-358.

(r, ϕ, z) are given by[4]

$$\psi = e^{-jn\phi} [AH_n^{(2)}(kr) + BH_n^{(1)}(kr)], \tag{2}$$

where ψ = the scalar potential of the wave.

$H_n^{(2)}$ = Hankel function of the second kind and represents outward-traveling waves,

$H_n^{(1)}$ = Hankel function of the first kind and represents inward-traveling waves,

n = order of the Hankel function,

A, B = arbitrary constants and correspond to incident and reflected waves respectively,

k = propagation constant which, in a lossless medium, is equal to $2\pi/\lambda$.

The corresponding fields are

$$E_z = \psi, \; E_r = 0, \; E_\phi = 0,$$

$$H_z = 0, \; H_r = +\frac{j}{\mu\omega}\frac{1}{r}\frac{\partial\psi}{\partial\phi}, \; H_\phi = \frac{-j}{\mu\omega}\frac{\partial\psi}{\partial r}. \tag{3}$$

In order to match the boundary condition at $r = a$, given by Equation (1), n must be taken as unity, and, thus,

$$E_z = e^{-j\phi} [AH_1^{(2)}(kr) + BH_1^{(1)}(kr)],$$

and

$$H_\phi = \frac{-j}{n_0} e^{-j\phi} [AH_1^{(2)\prime}(kr) + BH_1^{(1)\prime}(kr)], \tag{4}$$

where $n_0 = \sqrt{\frac{\mu}{\epsilon}}$ = intrinsic impedance of the medium.

Equations (4) can be rewritten in a form which emphasizes their traveling wave character. Thus,

---

[4] J. A. Stratton, *Electromagnetic Theory*, McGraw-Hill Book Company, New York, N. Y., 1941, pp. 360-361. Note that the expressions given here are the complex conjugates of those given in Stratton. This is because a different time dependence has been taken from that given in Stratton.

$$E_z = e^{-j\phi} G_1(kr) \left[Ae^{-j\Theta(kr)} + Be^{+j\Theta(kr)} \right],$$

and

$$H_\phi = -\frac{1}{n_0} e^{-j\phi} G_2(kr) \left[Ae^{-j\Psi(kr)} - Be^{+j\Psi(kr)} \right],$$

where

$$G_1(x) = \sqrt{J_1^2(x) + N_1^2(x)} = |H_1^{(1)}(x)|,$$

$$\Theta(x) = \arctan\left[\frac{N_1(x)}{J_1(x)}\right] = \operatorname{Arg} H_1^{(1)}(x),$$

$$G_2(x) = \sqrt{J_1'^2(x) + N_1'^2(x)} = |H_1^{(1)\prime}(x)|,$$

$$\Psi(x) = \arctan\left[\frac{-J_1'(x)}{N_1'(x)}\right] = \operatorname{Arg} -jH_1^{(1)\prime}(x),$$

$J_1(x), N_1(x)$ = Bessel functions of the first order and of the first and second kinds respectively.

$J_1'(x), N_1'(x)$ = derivatives of the functions with respect to their arguments.

(5)

It is worth noting at this time that the use of asymptotic forms[5] for the Bessel functions involved in Equations (5) will result in a considerable simplification. For large values of their arguments

$$G_1(x) \cong G_2(x) \cong \sqrt{\frac{2}{\pi x}},$$

and (6)

$$\Theta(x) \cong \Psi(x) \cong x - \frac{3\pi}{4}.$$

B. Impedance Expressions

The impedance at any point on the radial transmission line will be taken as the ratio of electric field to circumferential magnetic field at that point. Thus, from Equations (5),

---

[5] A. Sommerfeld, *Partial Differential Equations*, Academic Press, Inc., New York, N. Y., 1949, pp. 116-117.

$$Z(kr) = -Z_0(kr)\frac{Ae^{-j\Theta(kr)} + Be^{+j\Theta(kr)}}{Ae^{-j\Psi(kr)} - Be^{+j\Psi(kr)}}, \tag{7}$$

where

$$Z_0(kr) = \frac{n_0 G_1(kr)}{G_2(kr)}.$$

The constants A and B depend on the complex ratio of incident to reflected power. Explicit expressions for impedance can be obtained for various terminal conditions. If $Z(kb) = E_z/H_\phi$ evaluated at $r = b$ is regarded as known, it can be shown from Equations (7) that

$$Z(ka) = Z_0(ka)\frac{Z(kb)\cos[\Theta(ka) - \Psi(kb)] + jZ_0(kb)\sin[\Theta(ka) - \Theta(kb)]}{Z_0(kb)\cos[\Psi(ka) - \Theta(kb)] + jZ(kb)\sin[\Psi(ka) - \Psi(kb)]}. \tag{8}$$

The analogy to the usual transmission-line formula is evident, and, in fact, for large values of radius, the asymptotic expansions of Equations (6) can be used, and Equation (8) then reduces to exactly the usual transmission-line formula. For a short-circuit termination, $Z(kb) = 0$, and

$$Z(ka) = jZ_0(ka)\frac{\sin[\Theta(ka) - \Theta(kb)]}{\cos[\Psi(ka) - \Theta(kb)]}. \tag{9}$$

For an open-circuit termination, Z_b approaches infinity, and

$$Z(ka) = jZ_0(ka)\frac{\cos[\Theta(ka) - \Psi(kb)]}{\sin[\Psi(ka) - \Psi(kb)]}. \tag{10}$$

The wave impedance given above can be conveniently converted to "total" impedance expressions. Voltage is taken as positive when the top plate (plate in positive z direction from other plate) is positive with respect to the bottom plate. Radial current flow is considered positive when the current flow is outward on the top plate, and the "total" current is taken as the product of the current density and the circumference of the line. With these conventions, "total" impedance is obtained by multiplying the wave impedance by the factor $-l/(2\pi r)$.

It is no accident that the Equations (8)-(10) look almost exactly the same as those given by Ramo and Whinnery[3] for in-phase feed,

The difference, of course, is in the definition of the functions given by Equation (5) which is here appropriate to rotating phase feed.

C. Resonances

There are four types of resonances involved in open- and short-circuit-terminated radial transmission lines. The conditions for these resonances can be obtained through Equations (9) and (10).

The condition for parallel resonance of a short-circuit-terminated line is found from Equation (9) by setting

$$\cos [\Psi(ka) - \Theta(ka)] = 0,$$

which is equivalent to*

$$\frac{N_1(kb)}{J_1(kb)} = \frac{N_1'(ka)}{J_1'(ka)}. \tag{11}$$

The condition for series resonance of a short-circuit-terminated line is found from Equation (9) by setting

$$\sin [\Theta(ka) - \Theta(kb)] = 0,$$

which is equivalent to

$$\frac{N_1(kb)}{J_1(kb)} = \frac{N_1(ka)}{J_1(ka)}. \tag{12}$$

The condition for parallel resonance of an open-circuit-terminated line is found from Equation (10) by setting

$$\sin [\Psi(ka) - \Psi(kb)] = 0,$$

which is equivalent to

$$\frac{N_1'(kb)}{J_1'(kb)} = \frac{N_1'(ka)}{J_1'(ka)}. \tag{13}$$

The condition for series resonance of an open-circuit-terminated line is found from Equation (10) to be

$$\cos [\Theta(ka) - \Psi(kb)] = 0,$$

which is equivalent to

---

* See Appendix I.

$$\frac{N_1'(kb)}{J_1'(kb)} = \frac{N_1(ka)}{J_1(ka)}. \tag{14}$$

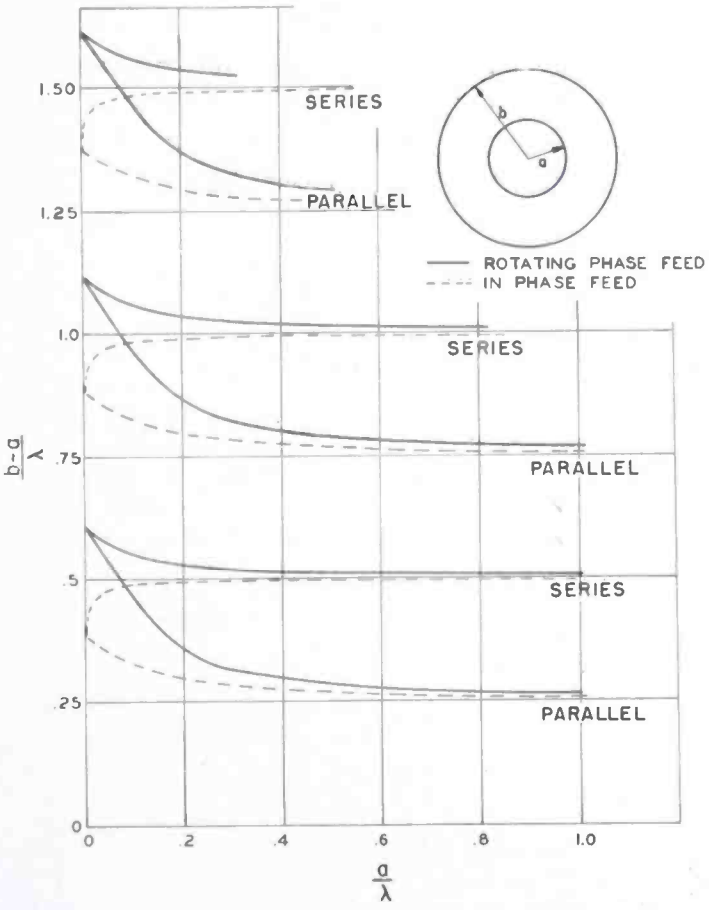

Fig. 2—Series and parallel resonances of short-circuit-terminated radial lines.

Curves illustrating the resonances of radial transmission line stubs fed in rotating phase are given in Figures 2 and 3. The resonances for in-phase feed are also given there for comparison.

The solution of Equations (11)-(14) is expedited by the use of curves given in Jahnke and Emde.[6] An additional curve supplementing those given in Jahnke and Emde is given here in Figure 4. If more accuracy is required than can be obtained from the curves, the points from the curve can be used as a starting point for a numerical solution by means of successive approximations.

It should be noted that the curves referred to in the previous paragraph can also be used conveniently in the design of a radial transmission line for a specified input reactance. This becomes evident when

[6] E. Jahnke and F. Emde, *Tables of Functions with Formulae and Curves*, Dover Publications, New York, N. Y., 1945, pp. 200-203.

the trigonometric functions in Equations (9) and (10) are expanded by the usual addition formulas.

D. Voltage and Current Distributions

The voltage and current distributions on the line can be obtained directly from the field expressions of Equations (2)-(5). Since the electric field has only a z component which is independent of the z coordinate, the voltage between any two opposite points of the line is

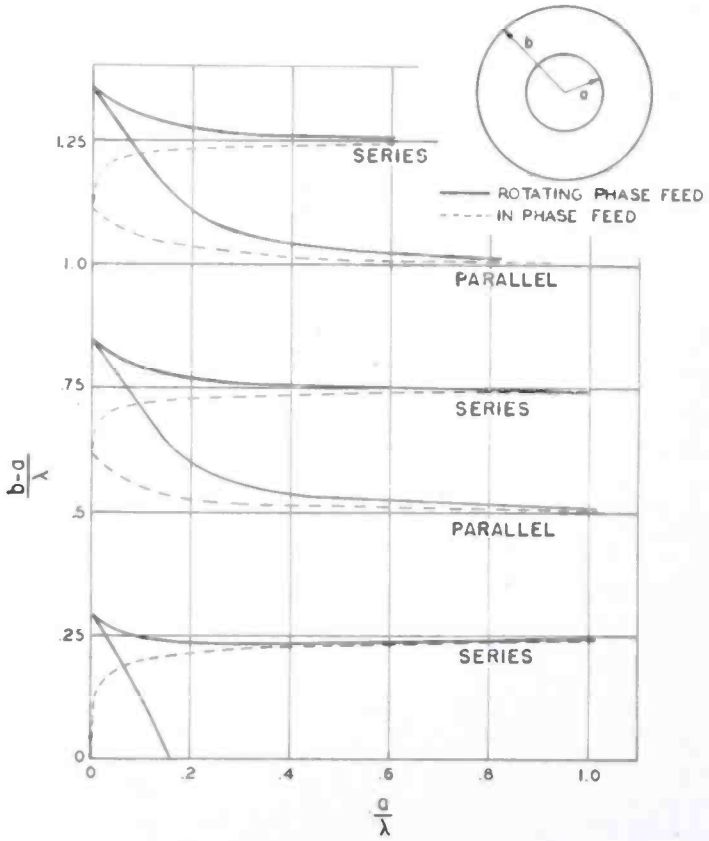

Fig. 3—Series and parallel resonances of open-circuit-terminated radial lines.

given by the product of the magnitude of the electric field times the height of the line. The current density on the parallel conducting plates is directly proportional to the magnitude of the magnetic field at the surface. The surface-current-density vector is given by

$$\overline{K} = \hat{n} \times \overline{H}, \tag{15}$$

where $\hat{n}$ is a unit vector directed from the conducting plates into the radial line.

E. Q of Short-Circuit Terminated Resonant Cavity

For the case of a short-circuit-terminated radial line it is found

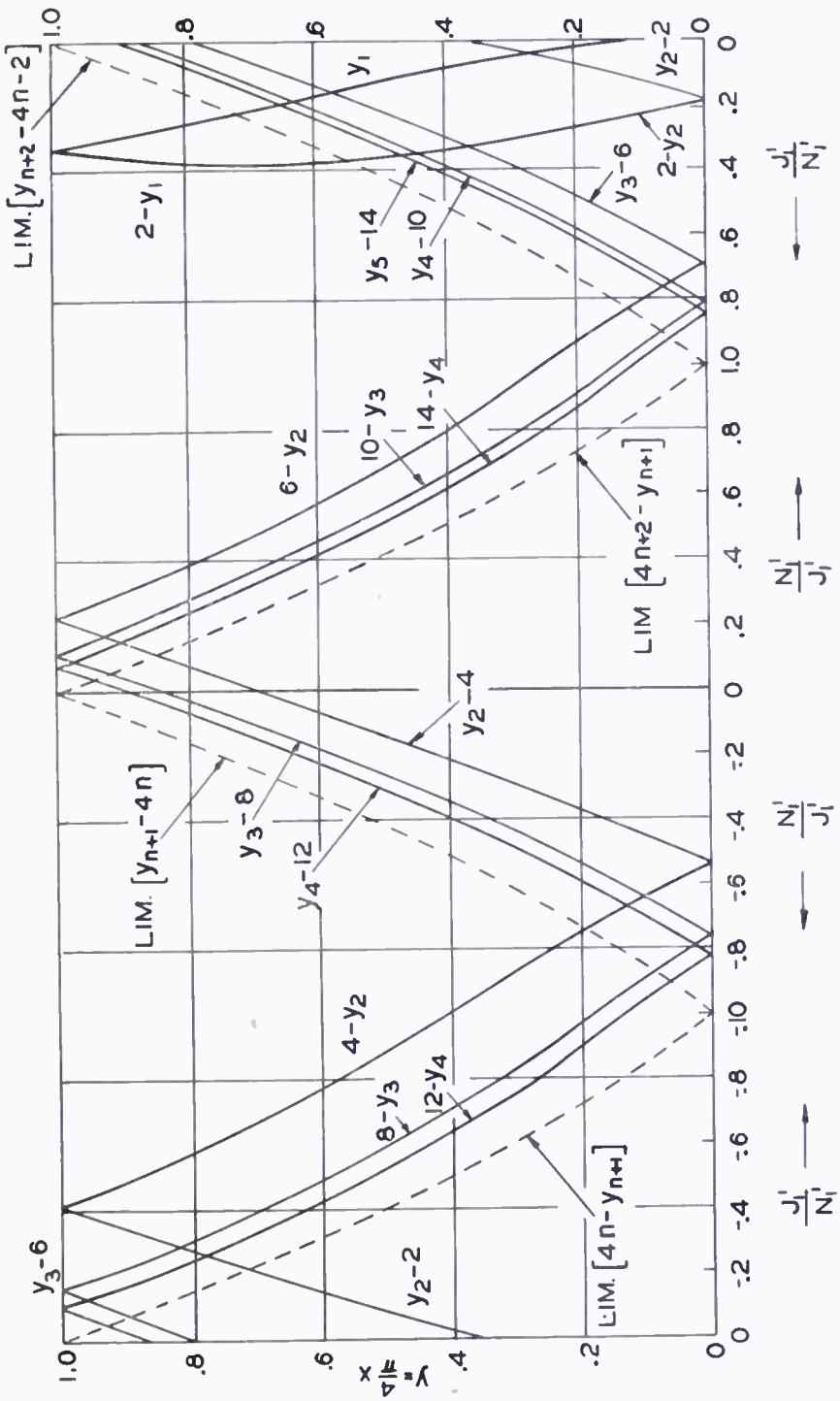

Fig. 4—Inversion of $N_1'\left(\frac{\pi}{4}y\right)/J_1'\left(\frac{\pi}{4}y\right)$.

from the field expressions (2) to (5) that

$$E_z = Be^{-j\phi} G_1(kr) \sin [\Theta(kr) - \Theta(kb)],$$

$$H_\phi = -j \frac{B}{n_0} e^{-j\phi} G_2(kr) \cos [\Psi(kr) - \Theta(kb)],$$

and

$$H_r = \frac{B}{n_0} e^{-j\phi} \frac{G_1(kr)}{kr} \sin [\Theta(kr) - \Theta(kb)]. \tag{16}$$

It is interesting to note that the radial component of magnetic field (and, hence, the circumferential component of surface current) varies inversely as the radius. Therefore, this component becomes increasingly negligible with respect to the other field components as the radius increases.

The definition of Q will be taken to be 2π times the ratio of the total stored energy to the energy dissipated per cycle. While the field expressions have been derived on the assumption that the walls of the line are perfectly conducting, the losses for high-conductivity walls can be approximated in the usual manner by integrating the power loss in the walls using the surface currents obtained from the perfect conductor assumption. The total power loss is

$$P_t = P_w + P_s + P_d, \tag{17}$$

where P_w is the copper loss in the walls of the radial line, P_s is the copper loss in the short-circuit termination, and P_d is the dielectric loss in the dielectric filling the radial line. For present purposes it will be assumed that P_s and P_d are negligible with respect to P_w. Now the power loss in the side walls is given by

$$P_w = 2\rho \iint \frac{1}{2} \bar{K} \cdot \bar{K}^* da,$$

$$= \rho \iint \bar{H} \cdot \bar{H}^* da, \tag{18}$$

where ρ is the surface resistivity of the material, and the integral is taken over one of the parallel plates of the radial line.

The average energy stored in the magnetic field is given by

$$T_{av} = \frac{\mu}{4} \iiint \bar{H} \cdot \bar{H}^* dv,$$

$$= \frac{\mu l}{4} \iint \bar{H} \cdot \bar{H}^* da. \tag{19}$$

where in the second equation the integration with respect to z has already been carried out so that the integral appearing there is the same as that in Equation (18) and l is the height of the radial transmission line.

At resonance the average energy stored in the electric field is equal to that stored in the magnetic field. Therefore, Q can be expressed as

$$Q = 2\pi \frac{2T_{av}}{P_w T}, \tag{20}$$

where T is the period. Upon simplification Equation (20) reduces to

$$Q = \frac{120\pi^2}{\rho} \left(\frac{l}{\lambda} \right), \tag{21}$$

which is the desired result.

It is interesting to note that as in the case of resonant uniform transmission line cavities, the Q is independent of the particular mode of resonance being used. It would appear that the Q could be increased indefinitely simply by increasing l. There are two factors that operate to limit the Q available in this manner. Firstly, the contribution of the short-circuit termination to the total losses has been neglected in the above determination of Q. These losses would increase as l was increased. Secondly, if operation is to be restricted to the transmission-line mode, l cannot be made larger than one-half wavelength. It can be shown that for reasonably large radii, the power lost in the short-circuit termination is given approximately by*

$$P_s = \frac{lP_w}{b-a}. \tag{22}$$

When the equation for Q is modified accordingly, it becomes

$$Q = \frac{120\pi^2}{\rho} \left(\frac{l}{\lambda} \right) \left[1 + \frac{l}{b-a} \right]^{-1}. \tag{23}$$

* See Appendix II.

It is interesting to compare the Q of a radial line cavity with that of other configurations. For a long radial line cavity constructed of copper for which l is one-quarter wavelength and which is operated at 820 megacycles,

$$Q = 39{,}600.$$

For a coaxial line cavity of maximum Q whose outer diameter is six inches,

$$Q = 18{,}400,$$

when operated under the same conditions. For a spherical cavity resonant in its dominant mode under conditions similar to those stated above

$$Q = 50{,}400.$$

The above figures are theoretical Q's, and it would be expected that actual practical Q's would be somewhat smaller in each case. Nevertheless, a useful comparison is obtained through these theoretical Q's.

III. Circular Polarization in Circular Waveguide

A. *Field Expressions*

Although the field expressions for dominant mode propagation in circular waveguide are given in many places, they will be repeated here for completeness. The fields for a TE_{11} circularly polarized wave in circular waveguide can be obtained from the scalar potential.

$$\psi = Ae^{-j\phi} J_1(\beta r)\, e^{-jhz} + Be^{-j\phi} J_1(\beta r)\, e^{+jhz}, \tag{24}$$

where

$$\beta^2 = k^2 - h^2, \tag{25}$$

and where β is determined from the first positive root of

$$J_1'(\beta a) = 0. \tag{26}$$

The first term in Equation (24) represents an incident wave, and the second term represents a reflected wave. k is the usual free space propagation constant, and a is the radius of the guide. The corresponding field components are

$$H_z = \beta^2 \psi,$$

$$H_\phi = \mp \frac{h\psi}{r},$$

$$H_r = \mp jh \frac{J_1'(\beta r)}{J_1(\beta r)} \psi,$$

$$E_z = 0,$$

$$E_\phi = j\mu\omega\beta \frac{J_1'(\beta r)}{J_1(\beta r)} \psi,$$

and

$$E_r = -\mu\omega \frac{\psi}{r}. \tag{27}$$

Where two signs are given in Equations (27) the top sign is applicable to the first term of ψ while the bottom sign is applicable to the second term.

B. Symmetrical Series Loading at Outer Guide Wall

In some applications it is desirable to load a circular waveguide transmitting circularly polarized power with a series load at the guide wall as shown in Figure 5. It will be assumed that the distance l

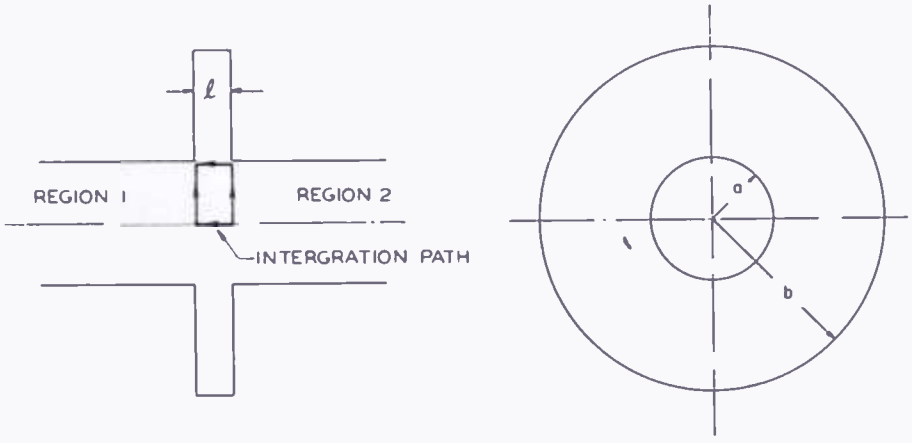

Fig. 5—Circular waveguide with series loading.

is much smaller than the guide wavelength. The object of the development to be given here is to find the reflection coefficient on the guide due to this series load. In other words, it is desired to find a characteristic impedance for the guide to which the series loading impedance can be normalized.

The circumferential component of magnetic field, H_ϕ, must be continuous across the discontinuity at the series load. That is to say, all of the axial current which flows into the series load must flow out the outer side. The corresponding value of E_z in the gap is

$$E_z = Z(ka)\ H_\phi, \tag{28}$$

where $Z(ka)$ represents the wave impedance in the gap. Outside the gap

$$E_z = 0, \tag{29}$$

on the guide walls.

Now the field quantities satisfy the following integral relation:

$$\oint_C \bar{E} \cdot d\bar{s} = -\frac{\partial}{\partial t} \int_S \bar{B} \cdot \hat{n} da,$$

$$= -j\mu\omega \int_S \bar{H} \cdot \hat{n} da, \tag{30}$$

for fields periodic in time. The curve C is any closed curve in a region in which the field quantities satisfy Maxwell's equations, and S is any surface which spans the curve C. In particular, if the integration path indicated in Figure 5 is taken as the curve C, and S is taken as the plane rectangular area which spans the curve, we can write

$$\oint_C \bar{E} \cdot d\bar{s} = -j\mu\omega \int_S H_\phi da. \tag{31}$$

Since H_ϕ is continuous across the gap, the integration with respect to z can be performed to obtain

$$\oint_C \bar{E} \cdot d\bar{s} = -j\mu\omega l \int_0^a H_\phi dr. \tag{32}$$

Equation (32) together with the continuity of H_ϕ are sufficient to determine the reflection coefficient introduced by the series load.

The guide is assumed to be matched to the right of the discontinuity, i.e., in region 2, and in this region, then,

$$\psi_2 = e^{-j\phi} J_1 (\beta r) e^{-j\beta z}. \tag{33}$$

In region 1 there may be both an incident and reflected wave so that

$$\psi_1 = e^{-j\phi} J_1 (\beta r) [A e^{-j\beta z} + B e^{+j\beta z}]. \tag{34}$$

Referring to the field expressions (27) it is seen that the continuity

of H_ϕ requires that

$$A - B = 1, \tag{35}$$

where z has been taken equal to zero at the discontinuity. Insertion of the field expressions into Equation (32) yields

$$A + B = 1 - jhl - \frac{2\pi h_i J_1(\beta a)}{n_0 \int_0^{\beta a} \frac{J_1(x)}{x}\, dx} \cdot \frac{Z(ka)}{2\pi ka}. \tag{36}$$

It is noted that from symmetry $E_z = 0$ on the portion of the integration path along the axis of the circular waveguide (See Figure 5). The magnitude of the second term on the right of Equation (36) is the electrical length of the gap. It will be assumed that the gap is small enough that this term can be neglected relative to the other terms of Equation (36). This is equivalent to taking the right-hand side of Equation (32) to be zero.

Now Equations (35) and (36) are to be compared to the corresponding equations one would obtain on a uniform transmission line from the transmission line equations. These are

$$A - B = 1,$$

and

$$A + B = 1 + \frac{Z}{Z_0}. \tag{37}$$

It is seen that there is a direct comparison. If the total input impendance of the series load is taken as

$$Z = -Z(ka)\,\frac{l}{2\pi a}, \tag{38}$$

then the characteristic impedance of the guide is identified as

$$Z_0 = n_0 \frac{k \int_0^{\beta a} \frac{J_1(x)}{x}\, dx}{2\pi h J_1(\beta a)},$$

$$= \frac{1}{\sqrt{1-\left(\frac{f_c}{f}\right)^2}} \frac{60}{J_1(\beta a)} \int_0^{\beta a} \frac{J_1(x)}{x}\, dx. \qquad (39)$$

Equations (38) and (39) give the desired results by which the reflection coefficient on the guide due to a symmetrical series load can be obtained.

The series load impedance given by Equation (38) is the same as the one that would be obtained from the quotient of the total voltage across the load and the "total" axial current flowing into the load.

The definite integral involved in Equation (39) can be readily evaluated by substituting for $J_1(x)$ its Maclaurin series expansion and integrating term by term. It is found that

$$Z_0 = \frac{82.601}{\sqrt{1-\left(\frac{f_c}{f}\right)^2}} \text{ ohms.} \qquad (40)$$

As was to be expected, the functional dependence on frequency of the characteristic impedance defined here is the same as that for other definitions of characteristic impedance.*

It may be noted that in obtaining the result of Equation (40) the field expressions used for the circular waveguide and radial transmission line were those for the dominant modes only. This is valid in obtaining a characteristic impedance for the waveguide, but it should be appreciated that a number of higher order modes will be excited at the junction between the waveguide and the transmission line. This will result in a slight deviation from the performance predicted by the present theory. The derived characteristic impedance will, however, not be altered by the presence of higher order modes.

C. *Wall Current in Guide for Given Amount of Power Transfer*

In the utilization of series loading of the type described in the preceding section, one is directly concerned with the axial current flowing in the guide wall. It is proposed here to determine a characteristic impedance of the guide (different from that obtained in the previous section) which can be used to determine the "total" axial current flowing in the wall of a matched circular guide when the power being transferred is known. The term "total" axial current is defined

* pp. 6-8, Reference (2).

as the product of the axial current density and the circumference of the guide.

The power being transferred in the guide is found from the usual expression

$$P_z = \frac{1}{2} \int_S (\overline{E} \times \overline{H}^*)_z \, da, \tag{41}$$

where the integral is to be taken over a cross section of the guide. Since the guide is matched, the scaler potential is given by

$$\psi = Ae^{-j\phi} J_1 (\beta r) \, e^{-jhz}. \tag{42}$$

When the corresponding field expressions are introduced into Equation (41) it is found that

$$P_z = \pi n_0 \, kh \int_0^{\beta a} [J_1'^2 (x) + J_1^2 (x)/x^2] \, x dx \, AA^*, \tag{43}$$

where the integration with respect to ϕ has already been carried out. The definite integral in Equation (43) can be readily evaluated by inserting the series expansions in place of the Bessel functions involved in the integrand and integrating term by term. When this is done it is found that

$$P_z = \pi n_0 kh \ (.40455) \ AA^*. \tag{44}$$

The axial current density is equal in magnitude to the magnitude of the circumferential magnetic field evaluated at $r = a$. If the "total" current is taken as the circumference of the guide times the current density, it is found from the field expressions (27) that

$$II^* = 2\pi^2 h^2 \, AA^* \, J_1^2 (\beta a), \tag{45}$$

where the current, I, is expressed as a root-mean-square current.

When AA^* is eliminated between Equations (44) and (45) it is found that

$$P_z = II^* \, Z_0,$$

where

$$Z_0 = \frac{71.695}{\sqrt{1 - \left(\frac{f_c}{f}\right)^2}} \text{ ohms.} \tag{46}$$

This is the desired result which relates axial current flow to the power being transferred. It is noted that this characteristic impedance has the same frequency dependance as the characteristic impedance which was derived for series loading purposes.

IV. Conclusions

Design equations and curves have been given for radial transmission lines excited in rotating phase. Special emphasis has been given to short-circuit-terminated radial line cavities. An expression for the Q of such cavities is given together with a comparison to other types of cavities.

Two definitions of the characterisic impedance of a circular waveguide transmitting circularly polarized energy have been given. These are useful in relating series loading to the reflection coefficient on the guide, and in determining the current flowing in the guide walls.

Although it has not been the purpose of this paper to present experimental data, it should be mentioned that the main theoretical results have been verified experimentally. A subsequent paper is planned which will describe in detail the experimental data in connection with specific equipments.

Appendix I—Derivations of Formulas Involving Impedance of Radial Line Cavities

Equations (11) to (14) can be readily derived through the application of trigonometric identities. Equation (11) will be derived to illustrate the procedure.

The condition

$$\cos\left[\Psi\,(ka) - \Theta\,(kb)\right] = 0, \tag{47}$$

is replaced by the equivalent condition

$$\Psi(ka) - \Theta(kb) = (2n+1)\left(\frac{\pi}{2}\right) \tag{48}$$

From this it follows that

$$\cot\left[\Psi(ka) - \Theta(kb)\right] = \frac{1 + \tan\Psi(ka)\tan\Theta(kb)}{\tan\Psi(ka) - \tan\Theta(kb)} = 0. \tag{49}$$

Utilizing the definitions given in Equations (5) it follows that

$$1 - \frac{N_1(kb)\, J_1'(ka)}{J_1(kb)\, N_1'(ka)} = 0, \tag{50}$$

which is equivalent to

$$\frac{N_1(kb)}{J_1(kb)} = \frac{N_1'(ka)}{J_1'(ka)}, \tag{51}$$

which is the desired result.

It was mentioned at the end of Section II.B that a radial line could be conveniently designed to a specified input reactance. An example will be carried through here to illustrate the process. Suppose that the inner radius, a, and input reactance, X, of a short-circuit-terminated radial line cavity are specified. Then from Equation (9) it is found that

$$X = Z_0(ka)\, \frac{\sin\left[\Theta(ka) - \Theta(kb)\right]}{\cos\left[\Psi(ka) - \Theta(kb)\right]}. \tag{52}$$

It is desired to solve this equation for b. By employing the usual trigonometric addition formulas, it can be shown that

$$\tan \Theta(kb) = \frac{\sin \Theta(ka) - \dfrac{X}{Z_0(ka)} \cos \Psi(ka)}{\cos\left[\Psi(ka) - \Theta(kb)\right] \dfrac{X}{Z_0(ka)}}. \tag{53}$$

The right-hand side of this equation is expressed entirely in terms of known quantities so that the unknown quantities have been separated from the known. By definition, the left-hand side is equal to $\dfrac{N_1(kb)}{J_1(kb)}$ so that the curves given by Jahnke and Emde[6] can be used conveniently to obtain a solution.

Appendix II. — Derivation of Equation for Termination Losses in Radial Line Cavities

Equation (22) gives a relation between the losses in the short-circuit termination of a radial line cavity and the losses in the walls. This is an approximate formula based on the validity of asymptotic expansions for the Bessel functions appearing in the integrand of

Equation (18). The asymptotic expansions are actually quite good for reasonably large radii.

When Equation (18) is written out in full using the field expressions of Equation (16), it is found that

$$P_w = \frac{\rho BB^*}{{n_0}^2} \int_0^{2\pi} \int_a^b \left[G_2^2(kr) \cos^2 [\Psi(kr) - \Theta(kb] \right.$$

$$\left. + \frac{1}{(kr)^2} G_1^2(kr) \sin^2 [\Theta(kr) - \Theta(kb)] \right] r dr d\phi. \tag{54}$$

If the asymptotic forms of Equation (6) are introduced into this last equation, and all terms of higher order than $1/kr$ are discarded, Equation (54) becomes

$$P_w = \frac{4\rho BB^*}{k^2 {n_0}^2} \int_{ka}^{kb} \cos^2 (x - x_b)\, dx,$$

$$= \left[\frac{2\rho BB^*}{k^2 {n_0}^2} \right] k(b-a) \left[1 + \frac{\sin 2\theta}{2\theta} \right], \tag{55}$$

where $x = kr$, $x_b = kb$, and $\theta = k(b-a)$. For a resonant cavity this reduces to

$$P_w = \left[\frac{2\rho BB^*}{k^2 {n_0}^2} \right] k(b-a). \tag{56}$$

To determine the power lost in the short circuit termination the integration of Equation (18) is carried out over the short circuit termination rather than the side walls. Thus,

$$P_s = \frac{1}{2} \rho \iint \overline{H} \cdot \overline{H}^* da,$$

$$= \frac{\rho BB^*}{2{n_0}^2} G_2^2(kb) \int_0^{2\pi} \int_0^l b\, dz d\phi, \tag{57}$$

which becomes

$$P_s = \left[\frac{2\rho BB^*}{{n_o}^2}\right]\left[\frac{l}{k}\right], \tag{58}$$

when the integration is carried out and the asymptotic form of Equation 6 is inserted for $G_2(kb)$.

Combining equations (56) and (58), it is found that

$$\frac{P_s}{P_w} = \frac{l}{b-a}, \tag{59}$$

which is the desired result.

TELEVISION TRANSMITTER CONSIDERATIONS IN COLOR BROADCASTING*

By

T. M. Gluyas, Jr.

RCA Engineering Products Division,
Camden, N. J.

Summary—The performance requirements for a compatible-color-television transmitter are somewhat more stringent than those for a monochrome transmitter. This paper gives a quantitative evaluation of some of these requirements. Amplitude-versus-frequency response, linearity, and differential phase response affect large-area color fidelity. Amplitude-versus-frequency response and envelope delay determine transient response, or the quality of color edges. Adequate frequency response is comparatively easy to obtain. Good linearity (differential gain constant within 20%) and prescribed envelope delay within ±.05 microsecond are obtained by predistortion in auxiliary apparatus. Care in circuit design and adjustment is required to obtain a low value of differential phase response because large signal conditions and nonlinear impedances result in variable phase in video circuits and variable envelope phase in single-sideband radio-frequency circuits.

A vestigial-sideband demodulator is desirable for color monitoring in order to observe transmitter chroma performance. Stringent demodulator performance specifications are imposed since the demodulator is an important tool for adjustment of the transmitter envelope delay.

Introduction

In a compatible-color-television broadcasting system, the transmitter must be able to transmit monochrome and color signals. Because of the similarity of the signals in the compatible system, a transmitter that performs well for monochrome will often be satisfactory for color broadcasting with only minor adjustments or modifications. However, special consideration must be given to certain requirements if color signals are to be transmitted without degradation.

There are also some system limitations that should be recognized. These have to do principally with the stringent bandwidth limitations necessary to prevent adjacent-channel interference. A discussion of these problems is given, and various solutions are suggested.

Interpretation of FCC Signal Specifications

It is of interest to consider those aspects of the FCC signal specifications which place limits on the signal quality and, therefore, affect transmitter design, adjustment, and operation.

* Decimal Classification: R583.4.

It is specified that a sine wave of 3.58 megacycles introduced at those terminals of the transmitter which are normally fed the composite color picture signal shall produce a response (as measured with a diode on the r-f transmission line supplying power to the antenna) which is down 6 ± 2 decibels with respect to the 200-kilocycle response, and in addition the response from 2.1 to 4.2 megacycles shall be flat within ±2 decibels. This says, in effect, that the chrominance signal should be about equal to the luminance signal and that the chrominance signal should have reasonably constant amplitude-versus-frequency response.

There is another rule which states that the angles of the subcarrier signals with respect to the burst phase when reproducing saturated primaries and their complements at 75 per cent of full amplitude shall be within ±10° of the correct value. The amplitude of the subcarrier shall be within ±20 per cent of the correct value and the ratio of the subcarrier to the d-c value (ratio of chrominance to luminance — or saturation) shall be within ±20 per cent of the correct value. This rule specifies the quality of the radiated signal, and only a portion of this tolerance can be assigned to the transmitter.

There are some other rules dealing with delay specifications, operating levels, etc., that can be described better with reference to the discussion and figures in later paragraphs.

Amplitude-versus-Frequency Response

Transmitter performance problems can be divided fairly well into those that affect the *color fidelity of large areas* and those that affect the *transient response or color edges*. However, some transmitter characteristics relate to both of these considerations. Frequency reponse is such a characteristic. The ratio of luminance to chrominance and, hence, the color saturation, is determined by the frequency response, and the frequency response in combination with the envelope delay determines the transient response and, therefore, the quality of color edges. Adequate frequency response is probably the most important single requirement for color since without the subcarrier response there will be no color. Fortunately it is one of the easier requirements to satisfy.

Figure 1A shows the idealized transmitter response (T), receiver response (R), and the channel space allocated to the I and Q color signals. The system amplitude response is the product $T \times R$. When the signal is demodulated in a television receiver, the resulting video frequency response is as shown in Figure 1C, curve Y. If the resulting video is again demodulated, this time in appropriate synchronous subcarrier detectors, a Q signal and an I signal will be recovered. The

I-channel amplitude-versus-frequency response is somewhat deficient in high-frequency response compared to the original video signal, *I'*, because the upper sideband of the subcarrier modulation is suppressed for modulating frequencies greater than 0.6 megacycle (3.58 + .6 = 4.18 megacycles above visual carrier). This is due to the bandwidth limitations imposed upon the receiver to prevent interference from the aural carrier and adjacent-channel signals and upon the transmitter to prevent adjacent-channel interference. A monitor switched from video line to demodulated signal should show a slight reduction in color resolution on the demodulated signal. The difference is of more academic than practical interest.

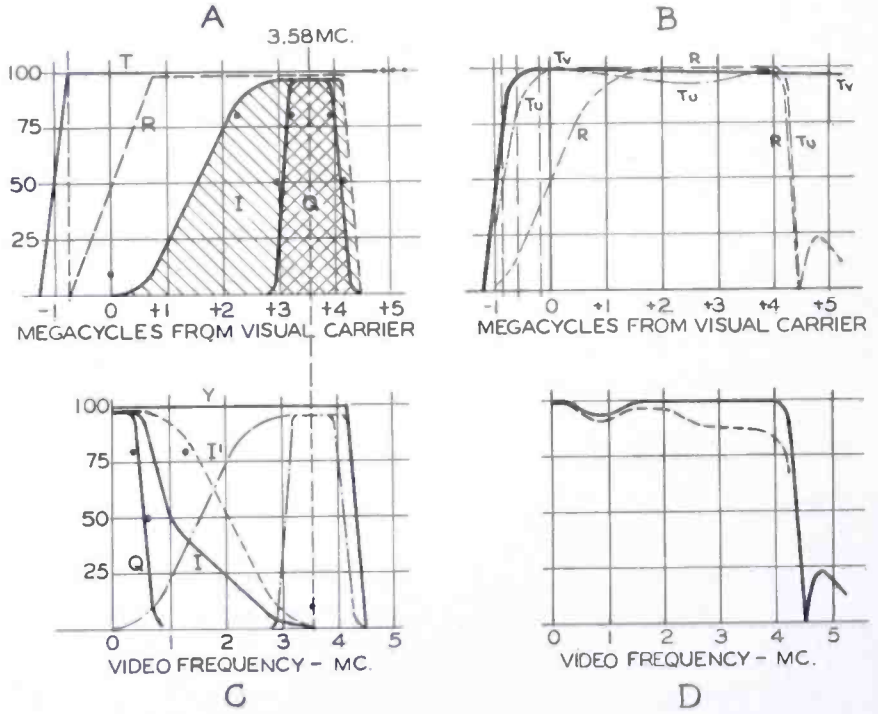

Fig.1—(A) Idealized amplitude-versus-frequency response of transmitter and receiver. (B) Typical amplitude-versus-frequency response of transmitter and receiver. (C) Idealized amplitude-versus-frequency response of demodulated signal. (D) Typical amplitude-versus-frequency response of demodulated signal.

Figure 1B shows the practical amplitude response obtainable with current transmitters and receivers, and Figure 1D shows the resulting video-frequency response at the output of the receiver second detector. The r-f phase-versus-frequency characteristic, which will be described later, was taken into account in obtaining the resulting video signal. Curves Tv and Tu are actually vestigial sideband filter response curves, but the over-all transmitter response will be little different except perhaps for slightly lower response in the 3-4.5 megacycle range. As

shown in Figure 1B, some visual transmitters cut off sharply at 4.5 megacycles above carrier to permit diplexing the sound, and some do not. In the latter case the response would still have to be limited to 4.75 megacycles so as to avoid adjacent-channel interference.

The 1-megacycle hole in the response of Figure 1D is produced by the failure of the upper and lower sideband responses of the receiver to complement each other properly. In some receivers this deficiency is improved by video frequency response manipulation. On the other hand, the hole may be deepened, as shown by the dotted line, by poor transmitter response in the lower sideband. The dotted line represents the approximate amount of degradation in the over-all frequency response that might be introduced by an acceptable transmitter.

Linearity

Transmitter *linearity* is one of the characteristics that affects *large-area color* and has little or nothing to do with transient response. It affects color saturation and color brightness. Nonlinearity is an inherent property of grid-bias modulation which is the modulation process employed in all modern television transmitters. It should be remarked parenthetically that plate modulation is no easy cure for this difficulty since it introduces other equally serious difficulties.

Because the usual modulation process is not linear, one must employ either special modulation techniques or apply negative feedback or predistortion. If predistortion is used, the d-c component must be inserted in the linearity-correcting circuits.

The modulation characteristic displayed in Figure 2 is perhaps a little more curved than that of the average transmitter, but is, nevertheless, typical of some transmitters. If the input signal represents definite steps or tones from light to dark with color information on each tone, it is clear that both the chrominance and luminance are altered by the curvature in the modulation characteristic. Although it may not be immediately obvious, the ratio of chrominance to luminance, which is color saturation, is also altered and in a direction to reduce the saturation of bright colors. Bright colors are reduced in both luminance and saturation.

With a test signal of the type shown, the variation in magnitude of the subcarrier pulses is called variation of differential or incremental gain. In this figure, the differential gain at white level is about 50 per cent of the differential gain at black level. With predistortion it is not difficult to adjust the over-all minimum differential gain to within 80 or 90 per cent of the maximum.

Differential Phase

With reference to Figure 2, it is vital that the transmitter retain constant phase of the subcarrier within very close limits at all brightness levels. Since the receiver 3.58-megacycle oscillator is synchronized by the burst at pedestal level, any phase shift at other brightness levels results in a distortion of hue. Generally, but not always, the phase shift or hue shift is greatest for bright colors such as bright yellow or flesh tones.

This transmission characteristic is sometimes called "differential phase," or "phase-versus-amplitude characteristic," or "phase-ampli-

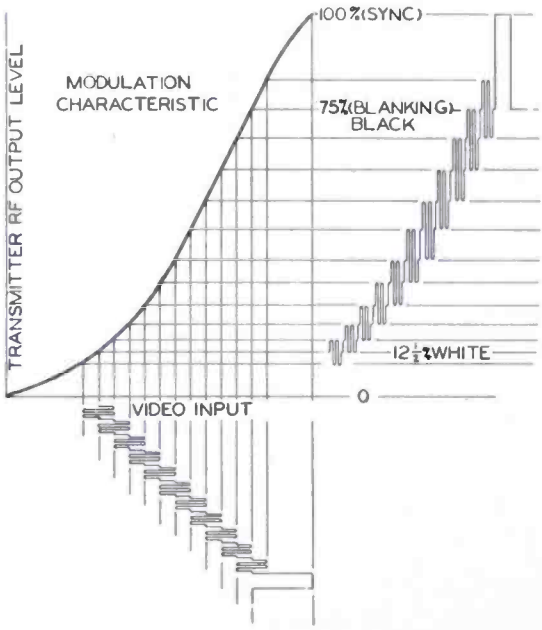

Fig. 2—Effect of nonlinear modulation characteristic on differential gain, and color saturation.

tude," or "phase shift versus brightness," "phase intermodulation," or perhaps other terms. It is a new concept and will no doubt be officially defined in due course.

Extended Amplitude Range

Figure 3 shows several scales that are used to define picture levels in transmitter operation: a modified I.R.E. scale; a scale based on 100 per cent peak transmitter output; and a new scale which is coming into use for color which specifies black as zero and white as 100. The numerals showing luminance levels and peak levels on the color waveforms are based on the latter scale.

One hundred per cent saturated colors can not possibly be trans-

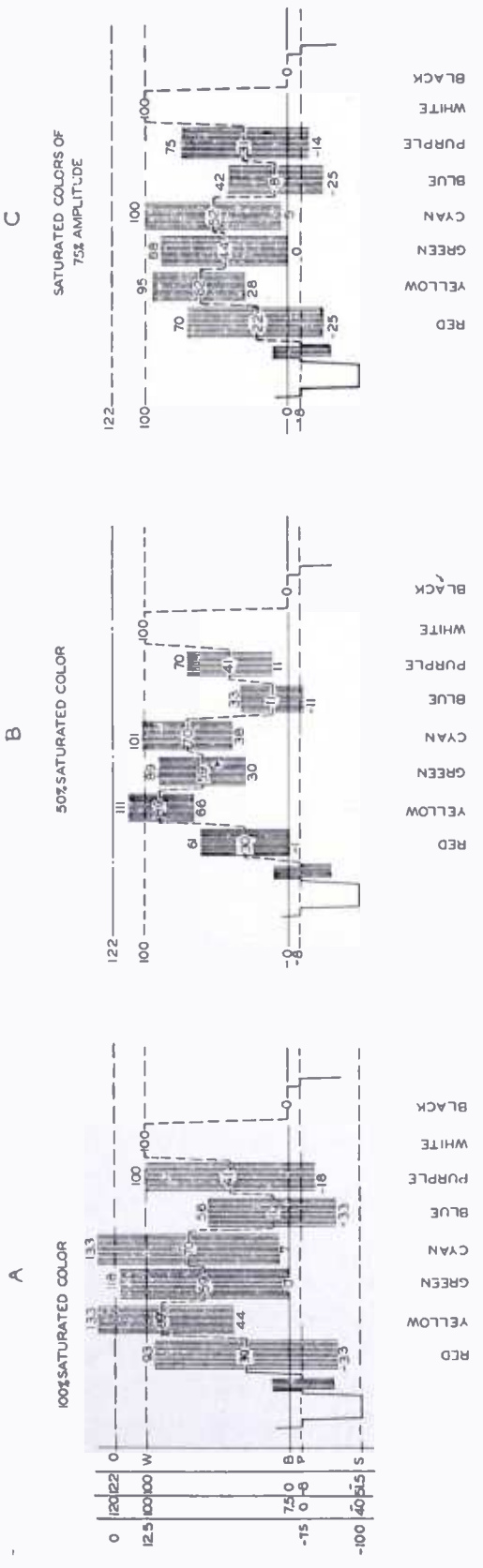

Fig. 3—Video waveforms of color-bar signals.

mitted without distortion because cyan and yellow call for overmodulation of the transmitter. Fortunately, 100 per cent saturated colors rarely appear in nature, and the output of a camera is more like the 50 per cent saturated colors shown in Figure 3B. Even this calls for modulating the transmitter in the "whiter than white" and "blacker than black" regions.

Figure 3C shows the prescribed waveform for saturated colors of 75 per cent amplitude. This does not call for modulating the transmitter beyond reference white nor is the luminance range very great, and it is not a very severe test of the ability of the transmitter to transmit bright desaturated colors without distortion. Differenial phase and differential amplitude tests and tests using standard saturated color bars of 75 per cent amplitude are all important.

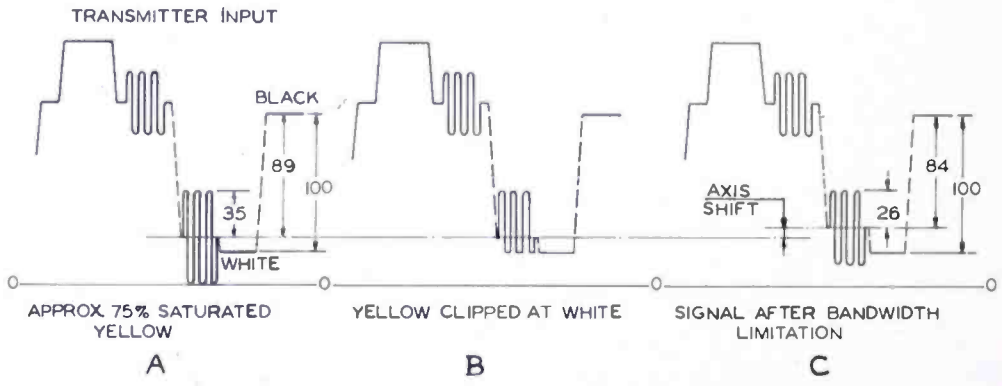

Fig. 4—Waveform illustrating effect of nonlinearity in the ultra-white region

Effect of White Compression

Since it is necessary to transmit waveforms that extend beyond reference white, and since it is not practical to make the transmitter linear to zero output, it is interesting to consider the effect of nonlinearity near zero output. Take the case of a 75 per cent saturated bright yellow that should modulate the transmitter to zero output. An exaggerated case of nonlinearity is a transmitter which clips completely at reference white as shown in Figure 4. Since the harmonics of the subcarrier cannot be transmitted, the system would recover the waveform of Figure 4C. Here both the luminance and chrominance have been reduced, and the resulting color has 95 per cent of its original brightness and 80 per cent of its original saturation. Since this is an exaggerated case, it is evident that transmitter nonlinearity in the "whiter than reference white" range is not excessively harmful.

White Stretching

A nonlinear modulation characteristic is generally corrected by a nonlinear video amplifier having a complementary transfer characteristic. In spite of the fact that intervening circuits between the two nonlinear circuits exclude most of the subcarrier harmonics, the compensation turns out to be fairly good.

Refer to Figure 5. The video signal is applied to a "white stretch" video amplifier (Figure 5A). The harmonics of the distorted output

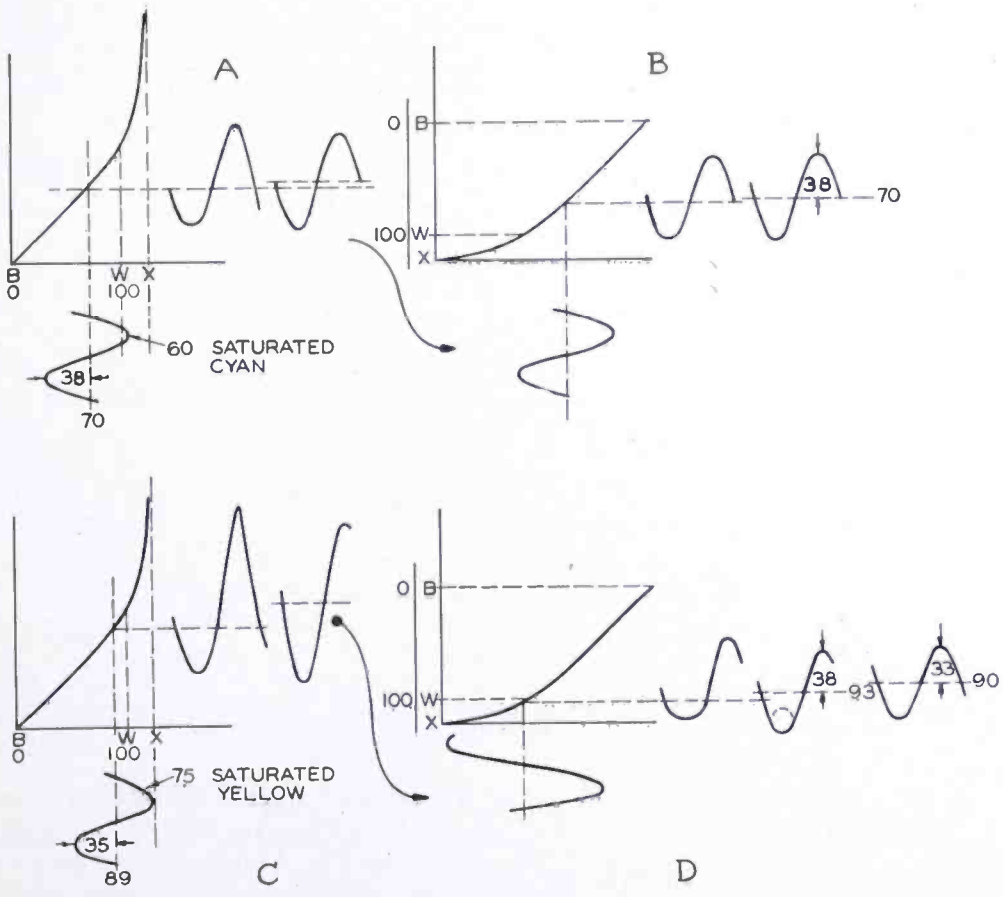

Fig. 5—Waveform illustrating effect of bandwidth limitation in the linearity correcting circuits.

signal are discarded, leaving a sinusoidal signal larger than the original with the axis shifted toward white. This pre-emphasized signal is applied to the modulator (Figure 5B). The resulting waveform shown in this illustration actually represents the envelope of the modulated carrier, but it may also represent the video signal recovered by the receiver. Upon again discarding harmonics, the signal is modified in amplitude and brightness as shown by the upper right-hand waveform. In the case of 60 per cent saturated cyan (Figures 5A and

B), the correction is perfect within the accuracy of graphical analysis. In the case of 75 per cent saturated yellow (Figures 5C, D), the predistortion tends to overmodulate the carrier. This generates harmonics in the receiver second detector, which are subsequently discarded, leaving a fundamental of slightly reduced amplitude. The net result is a slight loss of saturation for bright yellow.

Envelope Delay Requirements

Figure 6 depicts the transmitter envelope delay characteristic and its tolerances as specified by the FCC. This specification implies that the transmitter will correct for its own phase errors and, in addition, will introduce predistortion for the high-frequency envelope delay of the average receiver occasioned by the rapid cutoff at the upper edge of the band from full response at 4.2 megacycles above carrier to a

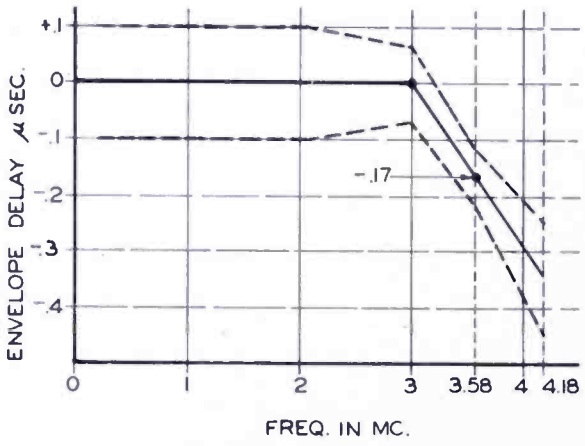

Fig. 6—FCC signal specification of envelope delay (dashed lines represent tolerance limits).

rejection of several thousand times at 4.5 megacycles above carrier. Another implication is that the receiver will either tolerate or correct for its own low-frequency phase errors.

The object of the envelope delay specification is to obtain a time match between the luminance and chrominance information and to obtain the best waveform for sudden transitions in the chrominance and luminance channels. The delay characteristic deals with the fidelity of *color edges* and is not related to the broad-area color fidelity. It is also *completely unrelated to the differential-phase problem.*

In order to obtain the specified envelope delay, delay equalizers or phase equalizers are required. The curves of Figure 7 show how the requirements for the phase equalizer are determined. The product of the receiver and the transmitter amplitude characteristics (Figure 7A) is the system amplitude characteristic (Figure 7C). In the lower

video-frequency range the receiver phase characteristic is ignored and the system phase characteristic (Figure 7C) is taken to be the transmitter phase characteristic (Figure 7B). The phase of the envelope is determined by adding vectorially the carrier and sidebands (example shown in Figure 7D). The video phase (Figure 7E) is the same as the system envelope phase, and the slope of the video phase characteristic is the transmitter delay that must be corrected.

Video predistortion is used to correct for imperfections in the r-f circuits but there is one limitation to this technique. The amount of correction that must be applied depends to a slight degree upon the receiver amplitude characteristic assumed because this determines how

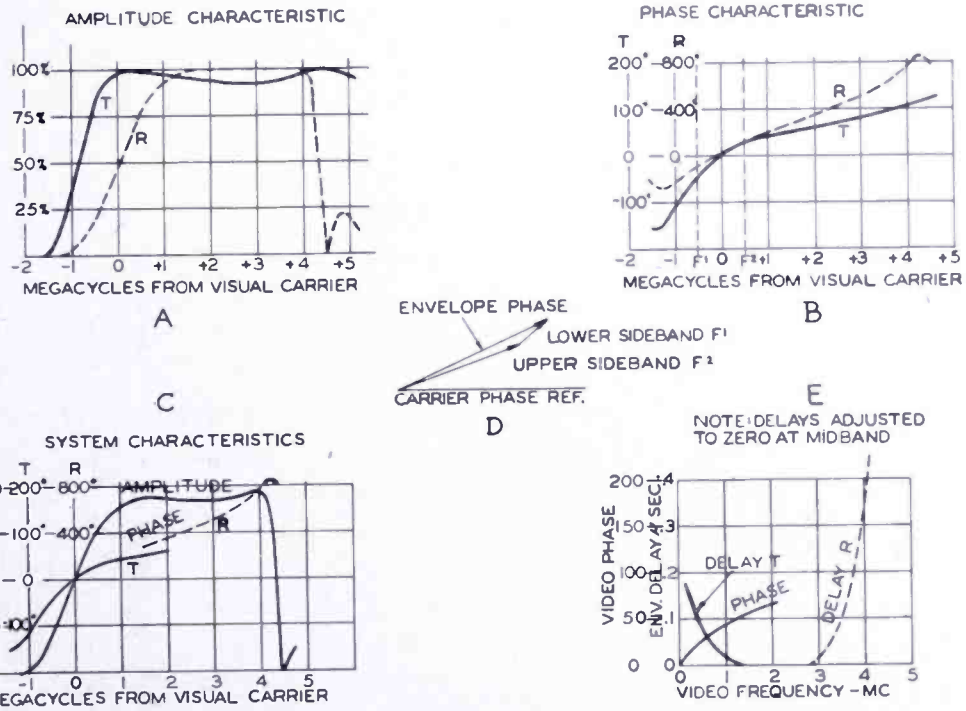

Fig. 7—Curves illustrating development of phase equalizer specifications. (A) Amplitude-versus-frequency response of transmitter and receiver. (B) Phase-versus-frequency response of transmitter and receiver. (C) System characteristics of amplitude-versus-frequency and phase-versus-frequency. (D) Vector diagram illustrating relations between envelope phase and the phases of carrier and sidebands. (E) Derived system phase characteristic and envelope delay.

much of the upper and lower sideband are added together to form the envelope. The correction cannot be perfect for every receiver. However, the over-all results are satisfactory.

Description of Phase Equalizers

Figure 8 illustrates the functional division of the circuits in a

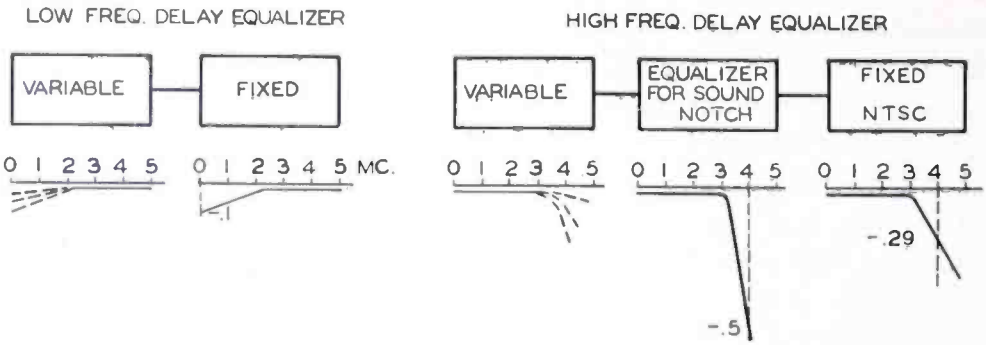

Fig. 8—Functional division of circuits in a commercial phase equalizer.

commercial phase equalizer. The low-frequency circuits are partly fixed and partly variable to accommodate a range of transmitter types and transmitter adjustments.

The high-frequency phase equalizer contains two principal fixed sections. One of these has the delay specified by the FCC and it is switched into the circuit when all other sections of the equalizers have been adjusted to produce an over-all constant time delay. The "sound notch equalizer" is employed only when the transmitter makes use of a notch-type diplexer for combining aural and visual outputs. In practice, a switch provides a choice of two networks for the notch equalizer having slightly different delay characteristics.

Figure 9 is a simplified schematic diagram of the receiver equalizer portion of the high-frequency equalizer. This portion contains about 20 per cent of the circuits of the high-frequency phase equalizer.

Figure 10 shows front and rear views of the high-frequency phase equalizer. It contains one 5-position switch and a number of toggle switches for adding or removing sections of the equalizer to obtain the required delay characteristic. The low-frequency unit, which is

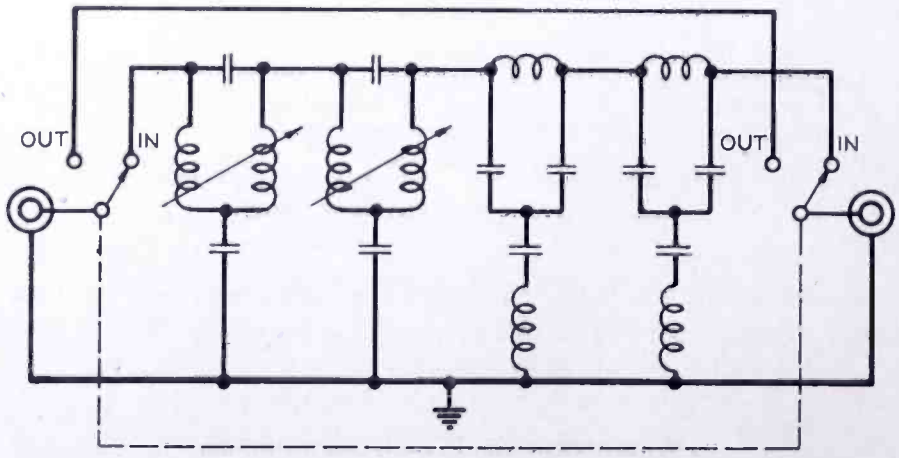

Fig. 9—Simplified schematic of the phase equalizer section which furnishes equalization for standard receiver envelope delay.

considerably smaller, employs one 4-position switch for delay adjustments.

Circuits Contributing to Differential Phase Shift

Most of the discussion thus far has dealt with the relation between color quality and certain transmitter characteristics, notably frequency response, linearity, and envelope delay. None of these are really new problems for the television engineer — they are actually little more than a tightening of the monochrome specifications. The new specifications are not particularly hard to meet.

On the other hand, the differential phase requirement is a new concept, and furthermore it is very difficult to carry out. The difficulty stems from the large-signal conditions that are encountered and the

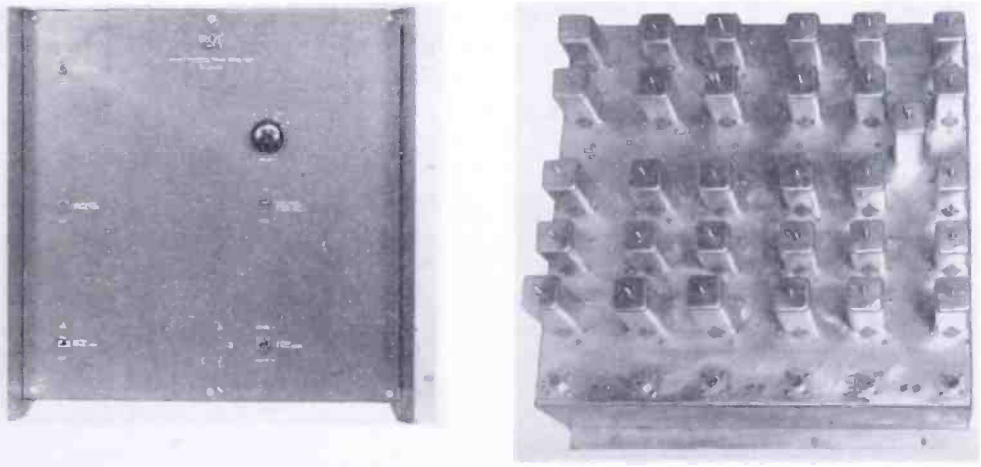

Fig. 10—High-frequency phase equalizer.

nonlinear impedances that result. The problem is encountered in both video and r-f circuits. Two examples of video problems and two r-f problems are chosen to illustrate the point.

Figure 11 represents a typical coupling circuit between a modulator and a modulated amplifier. The modulated amplifier draws some grid current when the video signal corresponds to black, but none when the picture is white. This loads the circuit at black level and alters the phase angle of the transfer impedance. The calculations tabulated in Figure 11 show a five-degree phase difference between black and white. One way to overcome this problem is to employ a very-low-impedance modulator such as a shunt-regulated video amplifier, and omit the coupling network.

Other types of coupling networks will exhibit smaller changes in transfer impedance phase angle than the illustrated circuit. Aside from

the differential-phase problem, the circuit of Figure 11 sometimes causes the modulator or video amplifier to overload at the subcarrier frequency, since the input impedance of the network rises at frequencies close to the cutoff frequency.

Figure 12 illustrates a video feedback amplifier wherein the loop gain changes from 5 near black level to 3.5 near white level. The interstage coupling networks in this example each have about 45° phase shift at the subcarrier frequency. In the diagram of the vector rela-

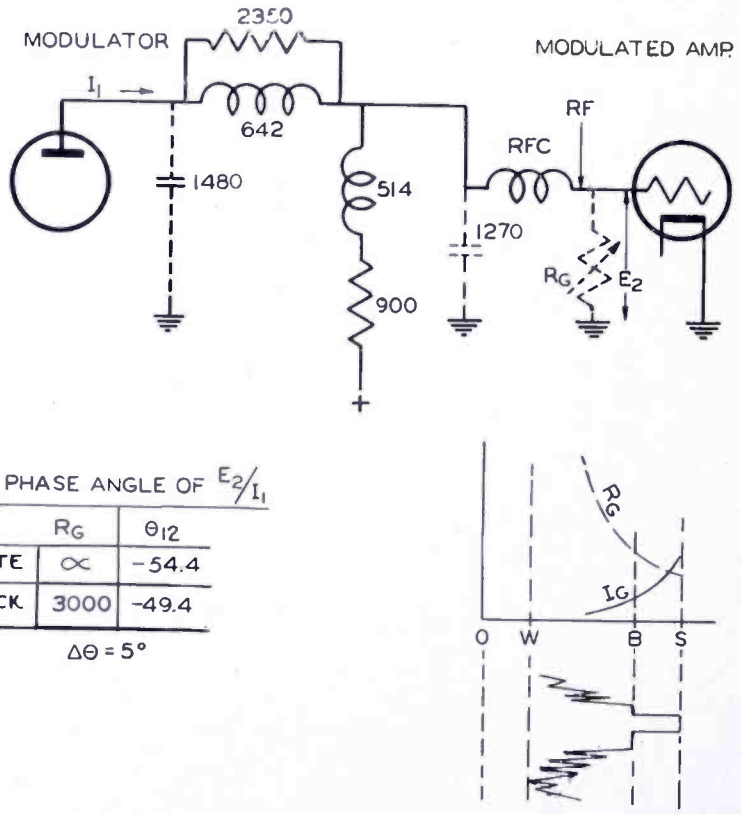

PHASE ANGLE OF E_2/I_1

	R_G	θ_{12}
WHITE	∞	-54.4
BLACK	3000	-49.4

$\Delta\Theta = 5°$

Fig. 11—Circuit and tabulation to illustrate differential phase shift in coupling network between modulator and r-f modulated amplifier.

tions between the various potentials acting in the feedback circuit, θ_{12} represents the phase shift between input and output terminals. When the loop gain changes, the phase shift between input and output becomes θ'_{12}. In this example the differential phase shift at subcarrier frequency is 5 degrees.

The amount of differential phase shift can be reduced by increasing the feedback, making the high-level stages more linear by individual stage feedback or increasing the static current, by reducing the circuit phase shift before feedback is applied, or by a combination of all of these techniques.

Figure 13 illustrates an r-f problem and shows the relation between

incidental phase modulation of the carrier and differential phase shift of the r-f envelope.

There are a number of ways in which a certain amount of incidental phase modulation of the carrier can take place, such as transit-time effects, residual feedback or feed through of r-f energy in an amplifier, or reaction on the r-f driver from a modulated amplifier or linear amplifier. Incidental phase modulation of the carrier results in differential phase shift of the envelope for single sideband operation, but

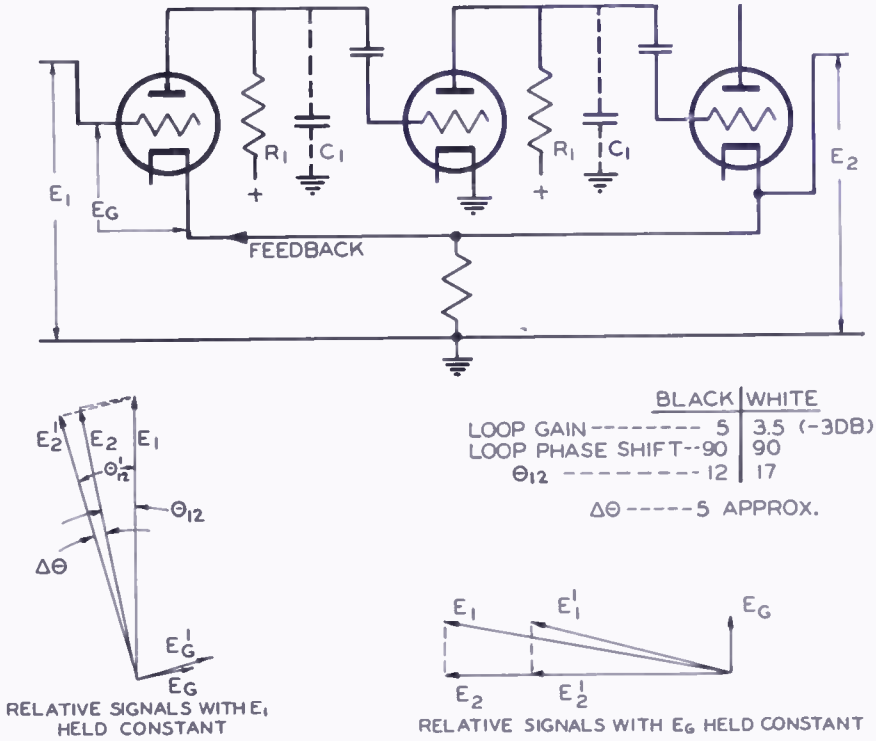

Fig. 12—Circuit, tabulation, and vector diagrams to illustrate differential phase shift in feedback video amplifier.

the relation between cause and effect is not obvious. The problem has been analyzed mathematically.[1]

Figures 13A and B are familiar representations of amplitude modulation and phase modulation except that, for simplicity, only the first-order phase-modulation sidebands are shown. Figure 13D represents simultaneous amplitude and phase modulation (such as incidental phase modulation) and is a combination of diagrams A and B. The envelope reaches a maximum at the instant when the carrier and sidebands add to form the vector *oa*. The envelope minimum is the resultant *oa'*. If only one sideband is present the envelope reaches a maximum when

[1] Unpublished analyses have been made by both G. L. Fredendall, RCA Laboratories, Princeton, and W. N. Parker, RCA Tube Division, Lancaster. The vector diagrams shown in Figure 13 are those of Parker.

the carrier and sideband add to form the vector *ob*. The single sideband case is diagramed in Figure 13C although the same information appears in the more cluttered diagram D.

The angle θ_v formed between loci *aa'* and *bb'* is the difference in phase between the double-sideband and single-sideband envelopes. It could be argued that the double-sideband envelope (ignoring phase

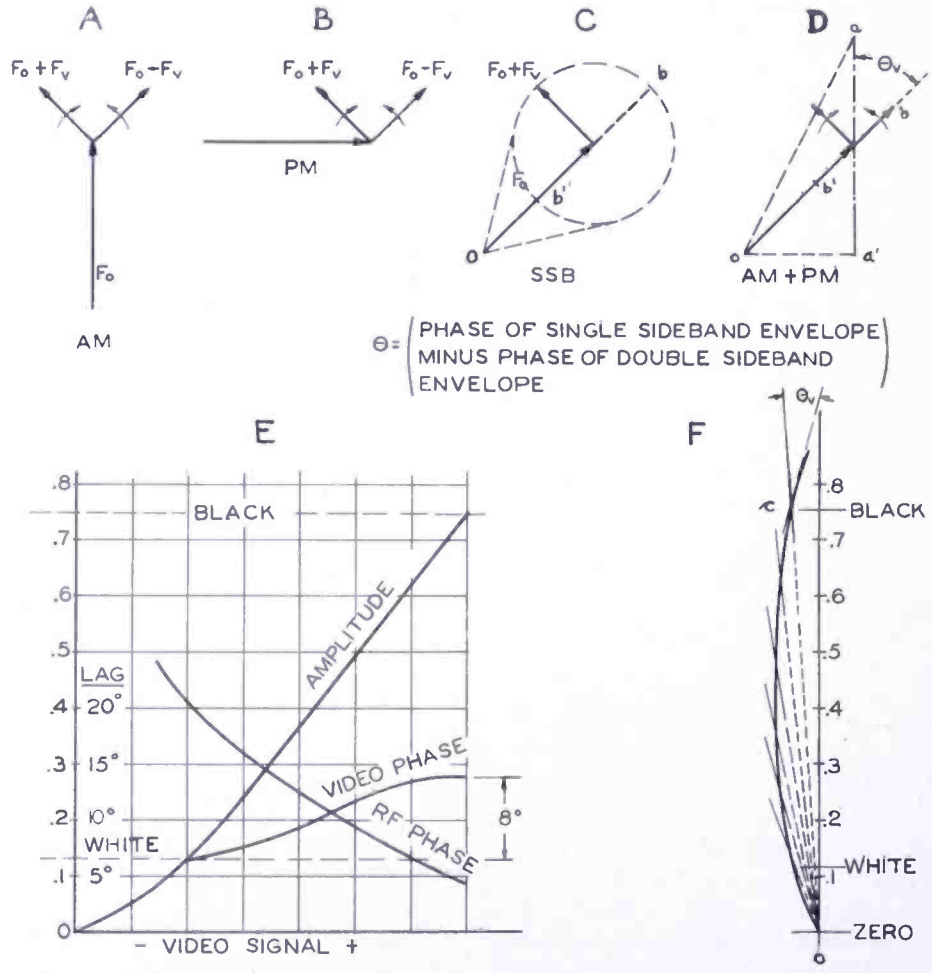

Fig. 13—Diagrams to illustrate relation between incidental phase modulation and vestigial sideband envelope differential phase. (A) Relation between carrier and sidebands for amplitude modulation. (B) Relation between carrier and first-order sidebands for phase modulation. (C) Relation between carrier, sideband, and envelope for single-sideband operation. (D) Relation between carrier, sidebands, and envelope for double-sideband and for single-sideband operation. (E) Amplitude and phase modulation characteristic and the phase of the single-sideband envelope (video phase). (F) Polar diagram of amplitude and phase modulation characteristic.

shift due to the associated circuits) is in phase with the modulating signal so that that θ_v also represents the phase shift between the single-sideband envelope and the modulating signal.

The envelope phase, per se, is of no special significance, but it is de-

sired that the envelope phase be independent of the picture brightness. The remaining two diagrams, Figures 13E and F, show that the envelope phase θ_v is a function of the transmitter phase modulation characteristic and, in the general case, the envelope phase is a function of the picture brightness.

Figure 13E, by way of example, postulates an amplitude and an r-f phase modulation characteristic. The same modulation characteristic is plotted in polar form in Figure 13F. Application of the arguments developed for diagram D indicates that the single-sideband envelope phase (θ_v), for small modulating signals (low amplitude of color subcarrier), is the angle formed between the radial and the tangent at each point on the polar plot of the modulation characteristic. For the example chosen, angle θ_v was obtained graphically at a number of brightness levels. Angle θ_v was then plotted as "video phase" in Figure 13E since this is the phase of the subcarrier that would be recovered from a vestigial sideband demodulator. In this example the differential phase shift from black to white is 8°. To simplify the geometric construction, a larger value of incidental phase modulation was chosen for the example than would normally be encountered.

In the discussion above, the differential phase shift resulted from the modulation process and subsequent elimination of one sideband, and was not a result of circuit phenomena. Coupled circuits loaded by the nonlinear impedance of an amplifier can introduce additional trouble.

Figure 14 shows a coupled circuit loaded by a grounded-grid linear amplifier. The tube chosen for this example has an input impedance of 70 ohms at black level and 100 ohms at white level. If the modulated amplifier has a high plate resistance and does not load the circuit, the amplitude and phase of the transfer impedance is as shown in the lower diagram. The single-sideband envelope is the beat between carrier (F_0) and subcarrier (F_1) and the envelope phase is the difference between the r-f phases of the circuit at these two frequencies. This varies as the level changes from black to white with an accompanying change in circuit loading. In the tabulation shown in Figure 14, the differential phase shift turns out to be 17°.

In practice, a single linear amplifier never produces as much as 17° of differential phase shift. Occasionally it may be as high as 10°, but often it is too small to measure. The actual circuit is a great deal more complicated than the simplified case used in the example. The plate resistance of the modulated amplifier is not negligible, and is a function of signal level. Often the modulated amplifier and linear amplifier are physically separated by a distance of several feet, and

the interconnecting transmission line and its coupling network play the role of middle circuit in a triple-tuned coupled circuit. The circuits may not be synchronously tuned. These complications make an accurate analysis difficult.

The variation in frequency response that results from the changing circuit loading has a direct effect on the picture quality in addition to the associated differential phase shift. The ratio of chrominance to luminance or color saturation is altered as a function of brightness.

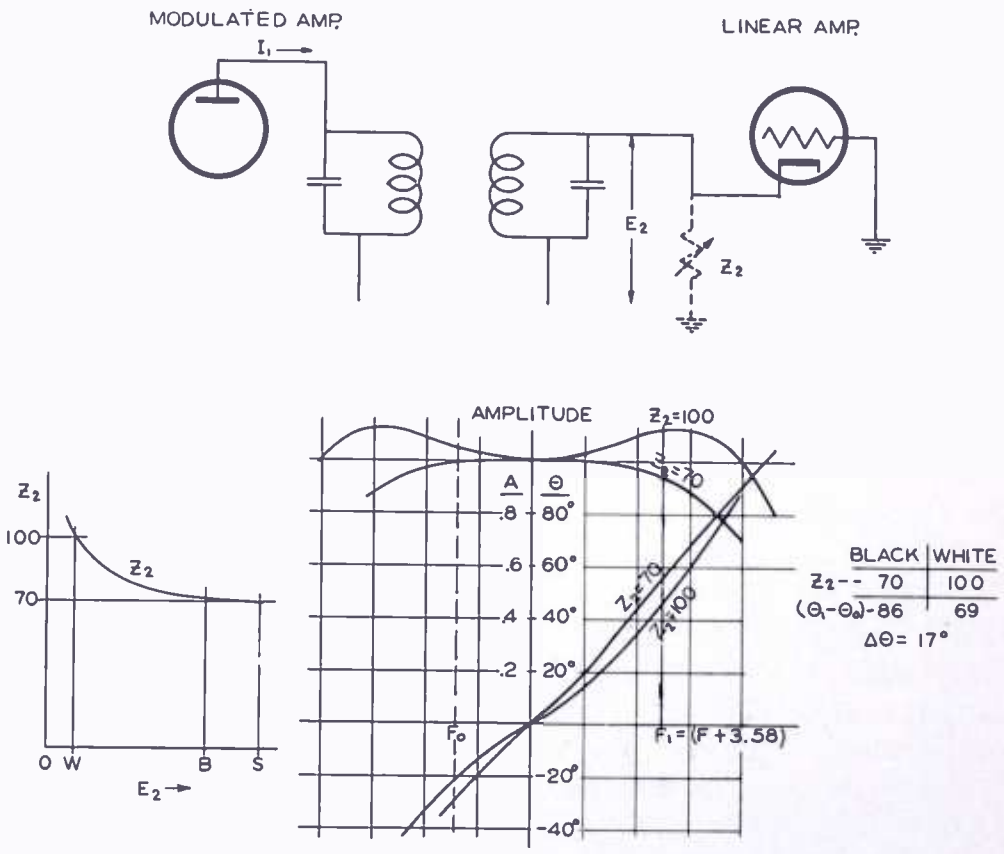

Fig. 14—Circuit diagram, impedance diagrams, and tabulation to illustrate differential phase shift of the single-sideband envelope in coupling networks for linear amplifiers.

This is not corrected by the white-stretch circuit, for although the latter can be set to give constant differential gain for any particular modulating frequency, it will not do so for all frequencies simultaneously. The variation in frequency response shown in Figure 14 (about 2 decibels from black to white) is approximately the maximum that has been observed in practice, and this has not been found to be particularly harmful.

Auxiliary Apparatus for Color Broadcasting

Figure 15 is a block diagram of the auxiliary apparatus and monitoring arrangement for color broadcasting. A bridging amplifier is used for monitoring the input unless the input signal apparatus provides its own monitoring output. Isolation amplifiers are used to obtain good sending-end and receiving-end termination of the phase equalizers. Transmitter linearity correcting circuits (white stretch) are built into the stabilizing amplifier.

The white-stretch circuit in the color stabilizing amplifier consists of several diodes shunted across the unbypassed cathode resistor of a

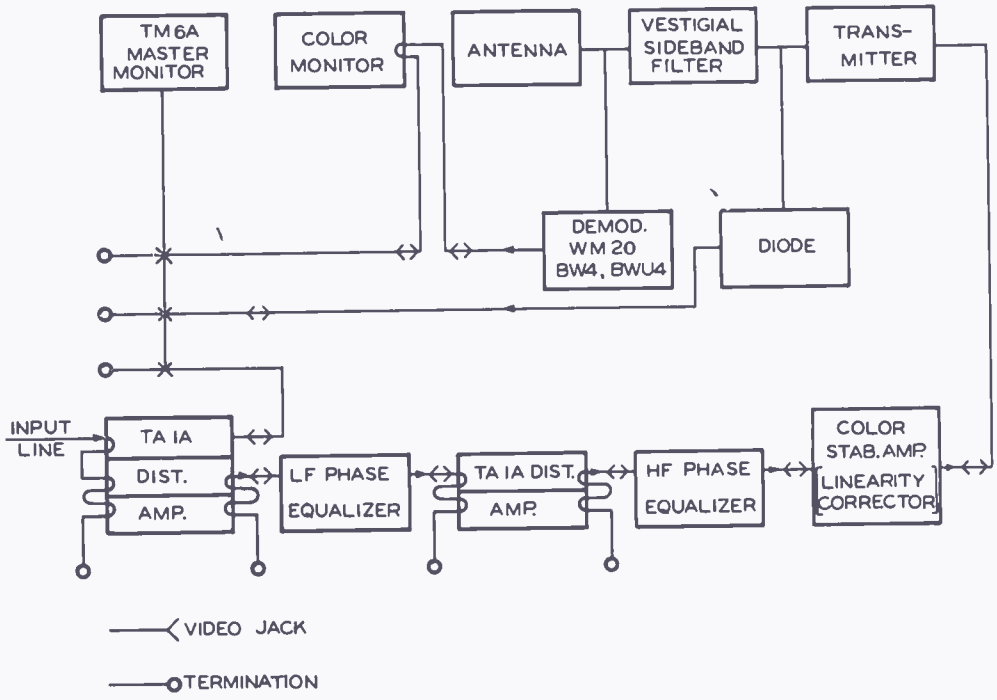

Fig. 15—Block diagram of transmitter, auxiliary apparatus, and monitoring equipment for color-television broadcasing.

video amplifier. A driven clamp circuit restores the d-c component at the grid of the amplifier. In series with each diode is a resistor and some fixed bias. When the diode conducts, it connects its associated resistor across the cathode resistor of the video amplifier thereby increasing the differential gain. The bias on each diode can be adjusted to start conduction at a desired brightness level. By individually adjusting the bias and series resistor for each diode, a variety of gain-versus-brightness curves can be obtained.[1] Adjustable capacitors are connected across the resistors associated with the diodes to keep the phase angle of the network constant as the resistors are added or subtracted by the action of the diode.

It is necessary to use a *vestigial sideband* demodulator for monitoring and therefore the output picture must be compared with the input picture in order to achieve its most effective monitoring. Intermediate monitoring points contain a certain amount of predistortion. The diode in the position shown might given an acceptable picture, but it will be low in chroma because the lower sideband is largely suppressed, and it will not be possible to judge, by monitoring with a diode, whether the transmitter is attenuating the subcarrier.

In addition to the external auxiliary apparatus, a "clamp softening" circuit must be added to any transmitter that employs driven clamp circuits to prevent these circuits from reducing the amplitude or

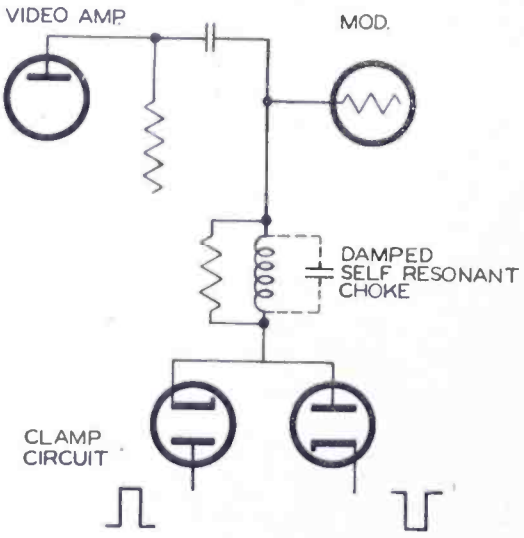

Fig. 16—Schematic diagram of "clamp softening" circuit.

affecting the phase of the synchronizing burst. The clamp softening circuit may simply be a resistor (e.g., 10,000 ohms) in series with the clamp circuit or, preferably, a network that has a high impedance at 3.58 megacycles and a low impedance at lower video frequencies. One arrangement commonly employed is shown in Figure 16.

Transmitter Adjustments

Transmitter adjustments normally made in order to meet the performance specifications for color broadcasting are:

1. Frequency response (and simultaneous adjustment for normal power output).
2. Linearity.
3. Differential phase (if there is an adjustment for this).
4. Envelope delay.

The adjustments should be performed in the order listed. Adjust-

ments of the tuned circuits to obtain proper frequency response, while simultaneously achieving normal peak power, will determine the operating conditions for the tubes and consequently determine the video signal level and the degree of linearity. Linearity correction and differential phase correction should be adjusted next. Finally, the delay equalizers are adjusted. The delay equalizers are passive networks and will not affect previous adjustments that have been made.

A sideband-response analyzer is the most satisfactory test instrument to enable frequency-response adjustment. Figure 17 shows the kind of display obtained when employing the sideband-response an-

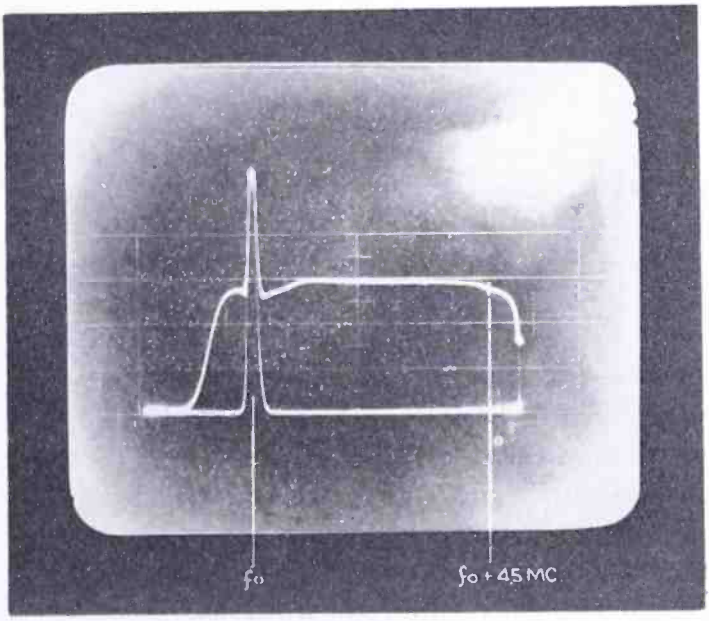

Fig. 17—Sideband response analyzer presentation of transmitter frequency response.

alyzer. The large spike is the carrier. The small spike is the 4.5-megacycle marker. The 5-megacycle high-frequency cutoff is produced by the video amplifier and the 1-megacycle cutoff below carrier is produced by the vestigial sideband filter. The dip near carrier may be imperfect neutralization of the modulated amplifier or it may be a poor tube in a video amplifier somewhere in the system — one with high cathode interface resistance.

The response from 1 to 4.5 megacycles is more uniform in this example than required, and should not be emulated in ordinary operating practice. The response shown by the dotted line of Figure 1D is more typical.

Adjustments of linearity, differential phase, and one method of adjusting envelope delay require test equipment that has been devel-

oped especially for color television. A description of such apparatus is outside the scope of this paper, but a very brief mention will be made of the application of these instruments to transmitter adjustments.

The linearity is adjusted using a linearity checker (stair-step generator with superimposed subcarrier). The differential phase is adjusted using the linearity checker in combination with a color-signal analyzer (basically a subcarrier phase detector and some adding circuits). For both of these tests a diode demodulator or a vestigial sideband demodulator may be employed. A diode demodulator is preferred because of its greater simplicity and smaller chance for contributory nonlinearity or phase error. If the diode is employed for differential phase measurements, it should be applied at a point in the system (e.g., after the vestigial sideband filter) where the frequency —3.58 megacycles (below visual carrier) is suppressed. This is necessary in order to include in the measurements the effect of any incidental phase modulation.

There is one fairly obvious precaution to be observed in the use of a diode demodulator for performance measurements involving the color subcarrier. Since one sideband is excluded and the carrier is at full amplitude, the degree of modulation will *appear* to be suppressed by 6 decibels. This should be taken into account when adjusting the subcarrier amplitude in the linearity checker.

Once the system linearity has been adjusted by predistorting the video signal, the gain control between the white stretcher and the transmitter modulator should not be adjusted except to correct for drift in gain of the intervening video stages. If the incoming video level changes, the correcting gain adjustment must be made by a control ahead of the white stretcher.

Phase Equalizer Adjustment

The final adjustment — adjustment to the prescribed envelope delay characteristic — can be made using either an envelope delay sweep generator or a square-wave generator. The former has the advantage that a direct reading is obtained of the system envelope delay and it is, therefore, possible to prove compliance with the FCC performance specification except at low video frequencies. It is also a more sensitive means of adjusting high-frequency envelope delay. The square-wave generator method will result in better low-frequency delay adjustment, but it does not give a quantitative measure of the envelope delay.

Using an envelope delay sweep and employing a diode detector after the vestigial sideband filter, the phase equalizers can be adjusted to

give a constant system time delay for frequencies between 2 and 4.2 megacycles. Although there is no doubt as to the soundness of this procedure, in practice it is difficult to adjust the high-frequency delay when the low-frequency reference is missing.

For low-frequency delay adjustment, a vestigial sideband demodulator must be used, and it must be *well corrected for its own low-frequency phase error.* The vestigial sideband demodulator would also be more convenient than a diode for high-frequency delay adjustment, but it would have to have either constant time delay within ±.02 microsecond to 4.2 megacycles (this can be approached with sound traps

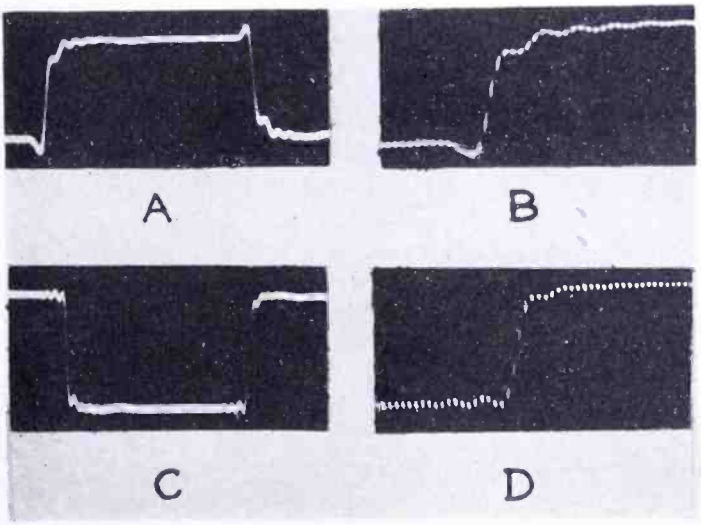

Fig. 18—100-kilocycle square-wave response of transmitter and vestigial sideband demodulator. (A) Uncorrected response. (B) Rapid scan (.05-microsecond markers) of uncorrected response. (C) Response after adjustment of phase equalizers. (D) Rapid scan (.05-microsecond markers) of equalized response.

switched out) or would have to match very closely the inverse of the FCC transmitter delay specification.

Figure 18 illustrates the use of a square-wave generator in adjusting the phase equalizers for best system envelope delay. Figure 18A is the uncorrected response. Figure 18B is the same, but scanned more rapidly and with 0.05-microsecond timing dots superimposed. Figure 18C is the corrected response after making phase equalizer adjustments, and Figure 18D is the fast sweep presentation of the corrected response. The leading transient and the trailing smear in Figures 18A and B are due to low-frequency phase errors in the transmitter. The high-frequency ringing is due to the 4.5-megacycle cutoff of the demodulator.

It is evident from Figures 18C and D that most of the low-frequency distortion is corrected. The residual low-frequency distortion may be

the uncorrected low-frequency phase error of the demodulator, or imperfect low-frequency amplitude response. The high-frequency ringing is reduced two-to-one in amplitude and is now symmetrical about the transition which is the proper condition when there is no phase distortion.

In these tests it is important to keep the depth of modulation low in order to minimize the disturbing influence of quadrature components.

Although the square-wave response is not greatly altered by considerable change in the adjustment of the high-frequency phase equalizer, one should not jump to the conclusion that high-frequency equalization is unimportant. The 100-kilocycle presentation is a good measure of the performance in the *luminance channel* only.

To obtain an equally reliable indication of transient response in the chrominance channel, it would be necessary to modulate a 3.58-megacycle subcarrier with a 100-kilocycle square wave to form a new test signal. The output of the regular demodulator would be followed by a synchronous detector to recover the initial 100-kilocycle square wave. Under these conditions, adjustment of the high-frequency equalizer would probably be as critical as adjustment of the low-frequency equalizer for the tests described in the preceding paragraphs

Acknowledgments

In this attempt to cover briefly all of the television transmitter problems and practices in color broadcasting, the efforts and ideas of many engineers have been freely used. Although it is difficult to single out individual work, the following have contributed important ideas in this field: G. L. Fredendall and W. C. Morrison of RCA Laboratories, T. J. Buzalski of the National Broadcasting Company, and N. J. Oman and J. W. Wentworth of the Engineering Products Division.

Special thanks are due to W. N. Parker for permission to use the analysis of incidental phase modulation, and to M. Feryszka who worked out many of the examples and curves used in this paper.

STUDIES OF THE INTERFACE LAYER IN OXIDE CATHODES*

By

L. S. Nergaard and R. M. Matheson

Research Laboratory, RCA Laboratories, Princeton, N. J.

Summary—*This paper presents new data on interface effects in commercial tubes and points up the complex nature of interface layers. Considerable stress has been placed on the latter because of its bearing on practical interface measurements. Certain precautions to be observed in making interface-resistance measurements have been suggested in the hope that the observation of these precautions may enable various workers in the field to obtain consistent and comparable results. Finally, the paper reports some exploratory experiments to determine the possible physical mechanisms which may lead to the observed complex behavior of a* $2BaO{\cdot}SiO_2$ *layer in contact with a metal and BaO or BaO + SrO. These experiments have not been carried to the point where they yield definitive results. They have been included so that the results may be available to others.*

Introduction

In the course of studies of the oxide cathode, it has been necessary to separate out the various mechanisms which contribute to the over-all behavior of the diodes in which the cathodes have been studied.[1,2] One of the separable effects is the high-speed ten-volt effect,[3] which is an anode effect, yet is easily confused with certain cathode effects. A second separable effect is that due to an insulating layer which may form at the interface between the base metal and the oxide of a cathode. No major effort has been devoted to either of these effects. They have been pursued until they were sufficiently understood so that their presence was easily recognized and their contribution to diode behavior could be separated out from the effects due to the oxide of the cathode. In the case of the interface layer, a simple circuit for measurement of the layer impedance was devised, the impedances of a substantial number of tubes were measured, and life

---

* Decimal Classification: R331.5.

[1] R. M. Matheson and L. S. Nergaard, "Decay and Recovery of the Pulsed Emission of Oxide-Coated Cathodes," *Jour. Appl. Phys.*, Vol. 23, pp. 869-875, August, 1952.

[2] L. S. Nergaard, "Studies of the Oxide Cathode," *RCA Review*, Vol. XIII, pp. 464-545, December, 1952.

[3] R. M. Matheson and L. S. Nergaard, "High-Speed Ten-Volt Effect," *RCA Review*, Vol. XII, pp. 258-268, June, 1951.

test data to determine the rate of growth of interface impedance is still being accumulated. In quite another connection, some of the electrical properties of barium-orthosilicate ($2BaO \cdot SiO_2$) were measured.[2]

In view of the practical importance of the interface layer and the widespread interest therein, it seems worthwhile to report on the information accumulated. It has also been noted that some of the various methods used to measure interface impedance do not yield like results when applied to the same tubes. Study at these laboratories of the electrical properties of $2BaO \cdot SiO_2$ suggests an explanation of the observed discrepancies and points to the precautions which must be taken if the various measurements are to yield consistent and coherent results.

Review of Interface Literature

The presence of, and to some extent the importance of, interface layers was first recognized by Wehnelt in about 1905. Somewhat later Arnold[4] observed a platinate interface layer on the platinum-iridium filaments he was using. In 1940, Rooksby[5] published the results of his X-ray studies of interface compounds. He identified a number of compounds including $2BaO \cdot SiO_2$, which has been the subject of much further study. In 1946, Fineman and Eisenstein[6] reported silicate interface layers in oxide-coated cathodes and described interface resistance measurements under pulse conditions. In 1949, Eisenstein[7,8] published an extensive paper on barium-orthosilicate interface layers. His paper describes the effect of such layers on cathode sparking and on cathode resistance. It also shows the rate at which the thickness of the layer increases on a cathode with 5 per cent silicon in the nickel base metal, and gives extensive data on the conductivity of $2BaO \cdot SiO_2$ and its temperature dependence.

About 1949, it became apparent that tubes in computer and time-division-multiplex service were failing at an early stage of life. It further appeared that the tubes that failed had been operating under very-low-duty conditions. The failures were soon correlated with the silicon content of the base metals used in the cathodes of these tubes, hence with $2BaO \cdot SiO_2$ interface layers. At the 1950 Conference on

---

[4] H. D. Arnold, "Phenomena in Oxide-Coated Filament Electron Tubes," *Phys. Rev.*, Vol. 16, pp. 70-82, July, 1920.

[5] H. P. Rooksby, "Applications of X-ray Technique to Industrial Laboratory Problems," *Jour. Royal Soc. Arts*, Vol. 88, pp. 308-336, 1940.

[6] A. Fineman and A. Eisenstein, "Studies of the Interface of Oxide Coated Cathodes," *Jour. Appl. Phys.*, Vol. 17, pp. 663-668, August, 1946.

[7] A. Eisenstein, "Some Properties of the Ba_2SiO_4 Oxide Cathode Interface," *Jour. Appl. Phys.*, Vol. 20, pp. 776-790, August, 1949.

[8] The chemical formula for barium orthosilicate is written $2BaO \cdot SiO_2$ by some authorities, Ba_2SiO_4 by others.

Physical Electronics, several papers on the interface problem were presented.

In 1951, Waymouth[9] and Eisenstein[10] published further studies of interface layers and their effects on the performance of tubes in practical circuits. In the same year Bounds and Briggs[11] published a paper on the nickel alloys used for oxide cathodes and described the effect of the alloying materials on cathode performance.[12]

Some Electrical Properties of Barium Orthosilicate

A considerable number of interface materials is known—tungstites, platinates, silicates, and titanates, for example. Of these, $2BaO \cdot SiO_2$ has the lowest conductivity and is therefore of most practical concern. These compounds are formed by residues of the reducing agents used to free the base-metal nickel from oxide, or by small amounts of specific reducing agents added to the base metal in controlled amounts to achieve easy activation and long life of the cathode.[11,13] The reducing agents diffuse out of the base metal and react with BaO to form the various interface compounds. For example, silicon diffuses out of the nickel and reacts with BaO to form silica and "excess" barium according to the equation

$$Si + 2BaO \rightarrow SiO_2 + 2Ba$$

The silica reacts with BaO to form the silicate

$$2BaO + SiO_2 \rightarrow 2BaO \cdot SiO_2$$

The complete reaction has two effects, (1) it produces excess barium which is desirable because it makes the cathode more active, and (2) it produces an insulating material which impairs the performance of the cathode.

---

[9] J. F. Waymouth, Jr., "Deterioration of Oxide Coated Cathodes Under Low Duty-Factor Operation," *Jour. Appl. Phys.*, Vol. 22, pp. 80-86, January, 1951.

[10] A. Eisenstein, "The Leaky Condenser Oxide Cathode Interface," *Jour. Appl. Phys.*, Vol. 22, pp. 138-148, February, 1951.

[11] A. M. Bounds and T. H. Briggs, "Nickel Alloys for Oxide-Coated Cathodes," *Proc. I.R.E.*, Vol. 39, pp. 788-799, July, 1951.

[12] In the past few years, interface problems have received attention at a number of conferences, for example, at the Conference on Electron Tubes for Computers at Atlantic City, N. J., December 11-12, 1950 and at the technical session on "Recent Developments in Electron Emitters" of the AIEE General Winter meeting in New York, January 21-25, 1952. Recent papers seem chiefly concerned with measurement methods and accumulated life-test data to which reference is made in a later section.

[13] H. E. Kern and R. T. Lynch, "Initial Emission and Life of a Planar-Type Diode as Related to the Effective Reducing Agent Content of the Cathode Nickel," *Phys. Rev.*, Vol. 82, p. 574, May 15, 1951.

The rate at which the interface layer forms is determined by the concentration of the reducing agent in the base metal, its diffusion through the base metal, the rate of the reaction between the reducing agent and the oxide, and perhaps by the rate at which one of the reactants can diffuse through the layer already formed. Eisenstein found that the silicate layer formed on a cathode having 5 per cent silicon in the nickel base reached a thickness of about 2×10^{-3} centimeter when operated at 1125° K for 100 hours.[7] Just how the apparent resistance of the layer depends on its thickness is not completely resolved. However, the experiments next considered suggest that the apparent resistance does not show a simple linear increase with thickness.

A sample of $2BaO{\cdot}SiO_2$ was prepared by firing barium oxide and silica in ortho proportions at 1630°K until the reaction was complete.

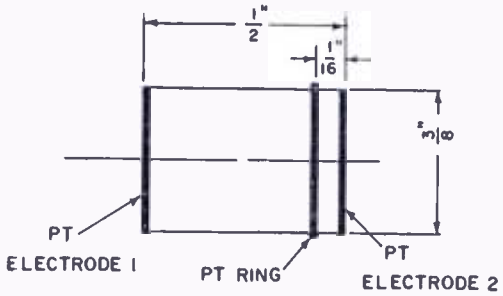

Fig. 1—Cylindrical sample of $2BaO{\cdot}SiO_2$ (Sample XXV-51) with platinum electrodes for resistance measurements.

The sample was a cylinder, ⅜ inch in diameter and ½ inch long. This cylinder was provided with platinum electrodes on its ends and a platinum "probe" ring about 1/16 inch from one end of the sample, as shown in Figure 1. These electrodes were painted and then fired on.

The first measurement made on the barium-orthosilicate cylinder was a measurement of the current decay under constant-voltage conditions. Such a decay curve is shown in Figure 2. It was obtained with the sample at 1210°K, with 100 volts applied across the sample in 1.5-second pulses at a repetition rate of ⅓ cycle per second. The initial current is 220 microamperes and the current decays to about 7 microamperes in 0.1 second. The decay is not exponential, but accords with the Sproull decay formula[14] up to about 4×10^{-2} second. Beyond 4×10^{-2} second there is a very slow downward drift not found in the Sproull formula. The Sproull formula was originally derived on the assumption that current decay in the oxide cathode results from the

[14] R. L. Sproull, "An Investigation of Short-Time Thermionic Emission from Oxide Coated Cathodes," *Phys. Rev.*, Vol. 67, pp. 168-178, March 1 and 15, 1945.

electrolytic transport of barium from the emitting surface. The observation of Sproull decay in the present experiment suggested that a similar mechanism might be operating, and that if some constituent of the silicate were transported electrolytically, the voltage distribution along the sample would not be linear. Accordingly, the voltage drops from electrode 1 to the platinum ring and from the platinum ring to electrode 2 in Figure 1, with current flowing from end to end in the sample, were measured. Electrode 2, which is closest to the ring, was positive. It was found that at higher temperatures the major

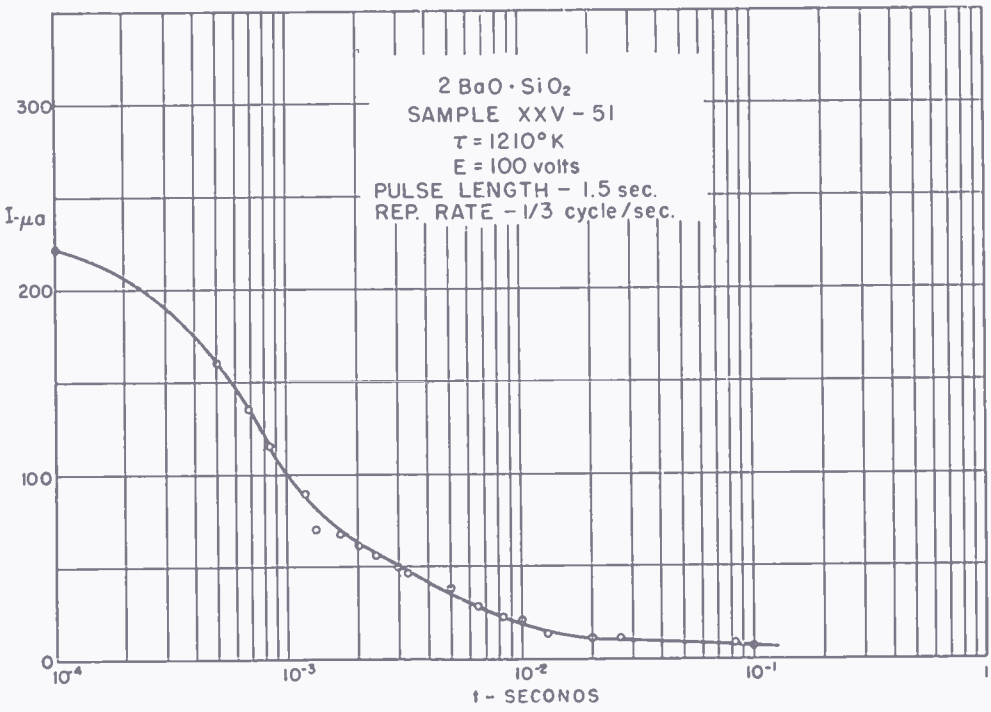

Fig. 2—The decay of current with time in sample XXV-51 of $2BaO{\cdot}SiO_2$ on application of a "unit-function" voltage.

fraction of the voltage drop occurred near the positive end. For example, at about 600°K only 5 volts out of 46 volts appeared between electrode 1 and the platinum ring. It appears that there is a depletion of some constituent at the positive end of the sample which raises the resistivity near the end. The behavior is similar to that observed earlier in a "Pyrex" glass sample at elevated temperatures.[2] The thickness of the depletion layer in the glass sample was measured and was found to be about 10^{-6} centimeter. The resistances of the silicate between electrode 1 and the ring (the "bulk resistance") and between the ring and electrode 2 (the "depletion layer resistance") were measured as a function of temperature from 700°K to 1100°K. The

bulk material shows an activation energy of about 0.80 electron-volt, the depletion layer an activation energy of about 1.2 electron-volts.

It now seems clear that the resistance of $2BaO{\cdot}SiO_2$ layer is not proportional to the thickness of the layer. Hence the thickness of a layer is not a simple measure of the resistance the layer will display.

In studies of the oxide cathode, It was found that the peak pulse current which may be drawn from an oxide cathode is a decreasing function of duty. Because the $2BaO{\cdot}SiO_2$ sample, like the oxide cathode, displays Sproull decay, it was thought that the silicate sample might

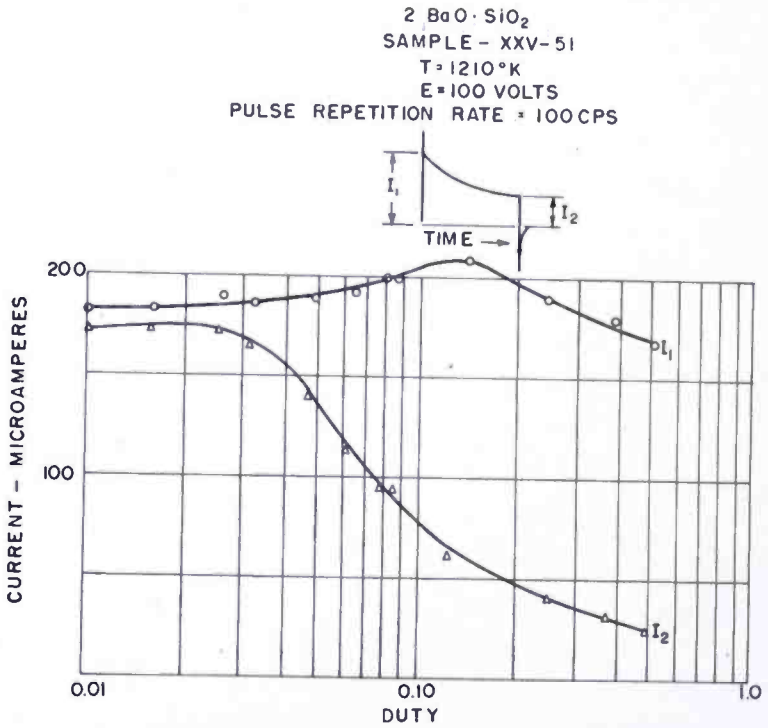

Fig. 3—The initial and final pulse currents in sample XXV-51 of $2BaO{\cdot}SiO_2$ as a function of duty.

display a similar behavior with duty. Figure 3 shows data exploring this possibility. The silicate sample was operated at 1210°K with 100-volt pulses applied at a repetition rate of 100 cycles per second. The duty was varied by varying pulse length. The initial current (I_1 in Figure 3), disregarding the initial spike, showed no marked change with duty (the initial spike and narrow part of the inverse spike were traced to stray capacitance in the measuring circuit). The final pulse current shows a marked dependence on duty.

Because an oxide cathode and the $2BaO{\cdot}SiO_2$ sample both show Sproull decay and exhibit depletion layers, it is of interest to inquire

why they differ in their behavior with respect to duty. An examination of the conditions of measurement for the two cases shows that the measurements were not made in the same way. The measurements on oxide cathodes were made in diodes. Hence, any polarization voltage developed in the cathode by current flow is impressed across the cathode–anode space in such a direction that no conduction current can flow through the external circuit during the off period. In the case of the silicate sample, the circuit was such that a depolarizing current could flow through the external circuit. The negative transient subsequent to the pulse may be such a depolarizing current. It has a height which is proportional to the total charge passed through the sample during the pulse, a behavior one associates with depolarization. Hence, it is possible that both would behave similarly under similar conditions of measurement and that the peak pulse current of the silicate sample would be a function of duty if no conduction current could flow through the external circuit between pulses. Unfortunately, the silicate sample was factured and such a measurement cannot now be made.

It is tempting to assume that $2BaO{\cdot}SiO_2$ is an impurity semiconductor and that the observed decay and voltage distributions result from an electrolysis of donors away from the positive boundary. If this assumption is made and if it is further assumed that the donors are similar to those in BaO, then the results of the foregoing experiments and the results of the experiments now to be described can be accounted for in a simple and coherent manner.

In the experiments described above, the measured resistances were very high—much higher than those observed in cathodes. It is believed that this occurs because the electrodes in the present tests were of platinum whereas the positive electrode in a cathode is BaO or (BaSr)O. Explicitly, and in terms of the model above, it is believed that donors can diffuse and electrolyze from the oxide into the silicate. Such diffusion and electrolysis can produce two effects:

(1) It can inhibit the formation of a depletion layer so that the apparent resistance of the interface layer is greatly reduced.

(2) It can increase the donor density in the interface layer so that the bulk resistance is reduced.

The following observations bear on these consequences of the electrolytic model and are interpreted in terms of the model.

It is observed that tubes which have aged without plate current show a much higher interface resistance than tubes which have aged in presence of substantial plate current. This observation suggests that the equilibrium distribution of donors between the oxide and the silicate is such that the silicate is relatively inactive. It is also observed that tubes which have aged without plate current show a marked

decrease of interface resistance when current is drawn for even moderate periods of time. The decrease of resistance is not permanent and the resistance increases as the cathode is aged without current. An example of this behavior is shown in Figure 4. This data pertains to three 6SN7–GT tubes which had interface resistances of 750, 330, and 93 ohms, respectively, measured at an anode current of 4 milliamperes. After the interface resistances had been measured, each of the tubes was operated at an anode current of 20 milliamperes for one minute after which the current was restored to 4 milliamperes and

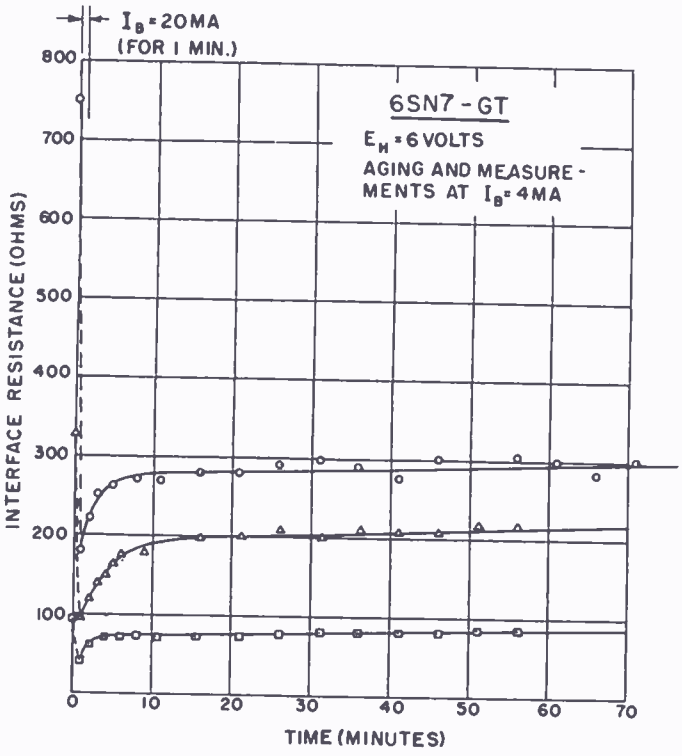

Fig. 4—The reduction of interface resistance as a function of time after passing excess current through the interface.

the interface resistance was measured as a function of time. The initial readings were obtained within 15 seconds after restoring the anode current to 4 milliamperes. The reduction in resistance immediately after drawing excess current, and the reduction in resistance after the first hour of aging at 4 milliamperes versus the initial interface resistance are plotted in Figure 5. The initial reduction in resistance is proportional to the initial resistance, approximately. The reduction after an hour of aging is proportional to the square of the initial resistance, approximately. The curves in Figure 4 show a slow upward trend after the initial rise. The data was extended for another seven hours for the uppermost curve. The resistance remained at about

300 ohms over this period. It appears that drawing excess current produces an activation of the interface layer which persists for at least a few hours. This behavior can be interpreted in terms of an electrolysis of donors into the interface layer by the excess current and a loss of donors by back diffusion when the current is small.

Whatever the details of the physical mechanism which leads to the behaviors described above, certain precautions to be observed in making measurements of interface resistance are indicated:

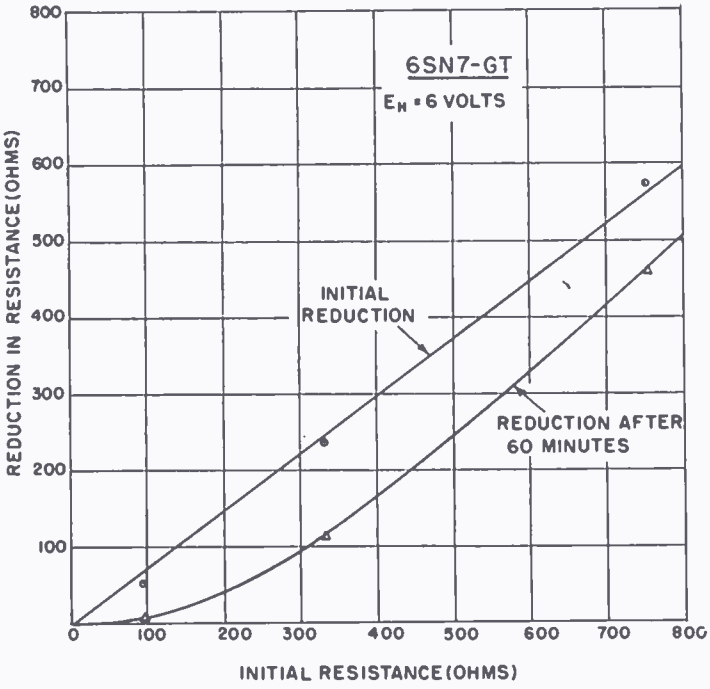

Fig. 5—The initial reduction in interface resistance and reduction in resistance after aging for an hour at 4.0 milliamperes plate current as a function of the resistance before passing excess current.

1. Measurements should be made at average currents comparable to those used in the aging processes if the measurements are not to change the quantities being measured.

2. If measurements are to be made at a specified current, adequate time for the realization of equilibrium must be provided.

3. Because the apparent resistance is a function of duty, all measurements must be made at the same duty if they are to show a simple correlation.

When interface layers are subjected to pulse operation, one or more short-time decays are observed. The time constants of these decays are of the order of 0.5-2 microseconds. These time constants appear to be more or less independent of the actual interface resistance.

Hence, it is difficult to account for them in terms of simple capacitances. It seems likely that the apparent capacitances are associated with an electronic or ionic blocking layer. It may be noted in passing that the dielectric constant of $2BaO{\cdot}SiO_2$ was measured by the immersion method using an acetone-benzene dielectric. The value was found to be $\epsilon = 12.4$.

The time effects described above may be represented approximately by the simple equivalent circuit shown in Figure 6. In the figure the diode represents the emitting surface, the interelectrode space and the anode of the actual diode. The electrical network represents the internal behavior of the cathode. R_0, R_1, and C_1, in combination, have a time constant of the order of 10^{-3} second, hence the combination represents the polarization mechanism which yields the slow decay. In the representation of practical tubes, R_1 is usually of the order of 5-10 times R_0. R_0, R_1, and C_2 in combination have a time constant

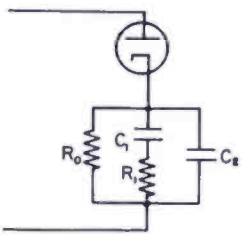

Fig. 6—The equivalent circuit of a diode having an interface layer. The diode is presumed to satisfy the Child–Langmuir law.

of the order of 1 microsecond, and hence represent the short-time-constant mechanism which is characteristic of interface layers. The circuit element which distinguishes the effect of an interface layer from other cathode effects is C_2. More detailed equivalent circuits are discussed elsewhere.[15]

The above equivalent circuit uses linear circuit parameters. This is an approximation as is apparent in the form of the current decay. If the decay effects are due to a depletion layer, the apparent resistance and capacitance are not linear. If the interface layer is thin and of low conductivity and if no depletion effects are apparent, the layer will act as a rectifying blocking layer with an exponential current–voltage characteristic. In neither case can the apparent circuit parameters be matched by linear circuit elements over an extended current range.

---

[15] R. M. Matheson and L. S. Nergaard, "A Bridge for the Measurement of Cathode Impedance," scheduled for publication in *RCA Review*.

Interface-Measurement Methods

A variety of methods has been used to measure interface resistance in tubes. Some of these methods will be described briefly. Their apparent relative merits will be outlined.

a. Simple Pulse Methods

In the simplest version of the pulse method, a constant-voltage pulse of about 10 microseconds duration is applied to the anode of the diode whose interface resistance is to be measured and the current decay is observed on an oscilloscope. The leading edge of the pulse should be steep enough so that there is no substantial decay during the time of application of the pulse, and the oscilloscope should have a bandwidth adequate to display the pulse accurately. The initial and final currents are determined from the oscilloscope display. If the current decay is small enough so that the diode impedance does not change appreciably with the change in current during decay, the decay may be regarded as due to the gradual insertion of the interface resistance in series with the cathode return. Hence, the interface resistance is

$$R_i = E\left(\frac{1}{I_\infty} - \frac{1}{I_0}\right)$$

in which E is the applied voltage, I_0 is the initial current, and I_∞ is the final current. If the decay is substantial, the change in diode impedance must be taken into account.

An alternative is to use a constant-current pulse and to display the voltage across the diode on an oscilloscope. In this case, the voltage rises from an initial value V_0 to a final value of V_∞. Because the diode resistance remains constant, the interface resistance is simply

$$R_i = \frac{V_\infty - V_0}{I}$$

in which I is the pulse current.

In the case of multielectrode tubes, the tubes are usually diode connected, i.e., all of the grids and anode are tied together. The alternative is to connect a multielectrode tube in its normal amplifier connection, drive the control grid with a constant-voltage pulse and observe the voltage pulse across the plate load. Because the interface resistance appears in the cathode circuit, it degenerates the transconductance of the tube. If g_{m0} is the transconductance of the tube in the absence of interface resistance and R_i is the interface resistance,

the apparent transconductance is

$$g_m = \frac{g_{m0}}{1 + g_{m0}R_i}.$$

This is the transconductance which is observed after pulse decay is complete or at frequencies low enough that the interface resistance is not shunted out by the apparent interface capacitance. In a high-μ tetrode or pentode, the voltage across the plate load at the beginning of a constant voltage pulse is

$$V_0 \approx g_{m0}R_pV_g$$

and after decay is complete is

$$V_\infty \approx g_mR_pV_g$$

where R_p is the plate-load resistance and V_g is the pulse voltage applied to the grid. Hence, the interface resistance is

$$R_i = \frac{1}{g_{m0}}\left(\frac{V_0}{V_\infty} - 1\right)$$

The amplifier connection has the advantage of yielding a certain amount of voltage gain. This is offset in part by the necessity of determining g_{m0}.

It should be noted that the foregoing method is exact only for triodes. In tetrodes, pentodes and other tubes having additional positive electrodes, the cathode current is not equal to the plate current, and the feedback voltage developed across a cathode resistance is not proportional to the plate current. If a triode connection cannot be used, corrections must be made to account for these additional currents.

In any of these pulse methods, the apparent capacitance may be computed from the measured resistances and the time constant of decay.

All of these methods suffer from a lack of accuracy, particularly when the interface resistance is very low. All of these methods have been used during the course of this study.

b. Pulse Comparison Method

This method, suggested by S. Nasto,* is essentially a refinement of the single-pulse methods. The tube under test, diode connected, is connected in parallel with an adjustable network which is an analog

* Tube Division, Radio Corporation of America, Harrison, N. J.

of the tube under test. The analog network consists of a resistor (the analog of the plate resistance of the tube under test) in series with a resistor and capacitor in parallel (the analog of the interface impedance). The tube and the analog network are driven by a pulse of about 10 microseconds duration at a repetition rate of 100 pulses per second. The current pulses through the tube and its analog are compared by displaying them alternately on the same oscilloscope. The analog network is adjusted to produce coincidence of the pulses and the interface resistance and capacitance are read directly.[16] Since this is basically the same method as the constant-voltage pulse method described previously, the change in diode impedance during decay must be corrected for if the decay is substantial.

c. The Wagner Method (1)

H. M. Wagner has modified the simple pulse methods described above so that he achieves a considerable advantage in accuracy.[17] He drives the diode-connected "unknown" tube with a constant-voltage pulse and views the current decay on an oscilloscope. He then inserts a "substitution resistor" in series with the tube and adjusts this resistor until the leading edge of the displayed pulse coincides with the previous position of the final current after decay. If the current decay is small, so that the diode resistance does not change appreciably, the inserted resistance is equal to the interface resistance. To increase the sensitivity, he divides off a fraction of the driving voltage and applies this voltage and the voltage across the tube-current-measuring resistor to a difference amplifier which drives the oscilloscope. Thus the oscilloscope displays only the amplified decay characteristic. By this means he achieves a sensitivity adequate to measure an interface resistance as low as one ohm.

Again, the apparent capacitance is determined from the time constant of decay and the interface resistance.

This measurement method is one of the simpler and more accurate methods which has been used at these laboratories.

A modification of this method in which the "unknown" tube is triode connected, the grid is driven with a square-wave voltage, and the current-measuring resistor and substitution resistor are inserted in the cathode return has also been used. This method has the advantages that the plate current can be adjusted independently of the signal

---

[16] The Clegg Laboratories Pulse Impedance Bridge, Model PIB1, which has a pulse generator and a synchronized switch for displaying alternate pulses built into the instrument, is readily modified to make this measurement.

[17] H. M. Wagner, "Cathode Interface Impedance and its Measurement," presented at the National Electronics Conference, Chicago, Ill., 1952.

voltage and that the tube need not be driven through current cutoff where the nonlinearity of the tube characteristic makes it difficult to match the voltage across the current-measuring resistor with the balancing voltage.

d. The Wagner Method (2)

A second method developed by Wagner compares the unknown tube, diode connected, with the analog network described above at two frequencies under small-signal conditions.[18] Because only two frequencies are used, only two parameters of the unknown can be determined. Accordingly, the capacitor of the analog network is chosen so that its reactance is small compared to the interface resistance at 10 megacycles and large compared to the interface resistance at 1 kilocycle. To make the measurement, the unknown tube is first driven by a 10-megacycle constant-current generator and the voltage across the tube is read with a vacuum-tube voltmeter. The analog network is then driven with the same constant-current and the R_p resistor is adjusted to obtain the same voltage as was obtained across the tube. This procedure is repeated with a 1-kilocycle constant-current generator except that now the resistor representing the interface resistance is adjusted to match voltages. Thus the R_p and interface resistance of the tube are determined.

This method is capable of an accuracy of about one ohm, and has the merit that only two simple oscillators and a vacuum-tube voltmeter are required. While several operations must be performed, they require no appreciable skill and the value of the interface resistance is obtained without computation.

e. The Transconductance Method

As noted in section (a), the apparent transconductance of a multielectrode tube is a function of the interface resistance. If the transconductance of a tube is measured at two frequencies, one high enough so that the apparent interface capacitance shunts out the interface resistance, the second low enough so that the interface capacitance does not shunt out the resistance, the interface resistance may be computed from the two transconductances by the formula

$$R_i = \frac{1}{g_{m1}} - \frac{1}{g_{m2}}$$

in which g_{m1} and g_{m2} are the "low" and "high" frequency transcon-

[18] H. M. Wagner, "Cathode Interface Resistance Test for Electron Tubes," presented at the Fourteenth Annual Conference on Physical Electronics, Massachusetts Institute of Technology, 1954.

ductances, respectively. Appropriate frequencies are 10 and 0.01 megacycles. If the lower frequency is chosen still lower, the long-time-constant effects begin to play a role. Much of our interface data has been acquired by this method. For low resistance values it suffers from the difficulties normal to all measurements or computations which depend on a small difference between large quantities.

f. A Bridge Method

This bridge method balances the unknown tube against a synthetic diode comprising a diode free from the defects under study in series with a suitable adjustable network (Figure 6). The details of the bridge are described elsewhere.[15] The bridge permits of considerable precision. However, in its present low-frequency form, this bridge does not separate out oxide effects and interface effects. Hence, it is suitable for measurements of interface impedance only when the interface impedance is high compared to the oxide impedance. This is usually the case with well-activated tubes having a considerable silicon content in the base metal, after the tubes have been aged at a low duty for some hundreds of hours. For making interface measurements early in the life of a tube, a pulse or high-frequency method is preferred to this bridge method.

In connection with the bridge circuit, it is worth noting that, in the form in which it has been built here, the bridge may be balanced and then switched to display the plate currents of the unknown and standard tubes on the horizontal and vertical axes, respectively, of an oscilloscope. If the display shows a marked and abrupt deviation from linearity, one of the two tubes is emission limited; which one is apparent from the direction of the deviation. In this manner, true emission limitations, unconfused by deviations due to cathode impedances, can be found.

g. The Frost Method

The method of Frost places the tube under test in its normal amplifier connection.[19] The grid is driven with a square wave from one half of a phase inverter. A resistance having a magnitude equal to the reciprocal of the transconductance of the tube under test is connected between the control grid and the anode. The anode is driven out of phase by the other half of the phase inverter. Hence, the current through the load resistor is zero if the tube has no cathode impedance. An amplifier driving an oscilloscope is used to observe the voltage

[19] H. B. Frost, "The Measurement of Cathode Interface Impedance," (Abstract), *Proc. I.R.E.*, Vol. 40, p. 230, February, 1952. Also reported at Twelfth Annual Conference on Physical Electronics, M.I.T., 1952.

across the plate load. If there is cathode impedance, the apparent transconductance of the tube becomes frequency sensitive and is not matched by the reciprocal g_m resistor, and a signal appears across the plate resistor. This signal is balanced out by a network in the cathode return which is the dual of the interface impedance (a network complementary to that of Figure 6). Because of the sensitivity of the circuit, stray capacitances must be balanced out by a neutralizing capacitor in order to achieve balance. Altogether, six parameters must be adjusted to achieve a balance: the reciprocal g_m resistor, the neutralizing capacitor, and the four elements of the complementary network.

This method is elegant and achieves a sensitivity and time resolution which do not seem to be matched by any other method. It has disclosed two time constants for interfaces in the microsecond range, one 0.1-1.5 microseconds; the second, 0.5-10 microseconds. Like all bridges which yield much information, a considerable amount of skill and time is involved in obtaining a balance. It is felt that this method is an elegant laboratory method but is not suitable for routine measurements on large numbers of tubes.

h. The Bartley and White Method

Bartley and White have used a comparison method for measuring interface impedance.[20] The tube under test is placed in its amplifier connection. The grid is driven by a square-wave voltage of several microseconds period. The output voltage of the tube is superposed on the square-wave input voltage in an oscilloscope display by an electronic switching circuit. Any distortion of the output wave shape by interface impedance is thus apparent. This measurement makes possible the selection of "standard" tubes which show no appreciable interface effects. In the measurement of interface impedance, the output voltage of the unknown tube is superposed on the output voltage from a standard tube, with both tubes driven by the same grid voltage. The two wave shapes are then made coincident by introducing resistance and capacitance in parallel, both in series with the cathode return of the standard tube. When the output-voltage wave shapes coincide, the inserted resistance and capacitance are equal to the apparent resistance and capacitance of the interface layer of the unknown.

Aside from the switching circuits required to superpose the voltages to be compared, the method is simple and direct. If the oscilloscope is preceded by an amplifier of adequate gain and bandwidth, it should be capable of considerable sensitivity and accuracy.

---

[20] W. P. Bartley and J. E. White, "Characteristic Shifts in Oxide Cathode Tubes," *AIEE Technical Paper*, pp. 52-53, December, 1951.

i. The McNarry Method

McNarry[21] makes the tacit assumption that a cathode exhibits zero resistance except for interface resistance and proceeds as follows. The diode-connected unknown is compared with a three-element passive network in a bridge. The unknown is operated at the desired d-c level and the bridge is driven with an a-c signal. The first of the three balances required to determine the interface impedance is made at a frequency of 10 megacycles. At this frequency, the interface impedance is negligible compared to the plate resistance of the diode, so that balance is achieved by adjusting a resistor R_0, which represents the plate resistance, in the standard arm of the bridge. The second balance is made at a frequency of 100 cycles. At this frequency, the apparent shunt reactance of the interface layer is large compared to the shunt resistance, so balance is achieved by inserting an additional resistance R_i, which represents the interface resistance, in series with R_0. The third balance is made at a frequency of 100 kilocycles by shunting R_i with a capacitance C_i. If the bridge ratio is unity, the bridge is direct reading and R_i and C_i are the interface resistance and capacitance respectively. The bridge measures low interface resistances within one ohm.

Unfortunately, the cathode impedance of a tube with zero interface resistance is not zero; the oxide resistance remains and may be substantial. Hence the bridge does not measure interface resistance directly. Just what it measures depends on the details of the circuit, particularly the balance indicator.

All of the above methods have their merits. The choice of circuit must be predicated on the application. For laboratory experiments where precision is desired (at the expense of time), certain circuits recommend themselves. For routine measurements of large quantities of tubes, other circuits are indicated. However, it must be stressed that the various methods will not yield the same results when applied to the same tubes. Methods which operate with a small signal superposed on a d-c bias are expected to yield a higher apparent interface resistance than those methods which employ a very small duty, because the former measure resistance after the decay of Figure 2 is complete and the latter make the measurement near the beginning of decay in Figure 2. Furthermore, the small-signal methods may change the apparent interface impedance of tubes which have been aged under cutoff conditions if the d-c cathode current is substantial in the test. Until the effects of current on the activity of interface layers have

[21] L. R. McNarry, "Bridge for Measuring the Interface Impedance of Oxide-Coated Cathodes," Report N.R.C. No. 2745 of the National Research Council of Canada.

been more thoroughly delimited, it seems wise to make measurements under conditions which resemble the aging conditions as closely as practicable.

Life Test

This section includes most of the pertinent data on interface effects in practical tubes which have been accumulated. Some of the data has been reported orally at various conferences. They are included here because of the evident interest in them.

a. 6SN7-GT's and 6SL7-GT's from Multiplex Equipment

Certain tubes operating at low duty cycle in time-division multiplex terminal equipment had failed. These tubes were sent here for study after their cathode resistances had been checked by the transconductance method described in the preceding section. The low-frequency transconductances were then computed from the measured high-frequency transconductances and measured cathode resistances for comparison with the measured low-frequency transconductances. The results are shown in Tables I and II. In Table I, I_p is the peak current to which the tube was driven in the bridge; R_k is the apparent cathode resistance at 60 cycles; V_k is the peak voltage drop across the apparent resistance; V_p is the peak applied plate voltage; and $I_p/V_0^{3/2}$ is the perveance of the tube, where $V_0 = V_p - V_k$.

It should be noted that in some cases the cathode drop amounts to 50 per cent of the applied voltage.

Table II compares the bridge measurements with the transconductance measurements. In Table II, g_{m0} is the transconductance at 10 megacycles (assumed to be the true transconductance of the tube); R_k is the apparent cathode resistance at 60 cycles; $g_m' = g_{m0}/(1 + g_{m0}R_k)$; g_m is the transconductance at 10 kilocycles; and D is the duty at which the tubes had operated in the multiplex equipment.

In some instances, the ratio of g_m/g_m' is considerably less than unity. This may be due to the fact that some of these tubes were subjected to emission checks after the transconductance measurements and before the bridge measurements. Operation of tubes under high current conditions reduces R_k, as was pointed out earlier. All of these tubes were checked for emission limitation up to at least one half ampere after the bridge measurements. In no instance was an emission limitation found.

b. Life-Test of Special 6AG7 Tubes

A group of 6AG7's having various cathode base metals were operated on life test for periods up to 3050 hours. The life-test data comprises the plate current at a standard voltage versus time, and

Table I—Measured Interface Resistances of Tubes Operated in Multiplex Service.

Tube Type	Tube No.	I_p Amps	R_k Ohms	V_k Volts	V_p Volts	V_k/V_p	$I_p/V_o^{3/2} \times 10^6$
6SN7–GT	1a	0.068	44	3.00	21.2	0.141	873
	b	0.032	317	1.01	19.8	0.510	1060
	3a	0.060	84	5.04	21.2	0.238	923
	b	0.034	322	11.1	21.2	0.528	1070
	14a	0.025	178	4.45	15.6	0.285	680
	b	0.042	213	8.9	21.2	0.419	966
	18a	0.025	250	6.25	17.7	0.354	618
	b	0.042	187	8.23	21.2	0.388	933
	30a	0.030	130	11.3	21.2	0.486	980
	b	0.044	179	7.9	21.2	0.372	900
6SL7–GT	1a	0.0216	480	10.4	21.2	0.491	610
	b	0.0136	256	3.48	10.0	0.348	825
	2a	0.0202	81	1.6	10.0	0.160	1030
	b	0.0184	142	2.6	10.0	0.260	920
	3a	0.016	203	3.2	10.0	0.320	905
	b	0.0106	483	5.1	10.0	0.510	980
	4a	0.0057	1010	5.8	10.0	0.580	670
	b	0.0088	615	5.4	10.0	0.540	890
	14a	0.0044	1670	7.3	10.0	0.730	995
	b	0.0104	465	4.83	10.0	0.483	881

Table II—Comparison of Measured and Computed Transconductances at 10 Kilocycles of the Tubes of Table I.

Tube Type	Tube No.	g_{mo} (10 mc)	R_k Ohms	$g_{m'}$ Comp.	g_m (10 kc)	$g_m/g_{m'}$	D
6SN7–GT	1a	2480	44	2230	2060	0.923	0.97
	b	2520	317	1400	1340	0.958	0.041
	3a	2520	84	2080	2140	1.03	0.97
	b	2560	322	1400	1420	1.01	0.041
	14a	2520	178	1760	1900	1.08	0.57
	b	2500	213	1630	1100	0.67	0.041
	18a	1440	250	1060	1460	1.36	0.45
	b	1060	187	885	400	0.45	0.041
	30a	1260	370	880	760	0.86	0.090
	b	2520	179	1740	1040	0.60	0.041
6SL7–GT	1a	1700	480	935	1120	1.20	1.0
	b	1680	256	1180	1320	1.12	1.0
	2a	1840	81	1600	1460	0.912	1.0
	b	1660	142	1340	1320	0.985	1.0
	3a	1740	203	1280	1340	1.05	1.0
	b	1580	483	893	1040	1.16	1.0
	4a	1100	1010	524	680	1.30	1.0
	b	1560	615	798	1040	1.30	1.0
	14a	1120	1670	582	500	0.860	1.0
	b	1100	465	730	800	1.10	1.0

Table III—Measured Interface Resistances of 6AG7's on Life Test

Group	Tube No.	I_p Amps	R_k Ohms	V_k Volts	V_p Volts	V_k/V_p	$I_p/V_o^{3/2} \times 10^6$
A N–34A Cutoff	1	0.038	180	6.8	10.7	0.64	4430
	2	0.064	78.4	5.0	10.9	0.46	4480
	3	0.064	91.3	5.8	11.7	0.50	4480
	4	0.058	113	6.6	12.1	0.55	4530
	5	0.064	71.5	4.6	10.6	0.43	4360
	6	0.052	86.2	4.5	9.5	0.47	4550
	7	0.051	83.5	4.3	9.2	0.47	4740
B N–34A Conduction	1	0.058	228	13.2	18.7	0.70	4570
	2	0.030	136	4.1	7.6	0.54	4600
	3	0.030	226	6.8	10.1	0.67	5000
	4	0.033	162	5.4	9.4	0.57	4150
	5	0.033	253	8.4	12.2	0.69	4480
	6	0.029	226	6.6	9.9	0.67	4870
	7	0.021	351	7.2	10.2	0.71	4070
	8	0.029	273	8.0	11.4	0.69	4610
C N–81 Conduction	1	0.067	37.3	2.5	8.5	0.34	4560
	3	0.042	106	4.5	9.2	0.49	4120

Table IV—Comparison of Measured and Computed Interface Resistances of Tubes of Table III.

Group	Tube No.	W/W_o Calc.	W/W_o Meas.	R_k Calc.	R_k Meas.	Life Hours
A N–34A Cutoff	1	0.195	0.234	115 Ω	180 Ω	1545
	2	0.615	0.472	25	78	2041
	3	0.402	0.350	53	91	2041
	4	0.490	0.380	39	113	2041
	5	0.640	0.432	23	72	2041
	6	0.326	0.339	66	86	1545
	7	0.390	0.370	55	83	2041
B N–34A Conduction	1	0.435	0.478	47	228	3053
	2	0.080	0.061	231	136	3053
	3	0.081	0.081	229	226	3053
	4	0.105	0.090	190	162	3053
	5	0.113	0.087	180	253	3053
	6	0.098	0.086	199	226	3053
	7	0.051	0.116	310	351	3053
	8	0.070	0.067	251	273	1545
C N–81 Conduction	1	0.338	0.303	66	37	3053
	3	0.191	0.305	117	106	3053

the power output of the tubes into a standard load versus time. Table III shows the results of bridge measurements on these tubes. The columns correspond to those of Table I. The tubes A and B have a high-silicon-content base metal (0.15-0.25 per cent silicon) and were run under cutoff and conducting conditions, respectively. Tubes C have

a low-silicon-content base metal (<0.01 per cent silicon) and were run under conducting conditions. It is worthy of note that in some of these tubes about 70 per cent of the applied voltage appears across the cathode.

Table IV compares the bridge measurements with the life-test data. The cathode resistance may be computed from the plate currents at the beginning and end of life if the drop in plate current is caused solely by an increase in cathode resistance. The required relation is

$$R_k = \frac{i_0^{2/3} - i^{2/3}}{P^{2/3}\, i}$$

in which i_0 is the initial current, i is the final current, and P is the perveance of the tube.

Columns 5 and 6 in Table IV compare the computed cathode resistances with those measured in the bridge. The ratio of the final g_m to the initial g_{m0} may be computed from the relation

$$\frac{g_m}{g_{m0}} = \frac{1}{1 + g_{m0} R_k}.$$

The ratio of the final power output into a standard load to the initial power output into the same load is approximately the square of the ratio of the final to initial g_m. Columns 2 and 3 of Table IV compare the ratio of final to initial output as computed and measured. It appears that the major cause of the decrease of plate current with life was the increase of interface resistance with life. The column on the extreme right shows the time at which the tubes were removed from the life-test racks. These tubes were also checked for signs of emission limitation up to about 0.5 ampere and none was found.

c. Life-Test Data on Special 6SN7-GT and 6SL7-GT Tubes Operating in Time-Division-Multiplex Terminal Equipment

The time-division-multiplex terminal equipment mentioned under (a) is now equipped with a series of 6SL7-GT's and 6SN7-GT's having various silicon-content base metals. These tubes are operated at a heater voltage of 6.0 volts to retard interface growth. After each 1000 hours of operation, the 10-megacycle and 10-kilocycle transconductances of these tubes are read. From the transconductances, the apparent interface resistances are computed. The data for the first 5000 hours was examined for significant differences which might be associated with the silicon content of the base metal, the average plate current, and the duty. The data was then grouped in accordance with

the operating conditions which seemed to produce differences. The average resistances versus life for each of the groups are shown in Figures 7, 8, and 9. An examination of the curves suggests that the original subdivisions were too fine and that the statistical variations far exceed the suspected correlations with plate current and duty. Figure 7 shows the variation of resistance with life of a group of 106 triode units with a relatively high silicon content in the base metal. The conditions of operation corresponding to each curve are shown

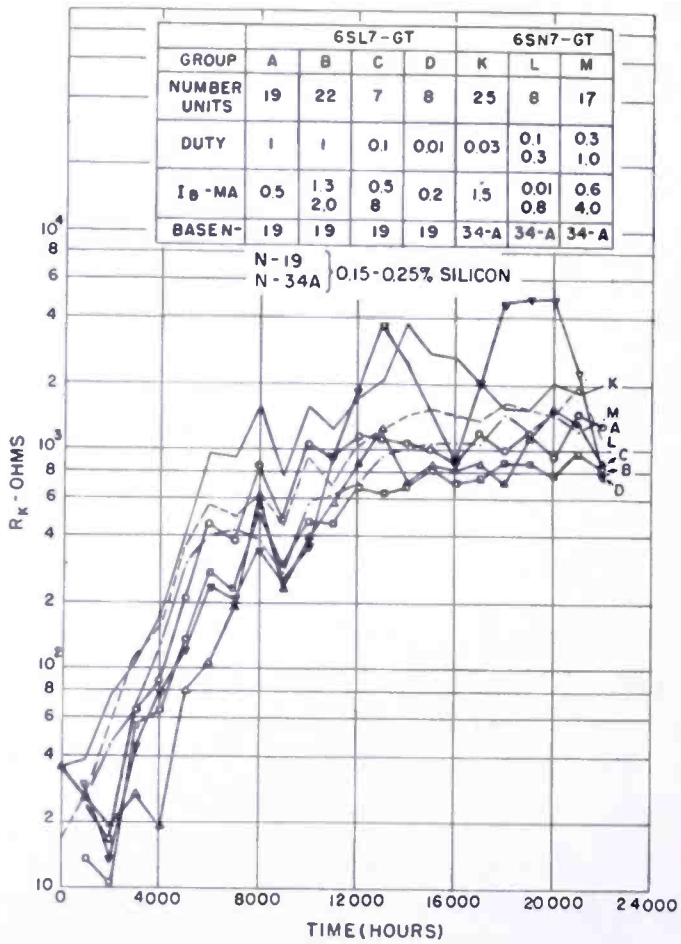

Fig. 7—The Interface resistances versus time of a set of tubes having 0.15–0.25 per cent silicon in the base metal.

in the box in the figure. It will be noted that the apparent resistance rises quite rapidly to a value of the order of a thousand ohms in the first 8000 hours and then shows a tendency to level off.

Figure 8 shows similar data on a group of 50 triode units having a lower silicon content base metal. The silicon content is less than ⅓ of that of the tubes of Figure 7 and the apparent resistance approaches a value of the order of ⅕ of that of the tubes of Figure 7. The same

rapid initial rise of resistance with life as observed previously is noticeable.

Figure 9 shows similar data on a group of 92 triode units some of which have a still lower silicon content. The same general behavior with life is observed. The resistance appears to level off at at about 70 ohms.

Because there appears to be no clear-cut correlation with plate current or duty, at least for the ranges of plate current and duty

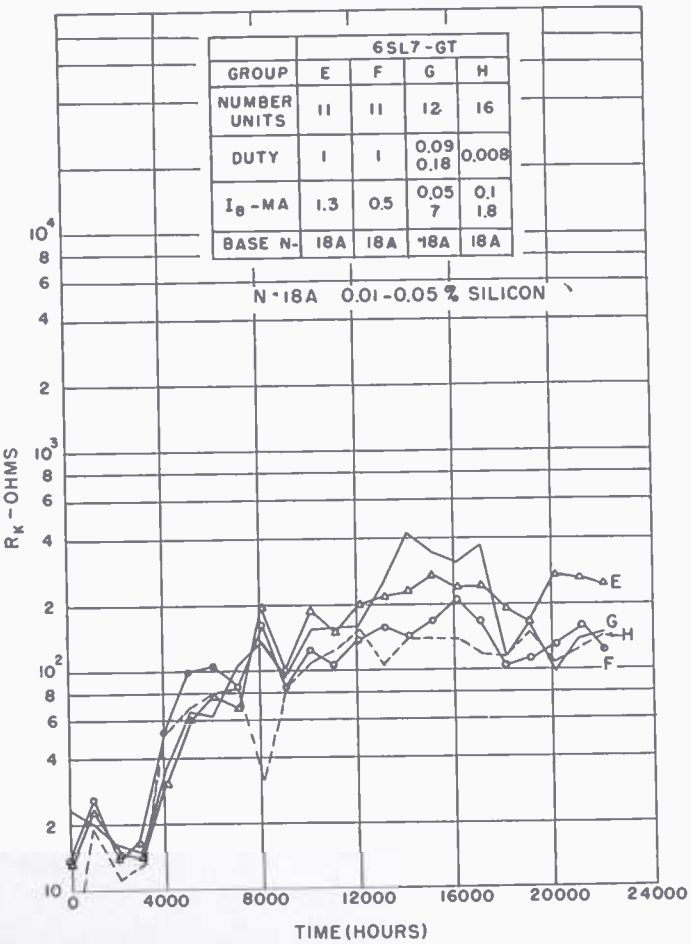

Fig. 8—The interface resistance versus time of a set of tubes having 0.01–0.05 per cent silicon in the base metal.

encountered in the multiplex equipment, the data was reduced to a unit cathode area basis and averaged by base metal. The results are shown in Figure 10. Two general conclusions can be drawn:

1. The interface resistances increase rapidly with time during the first 8000 hours and then show a tendency to saturate.

2. The "final" resistances are about in proportion to the original silicon contents of the base metals.

It is worth noting that the behavior of the resistance with time during the first few thousands of hours does not give a clear indication of what will happen subsequently.

Considered from an engineering standpoint, the implications of this data are self-evident. In view of the considerable investment in time required to obtain such data, it seems desirable to glean whatever further information is possible from it. The amount of fundamental physical information which can be abstracted is probably very small because:

1. The increase of interface thickness with time is not known.

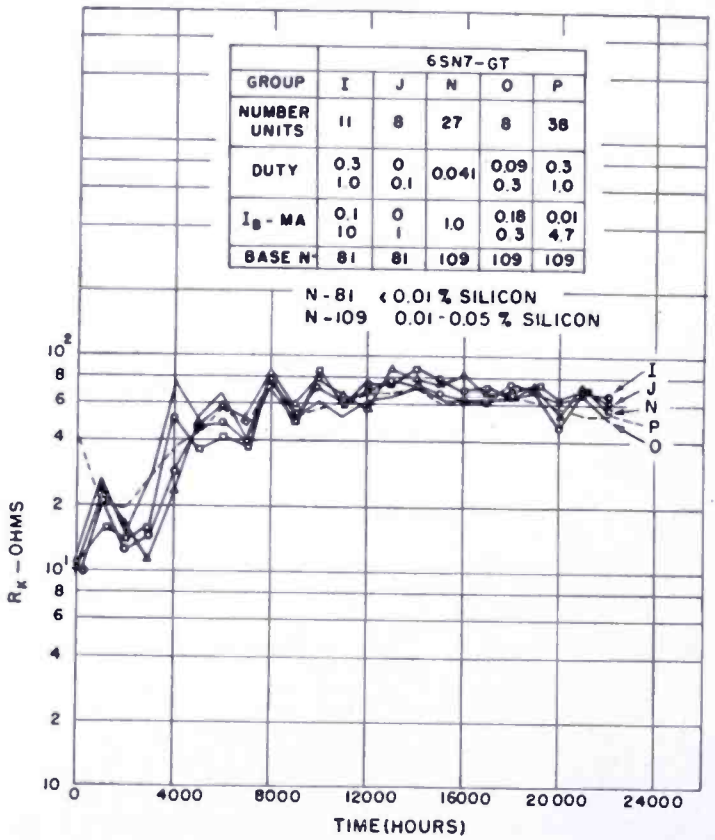

Fig. 9—The interface resistance versus time of a set of tubes having <0.01–0.05 per cent silicon in the base metal.

Hence, the dependence of interface resistance on layer thickness cannot be established. Furthermore, the process which determines the rate of growth cannot be separated out. The dominant process may be the rate of diffusion of silicon out of the base metal, the rate of diffusion of silicon or barium oxide through the interface layer, the rate of reaction between silicon and barium oxide, or perhaps one of these mechanisms early in life and another later.

2. It is not certain that the measurements from which the resist-

ances are derived do not affect the resistances and their rate of growth. The transconductances of the 6SN7-GT tubes are read at a plate current of 12 milliamperes and the transconductances of the 6SL7-GT tubes at a plate current of 4 milliamperes. These currents exceed the currents at which the tubes operate in the life test, with a few exceptions. If the usual pattern of behavior applies (the decrease of interface resistance with current noted in the section on the electrical properties of barium orthosilicate), the currents drawn during the measurements reduce the resistances at each reading. As the resist-

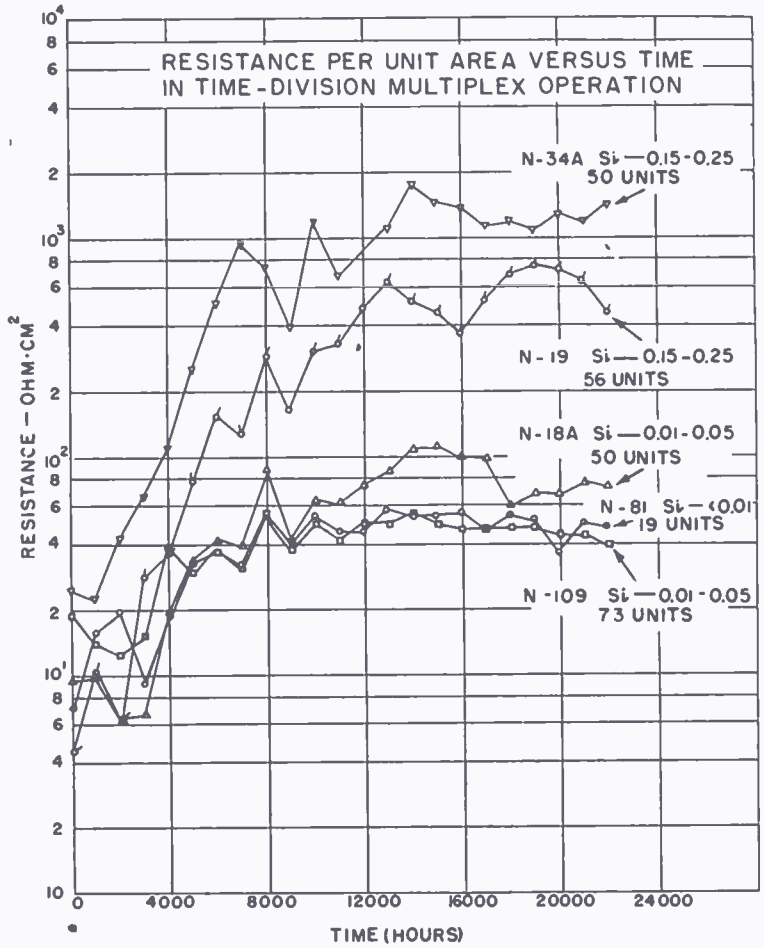

Fig. 10—The data of Figures 7, 8, and 9, reduced to a unit cathode area basis, with the type of base metal as a parameter.

ances increase with life the effect of the measurement current may also increase in such a manner that the asymptotic resistance observed in the life curves is simply an equilibrium between the rate of growth of resistance and the reactivation during each measurement. This possibility is suggested by the results shown in Figures 4 and 5.

To explore how the measurements might affect the life curves,

suppose that the resistance of the layer is proportional to its thickness and that the thickness is determined solely by the diffusion of silicon out of the nickel. Then it can be shown that after the first thousand or so hours of life, the resistance should approach an asymptotic value R_∞ according to the formula

$$R = R_\infty \left[1 - \left(1 - \frac{R_0}{R_x} \right) e^{-t/\tau} \right]$$

in which

$R_0 =$ resistance at the beginning of the life test,

$$\tau = \frac{1}{D} \left(\frac{d}{\pi} \right)^2 ,$$

$D =$ diffusion constant of silicon in nickel,

$d =$ thickness of the nickel.

Hence the rate at which the resistance increases is

$$\frac{\partial R}{\partial t} = \frac{R_\infty - R}{\tau} .$$

Now suppose the measurements reduce the resistance at the time of measurement in proportion to the resistance as in Figure 5. If this reduction is averaged over the time between readings, the differential equation becomes

$$\frac{\partial R}{\partial t} = \frac{R_\infty - R}{\tau} - \alpha R$$

where αR is the reduction due to the measurement. The asymptotic resistance then becomes

$$R'_\infty = \frac{R_\infty}{1 + \alpha\tau}$$

and the time constant becomes

$$\tau' = \frac{\tau}{1 + \alpha\tau} .$$

Hence, the life behavior is determined in part by the measurement, both as to the asymptotic resistance and the time constant.

This example has been used to stress a point made earlier, namely, that life data must be interpreted in terms of how the life tests are conducted and how the status of the tubes during life is determined. While life-test data on tubes periodically subjected to a current in excess of the operating current is of interest, it is also of interest to have data in which excess current is not drawn.

Conclusion

The reducing agents included in the base metal of oxide cathodes lead to the formation of insulating layers at the interface between the base metal and the oxide. The layer which forms when silicon is one of the reducing agents exhibits a resistance which is apparent early in the life of a tube and seriously impairs its performance in the course of time. Life data on tubes in practical applications is presented. It is found that tubes with 0.01 per cent silicon in the base metal develop an interface resistance of about 50 ohms for a square centimeter of cathode area and that tubes with 0.15-0.25 per cent silicon in the base metal develop an interface resistance of about 1000 ohms for a square centimeter of cathode area. These values are reached in about 10,000 hours after which the values remain more or less constant. The data extends to 22,000 hours.

Exploratory studies of the physical phenomena which account for the complex behavior of the interface layer are described. These studies lead to no firm physical model. However, they suggest certain precautions to be observed in making measurements of interface resistance if consistent results are to be obtained. The most important of these precautions is that measurements of interface resistance should be made at the cathode current at which the tubes normally operate; otherwise, the measurement itself may obscure the effect of the previous experience of the tube.

FACTORS IN THE DESIGN OF KEYED CLAMPING CIRCUITS*

By

ROLAND N. RHODES

Industry Service Laboratory, RCA Laboratories, Princeton, N. J.

Summary—*In the various signal-processing operations performed in the generation of the color television signal, it is sometimes necessary that the signals being processed possess their d-c component, and further be set at some definite d-c reference level. Keyed clamping circuits are usually employed to satisfy these requirements, and are commonly used for this purpose in such apparatus as linearity-correcting amplifiers, colorplexers, encoders, and stabilizing amplifiers.*

Several forms of keyed clamping circuits can be used. These include single, double, and quadruple diode types, as well as various triode types.[1] *At present, however, the most commonly employed clamp circuit is the double diode type, referenced against some fixed potential. The analysis in this paper is principally concerned with this particular circuit, but many of the results are applicable to the other forms of clamps.*

CIRCUIT DESCRIPTION

FIGURE 1a shows a typical keyed double diode clamping circuit as applied to a video amplifier chain. The video signal to be clamped, such as that of Figure 1b, appears at the plate of the amplifier T_{in}. This signal has lost its d-c component as can be deduced from the fact that its blanking level is not constant, but rather varies as a function of the video content in the signal. The clamping operation usually takes place during the latter part of the horizontal blanking period. At that time the clamping circuit is keyed on, and in effect "looks" at the video signal to see if its blanking level is constant and at a prescribed voltage. If it is not, the circuit operates to correct the situation, so that the video signal at the grid of T_{out} will appear as in Figure 1c.

The clamping circuit itself forms the grid return for T_{out} and consists of the circuitry associated with the diodes T_1 and T_2 and the triode driver T_3. A resistor R_i is commonly included in the circuit to help prevent the higher frequency components of the clamp keying pulses from appearing in the video signal on the grid of T_{out}. The diodes are connected in a bridge configuration. The lower arms of the

* Decimal Classification: R583.15.

[1] K. R. Wendt, "Television DC Component," *RCA Review*, Vol. IX, p. 85, March, 1948.

bridge consist of fixed resistors R_f and R_g, and a balancing potentiometer R_{bal}. The tap on R_{bal} is tied to the reference voltage E_3. The total resistance from this tap to point (b), the plate of T_2, is labeled R_2, and the total resistance from the tap to point (a), the cathode of T_1, is labeled R_1.

Clamping Operation

During the clamping interval a negative pulse is applied to the grid of the driver tube T_3 so that positive- and negative-going pulses appear across its plate and cathode loads respectively. These are the

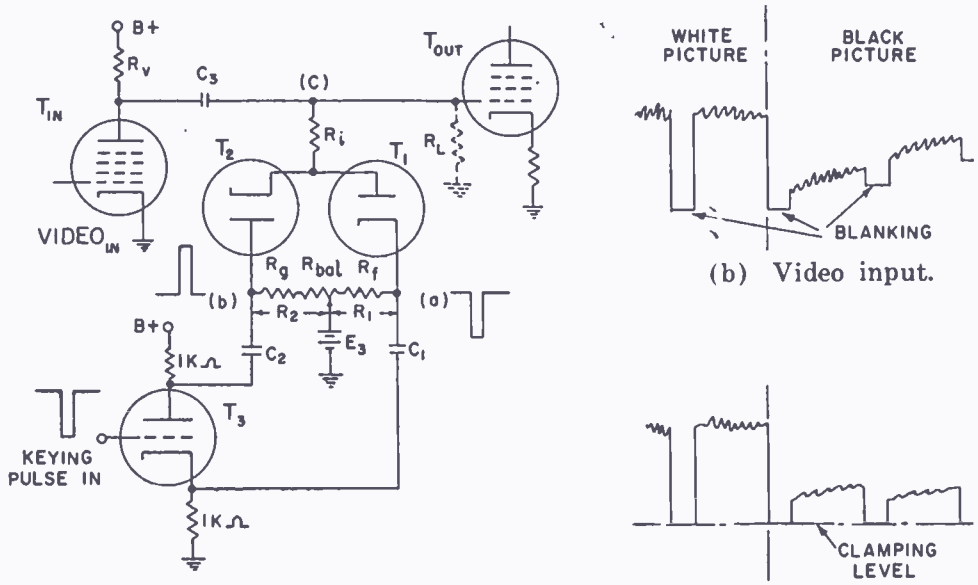

(a) Keyed clamping circuit.

(b) Video input.

(c) Video output.

Fig. 1—Keyed clamping operation.

clamp keying pulses. They are applied to the diodes causing them to conduct through the capacitors C_1 and C_2. Consequently, during the clamping interval electrons leave the upper plate of C_1, charging it in the positive direction, pass through the diodes, and enter the upper plate of C_2, charging it negative. This action develops a back bias voltage, approximately equal to the peak of the clamp pulses, across each of the capacitor–resistor combinations C_1R_1 and C_2R_2 of proper polarity to prevent diode conduction during the video interval.

The operation of the circuit when R_1 equals R_2 and the amplitudes of the keying pulses are equal, can be seen by considering what happens when a video signal which has lost its d-c component, such as that of Figure 1b, appears at the plate of T_{in}. As long as the blanking level of this signal is constant, the voltage during the clamping interval at the junction point (c) on Figure 1a remains the same as that of the

reference voltage E_3. Consequently, no charge flows into C_3 and any electrons leaving C_1 flow into C_2. However, when the picture content changes, as shown in Figure 1b, for example, the black level shifts upward and an unbalance voltage which is more positive than the reference voltage appears at the grid of T_{out} during the clamping interval.

Under these conditions, electrons are transferred from C_1 to C_3, so that the voltage of the blanking signal at the grid of T_{out} falls toward the reference voltage. If the video signal is such that its blanking level occurs at a voltage which is lower than the reference voltage, electrons are transferred from C_3 to C_2, and the voltage at the grid of T_{out} rises toward the reference voltage. In this manner, a clamping level equal to the reference voltage is maintained, and the d-c component is re-inserted into the video signal, which now appears at the grid of T_{out} as in Figure 1c. Undesirable low-frequency disturbances, such as hum or line bounce, are removed from the video signal by this same mechanism.

Clamp Level

It is usually necessary to set the clamping level at some specific voltage. This can be done by setting the reference voltage E_3 at the desired voltage, as discussed in the preceding section. However, the level can also be set by varying the relative sizes of R_1 and R_2 by means of a potentiometer such as R_{bal} of Figure 1.

In the latter case, the level setting takes place as follows: when the two diodes conduct during the clamping interval, the two capacitors charge in series, so that the electron charge is the same for both. Consequently, under equilibrium conditions they must each discharge an equal number of electrons through R_1 and R_2. If the two discharge resistors are equal, the voltage developed across them will be equal and opposite, and the clamping level will be equal to the reference voltage. However, when R_{bal} is adjusted so that R_1 and R_2 are not equal, the voltage across each of them will be proportional to their resistance. For example, if the tap on R_{bal} is moved to the left, R_2 decreases and R_1 increases, thereby making point (a) more positive and point (b) less negative. Consequently, the potential of the entire bridge circuit, and the resultant clamp level, is moved in the positive direction.

Effects of Leakage

The preceding analysis assumed that the resistance looking into the complete circuit from point (c) on Figure 1a was substantially infinite. However, under certain operating conditions, such as when there is leakage across the diodes or C_3 or when gas current or grid

emission occurs in T_{out}, the resistance looking into the circuit from (c) may be reduced sufficiently to affect the d-c level set by the clamp. This leakage resistance, labeled R_L, is drawn dotted in Figure 1a, and for purposes of analysis is shown returned to ground. Its value is usually not stable, but rather varies as a function of such things as ambient temperature and humidity, equipment warm-up conditions and other factors. Consequently it must be given due consideration in circuits where a high degree of stability of clamp level is required. In order to evaluate this effect, as well as some of the others which contribute to the stability problem, a more comprehensive analysis of the circuit is required. The analysis presented here, while not completely rigorous, yields results that are generally applicable within the limits of operating conditions usually encountered in television systems. It is based on conservation of the charge on the three capacitors involved in the circuit. As examples of the method, consider the cases

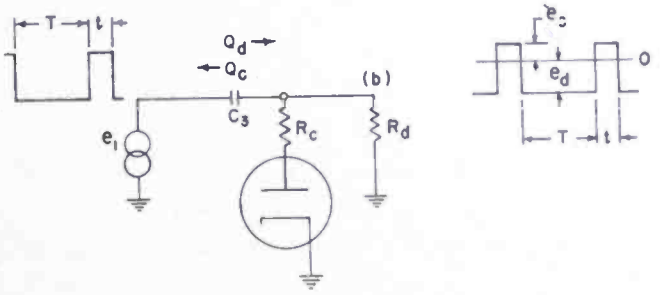

Fig. 2—D-C restorer.

of two somewhat simpler but closely related circuits—the d-c restorer, and the pulse peak detector.

D-C Restorer

Figure 2 shows a d-c restorer operating on a train of narrow pulses. The restorer is idealized to the extent that all the resistance in the charge path of the coupling capacitor C_3 is placed in series with the diode. If it is assumed further that the charging time constant R_cC_3 is long compared to the pulse-on period t, and the discharge time constant R_dC_3 is long compared to the pulse-off period T, and that t is much smaller than T, the d-c restored pulses appear at the point (b) as shown. The problem is to determine the amount by which the peaks of the pulses overshoot the reference potential, which in this case is ground. Since restoration takes place with respect to ground, the diode conducts and C_3 charges a number of electrons, Q_c, through R_c when the pulse goes above ground. During the rest of the interval the diode is cut off, and C_3 discharges a number of electrons, Q_d, through R_d.

The overshoot required for charging C_3 is the voltage labeled e_c and the discharge voltage is labeled e_d. Consequently,

$$Q_c = \frac{e_c}{R_c} t \tag{1}$$

$$Q_d = \frac{e_d}{R_d} T. \tag{2}$$

At equilibrium, $Q_c = Q_d$, and therefore

$$\frac{e_c}{e_d} = \frac{R_c}{R_d} \left(\frac{T}{t} \right) \tag{3}$$

Equation (3) is the d-c restorer equation. It depends on the fact that the amount of charge entering C_3 during t equals the amount leaving it during T under steady-state conditions. The lower the ratio e_c/e_d, the more efficient the d-c restorer at maintaining black-level. The controlling factors are the ratios of the charge-to-discharge path resistance and the discharge-to-charge time.

If it is assumed that all the charge path resistance is in the source, and that the diode has zero forward resistance, the voltage at (b) cannot rise above 0. However, the voltage e_c is still required to charge the capacitor, and under these conditions it will be developed across the source resistance. The result is that the value of e_d in the output remains the same as that called for in the equation, but that e_c is clipped off and will not appear in the output. Since ordinary d-c restorers have both source and diode forward resistance, some clipping of the signal always takes place, and it becomes increasingly severe as the ratio of the required charge voltage e_c to the discharge voltage e_d increases.

Pulse Peak Detector

Figure 3 shows a pulse peak detector. The time-constant assumptions are the same as in the previous case. The input pulses are shown at point (a) and the rectified output at (b). In this case the voltage available for charging C is equal to the difference in amplitude between the pulse height e_1 and the detected output E_2. The equations are set up in the same way as in the d-c restorer case by equating the charge and discharge of the capacitor C.

$$Q_c = \frac{e_1 - E_2}{R_c} t \tag{4}$$

$$Q_d = \frac{E_2}{R_d} T. \tag{5}$$

At equilibrium, $Q_c = Q_d$, and therefore

$$E_2 = e_1 \frac{R_d}{R_d + \frac{T}{t} R_c} \tag{6}$$

Equation (6) is in the form of a resistance voltage divider equation. The principal feature of this equation is the fact that the charge resistance R_c is multiplied by the ratio of discharge-to-charge times, and consequently appears to be a much larger resistor than it actually is.

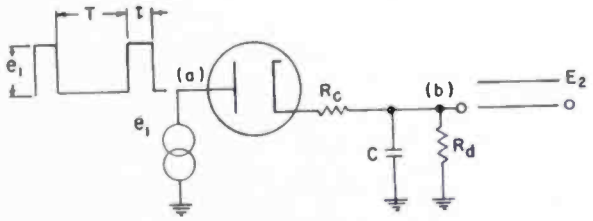

Fig. 3—Pulse peak detector.

Analysis of Keyed Clamping Circuits

With the preceding examples as background, further consideration can now be given to the loaded keyed clamp. The circuit is shown in Figure 4a, redrawn for purposes of analysis. The parenthetical circuit values are more or less typical. Two equal amplitude push-pull pulses labeled e_{+p} and e_{-p} are supplied by the generators shown. The two equal resistors, both labeled R_a, are the sums of the diode forward resistance and pulse source impedance in the two branches of the circuit. Again it is assumed that the various RC time constants are long compared to the duration of the pulses which act on them, and in addition, that R_1 and R_2 are both much larger than R_a, and that the leakage resistance R_L, though not infinite, is much larger than R_1 and R_2.

The circuit equations are set up in the same general way as in the two preceding cases. First we may note that when the circuit is in equilibrium the individual charge and discharge of each of the three

capacitors C_1, C_2, and C_3 must be equal. In addition, the sum of the charges on these three capacitors is constant. Consequently the first group of equations is

$$\begin{aligned} Q_{c1} &= Q_{d1} \\ Q_{c2} &= Q_{d2} \\ Q_{c3} &= Q_{d3} \\ Q_{c2} &= Q_{c1} + Q_{c3}. \end{aligned} \tag{7}$$

wherein the subscript c refers to the charge flowing during the pulse-on period t, and subscript d refers to the discharge flowing during the pulse-off period T. The numerical subscripts 1, 2, and 3 refer to the capacitors C_1, C_2 and C_3 respectively.

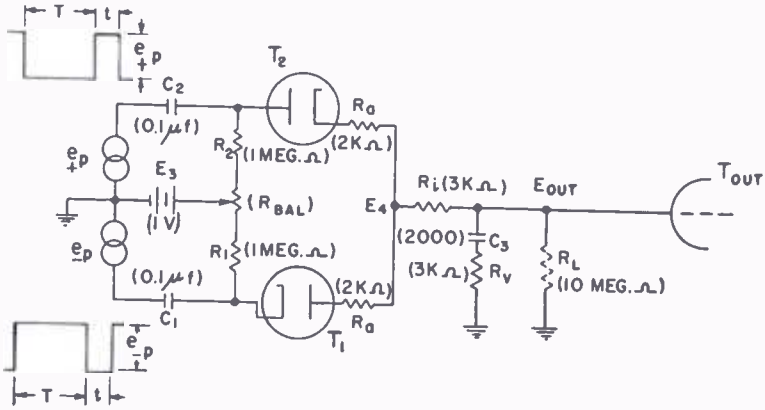

(a) Keyed clamping circuit.

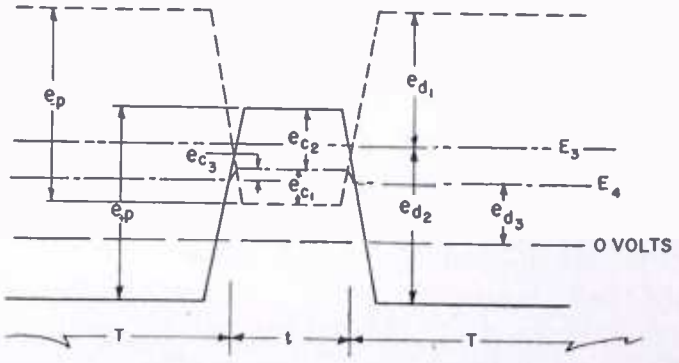

(b) Details of clamping pulses.

Fig. 4—Effects of leakage on clamping operation.

In order to obtain the required additional equations, the various voltage drops around the circuit due to the presence of the clamping pulses e_{+p} and e_{-p} are summed. Figure 4b is a somewhat exaggerated, expanded view of the pulses as they appear at the points labeled (1)

and (2) of Figure 4a, relative to the various d-c voltages involved in the circuit. In this figure E_3 was assumed to be some fixed positive potential above zero volts. The presence of the leakage resistance R_L causes the output voltage E_4 to be somewhat lower than it would be under open-circuit conditions. Considering the positive-going pulse which operates on T_2, it can be seen that T_2 will conduct when the pulse goes above the value of E_4. During this conduction time, the voltage E_4 rises due to the peak current flowing through R_v and R_i. This rise in voltage e_{c3} is the voltage available to charge C_3. The portion of the pulse voltage available for charging C_2 is then the difference between this peak voltage of E_4 and the peak voltage of the positive clamp pulse e_{+p} and is labeled e_{c2}. Similarly, the voltage available for charging C_1 is the difference between the peak voltages of E_4 and the negative clamp pulse e_{-p} and is labeled e_{c1}.

The discharge voltage of C_3, labeled e_{d3}, is substantially equal to the clamp output voltage E_4. Since during the discharge time T the diodes are nonconducting, C_1 and C_2 both discharge toward E_3, resulting in the discharge voltage e_{d1} and e_{d2} shown in the figure.

By adding up the voltages on the positive and negative pulses, the following two equations are obtained:

$$e_{+p} = e_{d2} - (E_3 - E_4) + (e_{c2} + e_{c3}) \tag{8}$$

and

$$e_{-p} = e_{d1} + (E_3 - E_4) + (e_{c1} - e_{c3}). \tag{9}$$

From Equations (7), (8), and (9) and the methods used in developing Equations (3) and (6), it can be shown that

$$E_4 = \frac{E_3 + e_p \dfrac{R_1 - R_2}{R_1 + R_2 + 2R_a\tau}}{1 + \dfrac{R_s\tau}{R_L} + \dfrac{1}{R_L}\left[\dfrac{(R_2 + R_a\tau)(R_1 + R_a\tau)}{R_1 + R_2 + 2R_a\tau}\right]} \tag{10}$$

where $\tau = T/t$, R_a is the combined pulse source and diode forward resistance, R_s is the sum of the video source resistance R_v and isolation resistance R_i, and R_L is the leakage resistance.

The expression

$$\frac{(R_2 + R_a\tau)(R_1 + R_a\tau)}{R_1 + R_2 + 2R_a\tau}$$

is the parallel resistance of $R_1 + R_a\tau$ and $R_2 + R_a\tau$ and can be represented by R_p. Since E_4 is substantially equal to the clamping level E_{out}, we have

$$E_{out} = \frac{E_3 + e_p \dfrac{R_1 - R_2}{R_1 + R_2 + 2R_a\tau}}{1 + \dfrac{R_p + R_s\tau}{R_L}}. \qquad (11)$$

Equation (11) is the clamping circuit equation.

Design Considerations

The clamping circuit equation is useful in bringing out many of the factors involved in the design of the circuit, especially insofar as stability of operation is concerned. For example, with the component values shown in Figure 4, if the ratio of pulse-off to pulse-on time (τ) is 40, and the bias voltage (E_3) is +1 volt and the leakage resistance (R_L) is substantially infinite, the clamping level (E_{out}) is also +1 volt. However, if for some reason a leakage current of one-tenth microampere flows, the effective leakage resistance drops to approximately 10 megohms, and the calculated clamping level drops to approximately 0.93 volt. This voltage will probably not be stable since it is dependent on the value of the leakage resistance.

It can be seen from the equation that in order to minimize the drift effects of R_L, the right hand term in the denominator should be very small compared to unity. This requires that leakage resistance R_L be large, and the $R_p + R_s\tau$ term be small. Insofar as R_L is concerned, leakage in the coupling capacitor C_3, the diodes, and the tube sockets can cause trouble in isolated instances, but these troubles can be avoided by employing reasonably high-quality components in the circuit. However, a more serious problem exists in those instances when it is necessary to clamp the grid of a tube of a type which is prone to either gas currents or grid emission. Under these conditions the effective value of R_L may be sufficiently low to cause clamp level instability. In many cases it is possible to increase R_L by running the tube "cool," that is, by operating the tube well within its rated dissipation and by reducing its filament voltage toward the lower limit of the manufacturer's tolerance.

Insofar as the $R_p + R_s\tau$ term is concerned, it is desirable to make it small. This requires that τ be as small as possible, that is, the clamp pulse be as long as the particular operating conditions permit. More-

over R_s, which is the sum of the video source resistance R_v and the isolation resistor R_i, and R_p, which is a combination of the resistors R_1, R_2 and $R_a\tau$, should be made very small compared to the leakage resistance R_L.

There is, of course, a lower limit to the values of these resistances due to other factors. For example, the factor which usually determines the lower limits of R_1 and R_2 is the amount of clamp pulse power available. This results because the clamp pulse source resistance in an actual circuit has some finite value, and as R_1 and R_2 are lowered, C_1 and C_2 discharge more heavily so that the peak charge current supplied to the diodes must also increase. Consequently the pulse source is more heavily loaded and the pulse voltage drops. It may be noted that since the diode forward resistance follows a three-halves power law, it decreases with increasing peak current. Consequently, R_a is lowered as the resistances of R_1 and R_2 are reduced, a factor which is beneficial insofar as clamp circuit stability is concerned.

The lower limit of clamp pulse voltage required depends on the largest amplitude video signal to be clamped. In order to prevent video signals from causing the diodes to conduct, the back bias voltages must be at least as large as the largest video signals; consequently the clamp pulses themselves must be at least this large and perhaps be 25 to 50 per cent larger. Keeping the clamp pulse height within these limits is desirable since it minimizes the amount of spurious clamp signal which can appear in the video signal and therefore permits the use of a small isolation resistor. In addition, as can be seen from the fraction in the numerator of the clamping circuit equation, increasing the pulse height makes the clamp output level more sensitive to a possible drift in the resistance values of R_1 and R_2. As a final observation, it may be noted that the fraction in the numerator of the equation also indicates one difficulty associated with setting the clamp level by varying the relative sizes of R_1 and R_2, namely, that the clamp level becomes sensitive to variations in clamp pulse amplitude.

MONOCHROME VIDICON FILM CAMERA*

By

W. L. Hurford and R. J. Marian

Engineering Products Division, Radio Corporation of America, Camden, N. J.

Summary—The Vidicon tube found its initial applications in the field of industrial television; however, its inherent characteristics coupled with the rapid advancement made in minimizing its limitations has made its use for regular broadcast television rather attractive. A television camera has performance characteristics dictated by the combination of the tube characteristics and the modification of those characteristics which are possible with the associated circuitry. These characteristics and the means taken in a film camera chain to exploit or modify the characteristics are the subject of this paper. The desirable features of the Vidicon and the circuit techniques to be discussed have combined to produce film pickup equipment representing a new high in the quality of film reproduction for television broadcasters.

Signal-to-Noise Ratio

THE Vidicon tube is characterized by very good signal-to-noise (S/N) ratio. The noise output of the Vidicon itself is that of a temperature-limited diode with a plate current equal to the signal electrode current of the Vidicon. This relationship is true for those cases where the current to the output element of a tube is small compared with the total beam current or cathode current.[1] Since the noise output of the Vidicon is very low, the S/N ratio of the film chain will be determined almost entirely by the characteristics of the video preamplifier. The input stage of the preamplifier consists of a 417A and a 12B4 in a cascode circuit. Such an arrangement has the good noise properties of a high g_m triode and the input impedance characteristics of a pentode. Miller-effect capacity at the input of the 417A is very small because the plate load, which is the driving point impedance of the cathode of the 12B4, is very low and hence very little signal voltage appears at the plate of the 417A. The stage gain, however, is high, being equal to the product of the transconductance of the 417A and the plate-load resistance in the plate circuit of the 12B4. The signal level is thus greatly increased and the favorable S/N ratio preserved. This good S/N ratio allows the application of aperture correction which may be used to improve the horizontal resolution.

---

* Decimal Classification: R583.12.

[1] Stanford Goldman, *Frequency Analysis, Modulation, and Noise*, McGraw-Hill Book Company, Inc., New York, N.Y., 1947; Ch. 7.

Aperture correction, which is a phase distortionless boosting of the high-frequency components of a signal, boosts the noise as well as the signal. The high-frequency S/N ratio is ordinarily rather poor compared to the S/N ratio at low frequencies. This is due to the loss of high-frequency signal components in the inevitable capacity shunting the camera-tube load resistance. For this reason aperture correction is acceptable only in a system having very good S/N ratio.

Aperture Correction

The response of the Vidicon in terms of television lines is plotted against zero line number as 100 per cent response in Figure 1. A frequency scale corresponding to line number is also shown in this figure.

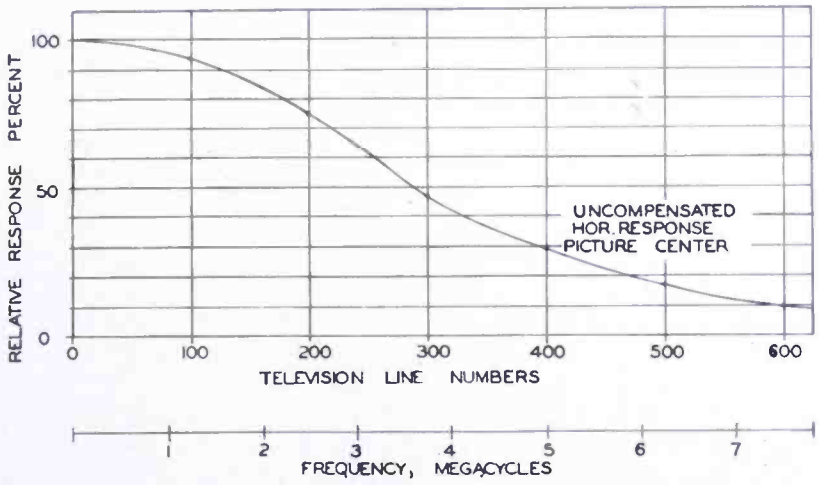

Fig. 1—Aperture characteristic of type 6326 Vidicon tube.

It is the reciprocal of this curve which should be applied to compensate for the aperture characteristic of the Vidicon tube. The Vidicon output signal versus frequency as modified by Vidicon output and preamplifier input capacity is also a curve similar to this; however, it should be compensated for by a network which is the dual of the effective parallel RC network at the Vidicon signal electrode, and not by the aperture correction circuit.

The aperture correction circuit employs an unterminated artificial transmission line driven from a source impedance equal to its characteristic impedance. The sending-end voltage is then[2]

$$e_s = e_g \cos\theta \angle -\theta$$

[2] R. C. Dennison, "Aperture Compensation for Television Cameras," *RCA Review*, Vol. XIV, pp. 569-585, December, 1953.

where θ is the line length in radians and e_g is the generator voltage. The receiving-end voltage is

$$e_r = e_g \angle -\theta$$

It is thus evident that the sending-end voltage and the receiving-end voltage are in phase for all frequencies, and may be combined in varying proportions to give various amounts of high-frequency boost without any consequent phase distortion. This fact is used to give a rising response characteristic such as one of those shown in Figure 2.

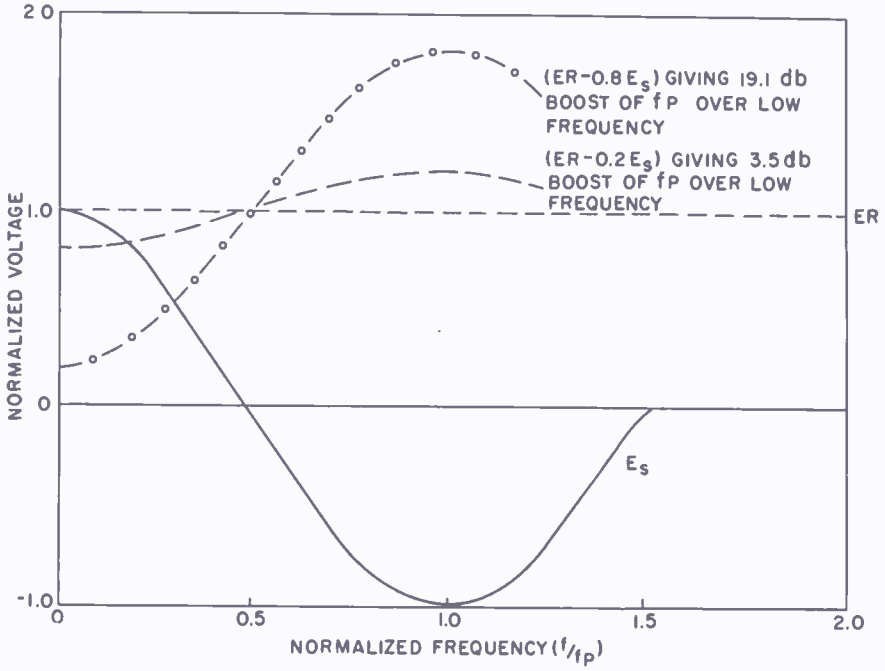

Fig. 2—Response curves obtainable from delay line type aperture correction circuit.

The combination of the proper rising response curve of Figure 2 with the Vidicon response curve of Figure 1 will give an over-all response curve which is approximately compensated or may even be peaked at the high-frequency end. As indicated in Figure 2, the sending-end and receiving-end voltages may be combined in various proportions to give various amounts of boost of the peaked frequency, f_p, over the low-frequency end of the spectrum. The choice of peaking frequency (determined by the electrical length of the line) and ratio of e_s/e_r is made to give a curve approximately the reciprocal of the Vidicon response curve up to the peaking frequency, f_p. f_p is ordinarily chosen at about 5 megacycles in order not to boost high-frequency noise excessively. Actually, of course, the Vidicon aperture is not the only

aperture in the over-all system. Equalization for the kinescope aperture could also be introduced at this point. Beyond the partial compensation for the scanning apertures which is thus provided, the use of additional phase-distortionless high-frequency boosting will "snap up" the picture detail.

Employed in this way, there will be small anticipatory and trailing overshoots and ringing due to the pass-band limitation. The effect, in the picture, is to frame dark areas with a fine white line, greatly enhancing the fine detail. For this reason the aperture correction circuit is provided with a tap switch allowing the selection of one of four different amounts of aperture equalization according to the needs of the system and the taste of the operator.

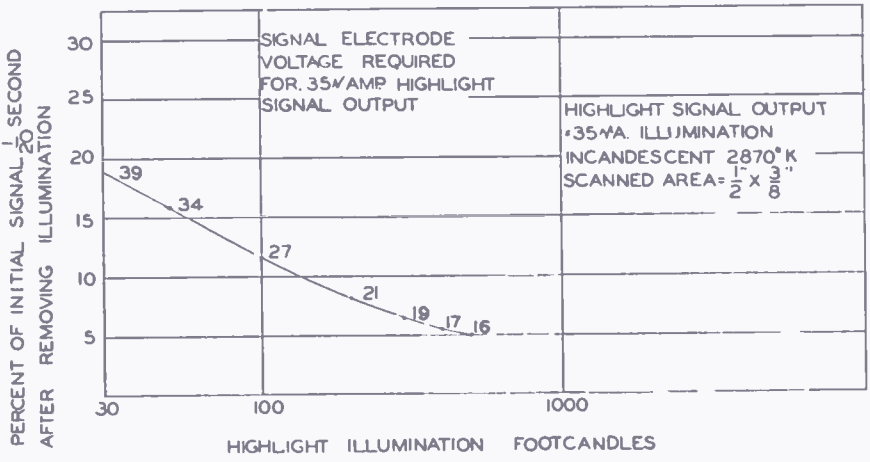

Fig. 3—Lag characteristic of type 6326 Vidicon tube.

Picture Lag and Flare

Lag is the persistence or retention of an image following the removal of the incident illumination, and is ordinarily measured as the per cent response at some time after removal of illumination to the response with illumination. Early Vidicon tubes showed a very marked picture lag. Tube improvements and better operating techniques have combined to reduce the lag problem to the point where the lag characteristic is satisfactory for film use. The lag characteristic of the Vidicon is shown in Figure 3 as a plot of per cent of initial signal at the end of 1/20 second versus highlight illumination. We may note, from this curve, that the lag is reduced from 19 per cent response after 1/20 second when the highlight illumination is 30 foot-candles to 7 per cent when the highlight illumination is 300 foot-candles. Intense highlight illumination is easy to obtain in the 0.625-inch diagonal normally projected on the face of the Vidicon, so that reasonable lag characteristics are available with the usual television projectors. We

may also note from Figure 3 that the signal electrode voltage needed to obtain a highlight signal output of 0.35 microampere decreases with increasing highlight illumination. If this information is used with the graph of the ratio of signal current to dark current versus signal electrode voltage which is plotted in Figure 4, it is seen that this ratio is raised from 15 to 1 up to 53 to 1 by going from a highlight illumination of 30 foot-candles to 300 foot-candles and adjusting to maintain the same signal current. The dark current is related to the "flare" signal, which is a spurious signal originating in the Vidicon tube itself. The larger ratio obtained with more intense highlight illumination in this example corresponds to a flare signal which is but a small percentage of peak-to-peak video. It is thus evident that operation at

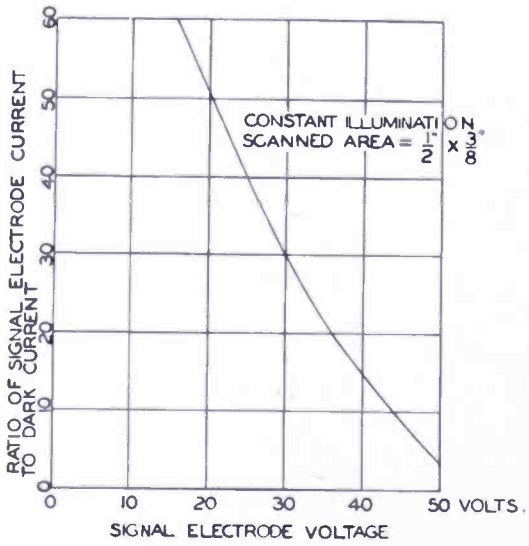

Fig. 4—Signal versus dark current characteristic of type 6326 Vidicon tube.

low target voltage and intense highlight brightnesses will produce a signal with satisfactory lag and "flare" characteristics. In discussing the lag characteristics of the Vidicon, it is of interest to note that lag, if not so long as to cause a noticeable tailing, is actually advantageous. In particular, it is the lag characteristic of the human eye which gives the sensation of motion from a series of still pictures, and in this application of the Vidicon, lag operates to limit the ratio of signal output during the time the face of the Vidicon is illuminated, to the signal output following the removal of illumination. Holding this ratio down helps in two ways. In the first place it greatly reduces the danger of overdriving any of the grids of the video amplifiers, and in the second place it makes possible the use of nonsynchronous projectors with long application time. In other words, it makes possible the use of ordinary movie projectors not specifically designed for

television use. However, some applications may find that the resultant 12 cycle flicker is excessive.

Shading

Of particular note, among the desirable characteristics of the Vidicon, is the fact that, since it is a photoconductive device rather than a photomissive one, it is free from the charge redistribution effects which exist in the iconoscope and the image orthicon. This allows the generation of an absolute black level in the output signal and greatly reduces the shading problems. In contrast with the iconoscope, there is no need for back and edge lighting of the scanned area. It is also worthy of note that the combination of very good S/N ratio and an absolute black level will produce a picture source very much better than previous type cameras for special effects applications such as the montage, where keying signal is produced from picture video.[3]

Transfer Characteristic

There is one other characteristic in which the Vidicon is quite different from other camera tubes and that is its transfer characteristic. The Vidicon transfer curve on a log log plot is nearly straight over a very wide range and shows no "knee" such as is obtained with the image orthicon or the iconoscope. The transfer characteristic of the Vidicon is shown in Figure 5. It is seen that the average slope of the transfer curve is about 0.65. In general, the effect of such an extended transfer characteristic is to give pictures of high contrast and range in the studio where the incident lighting is controlled and where the monitors have good highlight reproduction capability. The brightness range may, however, be somewhat excessive for the home receiver where the incident illumination is relatively high and the highlight capability low. It has been standard practice[4] to make the gamma of motion picture film lie between about 1.4 and 2.0 to make up for the loss of color. Using film of this type, it would be desirable for the over-all television system to have a gamma of about unity. (A gamma of 1.0 would be too low for studio or field use.) The gamma factors of the Vidicon and of the kinescope are fortunately somewhat complementary (0.65 for the Vidicon and about 2.0 for a kinescope under favorable conditions). The over-all gamma, assuming that the rest of the system is linear, would then be approximately 1.3. This

---

[3] W. L. Hurford, "Combined Special Effects Amplifier for TV," *Tele Tech*, pp. 50-94, November, 1951.

[4] I. G. Maloff, "Gamma and Range in Television," *RCA Review*, Vol. III, pp. 409-417, April, 1939.

figure may still be high for some home viewing conditions, resulting in compression of picture blacks. Because of this it may be desirable to modify the transfer characteristic of the equipment at the station to provide a gamma less than unity.

Optics

The small size of the Vidicon tube makes possible a small camera which is readily adaptable to a variety of mounting and multiplexing arrangements. The small picture diagonal also makes it easier to get fast lenses with short focal length. The short focal length gives a greater depth of focus than longer focal length lenses, facilitating setup of the optics in a multiplexing arrangement.

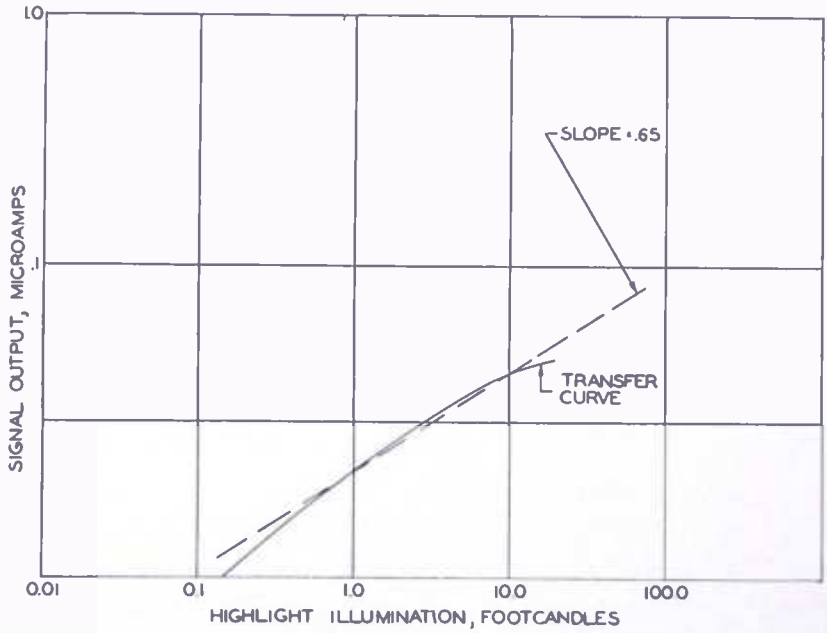

Fig. 5—Vidicon transfer characteristic.

Spurious Signals

One bothersome characteristic of the Vidicon tube is the generation of a spurious white signal at the edges of the scanned area. This signal is generated at all four sides of the scanned area but only shows up at the bottom of the picture when no steps are taken to eliminate it. This white signal does not show at the top or the left side of the picture because both horizontal and vertical flyback are complete and the forward trace has begun before the beam is unblanked. That is, the white signal has been generated but was covered by camera blanking. The white line at the right hand side of the picture is delayed by the amount of the camera cable delay and is then covered by the receiver

blanking so that it does not appear in the transmitted picture. The white line at the bottom of the picture although of the same width physically, on the photosensitive surface, is on a different time scale. It is about 2 or 3 lines in duration, hence camera cable delay and receiver blanking cannot operate to blank it out as they do for the right hand side. The manner of elimination on left, top and particularly the right hand edge, however, point the way for elimination of the line at the bottom of the picture. It is only necessary to delay vertical drive feeding the vertical sweep generator and also the vertical component of camera blanking so that standard receiver blanking will cover the white line generated by the camera.

The Type TK-21 Vidicon Film Camera Equipment

The TK-21 Vidicon film camera equipment was designed around the type 6326 Vidicon film pickup tube. The superior performance of this tube for film pickup use leaves little doubt but that the Vidicon tube will meet with universal acceptance in the field of television broadcasting. The major networks, as well as a number of stations in the field, are using this or a prototype of this equipment with success. The results have been such that it is difficult for an observer in the home to detect the difference between a "live" and a film broadcast.

Early in the design stage of this equipment, a decision was made to make the camera as small as consistent with good performance, to place only those components which were absolutely necessary in the camera, and to locate the remainder of the electronic circuitry in a standard rack where accessibility is at a maximum and where ventilation problems are at a minimum. Additionally, a control panel, which makes use of d-c controls, was to be located externally from the rack. This has been done in the design of the TK-21 film camera equipment.

This equipment consists of a Vidicon camera, a Vidicon control chassis, a Vidicon deflection chassis, a remote control panel, a master monitor, and two regulated power supplies. A block diagram of the film chain is shown in Figure 6.

Vidicon Camera

A side view of the camera with the cover removed is shown in Figure 7. The Vidicon tube, along with the deflection components, is located in the lower half of the unit. The video amplifier is located on a heavy, shock-mounted chassis at the top toward the front, while the blanking amplifier is located on the main chassis toward the top rear of the camera. The camera is connected to the rack-mounted units by

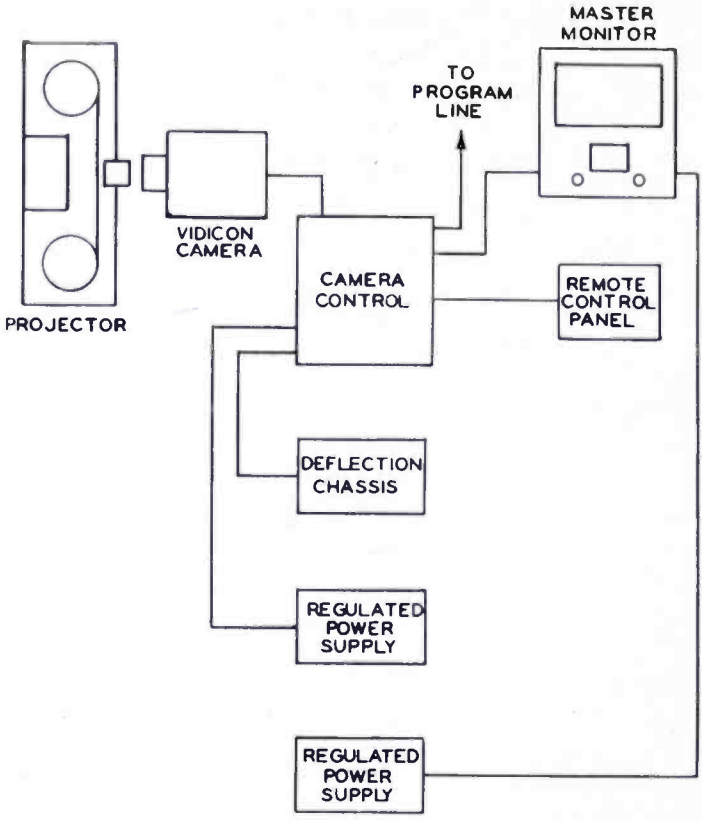

Fig. 6—TK 21 Vidicon film camera equipment.

means of a 24-conductor cable, three of the conductors being coaxial lines. The cable and connector are visible in Figure 7.

The output of the Vidicon feeds a cascode amplifier which makes use of a Type 417A high-transconductance triode as the input tube

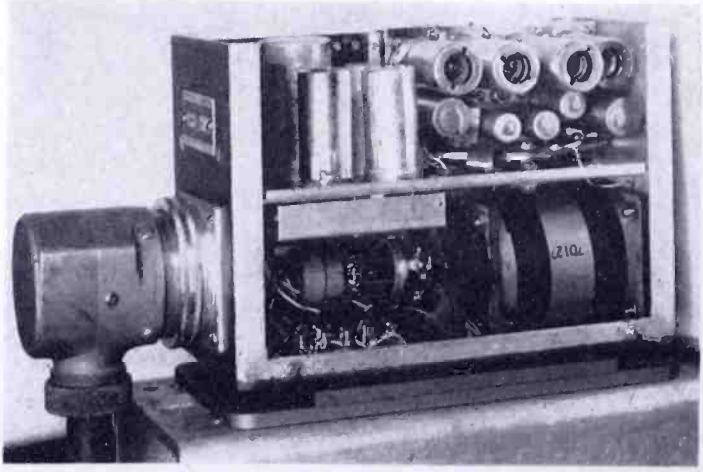

Fig. 7—Side view of the Vidicon camera with cover removed. The Vidicon tube and deflection components are located in the lower half of the camera. The video amplifier sub-chassis is located on the forward half of the shelf.

and a 12B4 high-perveance triode as the output tube of the amplifier. It is necessary to operate the 417A at the upper limit of its rated current to realize the g_m of approximately 25,000 micromhos. With this high g_m tube, heater voltage variations will result in tube current changes, which in turn vary the gain of the stage. A method of gain stabilization is used in the cathode circuit of the cascode stage as well as the following stage. The gain of the stages is within ±5 per cent over a +10 to —20 per cent change of heater voltage. It is interesting to note that, without gain stabilization, a —10 per cent change in heater voltage will drop the gain by about 40 per cent. To accomplish this stabilization, the cathode resistance is increased by about ten times normal value. The grid resistor is returned to a positive voltage to set the tube to the required operating plant. The cathode circuit then tends to hold the tube current to a constant value.

A cathode follower stage and a high-peaker stage in series, an arrangement which makes double use of the current, follows the cascode preamplifier. Because of the low input capacity of the cathode follower which is d-c coupled from the input stage, greater gain for a given bandwidth is realized from the cascode stage. An actual gain of approximately sixty for a bandwidth of 8 megacycles is realized from this amplifier. Following the high-peaker stage is a feedback type output stage which feeds .75 volt, peak-to-peak, to a 51-ohm line terminated at the Vidicon camera control chassis.

A composite blanking signal from the control unit is amplified and coupled to the cathode of the Vidicon to blank out the beam during the vertical and horizontal retrace time.

The deflection components are mounted along with various decoupling resistors and capacitors in the lower half of the camera, which is shown in Figure 7. Since the deflection driving tubes are located remotely from the camera, the horizontal and vertical windings of the deflection yoke function as terminations of transmission lines. In the horizontal case, the winding is a part of a constant impedance network which terminates a 51-ohm coaxial line while the vertical winding terminates directly an open wire pair in the camera cable. The deflection yoke is so designed that the horizontal and vertical windings may be rotated with respect to each other in initial adjustments for a minimum of geometric distortion. The focus coil is universally wound to achieve a highly uniform focus field for the Vidicon.

A heavy 1/16 inch thick mu-metal cylindrical shield, which has been hydrogen annealed after fabrication, encloses the focus coil. The purpose of this cylinder is twofold: to shield the Vidicon from stray fields, and to provide a return path for the deflection field. The align-

ment coils are located behind the focus coil over the end of the Vidicon gun structure and are used to orient the electron beam in the desired direction.

Vidicon Camera Control Chassis

The function of the camera control is to process the signal from the camera in such a manner that the output signal is in a form to feed directly to the modulator of a television transmitter. Some of the functions of the unit may or may not be used. Consider now the Vidicon camera control chassis, which is shown in Figure 8. The top unit is the camera control chassis, while the lower is the deflection

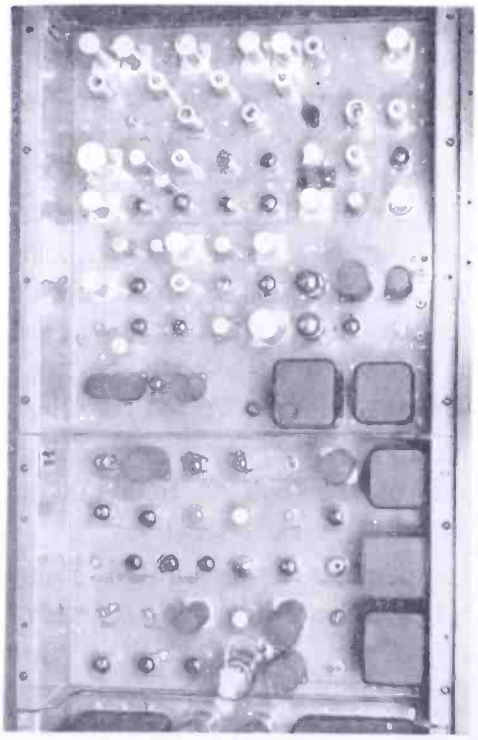

Fig. 8—The camera control chassis, upper unit, and deflection chassis, lower unit, mounted in standard rack.

chassis. The output line from the camera is terminated and the signal amplified in the first stage of this unit. A second high-peaker stage, which supplements the one in the camera and which compensates for short time constant streaking, follows the input stage. A gain-control stage follows, which is controlled by d-c from a gain control located on the remote control panel. The aperture circuits follow; these consist of a line driver, a delay line, and a mixing amplifier where fixed amounts of high-frequency boost may be added to the signal as desired. To accommodate both positive and negative film materials, both polari-

ties of video signal are made available by the following phase splitter stage. A video relay controlled from the remote control panel selects either plate or cathode output.

Next is a blanking modulator and clipping amplifier. The grid of this tube is clamped while the standard blanking signal is mixed in the cathode circuit. The blanking clipping function occurs in the plate circuit of this stage. The following video amplifier stage feeds a combination of several tubes which form a feedback-type output stage. Three low-impedance and well isolated outputs make possible input and output terminations of outgoing lines. Synchronizing signals may be mixed with two of these outputs. Several other stages which will not be discussed include a clamp pulse generator; synchronizing, setup, and blanking amplifiers; a bias voltage rectifier; and a bias voltage regulator.

A Vidicon picture without aperture compensation tends toward a soft appearance due to the aperturing effect of the scanning beam. A curve showing this effect is presented in Figure 1. Note that at 400 television lines or 5 megacycles the response is down to 30 per cent of the low-frequency response. In the Vidicon camera control, aperture compensation is added which brings up the "snap" and detail of the picture to exceed that of other pickup devices.

Deflection Chassis Unit

The primary function of the deflection chassis unit is to supply deflection and blanking voltages to the Vidicon camera. In addition, the unit includes a focus current regulator, a signal electrode current amplifier, and a Vidicon protection circuit. The chassis in the lower half of Figure 8 is the deflection chassis.

Horizontal driving pulses received from the synchronizing generator are amplified and differentiated, and the leading edge of the pulses are used to trigger a stabilized multivibrator circuit. The multivibrator circuit produces a driving pulse the width of which is adjustable to key a sawtooth generator. The width and amplitude of this generated drive pulse is practically independent of the amplitude and width of the incoming drive pulse from the synchronizing generator. The amplitude and width of this incoming pulse may vary from less than 50 to over 150 per cent of normal value without affecting the output of the multivibrator. The output of the sawtooth generator is amplified and fed to the grid of a 6CD6 tube operating in class A. The output is transformer coupled to a 51-ohm line which feeds the camera deflection yoke. Feedback from the plate of the output stage to the cathode of the previous stage is utilized to improve linearity,

which in this chain is accurate to within ±1.5 per cent of picture height.

The vertical deflection section of this unit must furnish deflection power which is delayed about 200 microseconds with respect to the vertical driving pulses from the synchronizing generator. The purpose of this delay is to eliminate the white line that normally occurs at the bottom of a Vidicon picture. A simplified combination pulse delay and sawtooth generator circuit is utilized in this unit.

The vertical-drive signal is applied through a diode to trigger a multivibrator, which generates a delayed drive pulse as well as a sawtooth voltage. This voltage is fed to the vertical output stage which is a cathode follower, the output line being connected in the cathode circuit. Feedback is used in the form of a voltage from the output cathode fed back to the center of the sawtooth charging resistor. The voltage reference to which the sawtooth capacitor charges varies with the sawtooth being generated. The output sawtooth, rather than being an exponential curve, is nearly linear, which results in vertical deflection linearity accurate to within ±1 per cent of picture height.

The purpose of the Vidicon blanking pulse is to render the beam active only during the forward scan. Normally, vertical and horizontal driving pulses are mixed and used for camera blanking. However, in the case of the Vidicon, the vertical pulse must be delayed, and it is desirable that the horizontal pulse be somewhat wider than retrace time.

In the vertical case, a delayed positive pulse is available from the multivibrator circuit. One of the waveforms of the horizontal multivibrator circuit has a sharp rise time and a relatively long decay time. By using this pulse in an adjustable clipper circuit, a pulse is obtained with a fixed leading edge and an adjustable trailing edge. This width is adjusted to cover up the horizontal deflection retrace. The two vertical and horizontal pulses are combined and fed to the camera through a coaxial line.

A Vidicon protection circuit is provided to prevent damage to the tube in case of deflection failure. In the vertical case, voltage across the yoke is amplified and rectified, and in the horizontal case, the large pulses across the primary of the horizontal output transformer are rectified. These two d-c voltages are utilized to bias on a 6AS6 tube in which a relay is connected in the plate circuit. Loss of either one of the voltages biases off the tube which causes the relay to drop out. This removes the wall voltage and grounds the wall electrode of the Vidicon causing the beam to become completely defocussed, preventing damage to the signal electrode.

Current to the focus and alignment coils in the Vidicon deflection yoke assembly is supplied from the deflection chassis unit. The voltage across a series resistor is applied to a direct-coupled amplifier, which in turn controls a series regulator. Regulated current is then supplied to the focus coil despite the fact that the total resistance of the circuit can vary considerably due to adjustment of the alignment coils, and heating. To set up and operate a Vidicon camera properly, it is desirable that the operator know the signal electrode current and voltage. The measurement of the voltage presents no problem. However, measurements of the signal electrode current does present somewhat of a

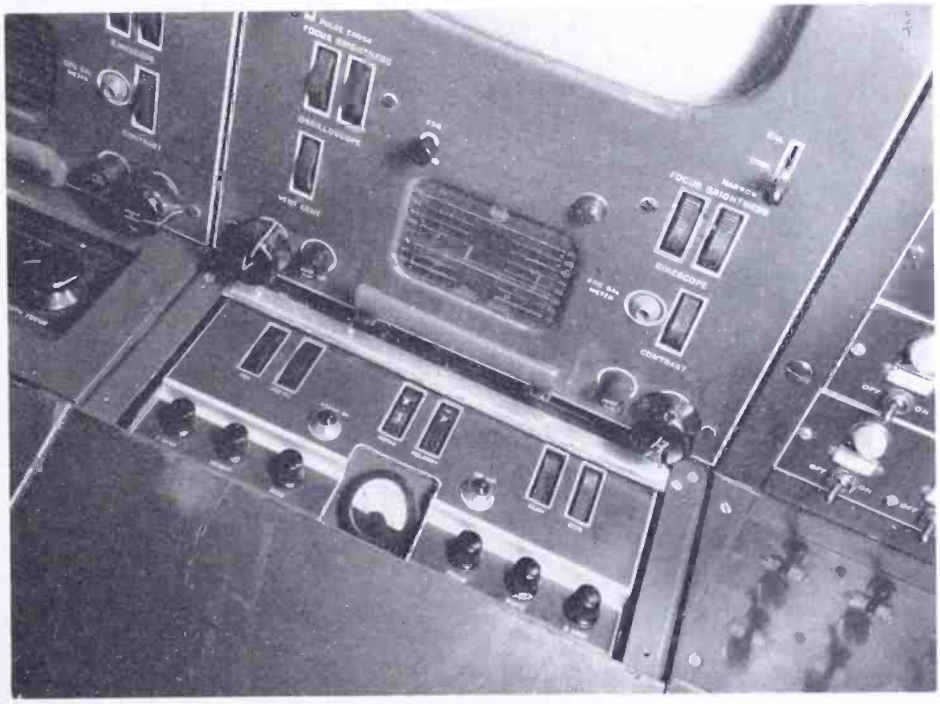

Fig. 9—Vidicon remote control panel. The unit is mounted in a standard console housing. A portion of the master monitor is visible in the upper center.

problem in that normal values are in the vicinity of 0.25 microampere. To do this, a bridge type of d-c amplifier is used to enable a 100 microampere meter to indicate full scale deflection at 0.5 microampere. The meter amplifier is located in the deflection chassis, while the meter is located in the remote control panel where it is visible to the operator.

Remote Control Panel

The remote control panel, as previously indicated, is located at the operating position in the console housing where the main master monitor is located. Operating controls such as gain, pedestal, beam,

and signal electrode voltage, as well as setup controls for size and centering and focus, are located in the panel. A "standby" as well as "on the air" tally, and a signal electrode current meter, provide a visible indication of the functioning of the system. Figure 9 illustrates the control panel mounted in the console housing. A portion of the master monitor is visible in the picture as well as a portion of the image orthicon studio camera control at the left and the power switching panel at the right.

Over-All Operation

Two modes of operation are possible for film pickup; the camera may be mounted directly on a projector by means of a bracket as is

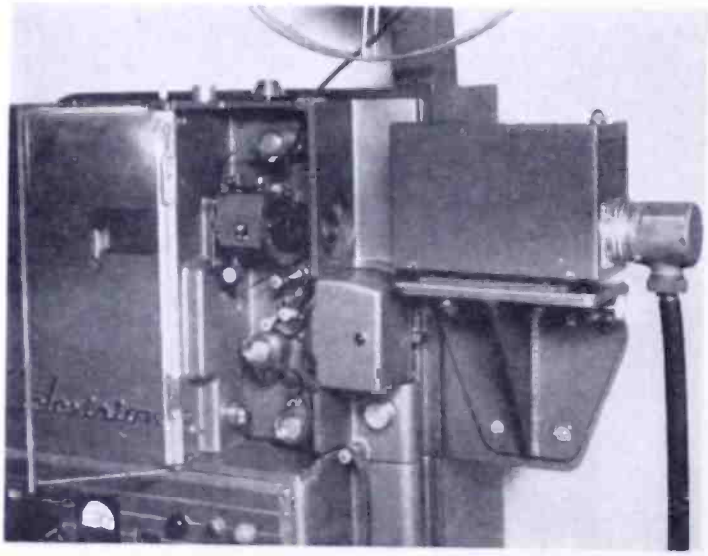

Fig. 10—Vidicon camera mounted directly on a 16-millimeter projector.

shown in Figure 10, or the camera may be mounted in a multiplexer as is shown in Figure 11. Use on a single projector is very convenient, but is somewhat uneconomical. Use of the camera with a multiplexer adds more complications so far as optical alignment is concerned; however, two movie projectors, one 2 × 2 inch transparent slide projector, and a single 4 × 5 inch opaque projector may be utilized with a multiplexer.

Because of the small size of the optical image (0.6 inch diagonal) on the face of the Vidicon, the problem is more involved than it is with the iconoscope film camera where the image is 4 × 5 inches. With a standard 4-inch projection lens, the 4 × 5 inch image is about three feet away from the projector. However, with the Vidicon, a 16-millimeter frame must be projected on the face at a 1 to 1 ratio.

This brings the camera up close to the projector and makes multiplexing with the regular mirror method practically impossible.

A shadow box or rear screen projection and front screen projection have been tried with unsatisfactory results; the camera made use of a lens as in direct pickup use. The screen material adds grain to the picture, and the loss of light is serious. If the screen of a shadow box is replaced with a large lens, these objections are removed. Therefore, a system was designed so that a 3 × 4 inch image is projected into the plane of a 5-inch lens. The lens acts as a collector and produces a cone of light down to a size where the camera lens can utilize the entire picture without much loss of light.

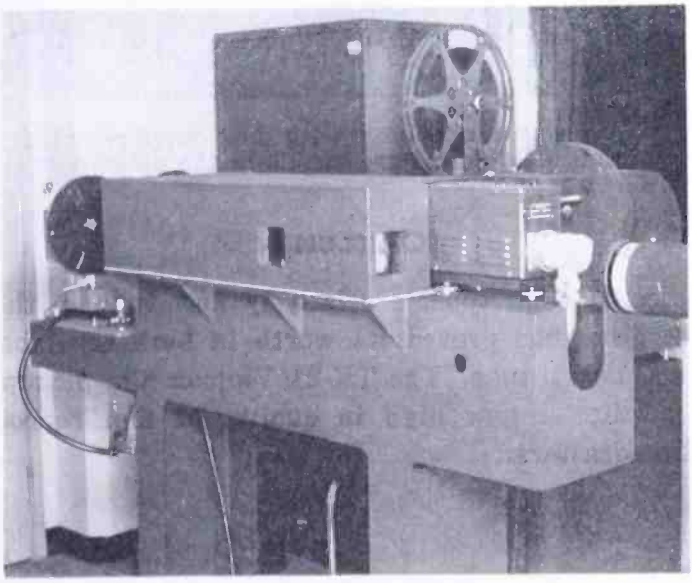

Fig. 11—Vidicon camera multiplexer. Permits four picture inputs to be fed to a single camera.

By making use of dichroic mirrors, two field lenses, and one sliding mirror, it is possible to make use of the four projector inputs mentioned above. The whole assembly is covered with a dust-tight cover. The images are projected through optical flat glass into the multiplexer. Figure 11 shows the multiplexer system in operation. Note the 2 × 2 inch slide projector at the left and the large lens of the opaque projector just visible at the right. Only one motion picture projector is shown in the photograph. However, the window through which the light from a second projector must pass is visible in the picture. Figure 12 shows another view of the Vidicon optical multiplexer with the dust cover removed. The dichroic mirrors and the two field lenses are visible in the picture.

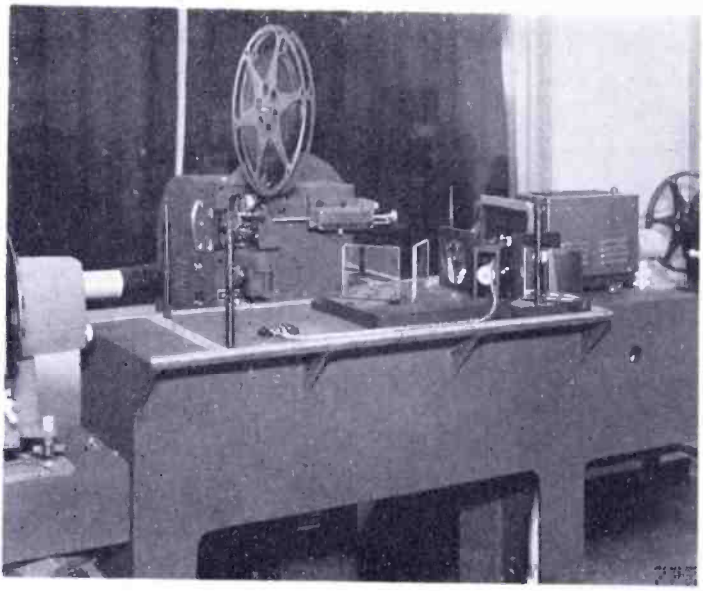

Fig. 12—Vidicon camera multiplexer with dust cover removed. The mirrors and field lenses are visible in the picture.

CONCLUSION

The Vidicon pickup tube, a relatively new tube in the television broadcasting field, has proved its worth in both the laboratory and field as a film pickup tube. The TK-21 Vidicon film pickup equipment has made possible a new high in quality of film reproduction for television broadcasters.

THE COMPLETE SPECIFICATION OF A NETWORK BY A SINGLE PARAMETER†

By

M. S. Corrington, T. Murakami, and R. W. Sonnenfeldt

RCA Victor Television Division,
Camden, N. J.

Summary—*If the transfer function of a linear passive network is defined as the output response divided by the input driving force, it can be written in either polar or Cartesian form,* $T(\omega)\, e^{i\theta(\omega)} = P(\omega) + i\, Q(\omega)$, *where* $T(\omega)$ *is the amplitude response,* $\theta(\omega)$ *is the phase characteristic,* $P(\omega)$ *is the in-phase component, and* $Q(\omega)$ *is the quadrature component. The transient response to a unit-step function,* $A(t)$, *can be determined within a constant from either* $P(\omega)$ *or* $Q(\omega)$ *alone.* $P(\omega)$, $Q(\omega)$, *and* $A(t)$ *are all related, and any one can be used to compute the other two. The derivation of these relations is valid for networks with either distributed or lumped constants, including transducers, and the question of minimum phase does not arise.*

A graphic method is described for computing $A(t)$ *from either* $P(\omega)$ *or* $Q(\omega)$ *and universal curves are included.*

Equipment is described which sweeps $P(\omega)$, $Q(\omega)$, *or a polar plot of* $T(\omega)$ *and* $\theta(\omega)$ *directly. An intensity frequency marker circuit is included which produces multiple, harmonically related dots on the sweep response. It is also possible to sweep the departure from phase linearity. By a heterodyne process the sweep can be used on low-pass or band-pass systems.*

Introduction

> *Fourier's Theorem is not only one of the most beautiful results of modern analysis, but it may be said to furnish an indispensable instrument in the treatment of nearly every recondite question in modern physics.*
> —Lord Kelvin and Peter Guthrie Tait, *Treatise on Natural Philosophy.*

FOR many years electronic engineers have been accustomed to think of the amplitude and phase response of the networks being designed for various applications. The laboratory test equipment includes oscillators, voltmeters, wave analyzers, etc., to measure the response to steady-state sine waves. Their educational background has taught the engineers to think in terms of steady-state network theory.

* Decimal Classification: R143.

† A substantial portion of the experimental part of this paper is being presented at the National Electronics Conference, Chicago, Ill., on October 5, 1954.

As the circuits become more complicated it is found that in many cases we do not have sine waves in the network. We are now thinking in terms of unit-step, ramp, sawtooth, and such wave forms, as well as the response to various pulses. In equipment where phase linearity is important it is now fairly common to use nonminimum net phase shift circuits, where the usual relations between amplitude and phase responses do not hold.

When an attempt is made to predict the transient response of a network from the steady-state response, it is necessary to consider both the amplitude and phase response, since it may not be known that the circuit is minimum phase. This is a difficult thing to do since it is necessary to work with two variables.

In this paper, it is shown that the amplitude and phase responses are not true parameters of the network. New parameters are introduced which completely specify the network and give a one-to-one correspondence between the transient and the steady-state response in all cases. It is no longer necessary to ask whether the network is mini-

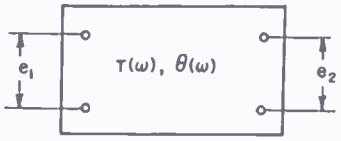

Fig. 1—Network with two pairs of terminals.

mum phase. Graphic methods for finding the relations between the parameters are given and test equipment is described.

Steady-State Response of a Network

In the linear, passive network of Figure 1, suppose that a sinusoidal steady-state driving force e_1 is applied to the input terminals. Let the resulting sinusoidal output response be e_2. The actual quantities may be voltages, currents, velocities, amplitudes, or other such quantities. The input and output signals need not be similar; one can be a current and the other a voltage, etc. The two sine waves can be written

$$e_1 = E_1 \sin(\omega t + \phi_1), \tag{1}$$

$$e_2 = E_2 \sin(\omega t + \phi_2), \tag{2}$$

where ω is the angular frequency and t is the time. Let the transfer function of the network be $T(\omega)$ and the phase response be $\theta(\omega)$. Then, by definition,

$$T(\omega) = \frac{E_2}{E_1}, \tag{3}$$

and

$$\theta(\omega) = \phi_2 - \phi_1 = \text{angle of lead.} \tag{4}$$

In general, $T(\omega)$ is an even function of frequency, and $\theta(\omega)$ is an odd function of frequency.

Since the system is assumed linear, the individual responses to any combination of waves can be added together to find the resultant output response. The steady-state solution for the response of the network of Figure 1 to a complex periodic input wave

$$e_1 = \sum_{n=0}^{\infty} E_n \cos(n\omega_0 t + \phi_n) \tag{5}$$

can be obtained by modifying the amplitude and phase of each term of Equation (5) in accord with $T(\omega)$ and $\theta(\omega)$. The sum is then evaluated to give

$$e_2 = \sum_{n=0}^{\infty} E_n T(n\omega_0) \cos[n\omega_0 t + \phi_n + \theta(n\omega_0)]. \tag{6}$$

Fourier Integral for Step-Function Response

When the driving force is not periodic, the same process can be used. The spectral density of the driving force $F(t)$, per cycle of bandwidth, is

$$G(\omega) = \int_{-\infty}^{\infty} F(t)\, e^{-i\omega t}\, dt. \tag{7}$$

The component of the complex input wave at frequency ω can be written as

$$\text{Differential driving force} = G(\omega)\, e^{i\omega t}\, df. \tag{8}$$

If each component of this differential driving force is modified in accord with $T(\omega)$ and $\theta(\omega)$, and the results integrated to give the total response, the result is

$$R(t) = \int_{-\infty}^{\infty} T(\omega)\, G(\omega)\, e^{i[\omega t + \theta(\omega)]}\, df$$

$$= \frac{1}{2\pi} \int_{-\infty}^{\infty} T(\omega)\, G(\omega)\, e^{i[\omega t + \theta(\omega)]}\, d\omega, \tag{9}$$

which is the Fourier integral for the transient response to the applied driving force.

When the driving force is the unit-step function, $U(t)$, applied at the origin, the spectral density is

$$G(\omega) = \frac{1}{i\omega}. \tag{10}$$

By Equation (9) the response of the network to a unit-step function is

$$A(t) = \frac{1}{2\pi i} \int_{-\infty}^{\infty} \frac{T(\omega)}{\omega} e^{i[\omega t + \theta(\omega)]}\, d\omega. \tag{11}$$

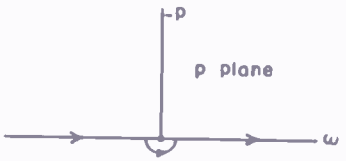

Fig. 2—Path of integration.

At the origin, if there is a pole, the path of integration must be deformed slightly to go below the pole, as shown by the small semicircle of Figure 2. This corresponds to a small amount of damping on the driving force, and prevents the transient from growing without limit.

The integral around the semicircle at the origin is πi times the residue at the point, or

$$\text{Integral over semicircle} = \pi i \left[\frac{1}{2\pi i} T(0) \right] = \frac{1}{2} T(0). \tag{12}$$

Since $T(\omega) = T(-\omega)$ and $\theta(\omega) = -\theta(-\omega)$, Equation (11) can be written

$$A(t) = \frac{1}{2} T(0) + \frac{1}{\pi} \int_{0}^{\infty} \frac{T(\omega)}{\omega} \sin[\omega t + \theta(\omega)]\, d\omega,$$

where $T(0)$ is the response of the system to zero frequency; it is the final steady-state value after the transient has died away.

Relations between the In-Phase and Quadrature Components of a Network and the Transient Response

If the transfer function of a network is $T(\omega)$ and the phase response is $\theta(\omega)$, the in-phase and quadrature components can be written

$$P(\omega) = T(\omega) \cos \theta(\omega), \tag{14}$$

and

$$Q(\omega) = T(\omega) \sin \theta(\omega), \tag{15}$$

so

$$P(\omega) + i\,Q(\omega) = T(\omega)\, e^{i\theta(\omega)}. \tag{16}$$

It is known from the physics of the network that $T(\omega)$ is an even function and $\theta(\omega)$ is an odd function of ω. Therefore

$$P(-\omega) = P(+\omega), \tag{17}$$

$$Q(-\omega) = -Q(+\omega), \tag{18}$$

$$P(0) = T(0), \tag{19}$$

and

$$Q(0) = 0. \tag{20}$$

The response of the network to a unit-step function at $T = 0$ is

$$A(t) = \frac{1}{2} T(0) + \frac{1}{\pi} \int_0^\infty \frac{T(\omega)}{\omega} \sin [\omega t + \theta(\omega)]\, d\omega \tag{13}$$

$$= \frac{1}{2} P(0) + \frac{1}{\pi} \int_0^\infty \frac{1}{\omega} [T(\omega) \cos \theta(\omega) \sin \omega t + T(\omega) \sin \theta(\omega) \cos \omega t]\, d\omega$$

$$= \frac{1}{2} P(0) + \frac{1}{\pi} \int_0^\infty \frac{P(\omega)}{\omega} \sin \omega t\, d\omega + \frac{1}{\pi} \int_0^\infty \frac{Q(\omega)}{\omega} \cos \omega t\, d\omega. \tag{21}$$

This equation is valid for all values of time $-\infty < t < \infty$.

It is a requirement of any physically realizable network that the network must not respond before the signal is applied. For $t < 0$ the

unit-step function has not been applied and the response is zero. Thus, changing t to $-t$ in Equation (21),

$$A(-t) = \frac{1}{2} P(0) - \frac{1}{\pi} \int_0^\infty \frac{P(\omega)}{\omega} \sin \omega t \, d\omega + \frac{1}{\pi} \int_0^\infty \frac{Q(\omega)}{\omega} \cos \omega t \, d\omega = 0. \qquad (22)$$

$$t > 0$$

Subtracting Equation (22) from Equation (21)

$$A(t) = \frac{2}{\pi} \int_0^\infty \frac{P(\omega)}{\omega} \sin \omega t \, d\omega. \qquad (23)$$

$$t > 0$$

Adding Equations (21) and (22)

$$A(t) = P(0) + \frac{2}{\pi} \int_0^\infty \frac{Q(\omega)}{\omega} \cos \omega t \, d\omega. \qquad (24)$$

$$t \geq 0$$

Equation (23) shows that the in-phase component, $P(\omega)$, of the transfer function completely determines the response to a unit-step function. Similarly, Equation (24) shows that the quadrature component, $Q(\omega)$, determines the step-function response uniquely except for the final steady-state value $P(0)$.

By differentiation of Equations (23) and (24), the impulse response is

$$h(t) = \delta(t) \, A(0) + \frac{2}{\pi} \int_0^\infty P(\omega) \cos \omega t \, d\omega \qquad (25)$$

$$= A(0) \, \delta(t) - \frac{2}{\pi} \int_0^\infty Q(\omega) \sin \omega t \, d\omega, \qquad (26)$$

$$t > 0$$

whenever the integrals exist. $\delta(t)$ is the unit-impulse function. This shows that either the in-phase or quadrature component of the network

completely determines the transient response to a unit impulse, within a constant.

Review of Assumptions Made

Since Equations (23) and (24) are the foundations for the rest of this paper, the conditions under which they were derived will now be summarized.

1. The network must be linear and passive. If amplifier tubes are used they must be used only to provide a change in level, with no distortion, and they must not produce sustained oscillations.
2. The transfer function, $T(\omega)$, of the network is the ratio of the output amplitude E_2 to the input amplitude E_1, for a steady-state sine-wave input. E_1 and E_2 may be any two similar or dissimilar but related quantities, such as current, voltage, velocity, force, etc. The results also apply to a two-terminal network if E_1 and E_2 are the two input quantities.
3. A physically realizable network must not respond before the driving force is applied. This is a very important condition and is the assumption that enabled the step-function response to be determined uniquely from either the in-phase component or the quadrature component. Later it will be used to determine the relation between $P(\omega)$ and $Q(\omega)$. Whenever the solution for the transient starts before the driving force is applied, it is an indication that non-physical assumptions have been made for $T(\omega)$ or $\theta(\omega)$.
4. The network may consist of either distributed or lumped constants, or a combination of the two. It may include transducers if they are linear.
5. The network need not be of minimum net phase shift type; the question is not raised.
6. The parameters of the network must not vary with time; $T(\omega)$ and $\theta(\omega)$ are functions of frequency only.

Derivation of Fourier Identity

The response of a network to a driving force $F(t)$ is

$$R(t) = \frac{1}{2\pi} \int_{-\infty}^{\infty} T(\omega)\, G(\omega)\, e^{i[\omega t + \theta(\omega)]} d\omega, \tag{9}$$

$$\text{where } G(\omega) = \int_{-\infty}^{\infty} F(t)\, e^{-i\omega t}\, dt, \tag{7}$$

$T(\omega)$ is the transfer function, and $\theta(\omega)$ is the phase response of the network.

Let the network be a direct connection with no impedance in series or shunt, so $T(\omega) = 1$ and $\theta(\omega) = 0$ at all frequencies. Then the response must be the same as the applied driving force, or

$$F(t) = \frac{1}{2\pi} \int_{-\infty}^{\infty} G(\omega)\, e^{i\omega t}\, d\omega,$$

$$\text{where} \qquad G(\omega) = \int_{-\infty}^{\infty} F(\lambda)\, e^{-i\omega\lambda}\, d\lambda$$

$$\text{or} \qquad F(t) = \frac{1}{2\pi} \int_{-\infty}^{\infty} d\omega \int_{-\infty}^{\infty} F(\lambda)\, e^{i\omega(t-\lambda)}\, d\lambda, \tag{27}$$

where $F(t)$ may be real or complex.

Since the Fourier identity is the limiting form of the Fourier series, the conditions on $F(t)$ are essentially the same as for the series. For the purpose of this text, $F(t)$ must be a bounded, single-valued function with not more than a finite number of maxima and minima, and a finite number of finite discontinuities in any finite interval. $F(t)$ must have absolute convergence; this means that the integral $\int_{-\infty}^{\infty} |F(\lambda)|\, d\lambda$ must exist. The Fourier identity converges to $F(t)$ at all points where $F(t)$ is continuous, and converges to the average of the right and left hand limits of $F(t)$ at each point where $F(t)$ is discontinuous. If $F(t)$ is complex, the real and imaginary components must each satisfy the above conditions.

Equation (27) can be rewritten

$$F(t) = \frac{1}{2\pi} \int_{-\infty}^{0} d\omega \int_{-\infty}^{\infty} F(\lambda)\, e^{i\omega(t-\lambda)}\, d\lambda$$

$$+ \frac{1}{2\pi} \int_{0}^{\infty} d\omega \int_{-\infty}^{\infty} F(\lambda)\, e^{i\omega(t-\lambda)}\, d\lambda$$

$$= \frac{1}{2\pi} \int_0^\infty d\omega \int_{-\infty}^\infty F(\lambda) \left[e^{i\omega(t-\lambda)} + e^{-i\omega(t-\lambda)} \right] d\lambda$$

$$= \frac{1}{\pi} \int_0^\infty d\omega \int_{-\infty}^\infty F(\lambda) \cos \omega(t-\lambda)\, d\lambda \qquad (28)$$

$$= \frac{1}{\pi} \int_0^\infty \cos \omega t\, d\omega \int_{-\infty}^\infty F(\lambda) \cos \omega\lambda\, d\lambda$$

$$+ \frac{1}{\pi} \int_0^\infty \sin \omega t\, d\omega \int_{-\infty}^\infty F(\lambda) \sin \omega\lambda\, d\lambda. \qquad (29)$$

If $F(\lambda)$ is an even function of λ, then

$$\int_{-\infty}^\infty F(\lambda) \sin \omega\lambda\, d\lambda = 0 \qquad (30)$$

if there are no poles on the axis, since the integrand is then odd. If $F(\lambda)$ is an odd function of λ, then

$$\int_{-\infty}^\infty F(\lambda) \cos \omega\lambda\, d\lambda = 0 \qquad (31)$$

if there are no poles on the axis, since the integrand is then odd. Thus we have the Fourier cosine formula

$$F(t) = \frac{2}{\pi} \int_0^\infty \cos \omega t\, d\omega \int_0^\infty F(\lambda) \cos \omega\lambda\, d\lambda \qquad (32)$$

if $F(\lambda)$ is even, and the Fourier sine formula

$$F(t) = \frac{2}{\pi} \int_0^\infty \sin \omega t\, d\omega \int_0^\infty F(\lambda) \sin \omega\lambda\, d\lambda \qquad (33)$$

if $F(\lambda)$ is odd.

Derivations of Relations between the In-Phase and Quadrature Components of a Network

From Equations (23) and (24)

$$A(t) = \frac{2}{\pi} \int_0^\infty \frac{P(\omega)}{\omega} \sin \omega t \, d\omega, \qquad t > 0 \tag{23}$$

and

$$A(t) = P(0) + \frac{2}{\pi} \int_0^\infty \frac{Q(\omega)}{\omega} \cos \omega t \, d\omega, \qquad t \geqq 0 \tag{24}$$

Make the change of variables $\omega \rightarrow \lambda$ and $t \rightarrow u$, and equate the two integrals. Then

$$P(0) + \frac{2}{\pi} \int_0^\infty \frac{Q(\lambda)}{\lambda} \cos \lambda u \, d\lambda = \frac{2}{\pi} \int_0^\infty \frac{P(\lambda)}{\lambda} \sin \lambda u \, d\lambda. \tag{34}$$

Multiply both sides of the equation by $e^{-\alpha u} \cos \omega u \, du$ and integrate from 0 to ∞.

$$P(0) \int_0^\infty e^{-\alpha u} \cos \omega u \, du + \frac{2}{\pi} \int_0^\infty \frac{Q(\lambda)}{\lambda} d\lambda \int_0^\infty e^{-\alpha u} \cos \lambda u \cos \omega u \, du$$

$$= \frac{2}{\pi} \int_0^\infty \frac{P(\lambda)}{\lambda} d\lambda \int_0^\infty e^{-\alpha u} \sin \lambda u \cos \omega u \, du. \tag{35}$$

By means of the known relations[1]

$$\int_0^\infty e^{-\alpha u} \cos \omega u \, du = \frac{\alpha}{\alpha^2 + \omega^2}, \qquad \alpha > 0 \tag{36}$$

and $$\int_0^\infty e^{-\alpha u} \sin \lambda u \cos \omega u \, du = \frac{\lambda \, (\alpha^2 + \lambda^2 - \omega^2)}{(\alpha^2 + \lambda^2 - \omega^2)^2 + 4\alpha^2\omega^2}, \quad \alpha > 0 \tag{37}$$

the first integral of Equation (35) becomes, in the limit as $\alpha \rightarrow 0$

$$\lim_{\alpha \rightarrow 0} P(0) \int_0^\infty e^{-\alpha u} \cos \omega u \, du = 0 \tag{38}$$

by Equation (36).

---

[1] Wolfgang Gröbner and Nikolaus Hofreiter, *Integraltafel, Zweiter Teil, Bestimmte Integrale*, Springer-Verlag, Wien and Innsbruck, 1950, p. 135, Equations (2a), (6b).

The second integral of Equation (35) becomes, after inversion of the order of integration,

$$\lim_{\alpha \to 0} \frac{2}{\pi} \int_0^\infty \frac{Q(\lambda)}{\lambda} d\lambda \int_0^\infty e^{-\alpha u} \cos \lambda u \cos \omega u \, du$$

$$= \lim_{\alpha \to 0} \frac{2}{\pi} \int_0^\infty e^{-\alpha u} \cos \omega u \, du \int_0^\infty \frac{Q(\lambda)}{\lambda} \cos \lambda u \, d\lambda$$

$$= \frac{Q(\omega)}{\omega}$$

by Equation (32), since $Q(\lambda)/\lambda$ is an even function of frequency. The integral on the right side of Equation (35) becomes, in the limit

$$\lim_{\alpha \to 0} \frac{2}{\pi} \int_0^\infty \frac{P(\lambda)}{\lambda} d\lambda \int_0^\infty e^{-\alpha u} \sin \lambda u \cos \omega u \, du$$

$$= \frac{2}{\pi} \int\!\!\!\!\!\!-_0^\infty \frac{P(\lambda)}{\lambda^2 - \omega^2} d\lambda \tag{40}$$

by Equation (37). The sign $\int\!\!\!\!\!\!-$ means the Cauchy principal value.[2]

When Equations (38), (39), and (40) are substituted into Equation (35), the result is

$$Q(\omega) = \frac{2\omega}{\pi} \int\!\!\!\!\!\!-_0^\infty \frac{P(\lambda)}{\lambda^2 - \omega^2} d\lambda. \tag{41}$$

By means of the known result[3]

$$\int\!\!\!\!\!\!-_0^\infty \frac{d\lambda}{\lambda^2 - \omega^2} = 0, \quad \omega \neq 0. \tag{42}$$

---

[2] If there is a singularity at $x = \alpha$, $a < \alpha < b$, then

$$\int\!\!\!\!\!\!-_a^b = \lim_{\epsilon \to 0} \left[\int_a^{\alpha - \epsilon} f(x)\,dx + \int_{\alpha + \epsilon}^b f(x)\,dx \right]$$

[3] Reference (1), p. 14, Equation (10b).

Equation (41) can be rewritten

$$Q(\omega) = \frac{2\omega}{\pi} \int_0^\infty \frac{P(\lambda) - P(\omega)}{\lambda^2 - \omega^2} d\lambda, \tag{43}$$

where it has been written in this form to eliminate the pole at $\lambda = \omega$. To derive equivalent results for computing $P(\omega)$ from $Q(\omega)$, multiply both sides of Equation (34) by $e^{-\alpha u} \sin \omega u \, du$ and integrate from 0 to ∞.

$$P(0) \int_0^\infty e^{-\alpha u} \sin \omega u \, du + \frac{2}{\pi} \int_0^\infty \frac{Q(\lambda)}{\lambda} d\lambda \int_0^\infty e^{-\alpha u} \cos \lambda u \sin \omega u \, du$$

$$= \frac{2}{\pi} \int_0^\infty \frac{P(\lambda)}{\lambda} d\lambda \int_0^\infty e^{-\alpha u} \sin \lambda u \sin \omega u \, du. \tag{44}$$

By means of the known relations[4]

$$\int_0^\infty e^{-\alpha u} \sin \omega u \, du = \frac{\omega}{\alpha^2 + \omega^2}, \quad \alpha > 0 \tag{45}$$

and

$$\int_0^\infty e^{-\alpha u} \cos \lambda u \sin \omega u \, du = \frac{\omega(\alpha^2 + \omega^2 - \lambda^2)}{(\alpha^2 + \omega^2 - \lambda^2)^2 + 4\alpha^2 \lambda^2}, \quad \alpha > 0 \tag{46}$$

the first integral of Equation (44) becomes in the limit as $\alpha \to 0$

$$\lim_{\alpha \to 0} P(0) \int_0^\infty e^{-\alpha u} \sin \omega u \, du = \frac{P(0)}{\omega} \tag{47}$$

in accord with Equation (45). The second integral of Equation (44) becomes in the limit

$$\lim_{\alpha \to 0} \frac{2}{\pi} \int_0^\infty \frac{Q(\lambda)}{\lambda} d\lambda \int_0^\infty e^{-\alpha u} \cos \lambda \, u \sin \omega u \, du$$

$$= \frac{2\omega}{\pi} \int_0^\infty \frac{Q(\lambda)}{\lambda(\omega^2 - \lambda^2)} d\lambda \tag{48}$$

[4] Reference (1), p. 135, Equations (1a), (6b).

in accord with Equation (46). If the order of integration is changed in the integral on the right-hand side of Equation (44), we have

$$\lim_{\alpha \to 0} \frac{2}{\pi} \int_0^\infty e^{-\alpha u} \sin \omega u \, du \int_0^\infty \frac{P(\lambda)}{\lambda} \sin \lambda u \, d\lambda = \frac{P(\omega)}{\omega} \tag{49}$$

in accord with Equation (33), since $P(\lambda)/\lambda$ is an odd function of λ. Substituting Equations (47), (48), and (49) into Equation (44), we have the result

$$P(\omega) - P(0) = -\frac{2\omega^2}{\pi} \int_0^\infty \frac{Q(\lambda)}{\lambda\,(\lambda^2 - \omega^2)} d\lambda. \tag{50}$$

Using Equation (42), Equation (50) can be written

$$P(\omega) - P(0) = -\frac{2\omega^2}{\pi} \int_0^\infty \frac{\dfrac{Q(\lambda)}{\lambda} - \dfrac{Q(\omega)}{\omega}}{\lambda^2 - \omega^2} d\lambda. \tag{51}$$

Equation (51) was written in this form to remove the pole at $\lambda = \omega$.

Restrictions on the Derivations

It should be noted that there are very few restrictions on the above derivations. It was assumed that the linear network satisfied the condition that the transfer function is single-valued, bounded, has not more than a finite number of finite discontinuities and a finite number of maxima and minima in any finite interval. The integral $\int_0^\infty \left| \frac{P(\lambda)}{\lambda} \right| d\lambda$ must converge absolutely. The question as to whether the network is of minimum phase does not arise. It is required that the network must not respond before the signal is applied; this is a requirement of a "physical" system. It is not necessary to know whether the network is formed of lumped constants, distributed constants, or whether it includes transducers for changing from one kind of a system to another, such as from an electrical system to a mechanical one.

When Equation (43) is used, it is evident that the in-phase component $P(\omega)$ completely and uniquely determines the quadrature component $Q(\omega)$. It also completely and uniquely determines the transient response to a unit-step function, as shown by Equation (23). It is therefore a true parameter of the network.

If the transfer function, $T(\omega)$, and the phase response, $\theta(\omega)$, of a network are given, it is possible to compute the transient response from Equation (9). It is not possible to use either one alone to find the transient unless it is known that the network has a minimum net phase shift.

In Bode's[5] book on networks, he has shown that the relations derived in Equations (43) and (51) give the relation between $T(\omega)$ and $\theta(\omega)$ if $T(\omega)$ is expressed in a neper or logarithmic scale and $\theta(\omega)$ is in radians. In a transfer function of nonminimum-phase type, there will be zeros of the function in the right half of the complex frequency plane. When the logarithm is taken, the zeros become negative poles since $\log_e 0 = -\infty$. When Bode derived his equations, he used a contour integral which surrounded the right half of the complex frequency plane and he assumed there were no poles in the right half plane. If there are such poles it is necessary to add some correction terms to his formulas.[6] Since poles of $P(\omega)$ in the right half plane indicate an active, unstable network, they will not exist in the passive networks we are considering. Therefore, Equations (43) and (51) will always hold for $P(\omega)$ and $Q(\omega)$ and the question of minimum phase shift need not be raised. It is permissible to have zeros of $P(\omega)$ or $Q(\omega)$ in the right half plane since the logarithm is not taken.

One-to-One Correspondence Obtained

In general, it is difficult to examine a network to decide whether it is minimum phase. For example, in a bridged-T network it may be minimum or nonminimum phase depending upon the numerical values of the circuit constants. The recent developments in color television receivers indicate that the circuits where accurate control of the transient response is important will usually be nonminimum phase to preserve phase linearity. For this reason it is desirable to discontinue the use of sweeps for measuring $T(\omega)$ and to replace them with sweeps for displaying either $P(\omega)$ or $Q(\omega)$. Then there will be a one-to-one correspondence between the frequency response and the

---

[5] Hendrik W. Bode, *Network Analysis and Feedback Amplifier Design*, D. Van Nostrand Company, Inc., New York, N. Y., 1945, Chapter 14.

[6] François-Henri Raymond, "Transformées de Hilbert et Relations de Bayard-Bode," Annales des Télécommunications, Vol. 6, pp. 262-272, October, 1951.

ient response in all cases. This will make it much easier to predict how each part of the $P(\omega)$ or $Q(\omega)$ response will affect the transient response.

When Equation (51) is compared with Equation (24), it is evident that the quadrature component, $Q(\omega)$, of the network also completely and uniquely determines the in-phase component, $P(\omega)$, and the unit-step response, $A(t)$, within an arbitrary additive constant, $P(0)$.

This leads to a very interesting conclusion. If a certain network with in-phase component $P(\omega)$ has a unit-step response $A(t)$, then the ω-axis can be moved up or down by any arbitrary amount $P(0)$ simultaneously on the two curves. For example, in Figure 3(a), let the low-pass filter of characteristic $P(\omega)$ have the step response $A(t)$ of Figure 3(b). Then the low-pass filter can be changed to a high-pass filter by moving the origin up to 1, as shown by the dotted line. The change in Figure 3(b) will be to move the origin exactly the same amount, as shown by the dotted line.

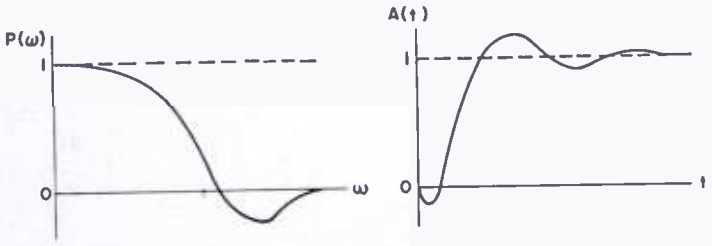

Fig. 3—(a) (left) In-phase component of network;
(b) (right) Unit-step response of network.

DERIVATION OF RELATIONS BETWEEN $A(t)$ AND $P(\omega)$ OR $Q(\omega)$

The response of a network to a unit-step function is given by Equations (23) and (24).

Using the identity[7]

$$\frac{2}{\pi}\int_0^\infty \frac{\sin \omega t}{\omega}\, d\omega = 1, \qquad t > 0. \tag{52}$$

Equation (23) can be written

$$A(t) - A(\infty) = \frac{2}{\pi}\int_0^\infty \frac{P(\lambda) - P(0)}{\lambda} \sin \lambda t\, d\lambda, \qquad t > 0 \tag{23}$$

since $P(0) = A(\infty)$.

[7] Reference (1), p. 119, Equation (14a).

If both sides of Equation (23) are multiplied by $\sin \omega t \, dt$ and then integrated from 0 to ∞, the result, when Equation (33) is used, is

$$\frac{P(\omega) - P(0)}{\omega} = \int_0^\infty [A(t) - A(\infty)] \sin \omega t \, dt. \qquad (53)$$

Starting with Equation (24) similar results can be derived for $Q(\omega)$. Thus

$$A(t) - A(\infty) = \frac{2}{\pi} \int_0^\infty \frac{Q(\lambda)}{\lambda} \cos t\lambda \, d\lambda, \qquad t \geqslant 0. \qquad (24)$$

Multiply both sides by $\cos \omega t \, dt$ and integrate from 0 to ∞. Then

$$\frac{Q(\omega)}{\omega} = \int_0^\infty [A(t) - A(\infty)] \cos \omega t \, dt \qquad (54)$$

by Equation (32).

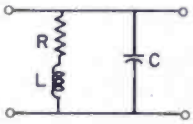

Fig. 4—Low-pass filter with shunt peaking coil.

The derivation of the fundamental relations is now complete. By Equations (23) and (24) it is possible to go from $P(\omega)$ or $Q(\omega)$ to $A(t)$. By Equations (43) and (51) it is possible to go from $P(\omega)$ to $Q(\omega)$ or vice versa. By Equations (53) and (54) it is possible to go from $A(t)$ to $P(\omega)$ or $Q(\omega)$. Thus any one of the three quantities determines the other two, and any one completely specifies the network within a constant.

$P(\omega)$, $Q(\omega)$, AND $A(t)$ CURVES FOR SHUNT-PEAKED CIRCUIT

Since the in-phase and quadrature components of a network are not as commonly used as selectivity curves, they will be illustrated by the shunt-peaked circuit of Figure 4.

The impedance across the terminals shown is

$$\frac{Z}{R} = \frac{1 + iQx}{1 - Qx^2 + ix}, \qquad (55)$$

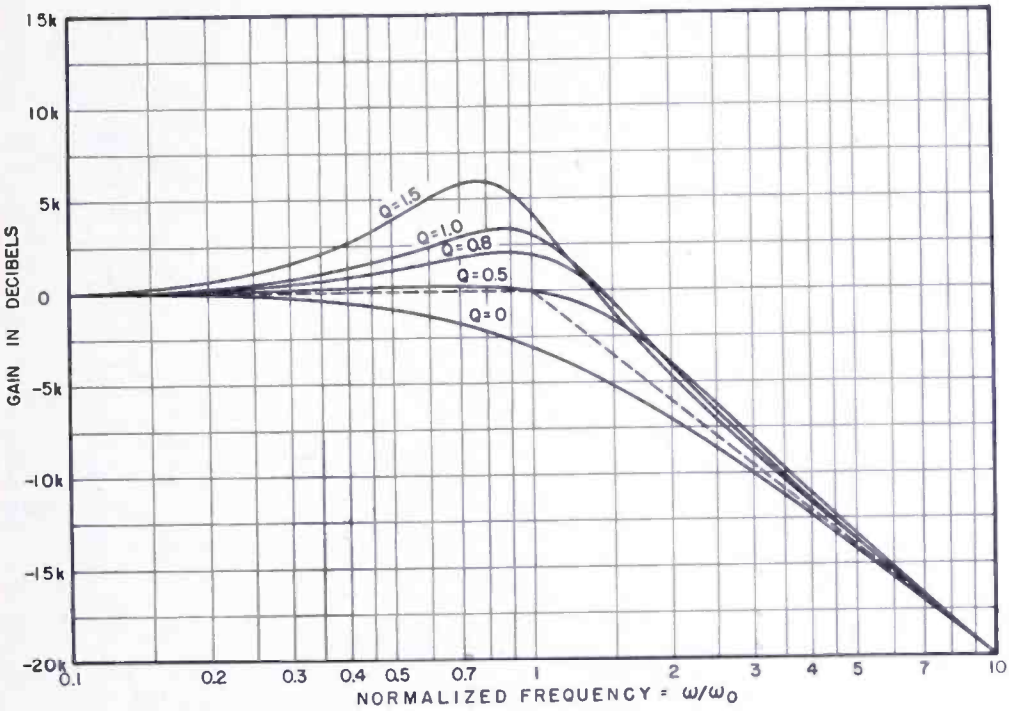

Fig. 5—Amplitude characteristics for low-pass filter.

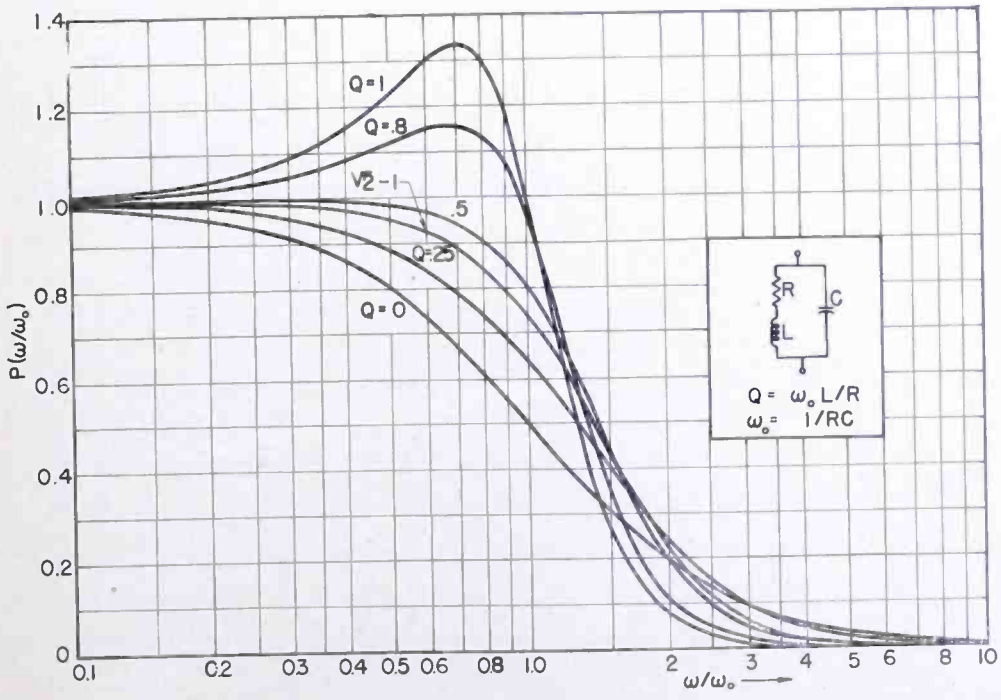

Fig. 6—$P(\omega/\omega_0)$ curves for minimum-phase shunt-peaked circuit.

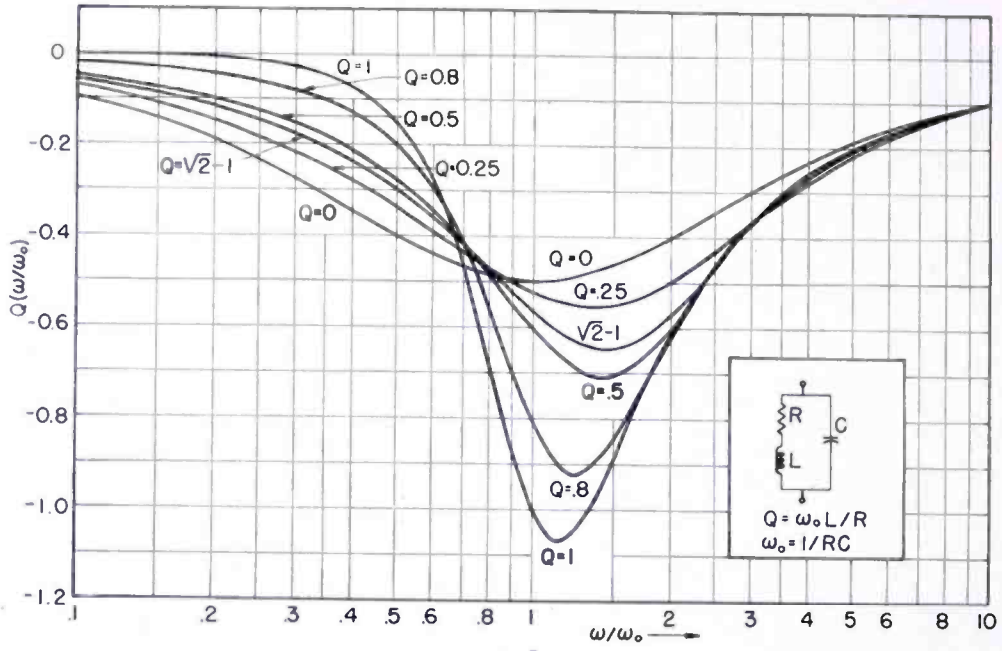

Fig. 7—$Q(\omega/\omega_0)$ curves for minimum-phase shunt-peaked circuit.

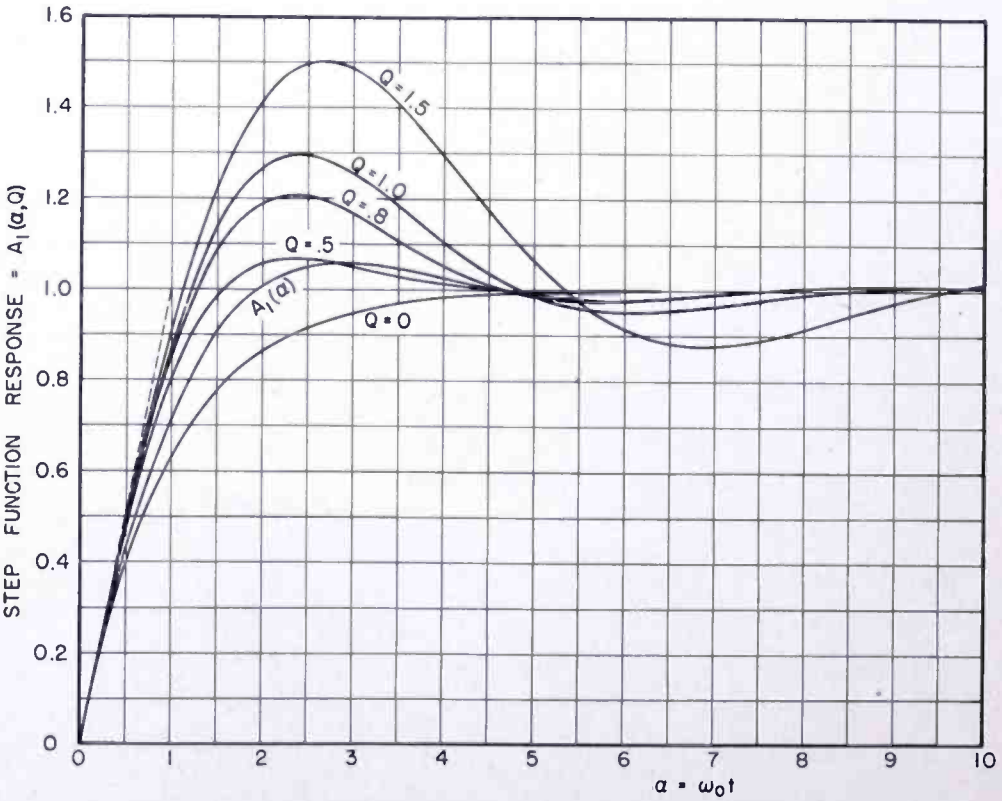

Fig. 8—Response to unit-step function, $A_1(\alpha,Q)$, low-pass filter.

where $\omega_0 = 1/RC$, $x = \omega/\omega_0$, and $Q = \omega_0 L/R$. If the Q of the circuit is varied by changing the inductance, L, of the peaking coil, the selectivity curves will be as shown by Figure 5, where the dotted line is the corresponding semi-infinite constant-slope low-pass filter. They all roll off at $6k$ decibels per octave at high frequencies, where k is the number of sections in cascade.

If Equation (55) is separated into real and imaginary parts, the result is

$$P(\omega) = \frac{1}{(1 - Qx^2)^2 + x^2} \tag{56}$$

and

$$Q(\omega) = \frac{Qx\,(1 - Qx^2) - x}{(1 - Qx^2)^2 + x^2}. \tag{57}$$

These equations are plotted in Figures 6 and 7, for various values of Q. The $P(\omega)$ curves all start out flat at $\omega = 0$ and the rise just before

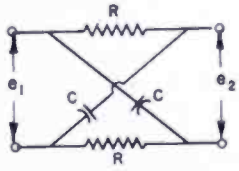

Fig. 9—Symmetrical lattice.

cutoff is determined by the amount of peaking. The $Q(\omega)$ curves come in asymptotically to zero at both ends of the frequency range and the maximum excursion increases uniformly with Q. The $P(\omega)$ curves do not cross the zero axis at any frequency, but the $Q(\omega)$ curves are positive at low frequencies if $Q > 1$.

The response of these filters to a unit-step function is shown by Figure 8. When $Q > 0.25$ there is a transient overshoot which increases with Q. The curve labeled $A_1(\alpha)$ is for one section of the semi-infinite constant-slope filter.

$P(\omega)$, $Q(\omega)$, AND $A(t)$ CURVES FOR NONMINIMUM-PHASE CIRCUIT

If the circuit of Figure 4 is cascaded with the all-pass lattice of Figure 9, which has the transfer function

$$\frac{e_2}{e_1} = \frac{1 - iQx}{1 + iQx}, \tag{58}$$

where $Q = \omega_0 RC$ and $x = \omega/\omega_0$, the resulting transfer function is obtained by multiplying Equation (55) by Equation (58). The new $P(\omega)$ and $Q(\omega)$ functions are

$$P(\omega) = \frac{1 - 2Qx^2}{(1 - Qx^2)^2 + x^2} \tag{59}$$

and

$$Q(\omega) = \frac{-Qx\,(1 - Qx^2) - x}{(1 - Qx^2)^2 + x^2}. \tag{60}$$

As is readily seen from Equations (55) and (58), the zero on the negative axis in the left half of the p-plane at $p = -1/Q$, has been moved to the corresponding point in the right half plane. The circuit is no longer minimum phase.

Since the all-pass lattice does not change the amplitude response of the system, the curves of Figure 5 can be used for the new network also. The two networks thus have the same amplitude response but different phase responses.

The $P(\omega)$ and $Q(\omega)$ curves for the two circuits in cascade are shown by Figures 10 and 11. The $P(\omega)$ curves all cross the zero axis at $\omega/\omega_0 = 1/(2Q)^{1/2}$, and approach the zero axis asymptotically at high frequencies. Similarly, the $Q(\omega)$ curves start out in the negative direction, reach a minimum, cross the axis at $\omega/\omega_0 = (Q + 1)^{1/2}/Q$, and approach the zero axis asymptotically at high frequencies.

The corresponding response to a unit-step function is shown by Figure 12. In each case there is a precursory negative swing followed by the main rise and the final value of unity.

It can thus be seen that even though the two circuits have the same amplitude response the transient responses are different. The $T(\omega)$ curve is therefore not a true parameter of the network, since it cannot be used to determine the other characteristics unless additional information is supplied. The $P(\omega)$ and $Q(\omega)$ curves do contain all the desired information and are therefore true parameters.

Graphic Solution for Finding $A(t)$ from $P(\omega)$

In order to obtain universal curves that can be moved along the ω-axis, a logarithmic frequency scale will be used. In Figure 13 let $P(\omega)$ be the straight-line segments shown, where $u_1 = \log \omega_1/\omega_0$, $u_2 = \log \omega_2/\omega_0$, $\beta = \omega_2/\omega_1$, and $\omega_0^2 = \omega_1\omega_2$.

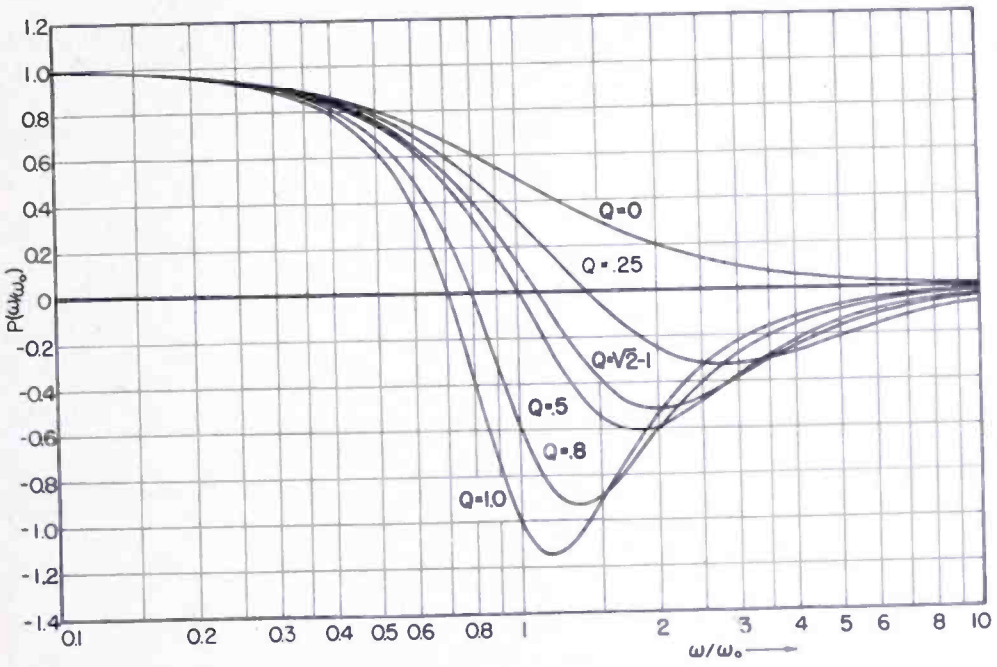

Fig. 10—$P(\omega/\omega_0)$ curves, zero moved to right half plane.

Then $P(\omega) = k \log \beta = 1, \qquad 0 \leq \omega \leq \omega_1$

$$= -k \log \frac{\omega}{\omega_0 \sqrt{\beta}}, \qquad \omega_1 \leq \omega \leq \omega_2$$

$$= 0. \qquad \omega_2 \leq \omega < \infty$$

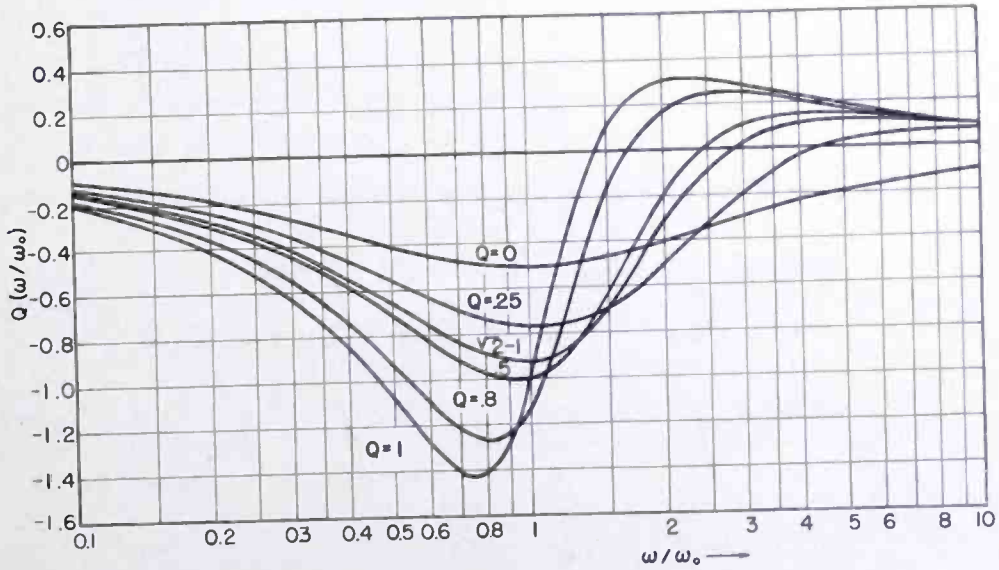

Fig. 11—$Q(\omega/\omega_0)$ curves, zero moved to right half plane.

Substituting in Equation (23)

$$A(t) = \frac{2}{\pi} \int_0^\infty \frac{P(\omega)}{\omega} \sin \omega t \, d\omega, \tag{23}$$

we have

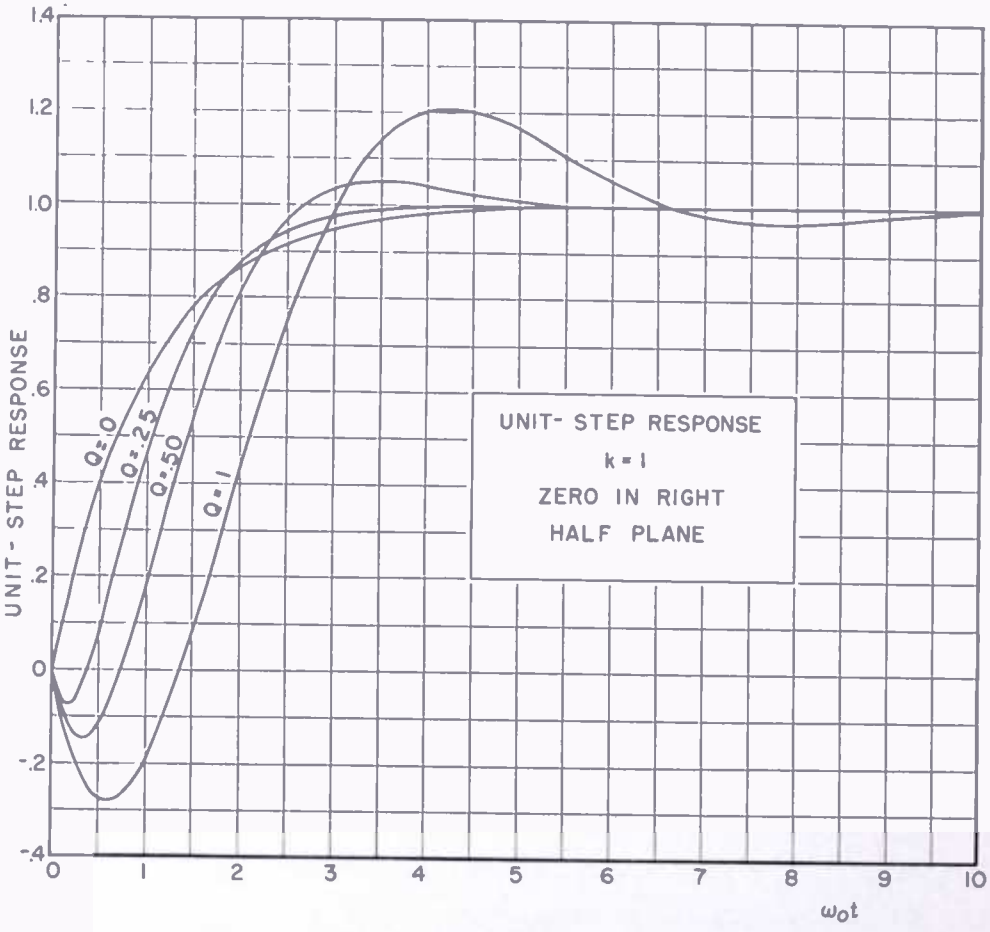

Fig. 12—Effect of moving one zero to right half plane, $k = 1$.

$$A(\omega_0 t) = \frac{2k \log \beta}{\pi} \int_0^{\omega_0/\sqrt{\beta}} \frac{\sin \omega t}{\omega} d\omega - \frac{2k}{\pi} \int_{\omega_0/\sqrt{\beta}}^{\omega_0\sqrt{\beta}} \log \frac{\omega}{\omega_0\sqrt{\beta}} \frac{\sin \omega t}{\omega} d\omega$$

$$= \frac{2k \log \beta}{\pi} \int_0^{\omega_0 t/\sqrt{\beta}} \frac{\sin s}{s} ds - \frac{2k}{\pi} \int_0^{\omega_0\sqrt{\beta}} \log \frac{s}{\omega_0\sqrt{\beta}\, t} \frac{\sin s}{s} ds$$

$$+ \frac{2k}{\pi} \int_0^{\omega_0 t/\sqrt{\beta}} \log \frac{s}{\omega_0 t\sqrt{\beta}} \frac{\sin s}{s} ds. \tag{61}$$

Using the identity

$$\int_0^x \frac{\text{Si}\,(s)}{s}\,ds = \int_0^x \frac{ds}{s}\int_0^s \frac{\sin t}{t}\,dt$$

$$= \int_0^x \frac{\sin t}{t}\,dt \int_t^x \frac{ds}{s} = -\int_0^x \log\frac{t}{x}\,\frac{\sin t}{t}\,dt, \qquad (62)$$

$A(\omega_0 t)$ can be written

$$A(\omega_0 t) = \frac{2k}{\pi}\int_{\omega_0 t/\sqrt{\beta}}^{\omega_0 t\sqrt{\beta}} \frac{\text{Si}\,(s)}{s}\,ds$$

$$= \frac{2k}{\pi}\left[\text{Im}\,E_1\,(\omega_0\sqrt{\beta}\,t) - \text{Im}\,E_1\,(\omega_0 t/\sqrt{\beta})\right] \qquad (63)$$

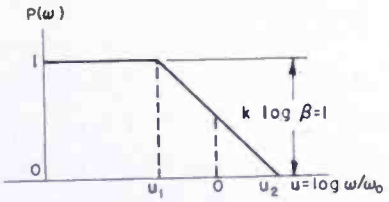

Fig. 13 — Straight-line segments for $P(\omega)$.

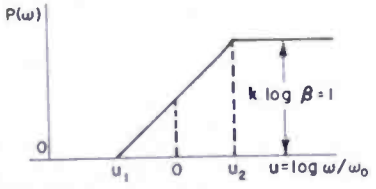

Fig. 14 — Straight-line segments for $P(\omega)$.

in the notation of Bouwkamp.[8] These functions were also tabulated by Hallén.[9]

If a high-pass filter of Figure 14 were used instead of Figure 13, the sum of the two gives the all-pass system with $A(t) = 1$. By subtracting the two results $A(\omega_0 t)$ for Figure 14 is

$$A(\omega_0 t) = 1 - \frac{2k}{\pi}\left[\text{Im}\,E_1\,(\omega_0 t\sqrt{\beta}) - \text{Im}\,E_1\,(\omega_0 t/\sqrt{\beta})\right]. \qquad (64)$$

A family of curves has been computed for various values of β, using Equation (63); they are given by Figures 15 and 16.

Example: Find the response to a unit-step function of the shunt-

[8] C. J. Bouwkamp, "Concerning a New Transcendent, Its Tabulation and Applications in Antenna Theory," *Quarterly Applied Mathematics*, Vol. 5, pp. 394-402, January, 1948.

[9] Erik Hallén, "Iterated Sine and Cosine Integrals," *Transactions of the Royal Institute of Technology*, Stockholm, Sweden, No. 12, pp. 3-6, 1947.

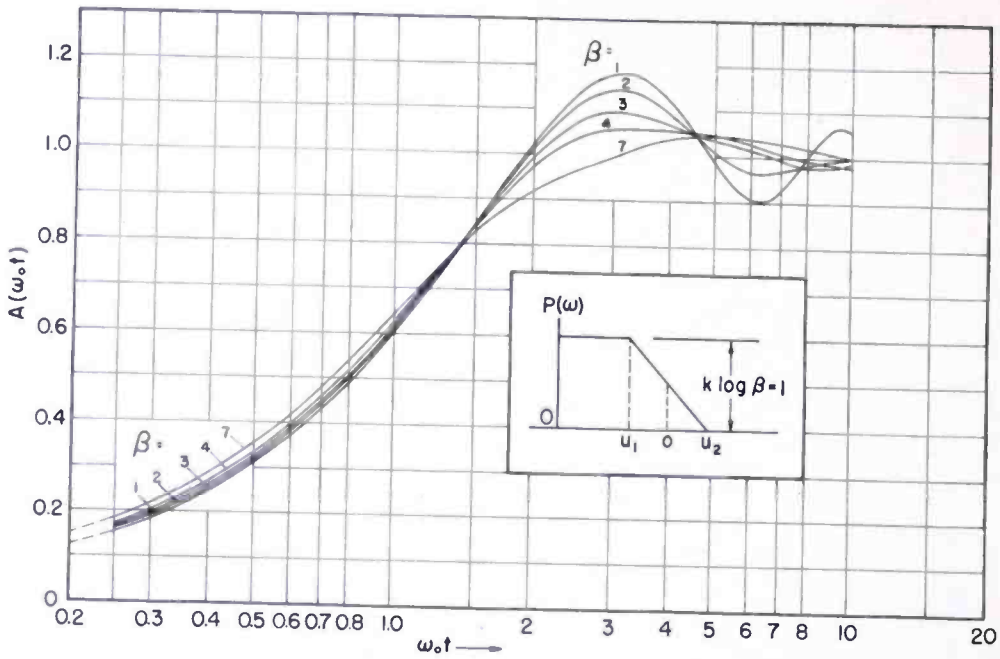

Fig. 15—Universal curves $P(\omega)$ to $A(t)$.

peaked low-pass filter, $Q = 1.0$, with the $P(\omega)$ characteristic shown by Figure 6.

The curve for $P(\omega)$ is approximated by the straight line segments shown on Figure 17. The first approximation is the line A B C D, with $\beta = 1.8$, $\omega_0 = 1.12$ and $P(\omega) = 1.13$. The curve for $\beta = 1.8$, obtained

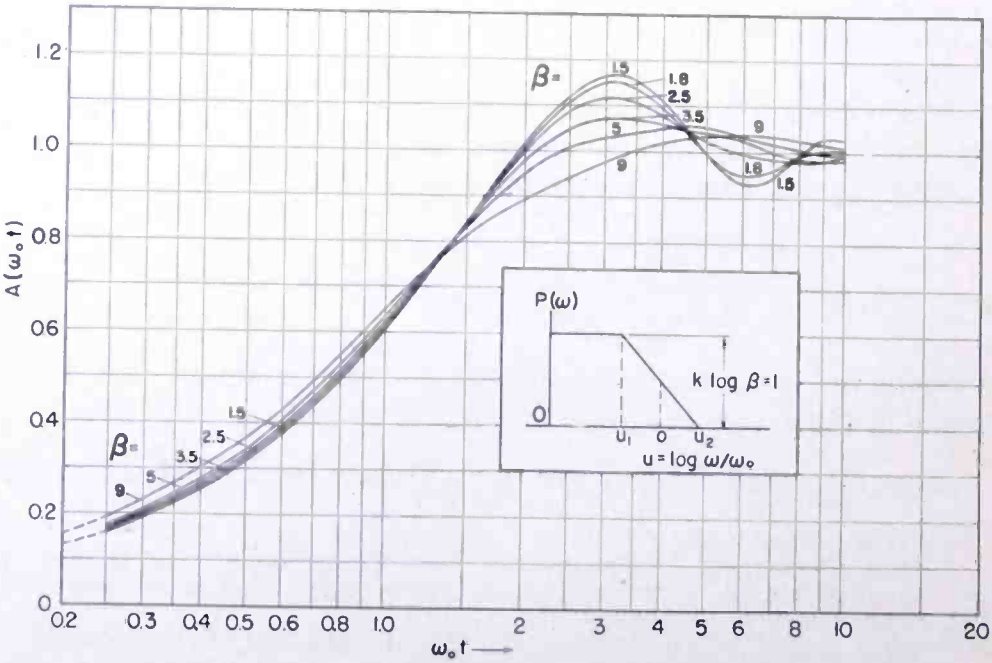

Fig. 16—Universal curves $P(\omega)$ to $A(t)$.

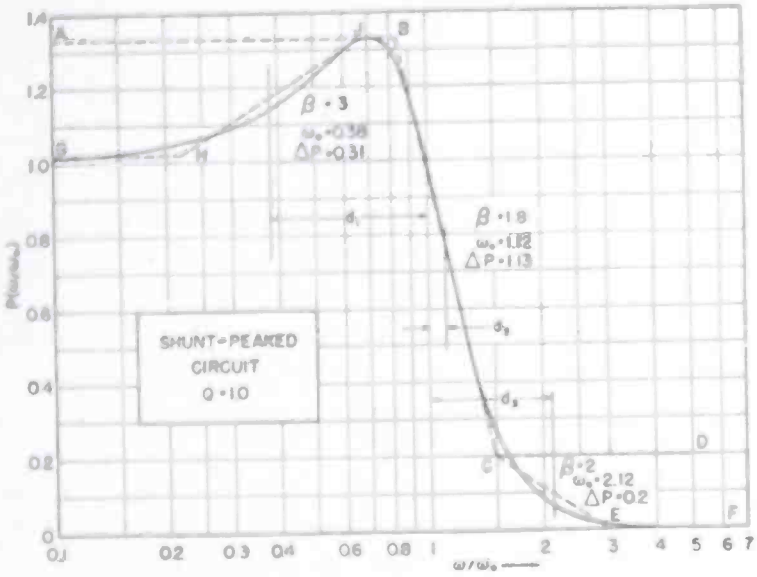

Fig. 17—Graphic solution for $A(t)$ from $P(\omega)$.

from Figure 16, is multiplied by 1.13 by means of proportional dividers, and plotted on semilog paper. The paper was then moved to the left a distance equal to d_2 on Figure 17 and plotted on Figure 18 as shown.

The step G H J B has a negative jump of 0.31 and corresponds to $\beta = 3$. The curve of Figure 15 was moved a distance d_1 to the right on Figure 18 and multiplied by 0.31. The minus sign shows that it is to be subtracted from the others.

In a similar manner the curve for the jump C E F is plotted on Figure 18 and moved a distance d_3 to the left as shown. When the

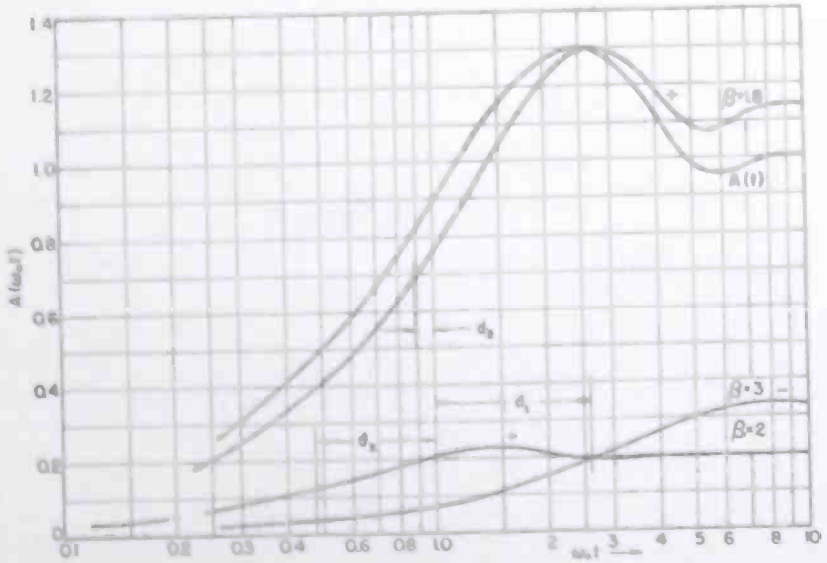

Fig. 18—Graphic solution for $A(t)$ from $P(\omega)$.

three curves are added and the sum is plotted on a linear time scale, the result is shown by the crosses of Figure 19. The solid curve is the theoretical one, and the error is seen to be very small.

Graphic Solution for Finding $A(t)$ from $Q(\omega)$

A set of universal curves for solving this problem will be derived in the same way as for the $P(\omega)$ curves just completed. A logarithmic frequency scale will be used as before. In Figure 20 let $Q(\omega)$ be the straight line segments shown. Using the same notation as before

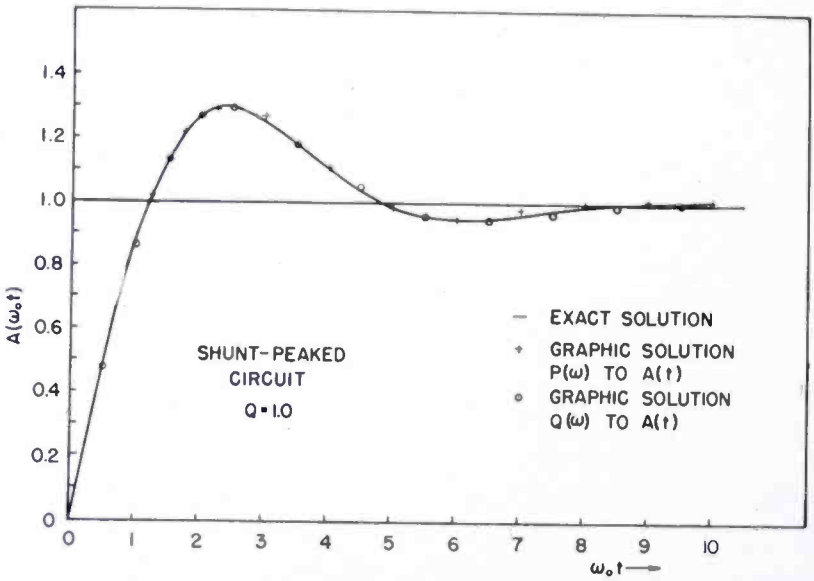

Fig. 19—Graphic solution of $A(t)$ from $P(\omega)$.

$$Q(\omega) = 0, \qquad 0 \leq \omega \leq \omega_1$$

$$= -k \log \frac{\omega\sqrt{\beta}}{\omega_0}, \qquad \omega_1 \leq \omega \leq \omega_2$$

$$= -1, \qquad \omega_2 \leq \omega < \infty.$$

Using Equation (24),

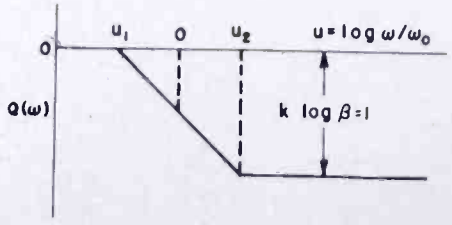

Fig. 20—Straight-line segments for $Q(\omega)$.

$$A(\omega_0 t) - A(\infty) = \frac{2}{\pi}\int_0^\infty \frac{Q(\omega)}{\omega}\cos \omega t \, d\omega \qquad t > 0 \qquad (24)$$

$$= -\frac{2k}{\pi}\int_{\omega_0/\sqrt{\beta}}^{\omega_0\sqrt{\beta}} \log \frac{\omega\sqrt{\beta}}{\omega_0}\,\frac{\cos \omega t}{\omega}\, d\omega$$

$$-\frac{2k}{\pi}\int_{\omega_0\sqrt{\beta}}^{\infty} \log \beta\,\frac{\cos \omega t}{\omega}\, d\omega$$

$$= -\frac{2k}{\pi}\int_{\omega_0 t/\sqrt{\beta}}^{\infty} \log \frac{s}{\omega_0 t/\sqrt{\beta}}\,\frac{\cos s}{s}\, ds$$

$$+\frac{2k}{\pi}\int_{\omega_0 t\sqrt{\beta}}^{\infty} \log \frac{s}{\omega_0 t\sqrt{\beta}}\,\frac{\cos s}{s}\, ds. \qquad (65)$$

Using the identity

$$\int_x^\infty \frac{\mathrm{Ci}\,(t)}{t}\, dt = -\int_x^\infty \frac{dt}{t}\int_t^\infty \frac{\cos s}{s}\, ds$$

$$= -\int_x^\infty \frac{\cos s}{s}\, ds \int_x^s \frac{dt}{t}$$

$$= -\int_x^\infty \log \frac{s}{x}\,\frac{\cos s}{s}\, ds, \qquad (66)$$

the result is

$$A(\omega_0 t) - A(\infty) = \frac{2k}{\pi}\int_{\omega_0 t/\sqrt{\beta}}^{\omega_0 t\sqrt{\beta}} \frac{\mathrm{Ci}\,(s)}{s}\, ds$$

$$= -\frac{2k}{\pi}\left[\mathrm{Re}\, E_1(\omega_0 t\sqrt{\beta}) - \mathrm{Re}\, E_1(\omega_0 t/\sqrt{\beta})\right] + \frac{2\gamma}{\pi} + \frac{2}{\pi}\log \omega_0 t,$$

$$\gamma = 0.5772 \cdots \qquad (67)$$

in the notation of Bouwkamp.[8]

A family of curves has been computed for various values of β, using

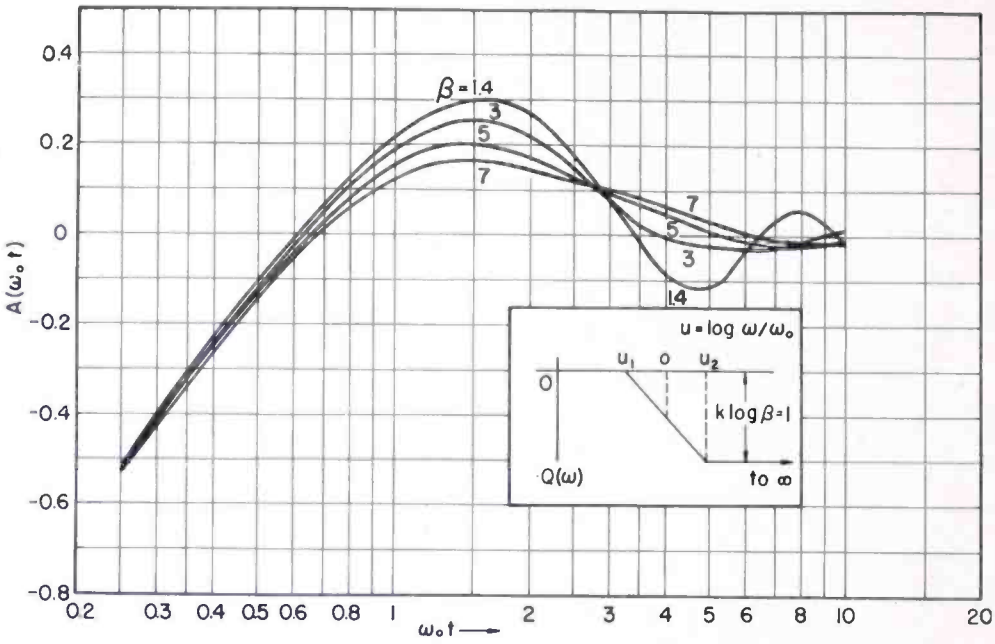

Fig. 21—Universal curves $Q(\omega)$ to $A(t)$.

Equation (67); they are given by Figures 21 and 22.

Example: Find the response of the shunt-peaked low-pass filter, $Q = 1.0$, with the $Q(\omega)$ characteristic shown by Figure 7, to a unit-step function.

The curve of Figure 23 for $Q(\omega)$ is approximated by the straight line segments A B C with $\beta = 2.25$ and $Q = 0.12$, line B D E with

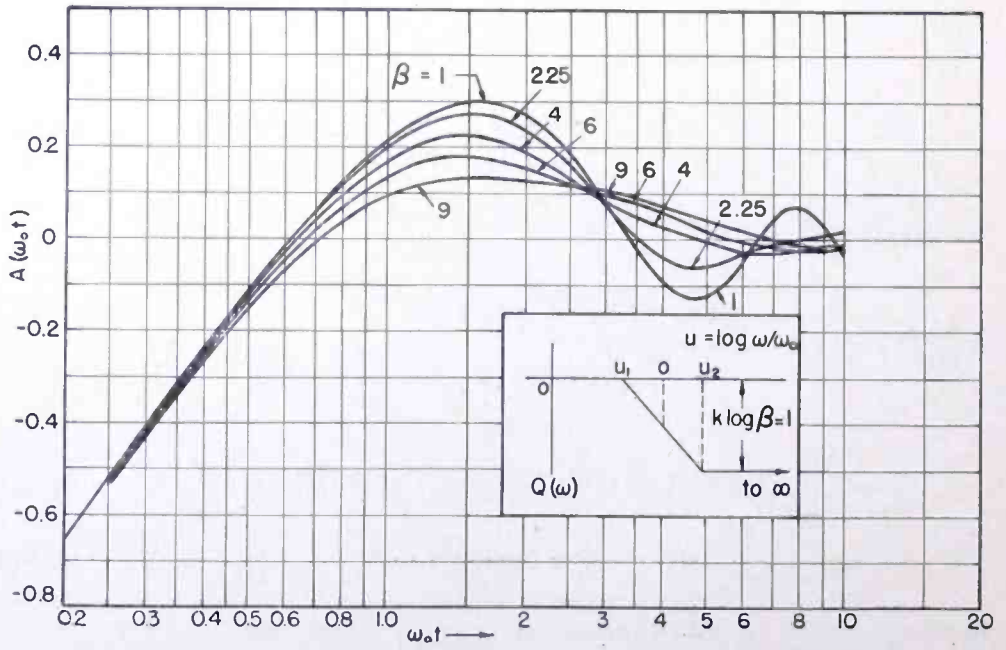

Fig. 22—Universal curves, $Q(\omega)$ to $A(t)$.

$\beta = 1.4$, etc. as shown. When the curves of Figures 21 and 22 are used in the same way that was done in Figure 17 for $P(\omega)$, the result is as shown by the circles of Figure 19. The errors are very small as shown.

Sweep and Display Equipment

The basic oscilloscope display is in the form of a polar diagram of the network output voltage, referred to the input voltage as the unit vector with zero phase. Frequency marking is obtained by Z-axis or intensity modulation of the display trace.

In addition to this display, which is a polar plot of $T(\omega)e^{i\theta(\omega)}$, displays for $P(\omega)$ and $Q(\omega)$ are available. The theoretical discussion

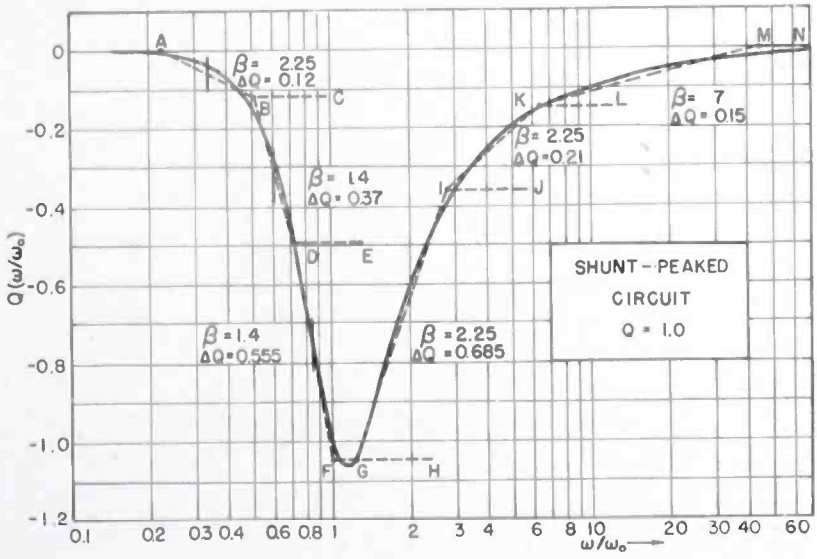

Fig. 23—Graphic solution, $A(t)$ from $Q(\omega)$.

has shown that $P(\omega)$, $Q(\omega)$, and $T(\omega)e^{i\theta(\omega)}$, are all true network parameters. For purposes of circuit alignment and circuit design, $T(\omega)e^{i\theta(\omega)}$ is usually most convenient. The sections that follow will describe the design, operation, and applications of the equipment.

Design Theory

To obtain $P(\omega)$, let the two voltages of Figure 1,

$$e_1 = E_1 \sin(\omega t + \phi_1) \tag{68}$$

and

$$e_2 = E_2 \sin(\omega t + \phi_2) \tag{69}$$

be applied to the grids of the modulator shown by Figure 24. If the

circuit is adjusted properly, the tube will multiply the two voltages together. The output is

$$e_1 e_2 = E_1 E_2 \sin(\omega t + \phi_1) \sin(\omega t + \phi_2)$$

$$= \frac{1}{2} E_1 E_2 [\cos(\phi_2 - \phi_1) - \cos(2\omega t + \phi_1 + \phi_2]. \tag{70}$$

When this output is passed through a low-pass filter, the term of frequency 2ω is removed so the output voltage is

$$e_3 = \frac{1}{2} E_1 E_2 \cos(\phi_2 - \phi_1)$$

$$= k\, T(\omega) \cos\theta(\omega) = k\, P(\omega), \tag{71}$$

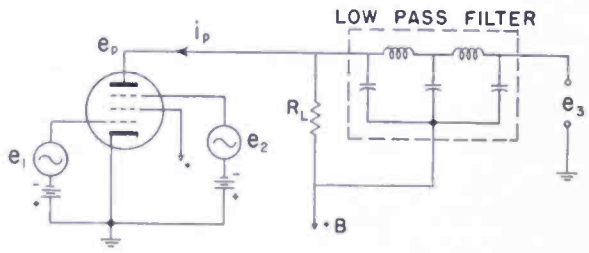

Fig. 24—Suppressor grid modulator.

where $k = \frac{1}{2} E_1^2$.

In a similar manner, $Q(\omega)$ can be obtained if the two voltages

$$e_1 = E_1 \cos(\omega t + \phi_1) \tag{72}$$

and

$$e_2 = E_2 \sin(\omega t + \phi_2) \tag{73}$$

are multiplied together. Thus

$$e_1 e_2 = E_1 E_2 \cos(\omega t + \phi_1) \sin(\omega t + \phi_2)$$
$$= E_1 E_2 [\sin(\phi_2 - \phi_1) + \sin(2\omega t + \phi_2 + \phi_1)]. \tag{74}$$

After passage through the low-pass filter,

$$e_3 = \frac{1}{2} E_1 E_2 \sin(\phi_2 - \phi_1)$$

$$= \frac{1}{2} E_1^2 \, T(\omega) \sin \theta(\omega)$$

$$= k \, Q(\omega), \tag{75}$$

where $k = \frac{1}{2} E_1^2$ as before.

Although a simple modulator followed by a low-pass filter will perform the required multiplication, a balanced phase detector[10] gives the desired result without critical adjustments. Figure 25 shows such a circuit. For proper operation in this equipment it is necessary that $e_1 >> e_2$, say 5 to 1 or more to allow for selectivity and attenuation in

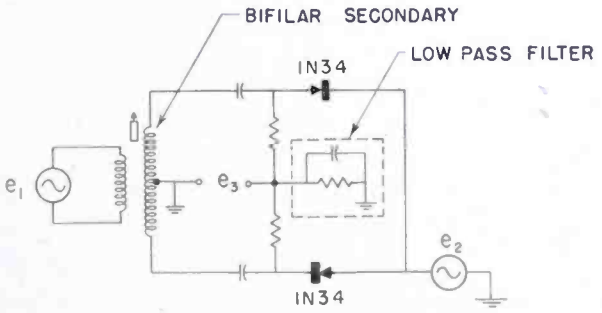

Fig. 25—Phase-sensitive detector.

the network under test. The low-pass filter is built-in as shown. A phase splitter can be used instead of the transformer and is preferable for wider bandwidths.

In order to sweep the entire frequency range of the filter, a fixed oscillator is usually beat with a frequency-modulated oscillator to produce the input signal e_1, as shown by Figure 26. The fixed-frequency oscillator is shifted 90 degrees with respect to the two channels as shown, so the two sweep voltages are always 90 degrees out of phase, as required by Equations (68) and (72). This is easy to do, since the fixed-frequency oscillator operates at one frequency only. Figure 27 shows the complete display arrangement.

To test a network, it is connected as shown by Figure 27. The input of the sweep, e_1, is fed to the $P(\omega)$ modulator, which is shown by Figure 25, and the output of the network, e_2, is also applied to the modulator. The output of the modulator is a voltage proportional to $P(\omega)$. In the same way, if the sweep which is shifted 90 degrees is used to drive the $Q(\omega)$ modulator as shown, the output will be a

[10] Britton Chance, Vernon Hughes, Edward F. MacNichol, David Sayre, and Frederic C. Williams, *Waveforms*, First Edition, McGraw-Hill Book Co., Inc., New York, 1949, p. 512, Figure 14.13.

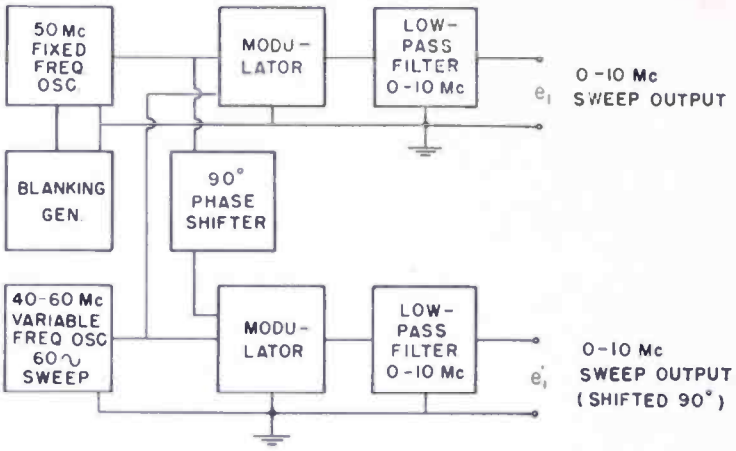

Fig. 26—Generation of sweep voltage.

voltage proportional to $Q(\omega)$. By connecting the two outputs to oscilloscopes as shown, it is possible to display $P(\omega)$, $Q(\omega)$ and the polar plot, $T(\omega)\ e^{i\theta(\omega)}$ simultaneously. Since the system will work for any fixed frequency, it is also possible to feed the outputs into automatic curve-drawing equipment and plot the $P(\omega)$ or $Q(\omega)$ response curves as a function of frequency directly. In this way it is possible to go down to as low a frequency as desired. Frequency markers are provided by modulation on the Z-axis of the scope at one or more frequencies.

Sweep Generator

Figure 28 shows the schematic for the sweep generator. The fixed-frequency oscillator operates at 25 megacycles with second-harmonic

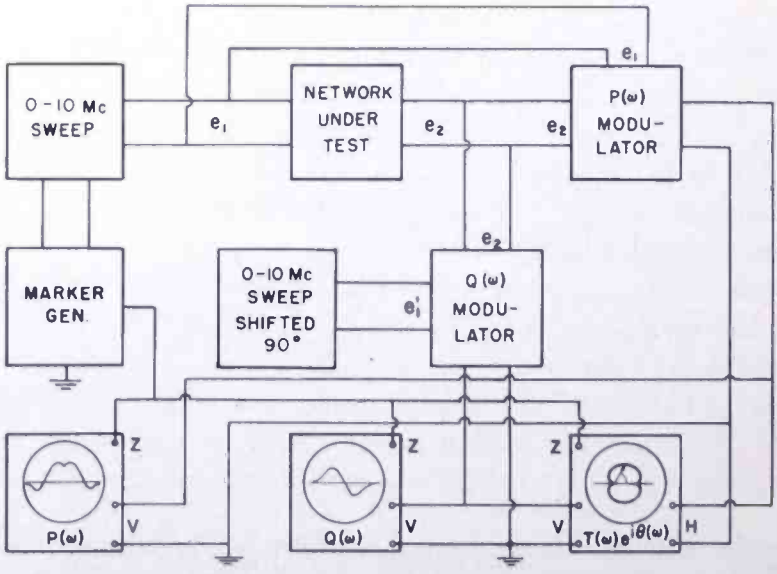

Fig. 27—Circuit for displaying $P(\omega)$, $Q(\omega)$ and $T(\omega)e^{i\theta(\omega)}$ simultaneously.

selection in the plate circuit. The inputs to the two modulators are shifted 90 degrees with respect to each other by the two *RC* networks. The two capacitors, C_1 and C_2, are adjustable to obtain this 90-degree phasing after the 25 megacycle oscillator is tuned. The variable-frequency oscillator is frequency modulated at a 60-cycle repetition rate with a maximum variation from 40 to 60 megacycles. Direct current on the moving coil of the 60-cycle variable capacitor serves to locate the center frequency, while an a-c source in series with the d-c source determines the deviation.

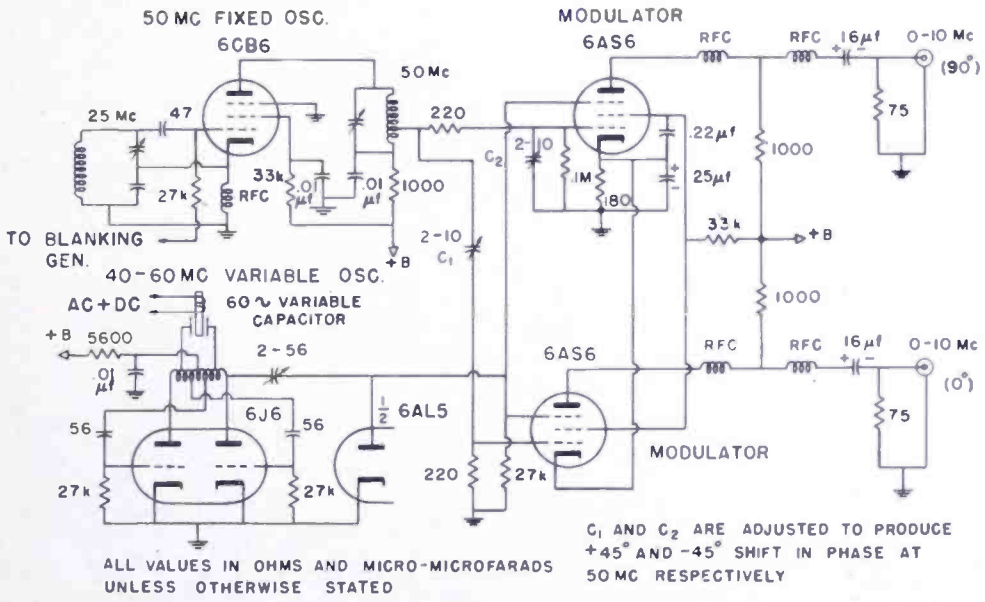

Fig. 28—Sweep generators.

The two 6AS6 tubes are linear modulators with low impedance output. Radio-frequency chokes in the plate circuits suppress components at carrier and higher frequencies. Where larger sweep outputs are required, the 6AS6 modulators may be provided with higher load impedances and may be followed by cathode followers. Care must be taken to keep the impedances in the two channels identical, to preserve the 90-degree relationship over the entire sweep range. As shown by Figure 26, the fixed oscillator is blanked at a 60-cycle rate so that the sweep output is zero on alternate half cycles at the 60-cycle repetition rate.

The power supply should have less than 0.1 per cent hum, and should have at least two per cent regulation to insure a stable sweep output. The two oscillators should be well shielded and shock mounted in ceramic sockets. Every effort must be made to eliminate r-f radiation. Oscillator "pulling" should be eliminated by adequate isolation.

Marker Circuit

The marker circuit, Figure 29, is a delay line operated with a short-circuited receiving end and consequently a high standing-wave ratio. A diode rectifier followed by an *RC* filter picks off the envelope generated when the sweep voltage is applied to the line. In the four clipping amplifiers following the diode, pulses are obtained which coincide accurately with the cancellation points in the envelope of the delay line voltage. These clipping amplifiers are similar to television sync separators and are self-biased. The output pulses are used to

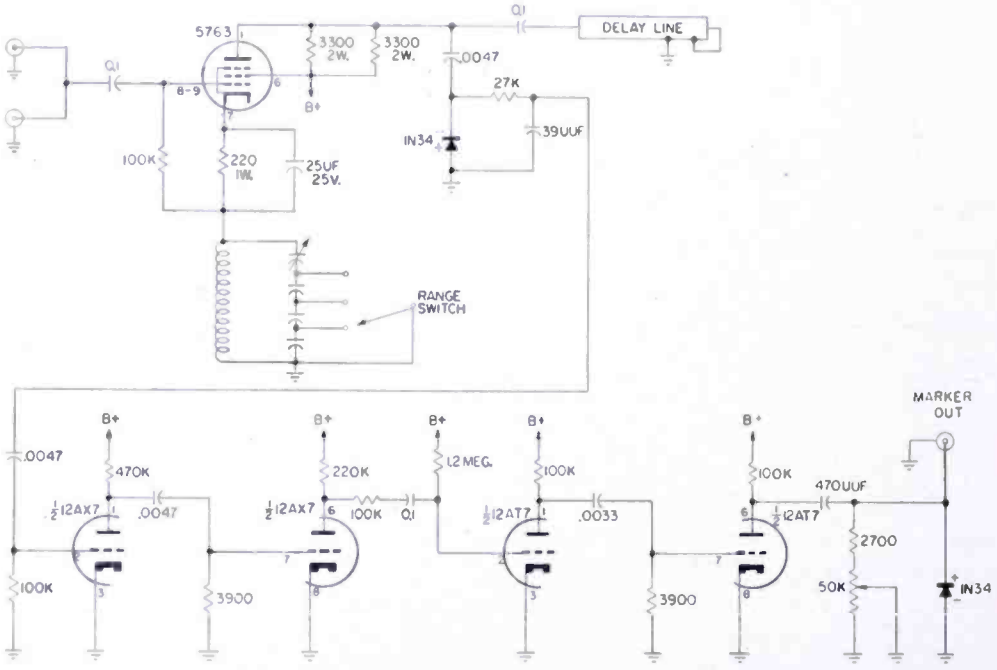

Fig. 29—Marker generator.

intensity-modulate the electron beam of the display to generate dot markers.

In the cathode of the delay-line driver tube is a parallel resonant circuit which may be tuned, by appropriate switching, between 0 and 10 megacycles. This provides an interpolation marker. The driving voltage for the delay line is sharply reduced at the resonant frequency of this circuit, causing a hole in the envelope at that frequency and providing an additional dot marker which is easily adjusted to any desired frequency. The calibration of this marker can always be compared to the delay-line marker dots, so accurate calibration is not needed. The dot markers are accurate to about ±25 kilocycles at 6 megacycles, with the error decreasing essentially linearly with frequency.

The line employed is 18¼ inches of HH2500.* The resulting marker dots are equally spaced every 500 kilocycles. The line may be cut for any other marker spacing, or other calibrated lines may be switched in and out, if desirable. A gain control for marker brightness is provided. These multiple, harmonically related markers are particularly suitable for the display described in this paper, but are also useful for other sweep measurements.

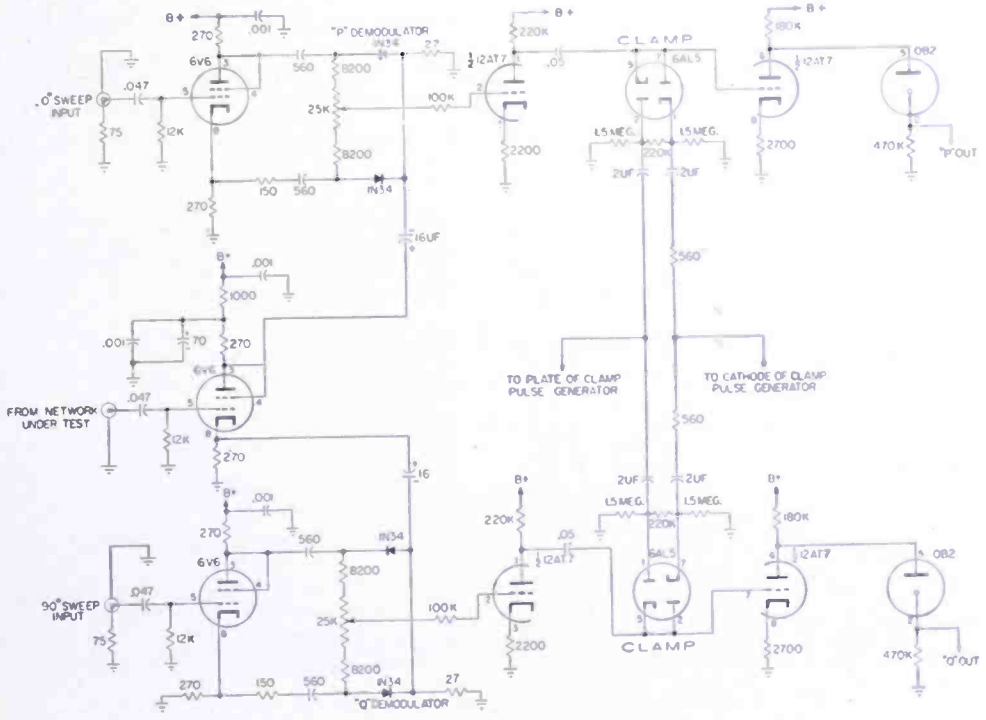

Fig. 30-A—Display unit.

$P(\omega)$ AND $Q(\omega)$ DISPLAY UNIT

The display unit, Figures 30 (a) and (b), consists of a well-regulated power supply, $P(\omega)$ and $Q(\omega)$ demodulators, and their associated amplifier and clamp circuits. The $P(\omega)$ demodulator is a phase-sensitive detector circuit[10] driven from a wide-band, low-impedance phase splitter. Two 1N34 diodes are used, and these are selected to have identical forward and back resistances. The second input for the $P(\omega)$ demodulator is the plate output from a preceding phase splitter which is driven by the output voltage of the network under test. The cathode of this phase splitter drives the $Q(\omega)$ demodulator; a phase splitter was chosen to obtain sufficient isolation between the $P(\omega)$ and $Q(\omega)$ demodulators. The output from the $P(\omega)$ demodulator is obtained

* Manufactured by the Columbia Technical Corporation, New York, N. Y.

from the center arm of a 25,000-ohm potentiometer which is set to balance the modulator. The desired output voltage has a 60-cycle repetition rate and contains frequency components up to several thousand cycles. The sweep frequency components existing at the center of the balance potentiometer are low-passed via the 100,000-ohm series resistor feeding into the shunt capacity of the first $P(\omega)$ amplifier which is d-c coupled. This amplifier has one per cent negative feedback because of the unbypassed cathode resistor. The plate of the first amplifier is capacity-coupled to the grid of the second amplifier, with a driven synchronous clamp on the grid of the second amplifier. The clamp sets the grid voltage during the blanked portion of the sweep as may be seen from Figure 31. At the top of this figure are shown

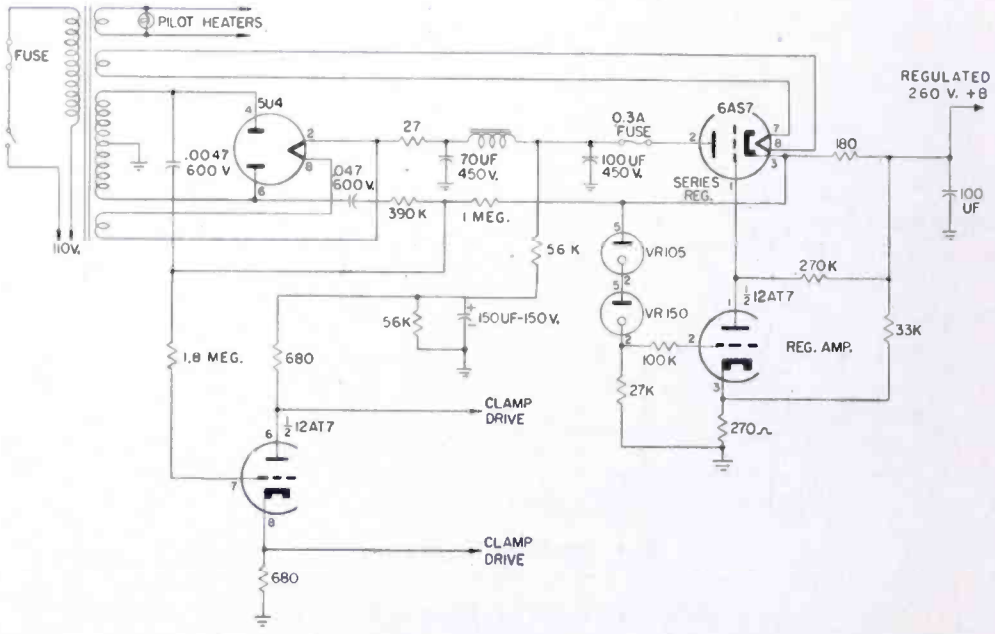

Fig. 30-B—Power supply for display unit.

typical $P(\omega)$ and $Q(\omega)$ waveforms obtained from a series-peaked low-pass filter. It will be noted that the clamps cause no significant transients, and their time position falls within the sweep blanking period. Figure 31(c) shows the clamp drive pulses.

It will be noted that the $P(\omega)$ and $Q(\omega)$ waveforms may contain a d-c component. It is therefore necessary either to d-c couple the entire display unit, or to insert the proper d-c by clamping. Since this equipment may be used to check the amplitude and phase response of complete systems, any variations in line voltage would normally cause a variation in d-c on these waveforms, and for that reason the synchronous clamp was chosen in preference to d-c coupling. By clamping on the blanked portion of the sweep output, d-c shifts caused by line

voltage variations are removed. The clamp time constants were carefully chosen to achieve this result. Another advantage of the clamp is that steady-state measurements can be made by turning off the a-c supply to the 60-cycle sweep capacitor unit, thereby removing the frequency deviation from the frequency-modulated oscillator. The d-c may then be adjusted to shift the frequency of the frequency-modulated oscillator to produce a desired steady beat frequency, which, however, will still be blanked on alternate half-cycles at 60 cycles because of the blanking on the fixed frequency sweep oscillator. In this case the $P(\omega)$ and $Q(\omega)$ voltages are merely 60-cycle square waves whose amplitude and polarity during sweep time will measure the transfer function of the network tested. The display for this case

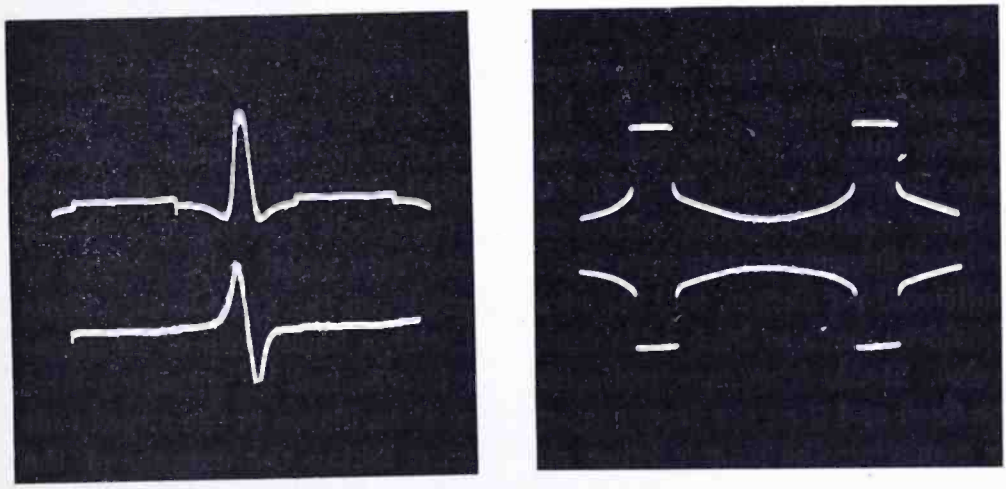

Fig. 31—a (upper left), b (lower left), and c (right).

consists of a single illuminated spot, marking the end of the transfer impedance vector. Such operation may be important when the network is such that normal sweep application would generate frequency-modulation transients, leading to erroneous results. This is the case with high-Q resonant systems (Q having its usual meaning here).

The second $P(\omega)$ amplifier has the desired output voltage plus the plate polarizing voltage in the plate output. This output is coupled through a voltage-regulator tube to remove a large portion of the polarizing voltage to lessen the requirements on the scope centering system.

The $Q(\omega)$ demodulator, amplifiers, and clamp are identical with the $P(\omega)$ channel in every respect except that the $Q(\omega)$ modulator driver is fed from the 90-degree sweep while the $P(\omega)$ modulator driver is fed from the zero-degree sweep. The display unit covers a frequency range from approximately 160 kilocycles to 12 megacycles. The range can be extended in either direction by appropriate changes in the

coupling networks and the modulator constants. The outputs are approximately 10 volts peak to peak for a sweep input of 0.1 volt. These voltages are sufficient to operate most commercial oscilloscopes and insure linear operation of all circuits involved.

The power-supply unit consists of a high gain series regulator, capable of producing a 260-volt B-supply with approximately one per cent regulation and less than 1 millivolt of hum. The clamping pulses are generated from the rectifier plate voltage, proper phasing being obtained via the RC coupling network in the 12AT7 grid circuit with grid-current limiting. The outputs are available across the 680-ohm plate and cathode resistors. The line plugs of the sweep unit and the display unit should either be provided with keys, or a single line plug should be used to insure proper phasing of sweep-blanking and clamp-pulse voltages.

Careful shielding is necessary to prevent any residual radio-frequency radiation from the high-frequency sweep oscillators from leaking into the display unit where it may be rectified on the demodulator diodes or by the $P(\omega)$ and $Q(\omega)$ high-gain amplifiers. To obtain further radio-frequency suppression, the leads feeding the phase-splitter demodulator-drivers were formed into small coils serving as additional r-f chokes, and the stray capacity on the demodulator feeds should be made as high as is consistent with a bandwidth of 12 megacycles. Radio-frequency radiation can be checked by disabling first the fixed and then the frequency-modulated oscillator in the sweep unit by removing the proper tubes and then checking the outputs of the $P(\omega)$ and $Q(\omega)$ amplifiers for zero output.

The cables feeding the $P(\omega)$ and $Q(\omega)$ phase splitters from the sweep unit are identical, to preserve the 90-degree phase relationship over the entire bandwidth, and the terminating resistors should be carefully selected for optimum termination to keep the standing-wave ratio on the feed lines very close to unity.

Operation of the Equipment

The equipment is operated by inserting the network or system to be tested between the terminals marked "network under test." It will be noted from the figures that the test circuit is then supplied from the zero-degree sweep, and its output voltage is applied to the phase splitter in the display unit to provide the second inputs to the $P(\omega)$ and $Q(\omega)$ demodulators. For the equipment shown here, the circuit under test should have 75-ohm input and output impedances. If necessary, impedance transformers can be used. The network may be of the minimum-phase-shift type, or nonminimum-phase shift; it may be

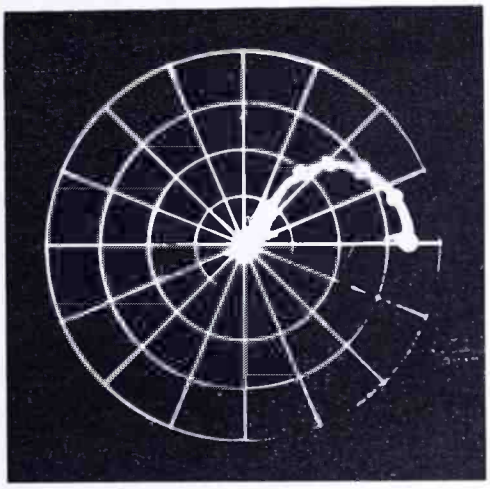

Fig. 32.

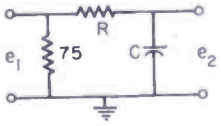

Fig. 33.

lumped constant or distributed, and it may include any number of linear stages and transducers, provided that it can be driven by a voltage and will have a voltage across its output terminals.

An understanding of the operation of this equipment is best gained from a discussion of typical test results. Figure 32 shows the display resulting when the network under test is the simple RC low-pass filter, as shown in Figure 33. The trace starts on the right of the diagram and proceeds in counter-clockwise fashion back to the origin. The amplitude is given by the radius vector connecting the trace to the origin, and the marking dots appear at 500-kilocycle intervals. It will be noted that the phase is far from linear with frequency, and that the amplitude decreases rapidly as the frequency increases. The total phase shift from zero to infinite frequency is 90 degrees. Figure 34 shows the response when an inductance is placed in series with the resistor as in the circuit of Figure 35. As is evident from the display,

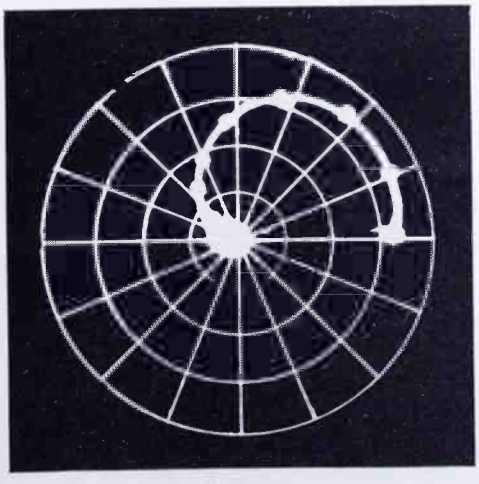

Fig. 34.

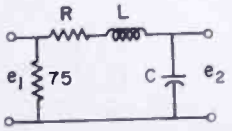

Fig. 35.

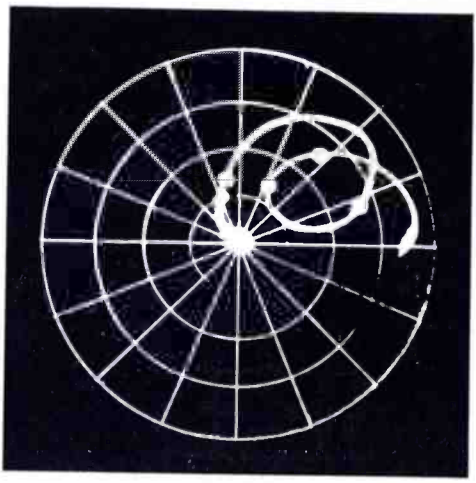

Fig. 36.

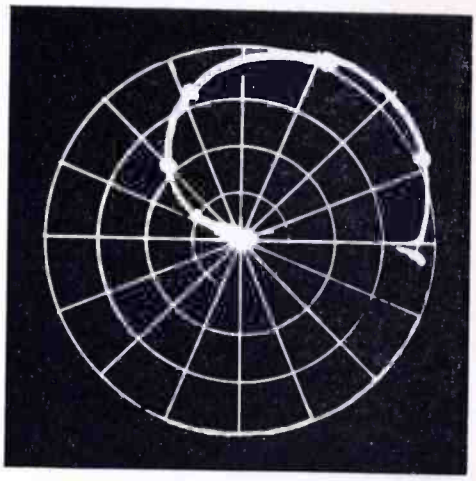

Fig. 37.

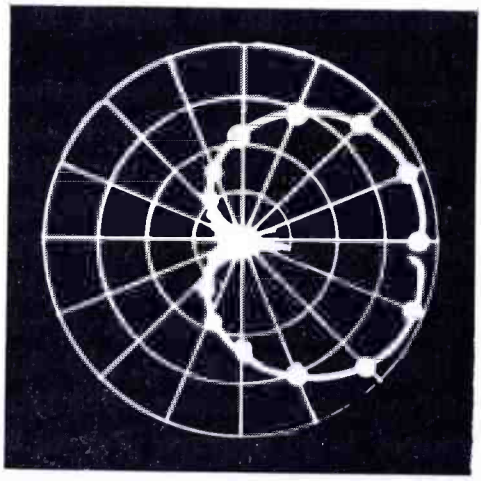

Fig. 38.

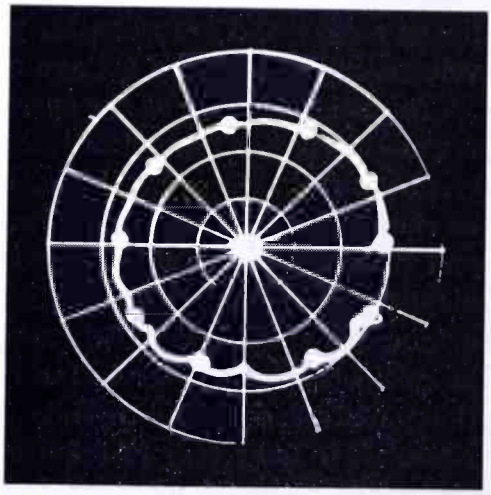

Fig. 39.

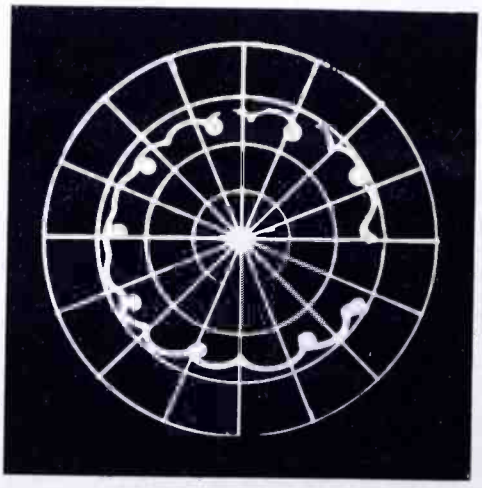

Fig. 40.

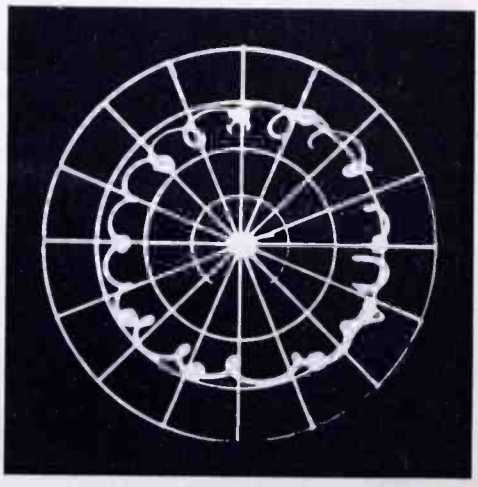

Fig. 41.

both the amplitude and the phase response of the circuit are considerably improved, as is predicted by theory for a series-peaked circuit with a Q of 0.3. The total phase shift of the circuit from zero to infinite frequency is seen to be 180 degrees. An enlarged version of Figure 34 is shown for illustrative purposes.

Figure 36 shows the display when a series resonant trap is added to the circuit. The phase oscillation near the rejection point is clearly evident. Figure 37 shows what happens when the peaking is increased, resulting in a rapid deterioration of the phase characteristic. The figures discussed so far were taken with the frequency-modulation sweep adjusted to deviate from 50 to 60 megacycles, so that the sweep output starts at zero and goes to 10 megacycles.

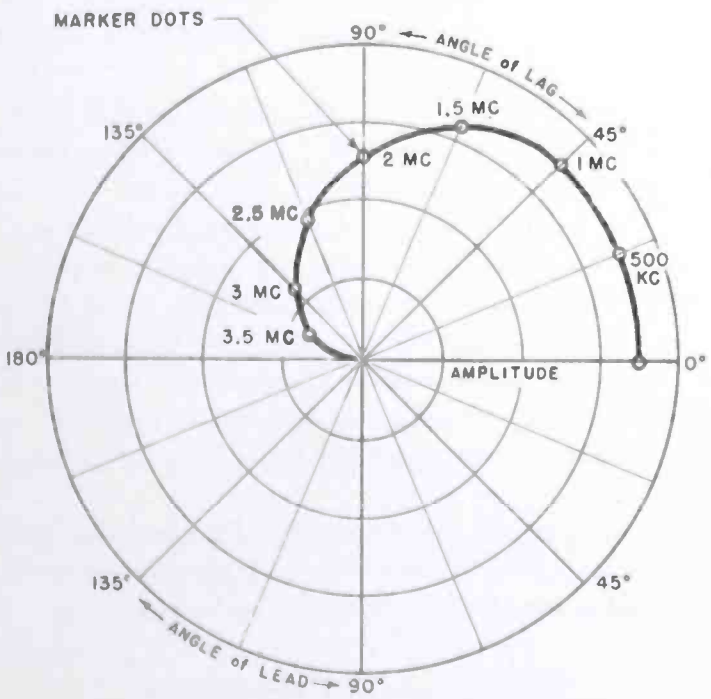

Fig. 34—Amplitude-phase characteristics.

Figure 38 shows what happens when the frequency-modulation sweep is adjusted to deviate from 40 to 60 megacycles, so that the sweep output starts at 10 megacycles and decreases to zero and then increases to 10 megacycles again before being blanked. Two display traces will be noted, substantially symmetrical about the horizontal axis. The degree of symmetry is a measure of the absence of frequency-modulation transients in the circuit under test, in the marker circuit, and in the demodulators, and shows substantially no evidence of hum. All of these effects separately and together would result in a degree of asymmetry about the horizontal axis determined by the severity of the

defects. Figure 31(a) shows the $P(\omega)$ function belonging to Figure 38, and Figure 31(b) shows the $Q(\omega)$ function going with the display of Figure 38.

As mentioned before, this equipment can be used for point-by-point measurements. In the absence of frequency-modulation transients, the vector radius should trace out the locus shown on the sweep display point by point, as the steady frequency is varied. In case an asymmetrical display is obtained with the double-sided sweep, it is then easy to check whether the asymmetry is due to hum or frequency-modulation transients simply by checking a few points on the curve in the steady state.

If the circuit under test is nonlinear, the display will also be asymmetrical. If hum and frequency-modulation transients can be eliminated as the cause, the degree of symmetry of the trace provides a good check on circuit linearity.

Because of the information available from the full sweep trace and its degree of symmetry, it is advisable to use it wherever convenient.

It should be realized that when the total phase shift exceeds 360 degrees the trace will become spiral and may be difficult to interpret at first glance. This difficulty is easily overcome by use of the interpolation marker which may be used to mark any point of interest. If desirable, the multiple harmonic markers can be removed by disconnecting the delay line in the marker chassis from the driver, in which case a single marker will be generated by the interpolation marker trap circuit. In that manner even the most complicated displays are rapidly and accurately interpreted.

Figures 39, 40, and 41 show the displays when the test circuit is a delay line with best termination, for too large a terminating resistor, and for too small a terminating resistor respectively.

ACCURACY OF THE EQUIPMENT

Experimental determination of the accuracy of this equipment has shown that the phase is given accurately within plus or minus 3 degrees in the range from 150 kilocycles to 8 megacycles in steady-state measurements, and in sweep measurements when frequency-modulation transients are negligible. The amplitude accuracy is within five per cent over the entire range in the absence of frequency-modulation transients. These values are well within the limits predicted by theory.

AUXILIARY EQUIPMENT

Several items of auxiliary equipment have been designed to increase

the usefulness of this equipment. Sometimes it is expedient to display the deviation from phase linearity rather than the phase curve itself, particularly in those instances where the total phase shift in systems under test is large, and where the desired objective is phase linearity. This can be done by inserting calibrated, constant-delay, nonselective (in the range of the equipment) lag lines in series with the sweep feeds to the display unit. The delay in each line is adjusted to the average delay of the circuit under test. Figure 42 shows this arrangement.

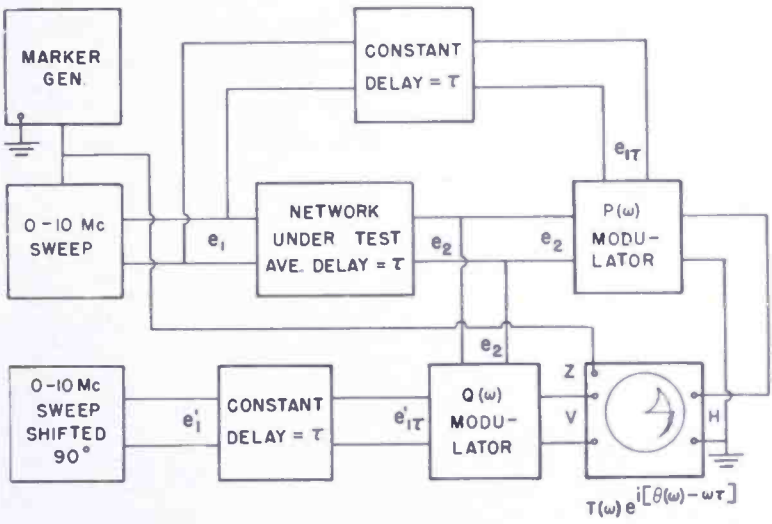

Fig. 42—Circuit for displaying deviation from phase linearity.

The $P(\omega)$ modulator has applied to its terminals the two voltages $e_{1\tau}$ and e_2 as shown in Figure 42. These may be expressed as follows:

$$e_{1\tau} = E_1 \sin(\omega t - \tau\omega) \tag{76}$$

since the phase shift of the lag line is $\theta_\tau = \tau\omega$, and

$$e_2 = E_2 \sin(\omega t - \theta), \tag{77}$$

where θ is the phase shift of the network under test.

The output voltage of the $P(\omega)$ modulator will therefore be the low-frequency component of the product $e_{1\tau} \times e_2$. This is, by Equation (71),

$$e_p = \frac{1}{2} E_1 E_2 \cos(\tau\omega - \theta) = k\, T(\omega) \cos(\tau\omega - \theta). \tag{78}$$

Similarly, the output voltage of the $Q(\omega)$ modulator will be, by Equa-

tion (75),

$$e_Q = -k\,T(\omega)\,\sin\,(\tau\omega - \theta). \tag{79}$$

The angle shown on the display is therefore the angle $(\tau\omega - \theta)$ which is the difference between the phase shift of the network and the linear phase function $(\tau\omega)$. In case the network under test is linear phase, the display will be a single horizontal line.

Heterodyne equipment has been designed to make possible measurements outside the basic 0 to 10 megacycle range of the equipment, as shown in Figure 43. Here the 0 to 10 megacycle sweep output is heterodyned with a fixed oscillator to produce frequency components in the range of the network to be tested. The output voltage from the network under test is beat against this same heterodyne oscillator, to

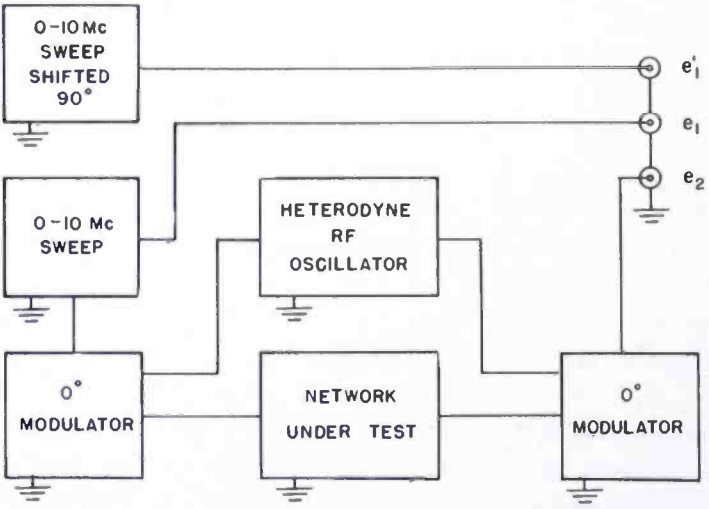

Fig. 43—Heterodyne method of shifting sweep frequency.

obtain an output between 0 and 10 megacycles. The resulting voltages e_1', e_1, and e_2 are fed to the display unit in the normal manner as shown by Figure 27. It will now be shown how this arrangement works.

The $P(\omega)$ and $Q(\omega)$ modulators are fed voltages e_1 and e_1' as before and as defined in Equations (68) and (72) respectively. Their input voltage, e_2, is found as follows:

The zero-degree modulator on the bottom left of Figure 43 has applied to it the voltages

$$e_1 = E_1 \sin\,(\omega t + \phi_1) \tag{68}$$

and the voltage produced by the heterodyne r-f oscillator

$$e_H = E_H \sin \omega_H t. \tag{80}$$

The voltage e_1 amplitude modulates the voltage e_H. The result is the test voltage

$$e_\tau = (1 + e_1)\, e_H = E_1 E_H \sin (\omega t + \phi_1) \sin \omega_H t + E_H \sin \omega_H t$$

$$= \frac{1}{2} E_1 E_H [\cos (\omega t - \omega_H t + \phi_1) - \cos (\omega_H t + \omega t + \phi_1)] + E_H \sin \omega_H t.$$

If the network is sufficiently selective (as is the case with most i-f amplifiers), ω_H can be chosen so that the carrier and one of the sidebands, say the lower, are rejected. The input voltage to the network under test which produces an output then becomes

$$e_\tau = -\frac{1}{2} E_1 E_H \cos (\omega t + \omega_H t + \phi_1). \tag{81}$$

If the network is linear and passive, its output voltage will be

$$e_0 = -\frac{1}{2} E_1 E_H T(\omega + \omega_H) \cos (\omega t + \omega_H t + \phi_2) \tag{82}$$

by use of Equations (2), (3), and (4).

The voltage e_0 is beat against the heterodyne oscillator in the zero-degree modulator on the bottom right of Figure 43 and the low-frequency terms are selected by the following display unit, Figure 27. The result is the product of Equations (80) and (82):

$$e_2 = -\frac{1}{2} E_1 E_H^2 T(\omega + \omega_H) \sin \omega_H t \cos (\omega t + \omega_H t + \phi_2).$$

The low-frequency component is

$$e_2 = \frac{1}{2} E_1 E_H^2 T(\omega + \omega_H) \sin (\omega t + \phi_2) = E_2 \sin (\omega t + \phi_2) \tag{83}$$

by letting $\frac{1}{2} E_H^2 = 1$.

When Equation (83) is compared with Equation (2), it is seen that the output amplitude E_2 and the phase shift of the network

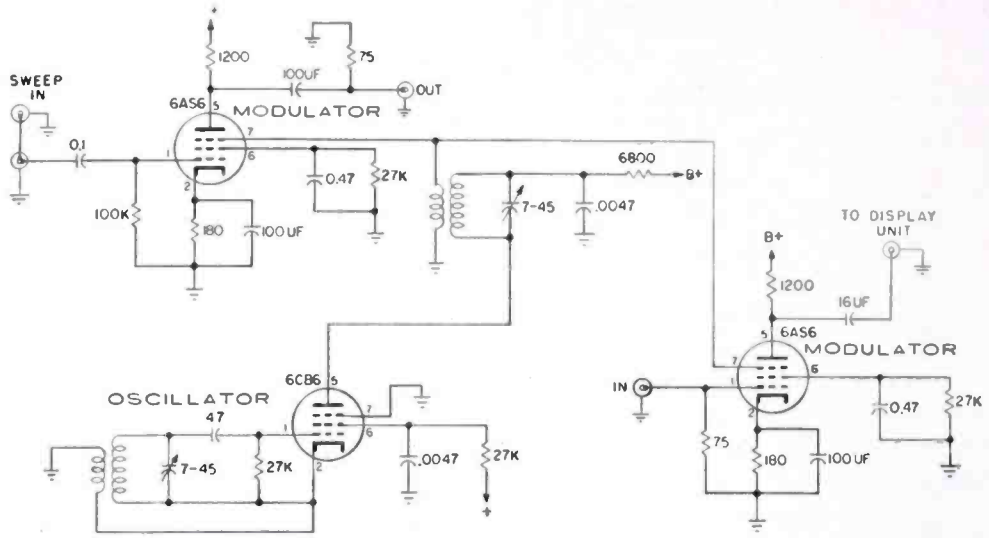

Fig. 44—Frequency shifter.

$(\phi_2 - \phi_1)$ are preserved in the heterodyne operation. It is evident from this analysis that the two modulators have carrier inputs (ω_H) that must be in phase and for this reason they have been labeled zero-degree modulators. Figure 44 is the schematic of the heterodyne unit. The 6CB6 is the oscillator, the two 6AS6 tubes are the modulators.

Figure 45 shows operation of the equipment when the network under test works in the normal range (40 to 60 megacycles) of the variable-frequency sweep oscillator. Voltages e_1 and e_1' are applied to the display unit as usual. The voltage e_2 is obtained by beating the output voltage of the network under test with the fixed sweep oscillator voltage in phase with the zero-degree sweep modulator. For this reason

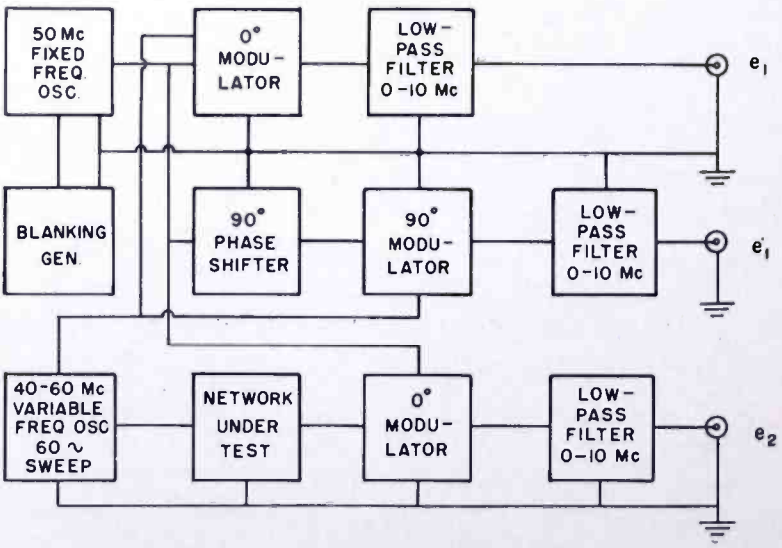

Fig. 45—40-60 megacycle sweep operation.

the modulator at the bottom of Figure 45 has been labeled zero-degree modulator. An analysis similar to that used for the arrangement of Figure 44 shows that the voltage e_2 obtained in Figure 45 has the correct amplitude and phase for proper operation of the display unit.

Conclusions

Equipment has been developed for the sweep display of the network transfer function as a vector plot. The equipment is useful in the design of amplifiers and complete systems whose phase and amplitude response determine system behavior. The equipment has been found to be accurate, reliable, and simple to use. It is useful for the sweep alignment of all kinds of amplifiers. When it is desired to compare two supposedly identical networks or to align simultaneously amplitude and phase response, the method is far more precise than conventional methods because the two variables are plotted simultaneously. If anything is wrong with the network, it will be impossible to get the right curve.

Feedback amplifiers and servo systems can be rapidly designed or analyzed by means of this display. Phase distortion studies can be made and the effects of gain-control settings and amplifier overload conditions can be rapidly ascertained.

Each time the phase angle increases by 90 degrees, either the $P(\omega)$ or the $Q(\omega)$ curve will go through zero. These zero crossings give accurate alignment points and the number of them will give the asymptotic rate of cutoff of the filter in multiples of six decibels per octave for minimum phase shift networks.

There is a direct and unique relation between either $P(\omega)$ or $Q(\omega)$ and the unit-step response $A(t)$. The universal curves and sweep equipment are very useful for computing or displaying circuit performance for any type of network such as lumped constant, distributed constants, minimum phase or nonminimum-phase shift. A set of universal curves is given to enable the computation of the transient from either $P(\omega)$ or $Q(\omega)$.

Additional References

E. Peterson, J. G. Kreek, and L. A. Ware, "Regeneration Theory and Experiment," *Bell Sys. Tech. Jour.*, Vol. 13, pp. 680-700, October, 1934.

J. R. Wait, "An Approximate Method of Obtaining the Transient Response from the Frequency Response," *Canadian Journal of Technology*, Vol. 31, pp. 127-131, June, 1953.

APPENDIX—RELATIONS BETWEEN $P(\omega)$ AND $Q(\omega)$

The following seventeen curves are based upon an analysis in a

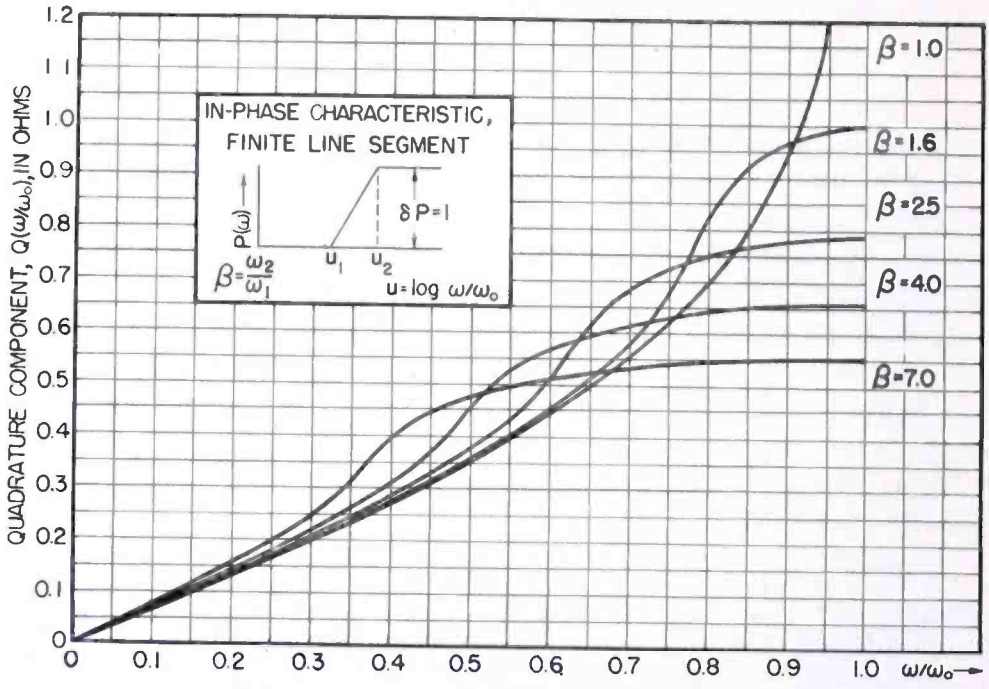

Fig. 46—Quadrature component for finite line segment in-phase characteristic.

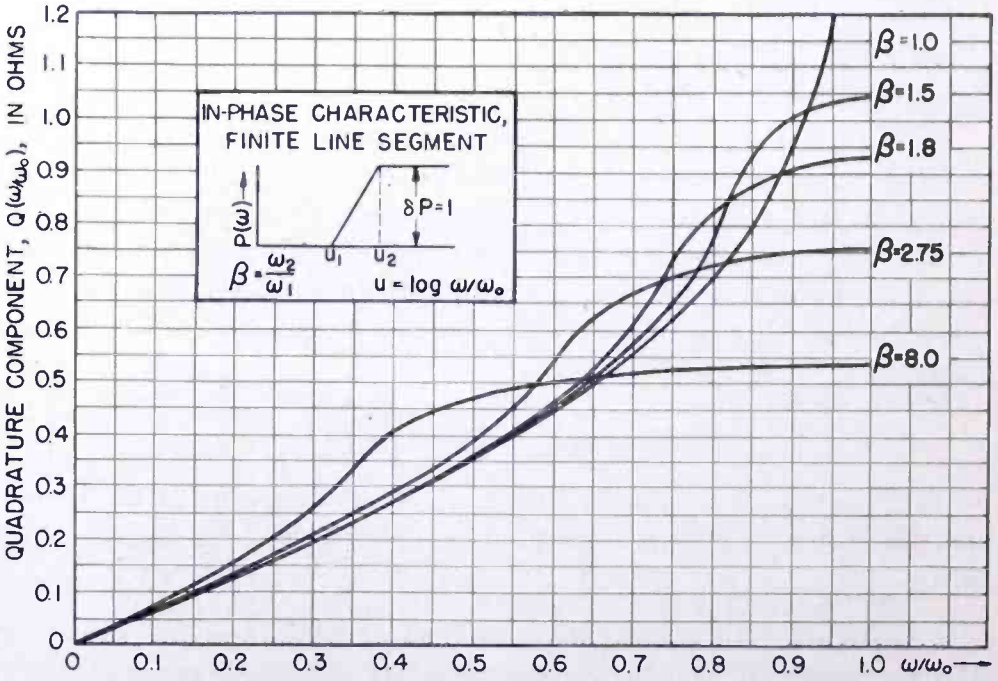

Fig. 47—Quadrature component for finite line segment in-phase characteristic.

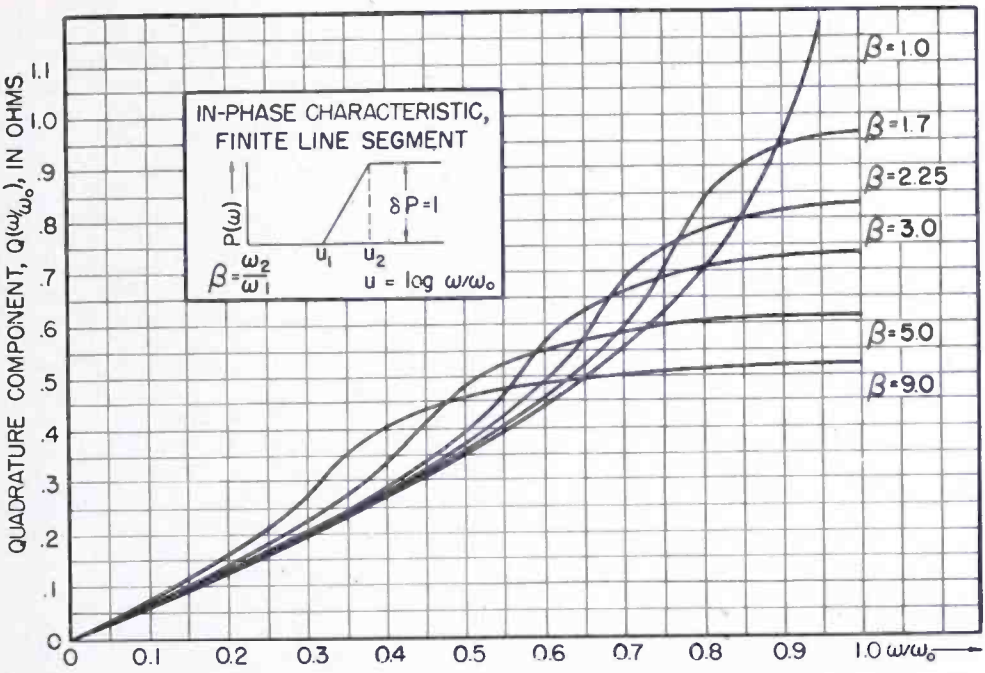

Fig. 48—Quadrature component for finite line segment in-phase characteristic.

previously published paper[11] and can be used to compute the $Q(\omega)$

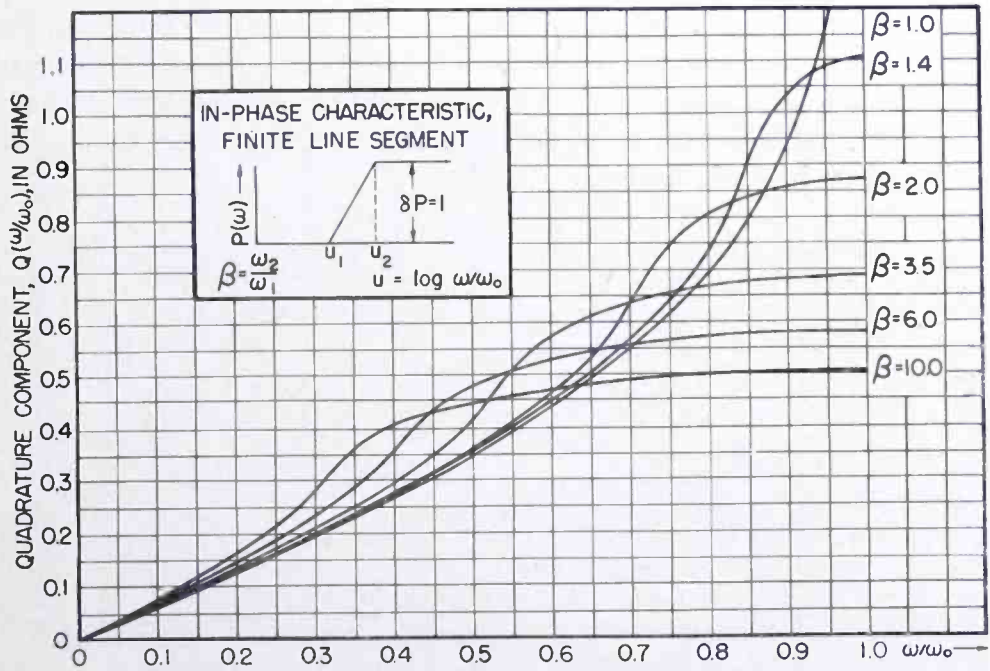

Fig. 49—Quadrature component for finite line segment in-phase characteristic.

[11] T. Murakami and M. S. Corrington, "Relation between Amplitude and Phase in Electrical Networks," *RCA Review*, Vol. 9, pp. 602-631, December, 1948.

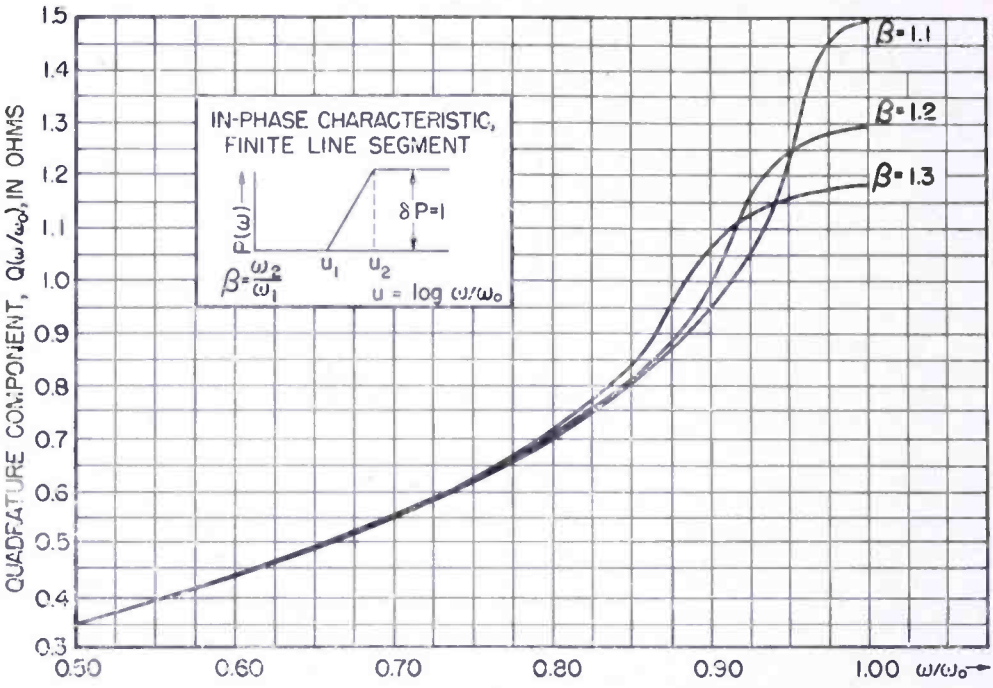

Fig. 50—Quadrature component for finite line segment in-phase characteristic.

response from a given $P(\omega)$ curve or the $P(\omega)$ response from a given $Q(\omega)$ curve. The graphic method of computation is the same as given in detail in that paper for the relations between amplitude and phase. The network need not be minimum phase and may have either distributed or lumped constants.

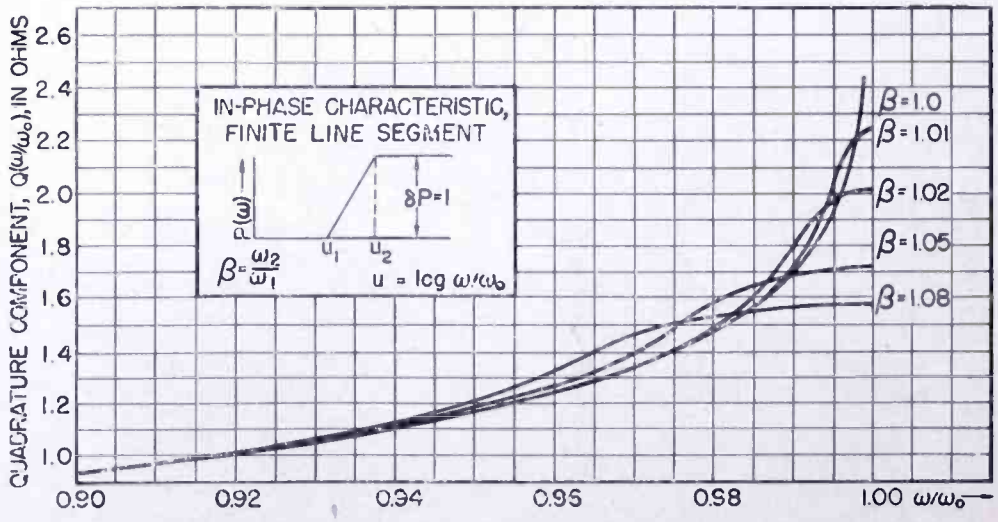

Fig. 51—Quadrature component for finite line segment in-phase characteristic.

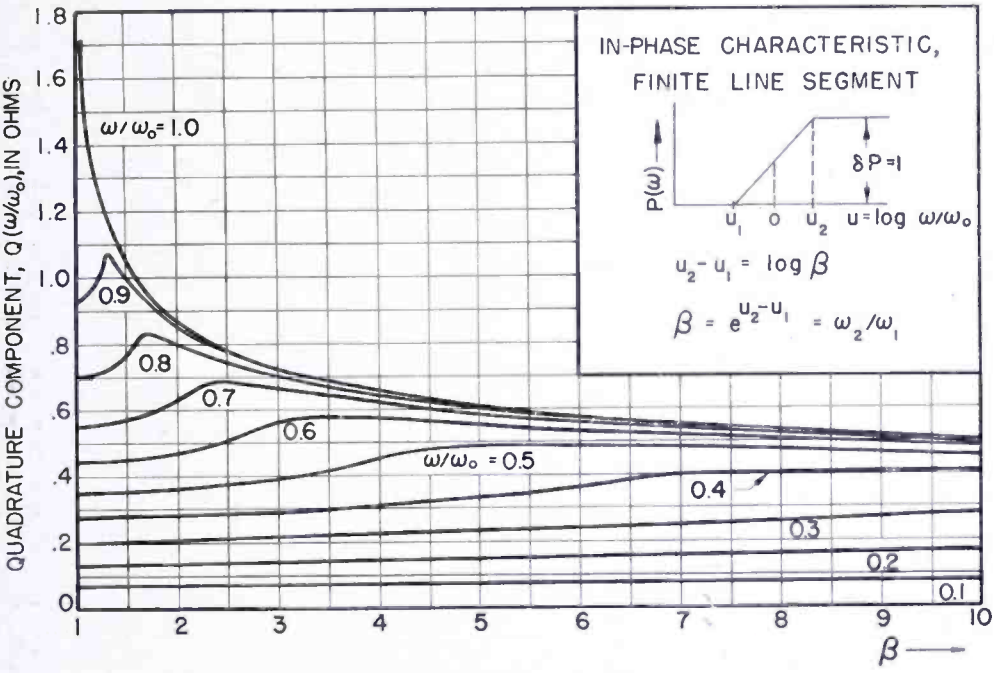

Fig. 52—Quadrature component for finite line segment in-phase characteristic.

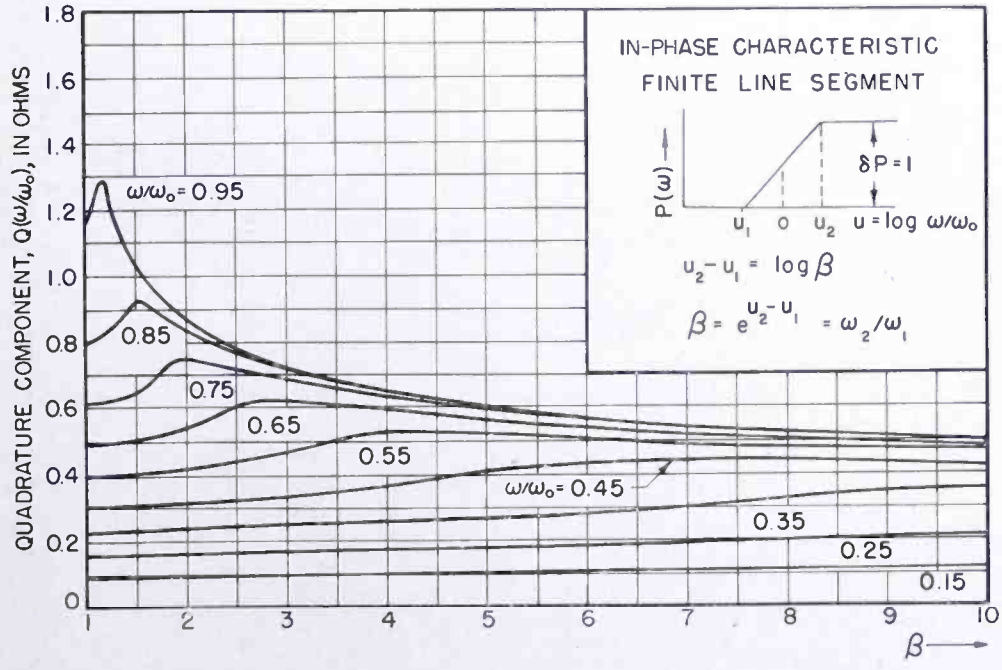

Fig. 53—Quadrature component for finite line segment in-phase characteristic.

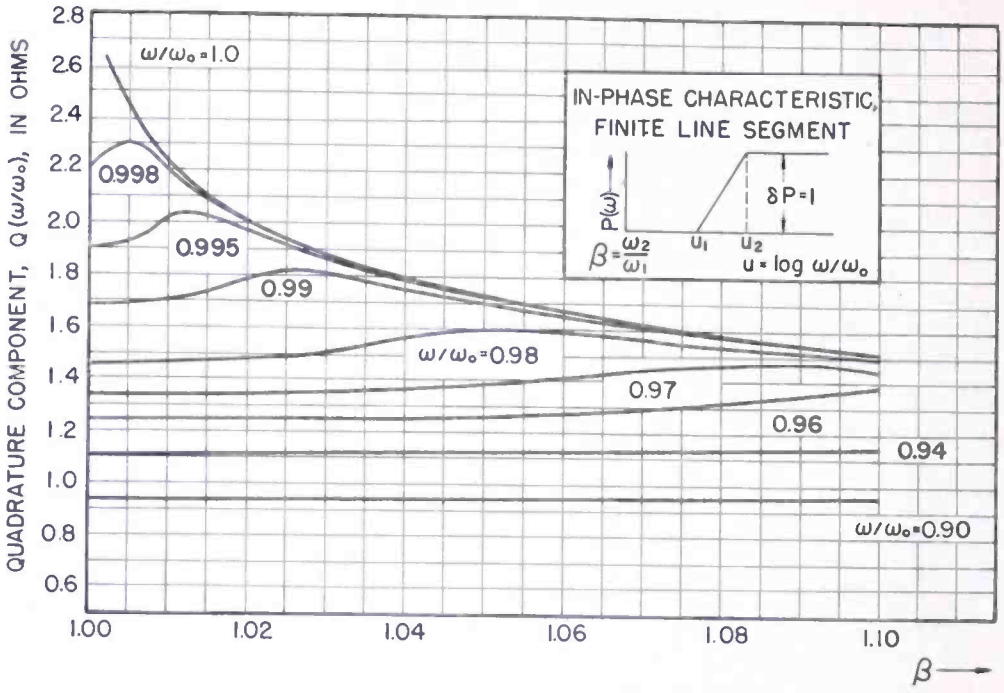

Fig. 54—Quadrature component for finite line segment in-phase characteristic.

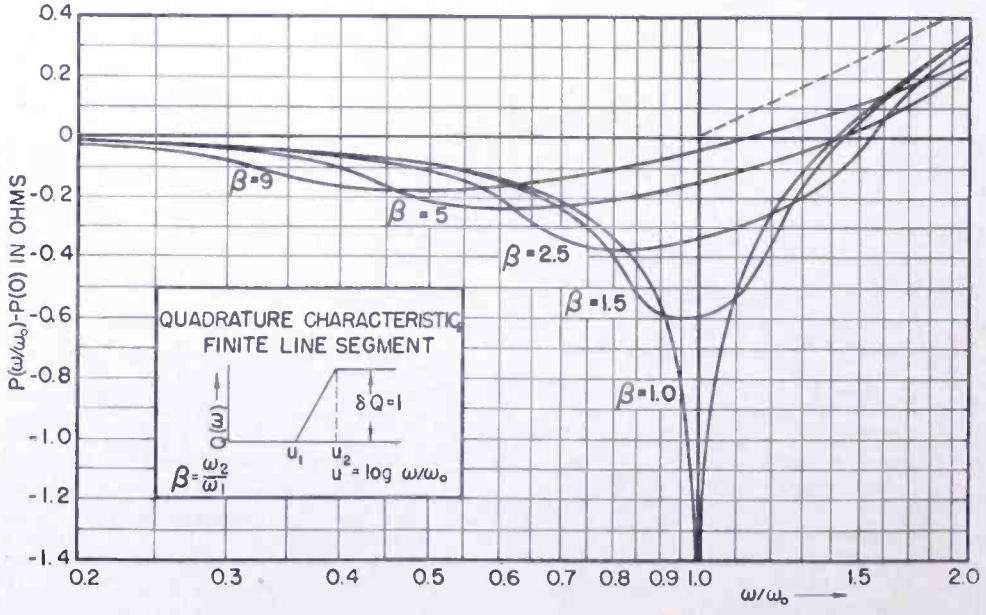

Fig. 55—In-phase component for finite line segment quadrature characteristic.

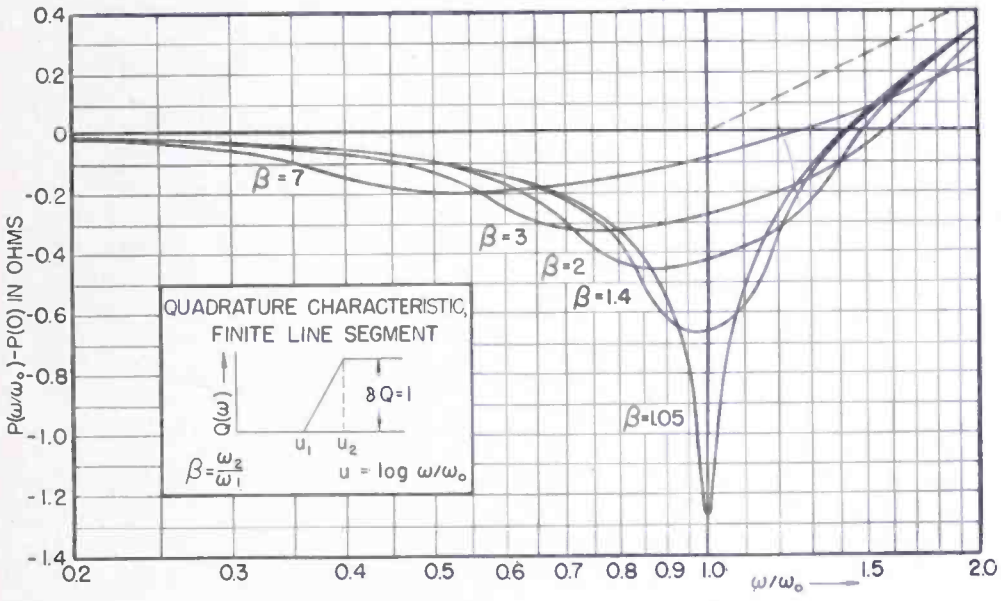

Fig. 56—In-phase component for finite line segment quadrature characteristic.

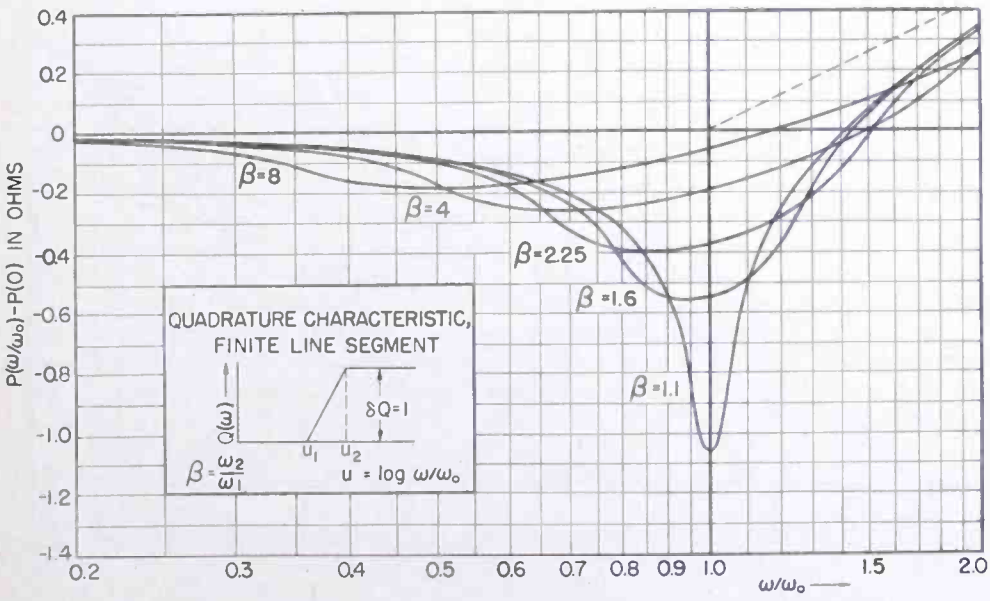

Fig. 57—In-phase component for finite line segment quadrature characteristic.

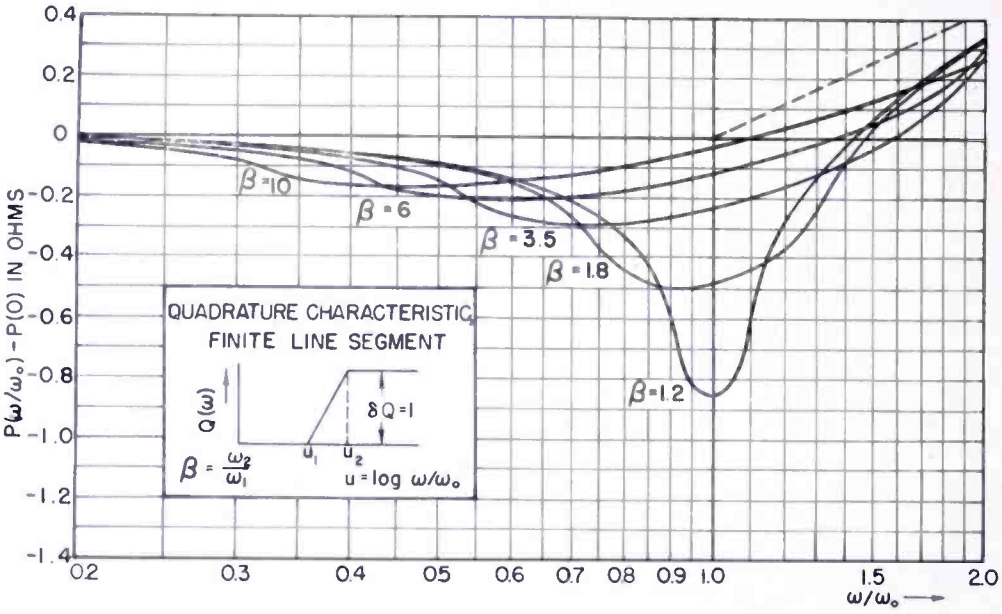

Fig. 58—In-phase component for finite line segment quadrature characteristic.

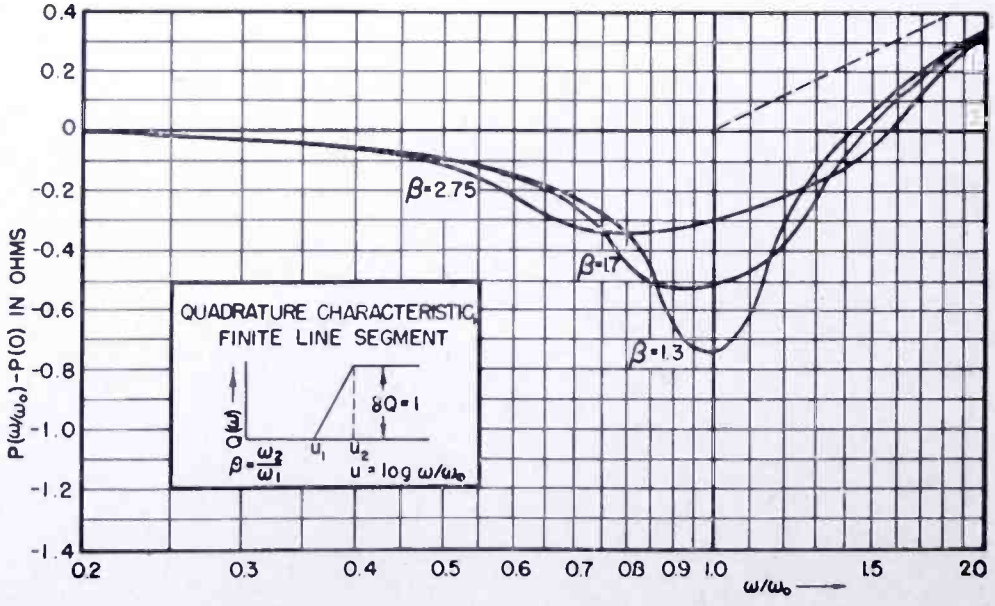

Fig. 59—In-phase component for finite line segment quadrature characteristic.

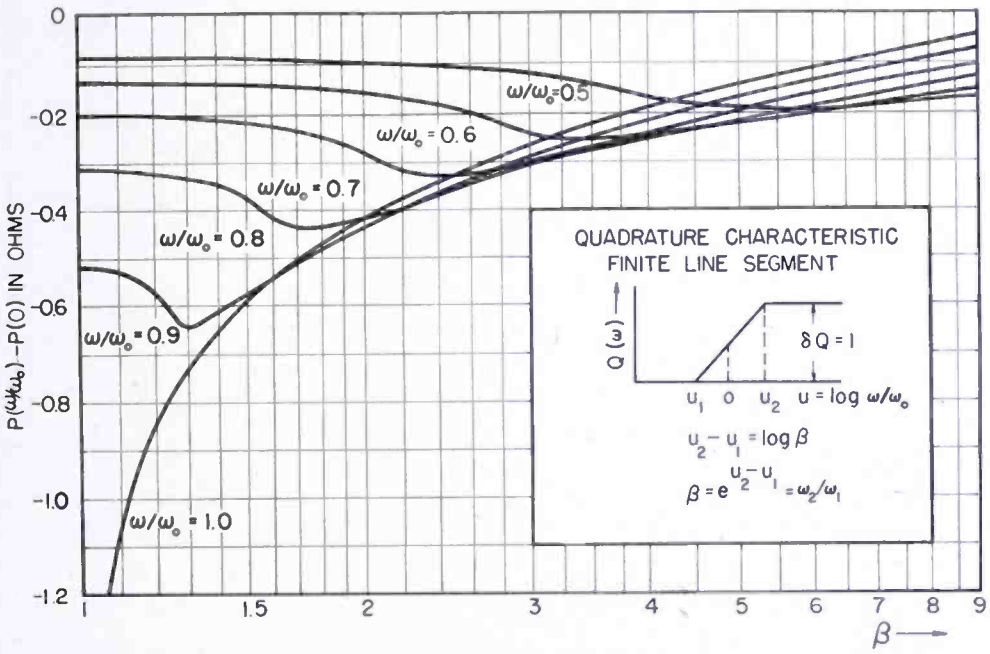

Fig. 60—In-phase component for finite line segment quadrature characteristic.

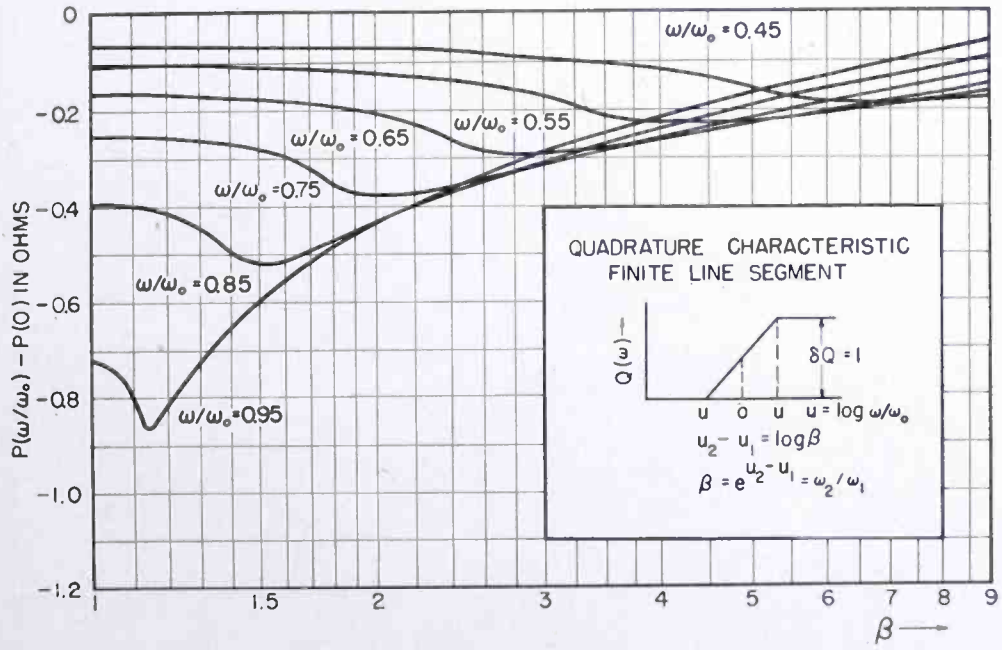

Fig. 61—In-phase component for finite line segment quadrature characteristic.

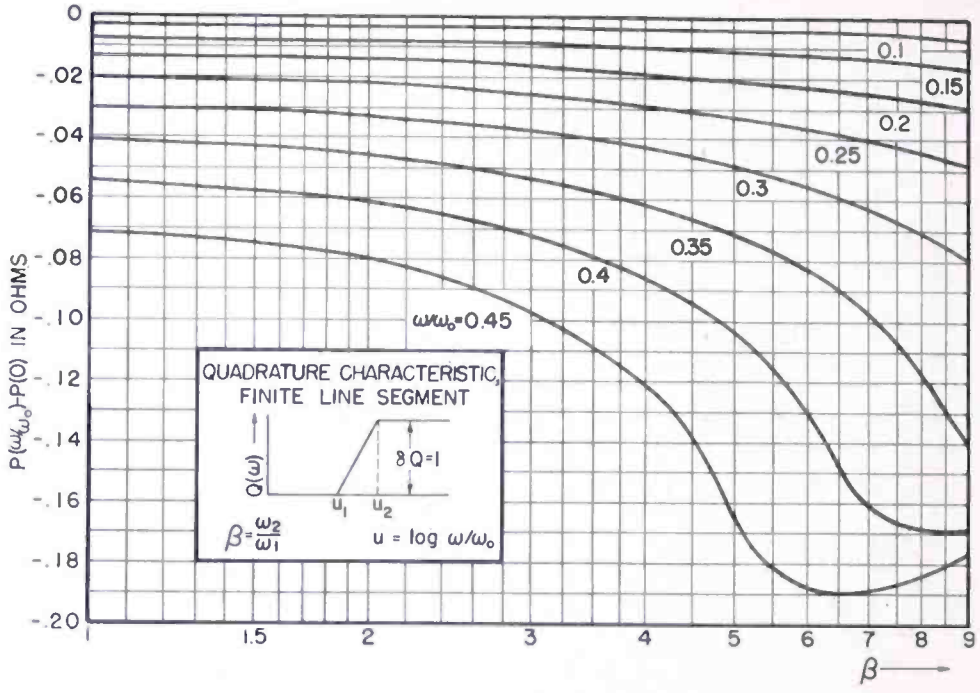

Fig. 62—In-phase component for finite line segment quadrature characteristic.

THE CT-100 COMMERCIAL COLOR TELEVISION RECEIVER*

By

L. R. Kirkwood and A. J. Torre

RCA Victor Television Division,
Camden, N. J.

***Summary**—This paper describes the first commercial color-television receiver produced by RCA. The receiver employs 37 receiving-type tubes, two selenium rectifiers, one silicon crystal, two germanium crystals, and one color kinescope. The receiver was designed to operate on the compatible color standards approved by the Federal Communications Commission on December 17, 1953. It is fully compatible—that is, once the receiver has been tuned, it will accept either color signals or the conventional monochrome signals with no further adjustment.*

Introduction

MODEL CT-100 is a color-television receiver using the 15GP22 kinescope. This kinescope is of the shadow mask type, enclosed in a round glass envelope, and giving a picture with a diagonal of approximately 12½ inches. A production quantity of the receivers was turned out early in 1954. This run showed that compatible color receivers could be built using normal factory techniques.

The CT-100 is designed to receive color-television signals of the type set forth in the compatible color standards adopted by the Federal Communications Commission on December 17, 1953. These signals include luminance, hue, and saturation information.

These are the three independent quantities which represent the video information necessary to reproduce color pictures.[1,2] The luminance information is essentially the same as the video signal in a monochrome transmission, and when displayed on a monochrome receiver, it gives a picture which is almost indistinguishable from a regular monochrome picture. The hue and saturation information is carried by a 3.579-megacycle subcarrier. The phase of the subcarrier relative to a synchronizing burst determines the hue, and the ampli-

---

* Decimal Classification: R583.5.

[1] G. H. Brown and D. G. C. Luck, "Principles and Development of Color Television Systems," *RCA Review*, Vol. 15, pp. 144-204, June, 1953.

[2] D. H. Pritchard and R. N. Rhodes, "Color Television Signal Receiver Demodulators," *RCA Review*, Vol. 14, pp. 205-226, June, 1953.

tude of the subcarrier relative to the luminance signal determines the color saturation.

In order to recover all of the video information, certain important receiver characteristics are necessary; the high-frequency response through the color demodulators must extend to at least 4.1 megacycles, and the phase characteristic must be linear. Also, the over-all amplitude characteristics must not vary or color saturation will be incorrect.

Fig. 1—The CT-100 color television receiver.

A block diagram of the color receiver is shown in Figure 2. The individual red, green, and blue video signals are derived by matrixing in the box labeled "video." The only new functions shown, compared to a black-and-white receiver, are color synchronization and convergence; however, closer tolerances are required of most of the other functions.

The r-f tuner is a UHF-VHF turret type. This unit provides independent adjustments for each channel and, therefore, consistent performance between channels. Experience has shown that tighter factory test limits can be held using such a unit.

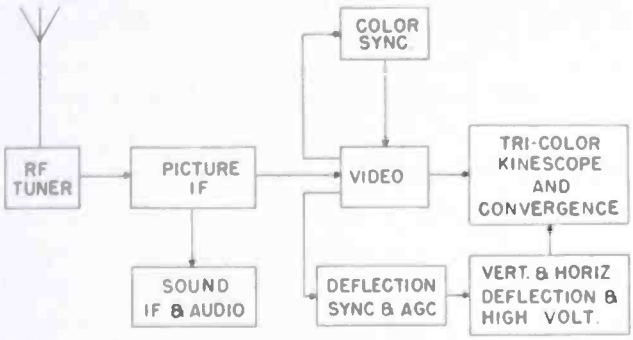

Fig. 2—Block diagram of the CT-100.

In order to facilitate manufacture, the set was designed to consist of a main chassis and three subassemblies: r-f; i-f, audio, and vertical deflection; and horizontal-deflection high voltage. These subassemblies are bolted together to form a single unit (Figure 3). The kinescope is secured to the cabinet. To assist in adjusting the kinescope, the top of the cabinet was made removable (Figure 4). Also, by removing the

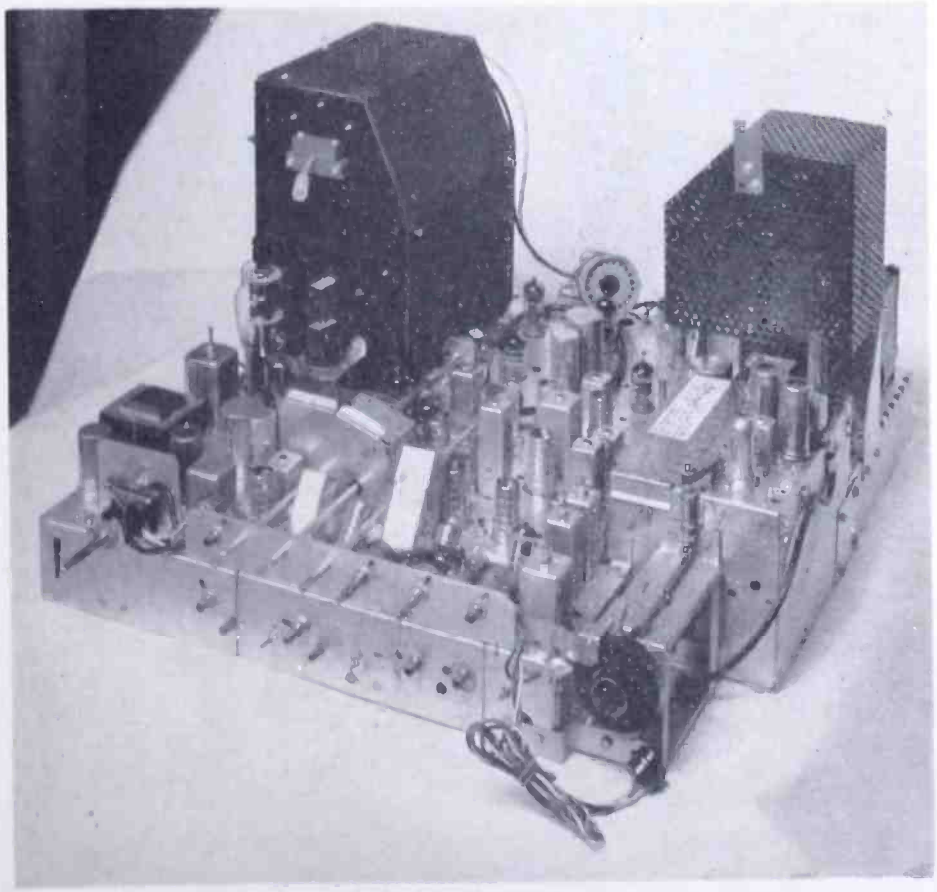

Fig. 3—Chassis of the CT-100.

control pencil box, other controls needed for setting up the kinescope are accessible.

In addition to the normal black-and-white controls, the receiver incorporates two new customer controls under the control panel—hue and color saturation. The d-c focus and convergence controls are accessible at the side of the cabinet.

To minimize radiation of color subcarrier frequency and harmonics, a metal back as well as a metal chassis bottom shield is used.

An intercarrier sound system is employed.

The receiver operates on 117 volts, 60 cycles, and is rated at 475 watts.

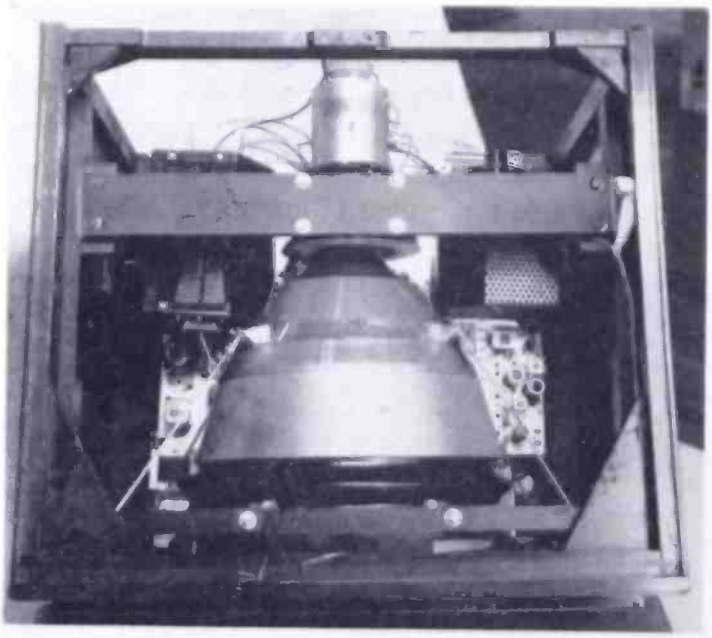

Fig. 4—Top view with the cover removed, showing how the kinescope is mounted.

The Cabinet dimensions are 40 inches high by 28 inches wide by 30⅝ inches deep, and the set weighs 175 pounds.

Maximum highlight brightness of 20 to 30 foot lamberts is attainable. Noise free operation is obtained from an 800 to 1000 microvolt signal and the receiver will synchronize on a signal as low as 15 microvolts. The schematic diagram is shown in Figures 5 and 6.

Circuit Description

Tuner

The r-f tuner is a three-tube, sixteen-position, turret-type tuner capable of covering any 16 of the VHF and UHF television channels, and providing a 40-megacycle i-f output. The tube complement con-

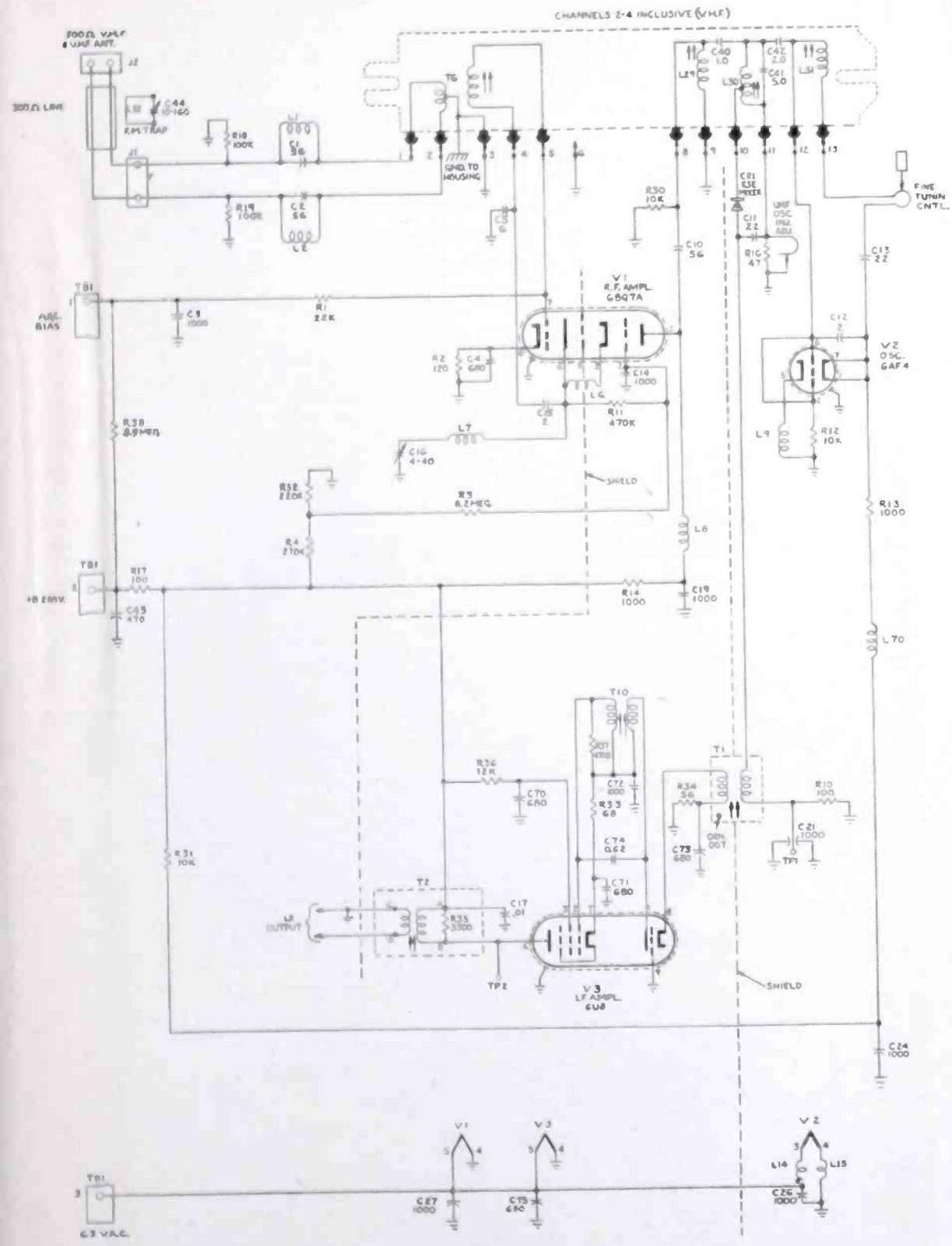

Fig. 5a– Schematic diagram of the tuner with channels 2-4 strip inserted.

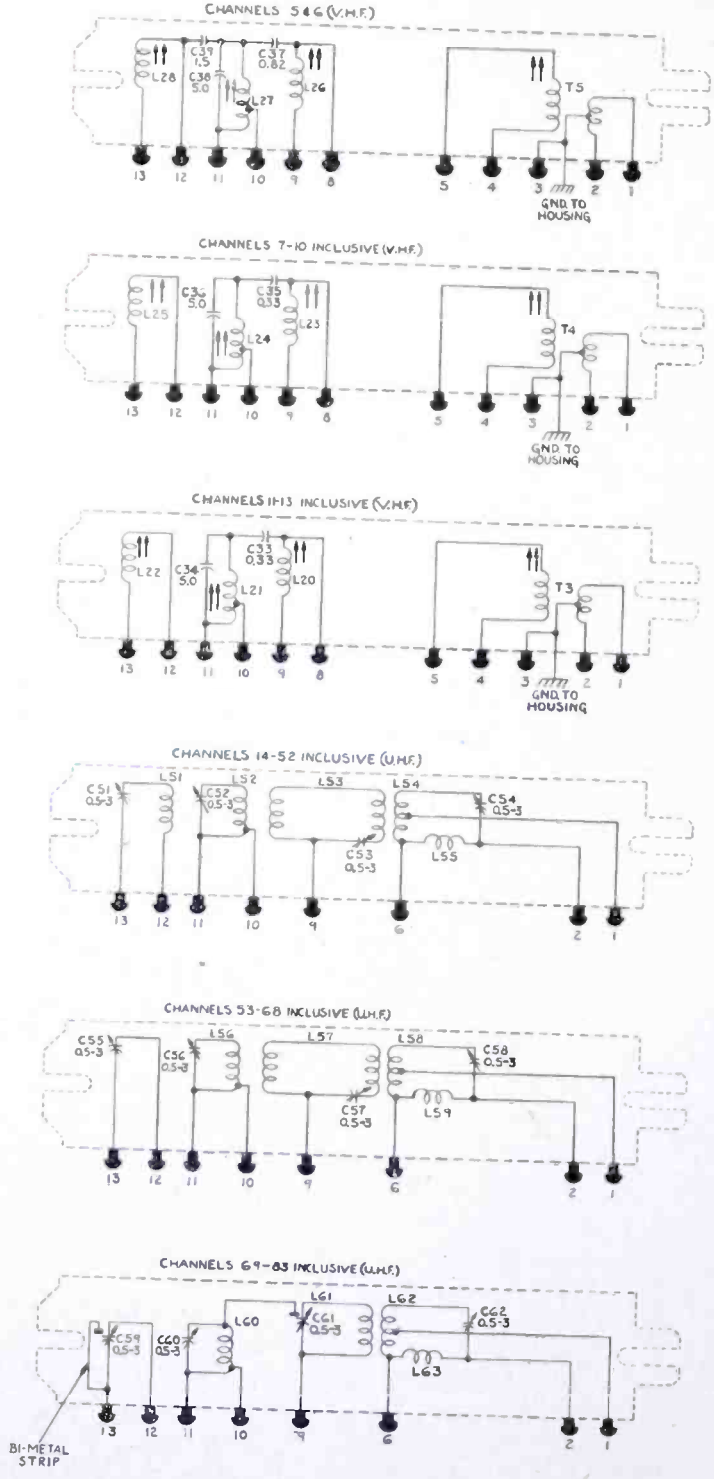

Fig. 5b—Strip assemblies for channels 5-83.

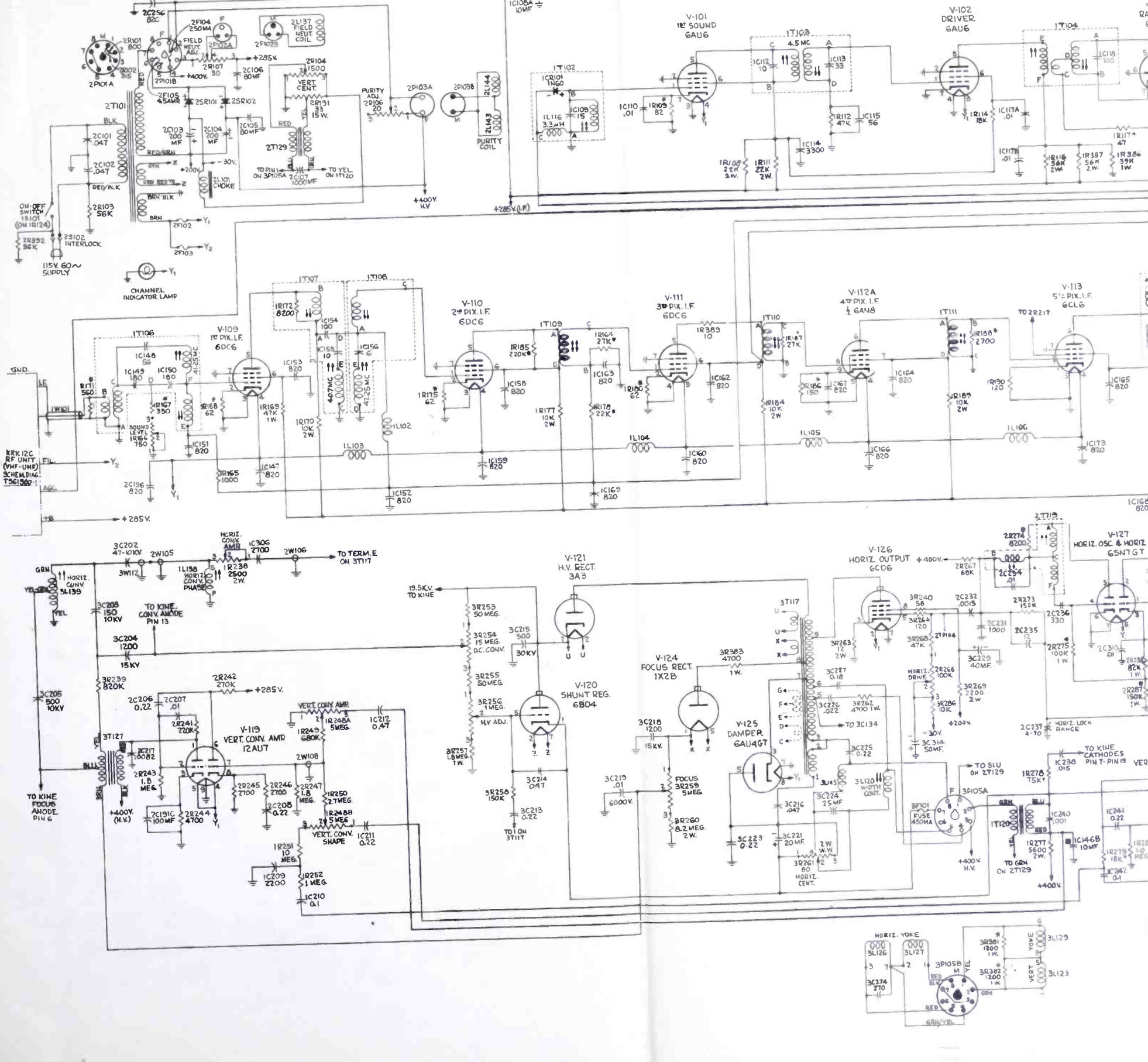
V-101
1ST SOUND
6AU6
V-102
DRIVER
6AU6
V-109
1ST PIX. I.F.
6DC6
V-110
2ND PIX. I.F.
6DC6
V-111
3RD PIX. I.F.
6DC6
V-112A
4TH PIX. I.F.
½ 6AN8
V-113
5TH PIX. I.F.
6CL6
V-119
VERT. CONV. AMR
12AU7
V-120
SHUNT REG.
6BD4
V-121
H.V. RECT.
3A3
V-124
FOCUS RECT.
1X2B
V-125
DAMPER
6AU4GT
V-126
HORIZ. OUTPUT
6CD6
V-127
HORIZ. OSC. & HORIZ.
6SN7GT
FIELD NEUT. ADJ.
FIELD NEUT COIL
VERT CENT
PURITY ADJ
PURITY COIL
CHANNEL INDICATOR LAMP
ON-OFF SWITCH
INTERLOCK
115V. 60~ SUPPLY
KRK 12G RF UNIT (VHF-UHF)
SCHEM. DIAG. T361300
HORIZ. CONV. AMR
HORIZ. CONV. PHASE
TO KINE CONV. ANODE PIN 13
TO KINE FOCUS ANODE PIN 6
TO KINE CATHODES PIN 7-PIN 19
TO TERM. E ON 3T117
VERT. CONV. AMP.
VERT. CONV. SHAPE
HORIZ. YOKE
HORIZ. OUTPUT
HORIZ. DRIVE
HORIZ. CENT.
HORIZ. LOCK RANGE
WIDTH CONT.
DAMPER
FUSE 450MA
+285V.
+400V.
+200V.
-30V.
19.5KV. TO KINE
15KV.
6000V.
+400V. H.V.

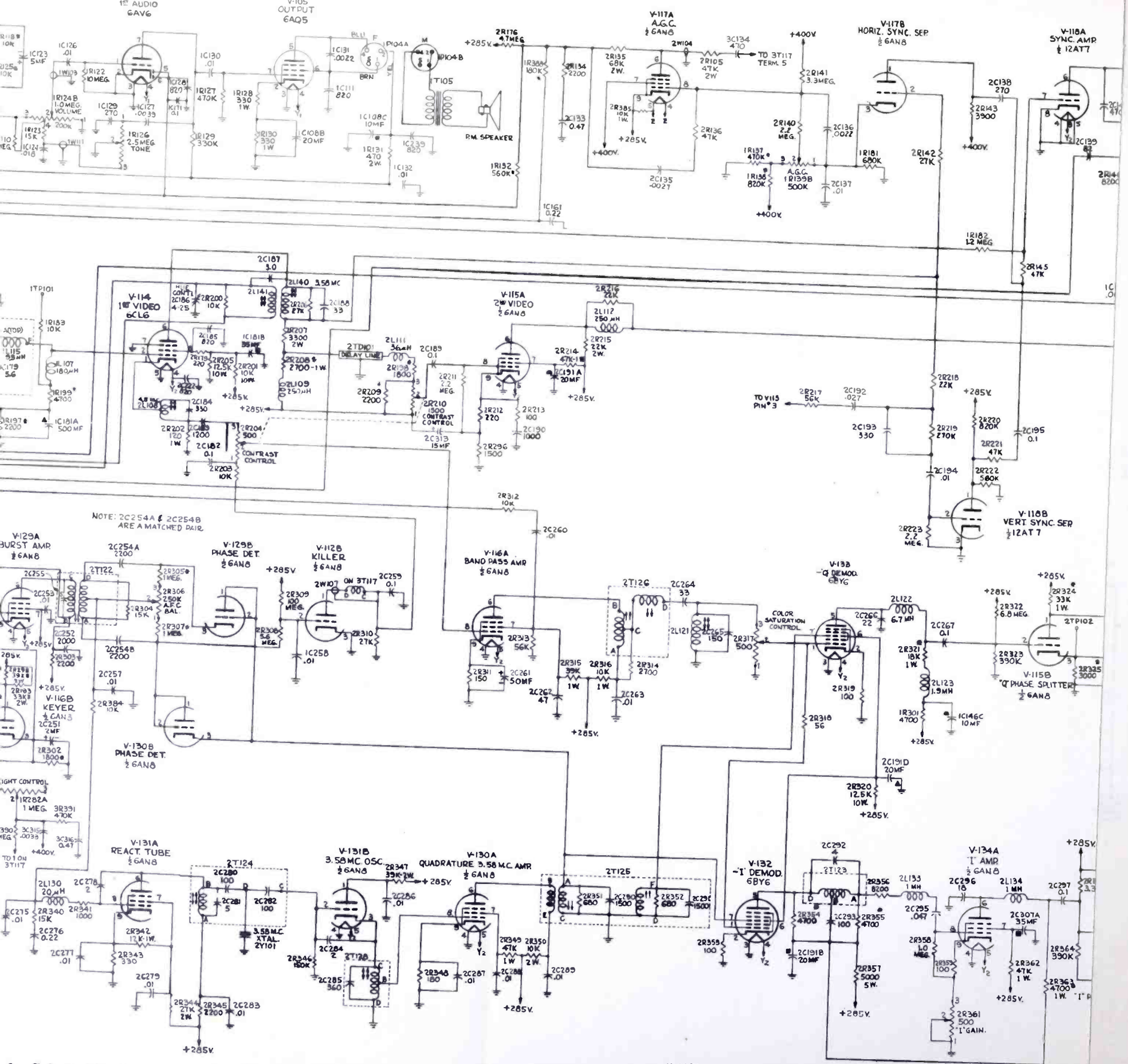

6—Schematic diagram of the CT-100.

K-1000
RESISTANCE VALUES ARE IN OHMS. CAPACITANCE VALUES LESS THAN 1.0 ARE IN MF AND ABOVE 1.0 ARE IN MMF EXCEPT AS INDICATED

sists of a VHF r-f amplifier, a VHF-UHF oscillator, and an i-f amplifier. A silicon crystal is used in the mixer circuit for both VHF and UHF. In the VHF range, a low-noise r-f amplifier feeds a crystal mixer which is followed by a low-noise i-f stage. For UHF the arrangement is similar except that there is no r-f amplifier.

VHF Circuits

The antenna input circuit consists of a link-coupled, single-tuned circuit with the 300-ohm balanced antenna input tapped down for impedance match. However, the constants and configuration have been selected to provide optimum noise factor for all channels rather than perfect impedance match between the antenna circuit and the r-f amplifier. Traps are placed in series with the primary of the input transformer to provide i-f attenuation. A tuned section of 300-ohm transmission line is mutually coupled to the input line to provide attenuation of signals in the FM broadcast band.

The r-f amplifier is a dual triode especially designed for driven-grounded-grid operation. It has the gain and stability of a pentode and the noise factor of a triode. Low output-to-input capacitance minimizes local oscillator feed-through. To prevent detuning of the input circuit with change in grid bias because of Miller effect and to improve the noise factor of the amplifier, a capacity bridge type of neutralization is used. The output of the r-f amplifier contains a capacity-coupled double-tuned circuit. The secondary is tapped for desired amplitude characteristic in accordance with the loading of the crystal diode. This low-noise silicon crystal mixer feeds a tuned bifilar transformer in the grid circuit of the i-f amplifier. Oscillator injection for the mixer is obtained through capacity coupling on the lower VHF channels, and mutual inductance coupling on the upper VHF channels.

The oscillator employs a temperature-compensated Colpitts circuit. Tuning is accomplished, as in the other r-f circuits, by switching in the correct inductance to resonate the tank circuit to the proper frequency. A fine-tuning control, located concentrically on the channel selector shaft, permits vernier adjustment of the local oscillator frequency.

UHF Circuits

On UHF, the 300-ohm balanced antenna input, which is the same as that used for VHF, is tapped into a triple-tuned preselector circuit. The output of the circuit is tapped for the crystal mixer circuit. Oscillator injection is obtained by means of an adjustable inductance in the ground side of the mixer circuit. The output of the mixer circuit is the same as for VHF.

The UHF oscillator circuit corresponds to that used for the VHF

sists of a VHF r-f amplifier, a VHF-UHF oscillator, and an i-f amplifier. A silicon crystal is used in the mixer circuit for both VHF and UHF. In the VHF range, a low-noise r-f amplifier feeds a crystal mixer which is followed by a low-noise i-f stage. For UHF the arrangement is similar except that there is no r-f amplifier.

VHF Circuits

The antenna input circuit consists of a link-coupled, single-tuned circuit with the 300-ohm balanced antenna input tapped down for impedance match. However, the constants and configuration have been selected to provide optimum noise factor for all channels rather than perfect impedance match between the antenna circuit and the r-f amplifier. Traps are placed in series with the primary of the input transformer to provide i-f attenuation. A tuned section of 300-ohm transmission line is mutually coupled to the input line to provide attenuation of signals in the FM broadcast band.

The r-f amplifier is a dual triode especially designed for driven-grounded-grid operation. It has the gain and stability of a pentode and the noise factor of a triode. Low output-to-input capacitance minimizes local oscillator feed-through. To prevent detuning of the input circuit with change in grid bias because of Miller effect and to improve the noise factor of the amplifier, a capacity bridge type of neutralization is used. The output of the r-f amplifier contains a capacity-coupled double-tuned circuit. The secondary is tapped for desired amplitude characteristic in accordance with the loading of the crystal diode. This low-noise silicon crystal mixer feeds a tuned bifilar transformer in the grid circuit of the i-f amplifier. Oscillator injection for the mixer is obtained through capacity coupling on the lower VHF channels, and mutual inductance coupling on the upper VHF channels.

The oscillator employs a temperature-compensated Colpitts circuit. Tuning is accomplished, as in the other r-f circuits, by switching in the correct inductance to resonate the tank circuit to the proper frequency. A fine-tuning control, located concentrically on the channel selector shaft, permits vernier adjustment of the local oscillator frequency.

UHF Circuits

On UHF, the 300-ohm balanced antenna input, which is the same as that used for VHF, is tapped into a triple-tuned preselector circuit. The output of the circuit is tapped for the crystal mixer circuit. Oscillator injection is obtained by means of an adjustable inductance in the ground side of the mixer circuit. The output of the mixer circuit is the same as for VHF.

The UHF oscillator circuit corresponds to that used for the VHF

range except that the tuning for the required channel is accomplished by using a variable capacitance in series with an inductance. The capacitance is preadjusted for the correct oscillator frequency.

Picture i-f Channel

The picture i-f amplifier is designed for a 45.75-megacycle picture carrier, 42.17-megacycle color subcarrier, and a 41.25-megacycle sound carrier. The amplifier consists of seven stages. The second detector uses a germanium crystal and is operated at six volts peak output level in the interest of linearity. The over-all sensitivity is approximately 14 microvolts across the antenna terminals for six volts peak at the second detector.

The noise factor of the tuner on UHF is determined primarily by the loss in the crystal mixer and the noise contributed by the first i-f amplifier following the mixer circuit. Therefore, a low-noise, grounded-grid triode-driven pentode is used for the first i-f stage. The cathode of this stage is fed from the crystal mixer by means of a single-tuned circuit. A double-tuned circuit is used as the interstage coupling between the plate of the triode and the grid of the pentode. The output network of the pentode is a link-coupled, bridged-T, m-derived, band-pass circuit with a rejection trap tuned for accompanying sound (41.25 megacycles). In order to reduce cross modulation, the sound carrier is attenuated as early as possible in the i-f amplifier.

The first picture i-f stage employs an m-derived, band-pass circuit with one rejection trap tuned for the desired skirt selectivity on the sound-carrier side (40.70 megacycles) and the other to the adjacent sound carrier (47.25 megacycles).

The second, third, and fourth picture i-f stages form a staggered triplet with the second and fourth stages tuned to the high- and low-frequency sides, respectively, of the passband. The third stage is tuned to approximately the center of the band.

The staggered triplet provides a means of compensating for production variations in the over-all amplifier, since each stage will affect a different portion of the passband.

The fifth picture i-f stage uses a bridged-π, m-derived, band-pass circuit and a mutually coupled absorption trap. The rejection traps are tuned for accompanying sound (41.25 megacycles) and adjacent sound (47.25 megacycles).

Curves of the individual stages are shown in Figure 7. The over-all curve is shown in Figure 8.

Sound i-f and Audio Channel

In most monochrome intercarrier sound receivers, the sound take-

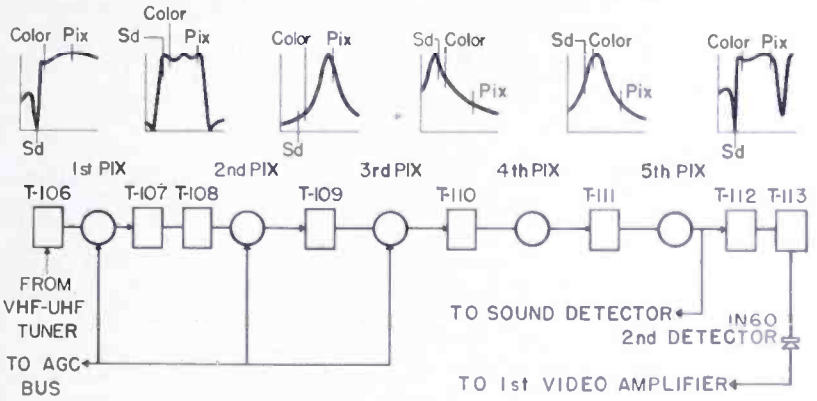

Fig. 7—Block diagram of the picture i-f channel with individual stage selectivities.

off is after the second detector. Also, it has been found that the optimum ratio of picture carrier to sound carrier at the detector should be approximately 15 to 1. However, in order to reduce the 920-kilocycle beat between sound carrier and color subcarrier so that it does not appear on the face of the kinescope, it is necessary to provide much greater attenuation of the sound. In the interest of sound gain, sound information should be taken off as late as possible in the i-f amplifier. In the CT-100, it is taken off after the fifth picture i-f tube. The required additional sound rejection is obtained by bridging the m-derived, band-pass circuit for maximum sound rejection.

The sound i-f detector is a germanium crystal diode feeding a single-tuned circuit in the grid of the 4.5-megacycle sound i-f amplifier. The output circuit is a high-impedance, double-tuned, band-pass transformer. Following is the driver for the ratio detector, which is operated with low screen voltage and grid leak bias in order to provide amplitude-modulation rejection. The ratio detector employs a double triode in a balanced detector circuit. The output from the ratio detector is fed to the first audio amplifier. A normal single-ended audio system is employed for the output.

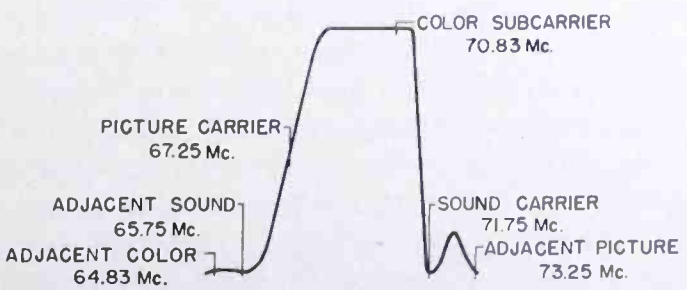

Fig. 8—Over-all r-f - i-f response on channel 4 (66-72 megacycles).

Video

The video section consists of a luminance channel, chrominance channel, and a matrix which combines the two channels. A block diagram is shown in Figure 9.

The luminance (Y) channel serves a purpose substantially similar to that performed in standard monochrome receivers—that of amplifying the luminance information to a level satisfactory for application to a kinescope. The only difference here is that the information is applied to the kinescope via the matrix.

The chrominance channel serves to recover the information contained in the color subcarrier and its accompanying sidebands. By the process of synchronous detection, two signals are recovered from the color subcarrier. These signals are called I (in phase) and Q (quadrature phase). Both the I and Q channels are band-limited according

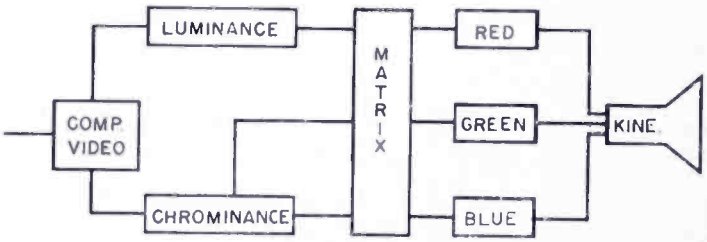

Fig. 9—Block diagram of the video section.

to FCC signal specifications. The I channel passes information up to approximately 1.5 megacycles. While band-limiting of these channels prevents crosstalk, it necessitates equalization of signal delay time among I, Q, and Y.

The matrix provides simultaneous red, blue, and green signals by combining predetermined proportions of Y, I, and Q information for application to the kinescope grids.

Luminance Channel

The first video amplifier provides both polarities of video, 4.5-megacycle attenuation by means of a cathode trap, and color subcarrier attenuation by a trap in the plate circuit. The grid is d-c coupled to the second detector load circuit which is raised slightly positive by a voltage divider. This biases the first video for more linear operation.

Sync-positive wideband video at the plate provides the luminance (Y) channel signal as well as the burst, sync, and AGC (automatic gain control) signals. The burst is taken off by capacity coupling a single-tuned circuit to the color subcarrier trap. Sync and AGC information are taken off just below the color subcarrier trap at a high video level. The luminance (Y) information is tapped down in the plate

circuit to match the impedance of the *Y* delay line. This delay line provides about 1.0 microsecond time delay for the luminance signal to effect time coincidence with the chrominance signals at the matrix junction point. The *Y* delay line is terminated in a network containing a potentiometer used as the contrast control in the *Y* channel. Ganged to this control is another potentiometer which is located in the cathode circuit of the first video and serves as the contrast control in the chrominance channel. These controls are mechanically coupled so they track from minimum, which is zero contrast, to maximum, keeping a constant ratio between luminance and chrominance for all contrast settings.

The *Y* section of the contrast control varies the signal applied to the second video amplifier. This stage amplifies the *Y* information to the level necessary for matrixing.

These video stages incorporate conventional series or shunt coil peaking in the plate circuits and *RC* peaking in the cathodes.

Chrominance Channel

The chrominance signal from the cathode of the first video amplifier is fed to the band-pass amplifier. The plate circuit of this stage contains the band-pass filter which removes the low-frequency components of the signal and retains the region of the color subcarrier and its sidebands. This filter has a bandwidth of approximately 2.4 to 5.0 megacycles, and is terminated by a potentiometer which serves as the color saturation control.

During each burst interval the band-pass amplifier is keyed off by applying to the screen of the tube a negative pulse derived from horizontal deflection. Keying the burst out in this manner avoids color kinescope background unbalance due to the d-c restorers clamping on demodulated burst rather than on tips of sync.

The grid circuit of the band-pass amplifier operates in conjunction with the "color killer." The "killer" stage is held at cutoff by negative d-c voltage developed by the burst phase detector. In the absence of burst, that is a standard black-and-white transmission, the "killer" stage conducts and biases the band-pass amplifier to cutoff, thereby assuring that no signal information passes to the demodulator grids via the band-pass filter.

Demodulation of the chroma signal is accomplished by two synchronous detectors; color subcarrier frequencies are applied to the outer grids while the chroma signal from the arm of the band-pass terminating potentiometer is applied to the inner grids.

The detected *Q* signal appears at the plate of the *Q* demodulator and is band-limited by a 0.5-megacycle low-pass filter. This signal is

fed to the Q phase splitter whose outputs provide the positive and negative Q signals necessary for matrixing.

The detected I signal appearing at the plate of the I demodulator is fed to a bridged negative mutual type filter which both limits the I channel bandwidth to 1.5 megacycles and provides high-frequency time delay compensation to match the Q time delay. The I signal is further amplified by the I amplifier pentode, and fed to the I phase splitter, which supplies the positive and negative I signals necessary for matrixing.

The proper ratio of I to Q signals is adjusted by a degeneration control in the I amplifier cathode circuit.

Matrix and Output

Fixed resistances are used in the matrixing. The adder and output stages for each color are combined in a twin triode.

D-C restoration is applied to the red, blue, and green output signals by a triple diode tube. The plate return circuits for these three restorers are arranged in a bridge circuit which is adjusted in such a way as to maintain proper tracking of the three kinescope grid bias values throughout the range of the master brightness control.

Deflection Synchronization

The synchronization signal is obtained from the plate circuit of the first video amplifier and is d-c coupled to the grid of the horizontal separator and a-c coupled to the grid of the vertical separator. Horizontal and vertical sync are added in the grid circuit which serves the function of sync amplifier and clipper. Variable clipping as a function of signal strength is obtained by connecting the grid resistor of the sync amplifier to the screen grid of the third picture i-f amplifier. Improved noise immunity in the vertical-deflection circuit is obtained by coupling negative noise pulses from the screen of the fifth picture i-f to the grid of the vertical-sync separator. The output of the sync amplifier is used for both horizontal- and vertical-sync information, vertical being fed through a printed integrator circuit for proper shaping before being applied to the vertical-deflection oscillator grid.

Automatic Gain Control

The AGC amplifier derives its control voltage from the cathode of the horizontal-sync separator. The magnitude of this voltage, together with the AGC control, determines the bias on the AGC tube. Plate supply is obtained from a horizontal kickback pulse, capacitively coupled to the yoke tap. The AGC tube conducts only at pulse time and is nonconducting during the remainder of the cycle. Negative

voltage is obtained by charging the plate capacitor and is applied to the i-f and r-f grids through suitable filter networks. A diode serves as a clamp on the r-f bias delaying the r-f bias for improved signal-to-noise ratio.

Horizontal Deflection and High Voltage

The horizontal-deflection system supplies the kickback pulses used in various circuits as well as the high-voltage potentials and horizontal scan. The horizontal-deflection output tube is driven by an oscillator and automatic frequency control circuit similar to that used in many monochrome receivers. A protective circuit which supplies fixed bias to the output tube grid is incorporated to protect the circuit against damage by failure of the horizontal-drive signal.

The ultor voltage is supplied by a single high-voltage rectifier rectifying the kickback pulse and is controlled by a shunt regulator. A high-voltage control which is part of the high-voltage bleeder varies the bias to the control grid of the high-voltage shunt regulator to adjust the high voltage. This type of regulation keeps a constant load on the high-voltage system. In order to maintain the static convergence potential at a fixed ratio with respect to the ultor voltage, the d-c convergence control is used as part of the high-voltage bleeder.

The focus voltage is derived from a separate rectifier tapped further down on the horizontal-deflection transformer, and the focus control is part of the bleeder on this rectifier.

Two separate windings, one of them tapped, provide kickback for "killer" bias rectification, band-pass keying, burst keying, and horizontal-deflection dynamic convergence signal.

The horizontal-deflection yoke is a-c coupled to the transformer. It is a series-connected yoke tapped up on the transformer so that both sides of the yoke carry pulse. This arrangement balances out much of the yoke ringing. In order to provide electrical centering to this arrangement and to keep centering current out of the transformer, two separate chokes are needed to connect in the centering control. One of these chokes is variable and serves as a width coil.

Since the yoke is tapped relatively high on the horizontal-deflection transformer, the vertical-deflection yoke has been isolated from a-c ground by a bifilar choke to prevent loading of the kickback pulse by the capacity between the horizontal- and the vertical-deflection windings in the yoke.

Vertical Deflection

Vertical deflection is supplied by a dual triode, the first half being a blocking oscillator and the second half driving the vertical-deflection

yoke section by means of an output transformer. Electrical centering is also used.

Color Synchronization

In order to recover the color information, it is necessary to generate a local subcarrier of proper frequency and phase. To accomplish this, phase reference information is transmitted as a component of the composite color signal. This color synchronizing information is transmitted in the form of a "burst" of approximately eight cycles of the color subcarrier frequency and appears immediately following each horizontal synchronizing pulse in the composite signal.

This burst is separated from the composite signal and is used in establishing the proper phase relationship between the transmitted signal and the local subcarrier. This subcarrier is generated by a quartz crystal oscillator whose exact frequency and phase is controlled by a reactance tube. The reactance tube derives its control information from an error signal proportional to the difference in phase between the transmitted burst and the local crystal oscillator output.

This color synchronizing channel includes a keyer wave-shaping stage, a keyed burst-amplifier stage, a phase detector, a crystal oscillator, a reactance tube, and a 3.579-megacycle amplifier.

The burst-amplifier stage is driven from a single-tuned coil coupled to the first video amplifier plate. A trimmer across the single-tuned coil provides hue control. The keyer tube is driven by a negative pulse derived from the horizontal deflection voltage. A positive flat-topped pulse from the plate is coupled to the low side of the burst input coil. The cathode of the keyer is connected to the cathode of the burst amplifier and bypassed providing an automatic adjustment of keying level.

The plate transformer of the burst amplifier has a high-impedance primary and a bifilar secondary tightly coupled to the primary. With a turns ratio of 6 to 1, the output is approximately 60 volts peak-to-peak of burst on either side of the secondary center tap.

The phase detector uses the triodes of two separate tubes connected as grid-cathode diodes with the plates connected to the grids. The phase detector compares the phase of the incoming burst signal with the phase of the locally generated signal. This locally generated signal is one output from a double-tuned transformer. The output of the phase detector is a d-c error voltage which is the reactance tube control signal.

The reactance-tube stage is of the capacitive type.

Operating the oscillator as a cathode follower has the basic advantage of eliminating the spurious oscillation to the reactance-tube plate

coil. For this type of circuit to oscillate, it is necessary for the cathode circuit to be resonant at a frequency lower than that of the crystal resonance. If the cathode circuit is tuned between the crystal resonance and the reactance plate coil resonance, it can then only oscillate at the crystal frequency.

The 3.579-megacycle double-tuned transformer amplifier is driven from tap on the oscillator cathode coil. A coupled transformer in the plate circuit yields low-impedance 3.579-megacycle voltages of the proper phase displacement for the demodulators. A tightly coupled tap from the primary provides *I*-phase color subcarrier to the *I* demodulator and reference phase color subcarrier to the phase detector. The secondary provides *Q*-phase color subcarrier to the *Q* demodulator.

Tri-Color Kinescopes

The tri-color kinescope, as used, is a simultaneous color display device. Structurally, the tube consists of three electron guns mounted with their axes parallel to the central axis of the tube, and spaced 120° apart. The focus electrode potential is adjusted to cause the beams to focus at the phosphor dot plate. All three beams pass through an electrostatic lens system, whose potential is adjusted to cause the three beams to converge at the phosphor plate. The three beams are electromagnetically deflected by a common yoke.

The control adjustments associated with the kinescope are of two categories, namely, static and dynamic.

Purity, center convergence, cutoff, and background tracking are all static adjustments. The purity adjustment permits alignment of the electron beams so that each beam falls only on the proper color dots.

Successful operation of a master background control requires that some provisions be made for the differences in the three phosphor efficiencies and also for the variation in gun characteristics. With the brightness control at maximum clockwise position the screen potential potentiometers are adjusted to give a gray low-light.

The low-light bias tracking is done by the blue and green dividers across the top portion of the master background potentiometer.

Center convergence of the three beams is done by adjusting the d-c potential of the convergence electrode for best super-positioning. Any residual error is due to mechanical inaccuracies of the gun alignments and is corrected for by the use of the individual beam convergence magnets.

Dynamic Convergence

Since the phosphor plate and the shadow mask are flat surfaces, the distance the beams must travel from the deflection plane to the

central area of the aperture mask is less than the distance they must travel when deflected away from central area. If the potential on the convergence electrode which was necessary to produce center convergence remained unchanged, the deflected beams would cross over before reaching the phosphor plate. To correct this condition, it is necessary to modulate the d-c potential on the convergence electrode in such a manner as to produce a larger convergence electrode voltage as the deflection angle increases. Since the tube focus is changed by the dynamic convergence voltage, it is also necessary to modulate this electrode.

The dynamic convergence and focus modulation voltages, each having the proper waveform, amplitude, and synchronism with deflection, are produced by linear addition of a variable shape vertical parabola with a variable phase horizontal sine wave. The composite alternating output voltage is coupled to the kinescope convergence electrode and focus electrode through the respective output taps.

The vertical-deflection dynamic convergence amplifier circuit combines, shapes, and amplifies the parabola and sawtooth waveforms derived from the vertical-deflection circuit for application to the kinescope.

Sine-wave horizontal dynamic waveform is derived from two cascaded series tuned circuits excited by horizontal kickback.

RCA TECHNICAL PAPERS†

Second Quarter, 1954

Any request for copies of papers listed herein should be addressed to the publication to which credited.*

"Aircraft Receiver for VOR-ILS and Communications," G. W. Gray, *Electronics* (June) 1954
"Application of Brewster's Angle to the Design of Coaxial-Line Components for Microwaves," B. A. Dahlman, *RCA Review* (June) 1954
"A Bridge for the Measurement of Cathode Impedance," R. M. Matheson and L. S. Nergaard, *RCA Industry Service Laboratory Bulletin LB-945* (May 11) 1954
"Broadbanding of Resonant-Type Microwave Output Windows," T. S. Chen, *RCA Review* (June) 1954
"Coining Cuts Costs of Magnetron Anodes," L. J. Caprarola, *Electronics* (May) 1954
"Color Subcarrier Frequency Measurement Equipment," P. T. Martin, *RCA Industry Service Laboratory Bulletin LB-951* (May 24) 1954
"The Complete Specification of a Network by a Single Parameter," R. W. Sonnenfeldt, T. Murakami, and M. S. Corrington, *RCA Industry Service Laboratory Bulletin LB-943* (May 10) 1954
"Design Considerations for Frequency-Shift-Keyed Circuits," W. Lyons, *RCA Review* (June) 1954
"The Design of IF Amplifiers for Color Television Receivers," M. D. Nelson and J. Avins, *RCA Industry Service Laboratory Bulletin LB-950* (May 20) 1954
"The Effect of Junction Shape and Surface Recombination on Transistor Current Gain," A. R. Moore and J. I. Pankove, *Proc. I.R.E.* (June) 1954
"Evacuating Photographic Materials for Use in Electron Optical Apparatus," J. H. Reisner, *Rev. Sci. Instr.* (May) 1954
"Factors in the Design of Keyed Clamping Circuits," R. N. Rhodes, *RCA Industry Service Laboratory Bulletin LB-946* (May 11) 1954
"Luminescence of the System $Zn_3(PO_4)_2$–$Cd_3(PO_4)_2$:Mn," A. L. Smith and A. D. Power, *Journal of the Electrochemical Society* (May) 1954
"The Metrechon—A Halftone-Picture Storage Tube," L. Pensak, *RCA Review* (June) 1954
"Microscope Controls Production," F. J. Herrmann, *Electronic Equipment* (May) 1954
"Microscopic Examination of Germanium Crystals and Transistors," S. G. Ellis, *RCA Industry Service Laboratory Bulletin LB-948* (May 17) 1954
"A Minimum Noise Figure for the Traveling-Wave Tube," S. Bloom and R. W. Peter, *RCA Review* (June) 1954
"New Manganese-Activated Fluoride Phosphors," A. L. Smith, *Journal of the Electrochemical Society* (April) 1954

† Report all corrections or addition to RCA Review, RCA Laboratories, Princeton, N. J.
* *RCA Industry Service Laboratory Bulletins* are not published and are issued only as a service to licensees of the Radio Corporation of America.

"A New System of Measuring and Specifying Image Definition," O. H. Schade, *National Bureau of Standards Circular 526* (April 29) 1954
"New 12½-KW UHF Filterplexer," R .L. Meisenheimer, *Broadcast News* (May-June) 1954
"On the Variation of Junction-Transistor Current-Amplification Factor with Emitter Current," W. M. Webster, *Proc. I.R.E.* (June) 1954
"Optimum Performance of Image Orthicons and Vidicons in Broadcast Service," R. G. Neuhauser, RCA Tube Division Publication (May 27) 1954
"Output Windows for Tunable Magnetrons," T. S. Chen, *Electronics* (May) 1954
"RCA's Versatile New Switcher," C. R. Monro, *Broadcast News* (May-June) 1954
"Resistivity Striations in Germanium Crystals," P. R. Camp, *Jour. Appl. Phys.* (April) 1954
"Some Properties of Germanium-Silicon Alloy Semiconductors," E. R. Johnson and S. M. Christian, *RCA Industry Service Laboratory Bulletin LB-949* (May 17) 1954
"Studies of the Interface Layer in Oxide Cathodes," R. M. Matheson and L. S. Nergaard, *RCA Industry Service Laboratory Bulletin LB-944* (May 11) 1944
"A Study of the Etching Rate or Germanium," P. R. Camp, *RCA Industry Service Laboratory Bulletin LB-947* (May 13) 1954
"A Switched-Zone Furnace for Germanium Purification," P. G. Herkart and S. M. Christian, *RCA Industry Service Laboratory LB-941* (April 1) 1954
"Synthesis of Constant-Time-Delay Networks," M. S. Corrington and R. W. Sonnenfeldt, *RCA Review* (June) 1954
"Synthetic-Pattern Generator for the Solution of Certain Instrumentation Problems in Television," R. C. Webb, *RCA Review* (June) 1954
"Transistor Equations Using h-Parameters," C. C. Cheng, *Electronics* (April) 1954
"Transistor Gun for TV," R .E. Lafferty, *Electronics* (May) 1954
"3-Vidicon Color Film Camera," H. N. Kozanowski, *Broadcast News* (May-June) 1954

AUTHORS

WARREN H. BLISS studied electrical engineering at Michigan State College, receiving a B.S. degree in 1928 and an M.S. degree in 1931. During the period, 1931-1943 he taught electrical engineering and communications courses at the University of Maine. After spending several summers with the research group at the RCA Communications terminal in New York City he joined RCA Laboratories as a full time research engineer in 1943. His work has included radio facsimile, high-speed-pulse radiotelegraphy, secrecy communication, and radar range circuit calibration. At present he is concerned with electronic counters and special cathode-ray tube display devices. Mr. Bliss is a Member of the Institute of Radio Engineers and the American Institute of Electrical Engineers.

M. S. CORRINGTON—(See *RCA Review*, Vol. XV, No. 2, June 1954, p. 271.)

THOMAS M. GLUYAS, JR. received the B.S. degree in Electrical Engineering from Pennsylvania State College in 1935. After 3 years spent with the Philco Corporation on television research, and 3 years developing television studio and FM transmitting equipment for KMBC in Kansas City, he joined RCA in the Spring of 1941. From 1941-1945 he was engaged in the design of shipborne radar antennas and a microwave radar system for fire control. Since 1945 he has been an engineer with the Television Transmitter Department and is now Supervisor of Advanced Development on television transmitters. Mr. Gluyas is Chairman of IRE Sub-Committee 15.6 on Standards relating to television broadcast transmitters.

WINSLOW L. HURFORD received the B.S. degree in Electrical Engineering from Lehigh University in 1948 and the M.E.E. degree from Syracuse University in 1953. He joined the Broadcast Studio Engineering Section of the General Electric Company in 1948. In 1953, he joined the Broadcast Studio Section of the RCA Victor Division in Camden, N. J. Mr. Hurford is a member of Tau Beta Pi, Eta Kappa Nu, the Scientific Research Society of America, and a Voting Associate of the Institute of Radio Engineers.

L. R. KIRKWOOD received the B.S. degree in Electrical Engineering in 1930 at Kansas State University. He joined the RCA Victor Division at that time to do design and development work on radios and phonographs. In this activity he made numerous fundamental contributions to the art and acquired many patents. His wartime assignments took in development of radar, navigation, and communications equipment for both Army and Navy. Following this, he did some of the very early color systems and receiver work for RCA, after which he returned to commercial radio engineering as manager of the department. In 1950, he became manager of the Color Product Development Section and organized this new activity. From 1950 to date, he directed and took part in all the receiver developments for color as well as take part in all major demonstrations and field tests. Mr. Kirkwood is a member of Phi Kappa Phi, Sigma Tau, Lambda Chi Alpha, and is a Senior Member of the Institute of Radio Engineers.

RALPH W. KLOPFENSTEIN received the B.S. degree in Electrical Engineering from the University of Washington in 1944 and the degree of M.S. in Applied Mathematics from Iowa State College in 1951. During 1945 and 1946 he served as a Radio Materiel Officer in the U. S. Navy and during 1947 and 1948 he was a Mathematics instructor at the South Dakota School of Mines and Technology. In 1948 he joined the Broadcast Engineering Section of the RCA Victor Division in Camden, N. J. where he worked on advanced development of television and FM transmitting antennas and filters. From the Fall of 1950 through the Spring of 1953 he served as mathematics instructor at Iowa State College. In September 1953 he joined the research staff at RCA Laboratories in Princeton, N. J. Mr. Klopfenstein is a Member of Sigma Xi, Phi Kappa Phi, and the Mathematical Association of America, and is a Senior Member of the Institute of Radio Engineers.

ROY J. MARIAN received the B.S. degree in Electrical Engineering from the University of Nebraska in 1949. From 1944 to 1946, he served with the U. S. Navy as an Aviation Electrician's Mate. In 1949, he joined the RCA Victor Division, Camden, New Jersey, as a specialized trainee. Since 1950, he has been working in the Broadcast Studio Engineering Section.

R. M. MATHESON received the A.B. degree from Cornell University in 1938 and the M.A. degree the following year. He attended graduate school at Princeton University in 1939 and 1940, holding a research assistantship during the latter year. From 1941 to 1946 he served in the U. S. Army Air Force, being released from active duty as a Captain. Prior to joining RCA in 1947, Mr. Matheson served as secretary to the Panel on Electron Tubes of the Joint Research and Development Board.

T. MURAKAMI received the B.S. degree in E.E. from Swarthmore College in 1944, and the M.S. degree from the Moore School of Electrical Engineering, University of Pennsylvania in 1947. From 1944 to 1946 he was an assistant and research associate in the Department of Electrical Engineering at Swarthmore College. Since 1946 he has been with the Advanced Development Section of the RCA Victor Television Division, Camden, N. J., working on radio frequency circuit development. Mr. Murakami is an Associate Member of the Institute of Radio Engineers and Sigma Xi.

LEON S. NERGAARD received the B.S. degree in Electrical Engineering from the University of Minnesota in 1927, the M.S. degree from Union College in 1930, and the Ph.D. degree from the University of Minnesota in 1935. From 1927 to 1930, he was in the research laboratory and vacuum-tube engineering department of the General Electric Company; from 1930 to 1933 a teaching assistant in the department of physics at the University of Minnesota; from 1933 to 1942 in the research and development laboratory of the RCA Manufacturing Company; and since 1942 at the RCA Laboratories Division in Princeton, N. J. Dr. Nergaard is a Member of Sigma Xi, the American Physical Society, the American Association for the Advancement of Science, and a Fellow of the Institute of Radio Engineers.

ROLAND N. RHODES received the degree of Bachelor of Electrical Engineering from the College of the City of New York in June, 1944. He then entered the U. S. Navy where he served until 1946. From 1947 to 1948 he was employed by Melpar Incorporated of Alexandria, Virginia. In 1948, he joined RCA Laboratories, Princeton, New Jersey where he is employed in the Industry Service Laboratory group doing research in the field of color television. He is an Associate Member of the Institute of Radio Engineers and a Member of Sigma Xi.

R. W. SONNENFELDT—(See *RCA Review*, Vol. XV, No. 2, June 1954, p. 272.)

ALTON JOHN TORRE received the B.S. degree in Electrical Engineering in 1943 at the University of Oklahoma, after which he joined the RCA Victor Division. His early work at RCA was connected with the design and development of airborne radar equipment. Following the war, his activities transferred to the home instrument field where he did design and development work on radio receivers. At present, he is manager of electrical engineering for the Color Product Development Section of which he has been a member since 1950. In this activity, he has taken part in practically all field tests and demonstrations as well as all color television receiver developments leading up to the commercialization of color. Mr. Torre is a member of Tau Beta Pi, Sigma Tau, Eta Kappa Nu, is a Senior Member of the Institute of Radio Engineers, and a registered engineer in the State of New Jersey.

CHARLES J. YOUNG received the A.B. degree from Harvard in 1921 and after completing the radio courses at the Harvard Engineering School joined the Radio Department of the General Electric Company, doing early work on wired radio and broadcast facsimile transmission. He transferred in 1930 to the engineering staff of the RCA Manufacturing Company at Camden, New Jersey where he was engaged primarily in development and design of electronic musical instruments, aircraft radio, and facsimile systems and apparatus. In 1942 he transferred to the RCA Laboratories at Princeton where he continued work on facsimile and also did development on electronic counters, memory devices, and electrophotography. Mr. Young received the Modern Pioneer Award, National Association of Manufacturers in 1946, is a member of Sigma Xi and a Fellow of the Institute of Radio Engineers.